Department of Electrical and Computer Engineering

A Study of Planar Inverted-F Antennas in a Dielectric Enclosure

Jianwei He

This thesis is presented for the award of
the Degree of Doctor of Philosophy
of
Curtin University of Technology

January, 2006

ABSTRACT

Demand for small and low-profile antennas has greatly increased due to the desire for miniaturisation of modern-day mobile radio electronic terminals. Such an antenna is often integrated into the dielectric casing of a terminal, or independently enclosed within a dielectric radome to provide a protection from operating environments and keep the system more compact. However, the dielectric casing or radome may interact strongly with the antenna and result in losses in performance. The primary focus of this dissertation is to investigate and enhance the performance of Planar Inverted-F Antennas (PIFAs) when enclosed in dielectric casings or radomes for applications in mobile radio communications.

PIFAs have attracted much interest due to their small volume, low profile structures and electrical characteristics compatible with existing specifications, making it a promising candidate for mobile radio applications. Therefore, the design of a single band PIFA on a finite ground plane, operating in the 900 MHz band is first presented. It is found that the effect of the finite ground plane must be considered to achieve an optimum performance of the PIFA. Then the performance of this antenna in the presence of a dielectric cover layer is investigated and evaluated in terms of resonant frequency, bandwidth and efficiency. In this study, the dielectric layer represents the dielectric casing of a device where the antenna is much closer to the top part of the casing than to the other side parts whose effect can then be ignored. Computer simulations of performance are based on the Method of Moments (MOM) and have been validated by measurements. This study shows that a dielectric cover layer will strongly interact with the antenna with the result that the antenna performance may move outside the design specifications. Therefore, it is concluded that the dielectric cover layer must always be taken into account in the design stage.

In addtion, the input and radiation characteristics of a PIFA enclosed within a rectangular dielectric radome for both the 900 MHz and 2400 MHz frequency bands are

analysed using the MOM. This research concentrates on the effect of each individual part of the rectangular dielectric radome on the overall performance. It is observed that each individual part has a different degree of effect on both the input and radiation characteristics of the PIFA, and that the effect is more significant at the higher frequency band. The study indicates that the effect of the dielectric radome on the performance of the antenna can be minimised by carefully choosing its location and orientation within the radome. Another indication is that an optimised dielectric radome design can both miniaturise the antenna and at the same time improve the bandwidth without sacrificing other performance parameters such as the gain.

Furthermore, an analytical approach based on the Transmission Line Model (TLM) is applied to estimate the input characteristics of a PIFA having a dielectric cover layer. The results calculated based on this approach are compared with MOM computed results. A reasonably good agreement between them has been demonstrated. It is suggested that the TLM model could form part of an efficient Computer Aided Design (CAD) tool for design engineers to provide initial design parameters.

Finally, a new dual-band PIFA is proposed. A design example for the Industrial, Scientific and Medical (ISM) frequency bands of 900 MHz and 2400 MHz is given. Measurement validation of the design is presented. The influence of the dielectric cover layer on the resonant frequency, bandwidth, gain and radiation patterns of this antenna is also examined by simulation. In this study, it is found that a simple capacitive disk arrangement not only provides a single feed for dual-band operation but also gives flexibility to allow individual control of the two desired band resonances.

ACKNOWLEDGEMENTS

I would like to express my sincere gratitude to Professor Kah-Seng Chung, my supervisor, for his guidance and support throughout my studies towards the Ph.D. degree.

I also would like to acknowledge the support of the Department of Electrical and Computer Engineering. Moreover, I would like to acknowledge financial assistance in the forms of an Australian Postgraduate Research Award from the Department of Employment, Education, Training and Youth Affairs and a MINECOM scholarship from Communications Technology Research Group (CTRG).

The thesis was written within CTRG and I wish to thank all its members for their support during the period of my study. In addition, I would like to thank Mr. Keith Rainbow for proofreading the thesis. Above all, my wife, Qiufang, son, Devin, and daughter, Jessie deserve my deepest gratitude for their remarkable patience and loving encouragement throughout my studies.

TABLE OF CONTENTS

LIST OF FIGURES

LIST OF TABLES

ABBREVIATIONS

ABC	Absorbing Boundary Condition
CAD	Computer Aided Design
DCS	Digital Communication System
dB	Decibel
dBi	Decibel gain with reference to isotropic antenna
EFIE	Electric Field Integral Equation
FDTD	Finite Difference Time Domain
FEM	Finite Element Method
FFT	Fast Fourier Transform
FS-PIFA	Full Short-circuit PIFA
GA	Genetic Algorithm
GHz	Gigahertz
GSM	Global System for Mobile communications
IFA	Inverted-F Antenna
ILA	Inverted-L Antenna
ISM	Industrial, Scientific and Medical
MLA	Meander Line Antenna
MOM	Method of Moments
MPIE	Mixed Potential Integral Equation
MTLA	Modified Transmission Line Antenna
MHz	Mega Hertz
NEC	Numerical Electromagnetic Code
PCB	Printed Circuit Board
PCS	Personal Communication System
PEC	Perfect Electric Conductor
PIFA	Planar Inverted-F Antenna
SAR	Specific Absorption Ratio
SET	Surface Equivalence Theorem
SIE	Surface Integral Equation

SIFA	Strip Inverted-F Antenna
SNM	Spatial Network Method
TLM	Transmission Line Model
UMTS	Universal Mobile Telecommunication System
VSWR	Voltage Standing Wave Ratio
WLAN	Wireless Local Area Network

LIST OF SYMBOLS

a_k	Complex coefficient in the k^{th} term
$\mathbf{A}$	Matrix
A_{lk}	Coefficient in the l^{th} row and k^{th} column element of matrix $\mathbf{A}$
b_l	Complex coefficient in the l^{th} term
B	Edge susceptance of patch
$\mathbf{B}_m$	Basis function
$\mathbf{B}_n$	Basis function
BW	Bandwidth
c	Wave propagation velocity in free space
c_n	Constant in the n^{th} term
C	Correction factor in the TLM of PIFA
C_l	Turning capacitor of loop antenna
$C_{L_1 e}$	Edge capacitance of patch at a side having a width of L_1
d	Thickness of dielectric layer, casing or radome
d_f	Distance between short-circuit plate (wire) and feed wire
d_{ij}	Coefficient in new quasi-static model
d_l	Distance from input terminal of loop antenna to tapping point
d_{top}	Separation between top patch and top radome
d_{side}	Separation between side edge of top patch and side radome
d_{open}	Separation between open end of top patch and side radome
d_{short}	Separation between short-circuit plate and side radome
D	Directivity
D_s	Distance from short-circuit plate to narrow side of finite ground plate
$\mathbf{E}$	Total electric field on surface
$\mathbf{E}_{inc}$	Incident electric field on surface
$\mathbf{E}_s$	Secondary electric field on surface
f	Frequency
$f_{\max}$	Maximum resonant frequency

$f_{\min}$	Minimum resonant frequency
f_o	Resonant frequency
$f(\mathbf{r})$	Current function
g	Air gap between patch and top dielectric layer, casing or radome
$g(\mathbf{r}')$	Excitation vector (incident electric field) function
g_f	Distance from feed wire to the long side of finite ground plane
g_i	Distance with respect to the initial position of short-circuit plate
g_s	Distance from the edge of short-circuit plate to the long side of finite ground plane
G	Gain
G_s	Surface-wave conductance of radiation edge
G_r	Radiation conductance of radiation edge
$\mathbf{G}(\mathbf{r} \mid \mathbf{r}')$	Green's function
H	Height of antenna
$H(s)$	Transfer function
$\mathbf{H}$	Total magnetic field
$\mathbf{H}_{inc}$	Incident magnetic field
$\mathbf{H}_s$	Scattered magnetic field
I_n	Current distribution coefficient
$\mathbf{J}$	Current density
M	Equivalent magnetic current density
$\mathbf{n}_{ji}$	Unit normal directed from region j to region i
Q	Quality factor
k	Wave number in medium
k_0	Wave number in free space
K	Operator
Δl	Transmission line extension due to the fringing effect
L	Operator
L_2	Length of antenna patch (wire)
L_1	Width of antenna patch

L_d	Internal length of rectangular radome
L_g	Length of finite ground plane
L_s	Inductance of short-circuit plate
P_{gen}	Power applied to antenna
P_{rad}	Radiated power of antenna
P_{loss}	Loss power in antenna
P_{num}	Simulated errors between power applied and the sum of radiation power and loss power
r_a	Radius of sphere containing antenna
$\mathbf{r}$	Vector position of the field point
$\mathbf{r}'$	Vector position of the source point
R	Point of top patch assembly
R_s	Resistor of short-circuit plate
s	Complex frequency $(= j2\pi f)$
S	Conducting surface
V_m	Excited voltage coefficient
w_m	Test function in the m^{th} term
W_d	Internal width of rectangular radome
W_e	Effective width of patch
W_s	Width of short-circuit plate
W_g	Width of finite ground plane
$\tan\delta$	Loss tangent
$\tan\delta_e$	Effective loss tangent
t	Thickness of conductive plate
T_l	Tapping point of loop antenna
Y_m	Mutual admittance between the two radiating edges of patch antenna
$Z^{(i)}$	Intrinsic impedance of region *i*
Z_0	Characteristic impedance in free space
Z_c	Characteristic impedance in medium
Z_f	Impedance of coaxial feed wire

Z_{in} Input impedance of antenna

Z_{mn} Impedance coefficient

Z_{ol} Open end load

Z_{sl} Short-circuit end load

Z_s Surface impedance of conductor

α Wave attenuation constant

β Wave phase constant

ρ Specific resistance of conductive plate

ρ_{Cu} Specific resistance of copper plate

ε Permittivity

ε_0 Permittivity of free space

ε_{eq} Equivalent dielectric constant

ε_{re} Effective dielectric constant

ε_r Relative dielectric constant

ε_{r1} Relative dielectric constant of layer 1

ε_{r2} Relative dielectric constant of layer 2

η Radiating efficiency

η_0 Wave impedance of free space

λ Wavelength in media

λ_0 Wavelength in free space

γ Complex wave propagation constant

μ Permeability

μ_0 Permeability of free space

ω Angular frequency ($=2\pi f$)

CHAPTER ONE

1. INTRODUCTION

1.1 Motivation

With the recent advances in wireless communications, the need for compact, low-profile, and high performance antennas has greatly increased. The greatest demand for these antennas is from personal communication systems (e.g. cellular phones, pagers and mobile data systems) and other mobile applications (e.g. global position systems, automobiles and trains). Depending on the applications, there are differences in antenna performance requirements (e.g. frequency, bandwidth, gain and polarisation). However, compact and low-profile antennas are essential for such applications, for either mechanical reasons or due to the miniaturisation of electronic devices in general.

Among the compact and low profile antennas, the Planar Inverted-F Antenna (PIFA) is a strong candidate for mobile devices because it has a compact size and a cross polarized radiation pattern and is also capable of covering popular wireless communications bands. However, PIFA requires a ground plane, but at the same time the ground plane should be small in order to fit it in mobile devices. The size and configuration of such a ground plane may therefore influence the PIFA performance.

Moreover, modern communication devices tend to house the antennas within their dielectric casing or radome for ergonomic reasons rather than have them located externally. Not only does this make the device more compact and appealing, but it also reduces the possibility of the antenna being physically damaged. Since such a dielectric casing is typically in the vicinity of the near field of the antenna, its effect could significantly impact the input impedance and radiation characteristics of the antenna element. Consequently, this may lead to poor performance of the overall antenna system due to the normally high Q factor of small antennas. Such a dielectric casing therefore has to be treated as part of the radiating system and its effect must be fully taken into account in the initial design phase of the overall antenna system.

Furthermore, modern wireless communication systems are usually operating in several frequency bands. Such multiband operation, in which different radio modules are integrated into the same device, is becoming a necessary feature for modern day applications. This has created the need for low profile multiband antennas.

In addition, numerical simulation techniques based on Method of Moments (MOM), Finite Element Method (FEM) and Finite Difference Time Domain method (FDTD) are powerful tools that could be used for predicting antenna performance in a complex environment. However, the large computing time associated with such techniques makes optimisation of the design parameters time consuming. Because of this, the use of the Transmission Line Model (TLM) as an approximate analytical tool could be effective during the initial design phase.

1.2 Objective of the Thesis

The objective of this research is to investigate the influence of a dielectric casing or radome on the performance of compact and low profile antennas, such as PIFAs, for applications in mobile communications. Through this study, a better understanding of the design considerations of such built-in antennas has been gained. The investigation is carried out for antennas operating in the Industrial, Scientific and Medical (ISM) frequency bands at both 900 MHz and 2400 MHz, by means of extensive numerical simulations in conjunction with measurement validations. Furthermore, an approximate analysis of a dielectric covered PIFA, based on the TLM, is presented. Such a model can be used as a fast Computer Aided Design (CAD) tool for engineers involved in the design of dielectric covered PIFA.

1.3 Organisation of the Thesis

This thesis is organised into eight chapters. Chapter 2 presents a background introduction to small and low profile antennas for wireless communications. It begins by giving a definition of small antennas. This is followed by a discussion of the fundamental limitations of small antennas. The techniques used for antenna

miniaturisations are then introduced and the advantages and disadvantages of each technique are explained. Finally, the properties of antennas required for mobile radio communications are characterised.

A review of literature related to this research is given in Chapter 3. Planar antenna structures considered for mobile radio communications are introduced. Among them, the PIFA (Taga *et al*, 1987) is often preferred. An extensive survey of the published results of research on PIFAs for mobile applications is presented. The effect of its operating environment on the performance of the PIFA is discussed. Also, the methods of analysis of mobile radio antenna systems are reviewed and the applications best suited to each method are discussed. Finally, several concluding remarks are presented.

In Chapter 4, the performance of a PIFA mounted on a finite ground plane and covered with a dielectric layer is investigated at 900 MHz using the MOM. First, an investigation of the performance of a PIFA mounted on a finite ground plane is presented in an attempt to enhance its performance. This investigation includes the influences on input characteristics (resonant frequency and bandwidth) due to the positions of the short-circuit plate and the feeding point, and the location where the antenna is mounted on a finite ground plane. After that, a PIFA with an enhanced bandwidth is designed and the effect due to the electrical parameters and physical configurations of the dielectric cover layer on the performance of this PIFA is investigated. Finally, measurements conducted to validate the numerical simulations are presented.

The input and the radiation characteristics of a PIFA enclosed in a rectangular dielectric radome are analysed using the MOM in Chapter 5. This study is focused on the effect of each individual part of the radome on both the input and the radiation characteristics of the PIFA, such as the resonant frequency, bandwidth and radiation patterns. The investigation is carried out at both 900 MHz and 2400 MHz, and a comparison between them is made.

The TLM is applied to a PIFA in Chapter 6 in an attempt to provide an efficient CAD tool for initial engineering design. A correction factor is introduced to compensate for the effect of the width of the short-circuit plate. The effect of the dielectric cover layer

is also included in the model. In addition, a comparison between the results obtained using the TLM and the full wave MOM simulated results is given.

In Chapter 7, a new single feed dual-band PIFA for wireless communications is proposed. The influences of individual composite parts on the input characteristics of the proposed dual-band PIFA are examined using the MOM. An investigation of the different configurations of the feed disk is also presented. Moreover, an example of this antenna, designed for the ISM frequency bands of 900 MHz and 2400 MHz, is given. The results measured on a fabricated antenna are provided to validate the simulation results. Furthermore, the effect of a dielectric cover on the input impedance and radiation characteristics of this dual-band PIFA is studied.

Finally, Chapter 8 concludes the thesis by stating the main findings of this research. Also, recommendations are made for future studies.

1.4 Summary of Original Contributions

To the best knowledge of the author, the following contributions have not been previously published by other researchers:

- The performance of a PIFA on a finite ground plane due to the location where the antenna is mounted has been investigated. The input characteristics of the PIFA as a function of the positions of the short-circuit plate and feeding point have also been examined. The numerical results obtained using simulations in this study should be valuable in the design of a PIFA that requires a small ground plane to achieve an optimal performance. Based on the above study, a PIFA on a finite ground plane with a bandwidth of 8.5% (VSWR $\leq$ 2) has been designed to operate in the 900 MHz band, and a prototype has been fabricated. The electrical performance determined by simulations shows good agreement with the measured results.

- The effect due to the thickness, dielectric constant and loss tangent of the dielectric cover layer on the performance of a PIFA operating at 900 MHz has been analysed numerically and experimentally. This study shows that the

dielectric cover layer could take the PIFA's performance outside the designed specifications. The results presented may be adopted in the design of a PIFA covered by a protective dielectric layer. Simulated and experimental results have been found to be in good agreement.

- The input impedance and radiation characteristics of the PIFA enclosed in a rectangular dielectric radome have been studied using the MOM for operation in the ISM 900 MHz and 2400 MHz frequency bands. The effects of the individual parts of the dielectric radome on both the input impedance and radiation characteristics of the PIFA are investigated. The analytical results indicate that the dielectric radome could have a significant effect on the performance of the antenna, particularly at a higher frequency. However, this effect could be minimised by optimising the position and orientation of a PIFA within a dielectric radome. In addition, the results give another indication that a dielectric radome could be beneficial to the antenna system, that is, an optimised dielectric radome design could miniaturise the antenna with the possibility of bandwidth improvement and without sacrificing other performance such as the gain.

- An analytical approach based on the TLM has been applied to estimating the input characteristics of a PIFA with a dielectric cover layer. The results calculated based on this model have been compared with the full wave MOM computed results. This model could form an efficient CAD tool for engineers to obtain initial design parameters.

- A new single feed dual-band PIFA using a capacitive feeding technique has been proposed. The influence of the individual composite parts on the input characteristics of the proposed dual-band PIFA has been studied to get a better understanding of the principle of this antenna. A design procedure for the proposed antenna, which was illustrated by an example of a dual-band PIFA for 900 MHZ and 2400 MHz ISM applications, has been presented. This antenna has been fabricated for the measurement validation. Also, the performance of this dual-band PIFA in the presence of a dielectric cover layer has been investigated. The analysis and design details presented here could be adopted

for engineers who are interested in utilising a low-profile dual-band PIFA for wireless communications. The interesting finding from this study is that the capacitive feed disk used in this design not only provides a single feed structure but also shows great flexibility to individually control the two desired resonances. Finally, the effect of a dielectric cover layer on this dual-band PIFA has also been studied. It is found that the dielectric cover layer could have a significant impact on the input and radiation characteristics of this dual-band PIFA, particularly at the higher frequency band. The analysis and design details for the antenna and the effect of the dielectric cover layer presented could be adopted as the starting points for engineers who are interested in utilising a low-profile dual-band or multi-band PIFA as an internal antenna for new wireless communication devices.

CHAPTER TWO

2. BACKGROUND

2.1 Introduction

Modern mobile radio communications have become an important part of telecommunications. Contemporary applications, such as paging and mobile phones, have shown a tremendous growth, and new applications are emerging every day: wireless computer links, wireless multimedia links, satellite mobile phones, wireless internet; just about everything "goes mobile".

Mobile terminals for wireless applications must be light, small, and should have low power consumption. Technology has evolved very quickly to satisfy these needs in a rapidly growing market: chips are becoming smaller, they consumer less current, they are more efficient, and they perform more complex operations. Such technologies have made the smaller sizes needed for a mobile application possible while at the same time functionalities have increased. Thus, it is necessary for antenna designers to create small and low profile antennas that are compatible with modern technology and satisfy the performance specifications, particularly with respect to bandwidth and power efficiency.

2.2 Definition of Small Antennas

Small antennas are usually divided into two distinct categories: "electrically small" and "physically small" antennas.

An "electrically small" antenna is one that can be bounded by the radiansphere, which is a sphere of radius $\lambda/2\pi$, where λ is the wavelength of the operating frequency (Fujimoto *et al*, 1987). A very short dipole is an example of this category.

"Physically small" is a relative term, and it describes antennas whose dimensions are regarded as small in a relative sense (Fujimoto *et al*, 1987). A millimetre horn antenna is an example.

2.3 Fundamental Limitations of Small Antennas

In this section, the fundamental limitations in the relationship between the maximum physical dimension of an antenna and the Q factor, bandwidth, efficiency, or gain are presented.

2.3.1 Quality factor *Q*

The Q factor here is defined as the ratio of 2π times the larger of the mean electric or mean magnetic stored energy to the power dissipated in radiation. For a small antenna, the minimum possible Q is expressed as (Chu, 1948),

$$Q \approx \frac{1}{(k\, r_a)^2}, \text{ for } kr_a \leq 1 \qquad (2.1)$$

where r_a is the radius of the sphere containing the antenna in metres (m); k, a wave number in radian per metre (rad/m), equals $2\pi / \lambda$ where λ is the wavelength in metres (m). This equation indicates that the Q increases dramatically as the radius of the sphere decreases. Therefore, the high Q of a small antenna leads to a fundamental limitation in its performance, especially its fractional impedance bandwidth.

2.3.2 Bandwidth

The analysis of electrically small antennas and the study of the effect of size reduction on radiation properties were initiated in the mid-1940's. Wheeler (Wheeler, 1947)

deduced a fundamental relationship between the maximum dimension $2r_a$ of an electrically small antenna, its maximum fractional bandwidth BW, and radiating efficiency η. This relationship can be written as

$$BW = \frac{2(kr_a)^2}{\eta} \tag{2.2}$$

Equation (2.2) confirms that the product of efficiency and bandwidth is related to the volume occupied by an antenna. The equation also indicates that the bandwidth or efficiency of an antenna becomes small when the size of the antenna is reduced. Indeed, as the size of an antenna decreases, its reactance increases, but its radiation resistance decreases. This implies that bandwidth may be gained at the price of radiation efficiency once the size of the antenna is constrained.

2.3.3 Gain

The works of Wheeler and Chu, on fundamental limits of small antennas, were extended by Harrington (Harrington, 1960) to include the effects of losses. This showed that a miniaturised antenna will show a higher concentration of surface currents than a standard antenna, and thus, the ohmic losses will be enhanced.

Moreover, Harrington proposed a very useful and simple formula to predict the directivity of a small antenna, that is, the directivity D of an antenna is expressed as

$$D = 2kr_a + (kr_a)^2 \tag{2.3}$$

Equation (2.3) can be used to predict a practical upper limit for the gain, G, of an antenna ($G = \eta D$). This formula provides a good approximation for standard antennas but is difficult to apply to small antennas, as they tend to have poor efficiency.

2.3.4 Polarisation

Antenna miniaturisation affects bandwidth, gain and efficiency, but can, in many cases, also affect polarisation purity due to the change of the antenna surface current distribution direction (Fujimoto *et al*, 1987; Fujimoto *et al*, 1994).

2.4 Antenna Miniaturisation

Techniques for making antennas smaller have been known for a long time, and many of them are described in standard text books (Lo *et al*, 1988; Johnson *et al*, 1984; Orr, 1978). The main design techniques in reducing physical size and enhancing the performance of an antenna, particularly planar antennas, are to use resistive or reactive loadings, to use high dielectric-constant materials, to use short-circuit plates or pins, to cut slots on resonant patches; and to fold resonant wires or patches. Many of these techniques have been used for mobile radio applications. These techniques are described below.

2.4.1 Using resistive or reactive loadings

An antenna smaller than a half-wavelength will have a strong reactive input impedance, which may be compensated for by resistive and / or reactive loadings. However, this loading will also reduce the efficiency of the antenna if the added elements have losses. For example, a thin plate element used to make a small loop antenna is inherently inductive, and this inductance may be significant at the frequency used. Resonance may be used to reduce this inductance at the working frequency. To achieve resonance, a capacitor C_l is used and tuned in parallel to the inductance of the loop, as shown in Figure 2-1 (Fujimoto *et al*, 1987). In Figure 2-1, a tap at an intermediate point on the loop element is taken to form a transformer circuit. The tapping point is indicated as T_l at a distance d_l from the input terminal of the loop.

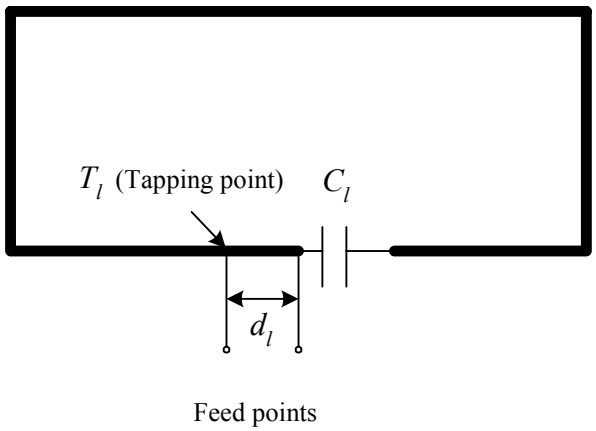

Figure 2-1 A small loop antenna with capacitive loading.

2.4.2 Using high-dielectric-constant materials

This is the most popular technique in reducing the size of a printed antenna. The principle is that the effective wavelength becomes shorter in a higher-dielectric constant material. Therefore, its size becomes smaller when an antenna is printed on such a material. The reduction ratio is approximately relative to the square root of the dielectric constant ε_r (James *et al*, 1989). A conventional patch antenna, using ε_r of 2 to 3, has a dimension of about $0.35\lambda_0$ (λ_0 is the wavelength in free space). With an ε_r of 10, the patch size reduces to about $0.2\lambda_0$. Useful as this is, it should be kept in mind that a higher dielectric constant, unfortunately, is often associated with a higher dielectric loss, which will lead to poor efficiency.

2.4.3 Using short-circuit pins or plates

Another popular strategy for making planar antennas smaller is to make use of short circuit pins or plates to the ground planes, as is the case in the example illustrated in Figure 2-2 (a) and (b). Here, the size of a microstrip patch can be reduced by half by inserting a short-circuit plate, which acts as a mirror, in the middle of the patch where the *E*-field is zero (James *et al*, 1989). When the width of this short-circuit plate is set

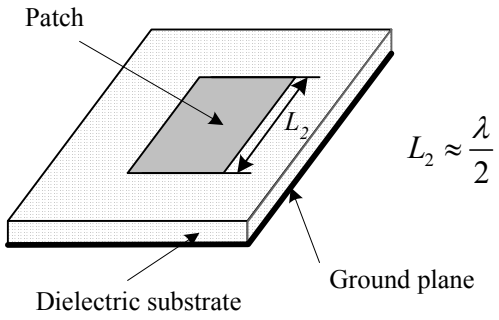

(a)

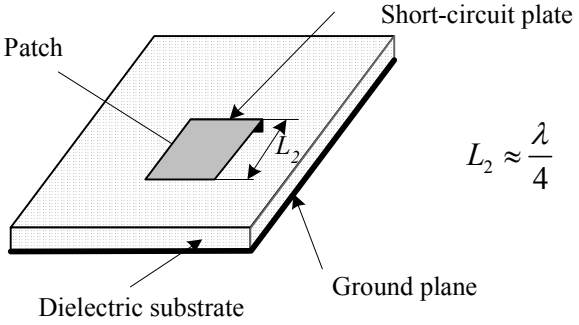

(b)

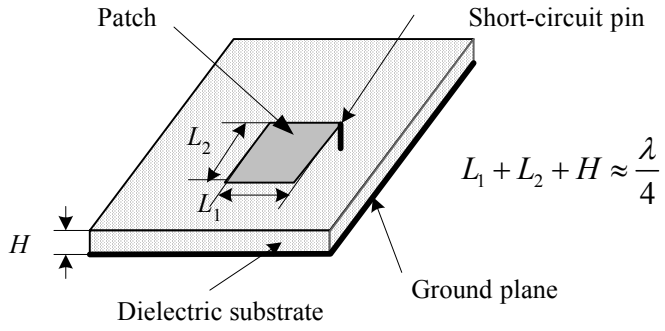

(c)

Figure 2-2 (a) A $\lambda/2$ microstrip patch antenna; (b) A $\lambda/4$ short-circuited microstrip patch antenna; (c) A miniaturised short-circuited microstrip patch antenna.

narrower than that of the microstrip patch, the effective inductance of the antenna element increases and the resonant frequency becomes lower than that of a conventional short-circuited microstrip patch antenna having the same sized planar element. As a result, the width of the short-circuited microstrip patch antenna can be further reduced, as shown in Figure 2-2 (c) (Hirasawa *et al*, 1992).

2.4.4 Cutting slots in resonant patches

Another way to make an antenna smaller is to introduce slots into the resonant patch (Bokhari, *et al*, 1996; Huang, 2001). In doing so, the current on the patch, and so the field underneath the patch, will be distributed from one edge of the patch to the opposite edge by a longer path around the slots, as shown in Figure 2-3. This longer path, in essence, reduces the resonant frequency or the physical size of the antenna. Depending on the length of slots, a 10 % to 20 % size reduction can be achieved. For example, a circular patch antenna developed by Huang for a Mars mission (Huang, 2001) using ε_r of 10 and four slots achieved a patch diameter of 110 mm (0.15λ) at the operating frequency of 400 MHz.

2.4.5 Folding the resonant wire or patch

Folding a resonant patch can reduce the planar antenna dimension by almost half. The configuration of a folded shorted-patch antenna is illustrated in Figure 2-4 (Li *et al*, 2002). Li *et al* designed a practical antenna for the Bluetooth ISM 2400 MHz frequency band using this technique. The length of the folded shorted-patch antenna becomes only $\lambda/8$, approximately four times smaller than a conventional patch antenna. It has an impedance bandwidth of 4%.

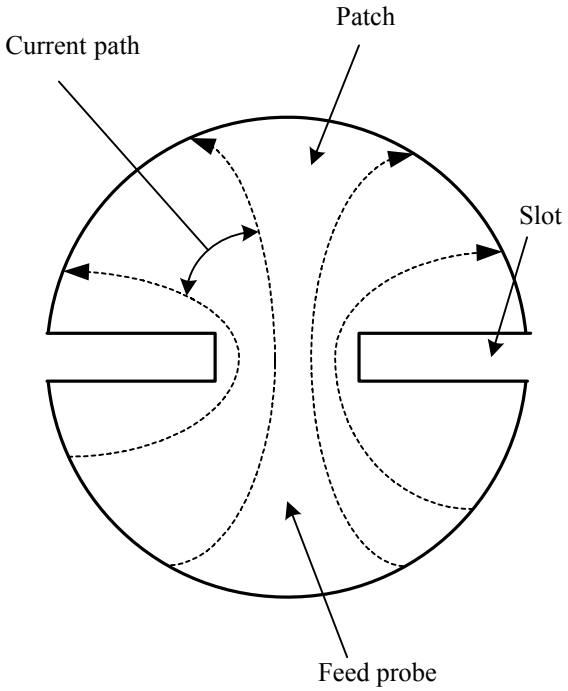

Figure 2-3 A patch with slots yields longer patch length of current flow.

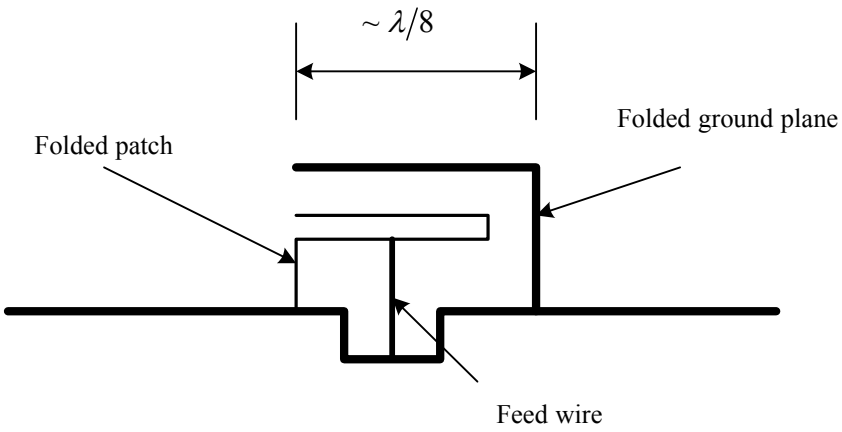

Figure 2-4 A folded shorted-patch antenna.

Conventional monopole antennas in the form of a straight rod are usually operated at a quarter wavelength, this means that, when operated at 900 MHz, which is the most popular frequency band in modern mobile communications, the monopole antenna requires a height of about 83.3 mm. Such a long antenna is impossible to fit into a small handset casing. Therefore, the folding technique mentioned above can be applied to make branch-line antennas. Figure 2-5 shows a branch-line planar monopole comprising two folded printed lines resonating at different frequencies for the Global System for Mobile communications (GSM) and Digital Communication System (DCS) bands (Wong, 2002). This kind of antenna, also called the Meander Line Antenna (MLA), may be used in small mobile radio terminals.

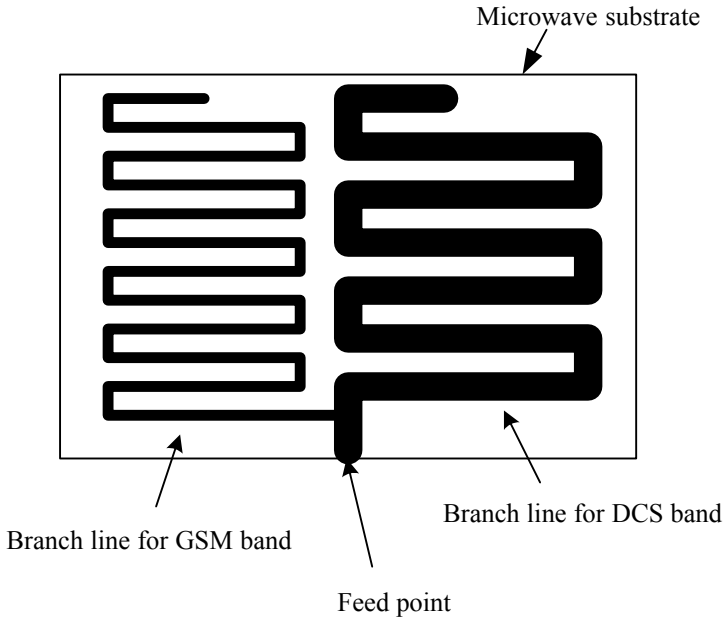

Figure 2-5 A GSM/DCS dual-frequency planar folded line monopole printed on a substrate.

2.4.6 Configuration optimising techniques

A recently emerging technique is the use of Genetic Algorithms (GA) to minimise the size of wire-type or printed antennas (Altshuler *et al*, 2000 and Altshuler, 2002). This antenna optimisation is very similar to biological genetic evolution where biological

configurations adapt their fitness to the natural environment by a huge number of chromosome sets with binary type genetic decisions. The antenna designed by this technique generally does not have a conventional shape. For example, by using this technique, a ten-segment self-resonant small wire antenna, as shown in Figure 2-6, falls within a cube having an edge side diameter of 0.038λ at a resonant frequency of about 400 MHz. This antenna achieves elliptical polarisation with near-hemispherical radiation coverage.

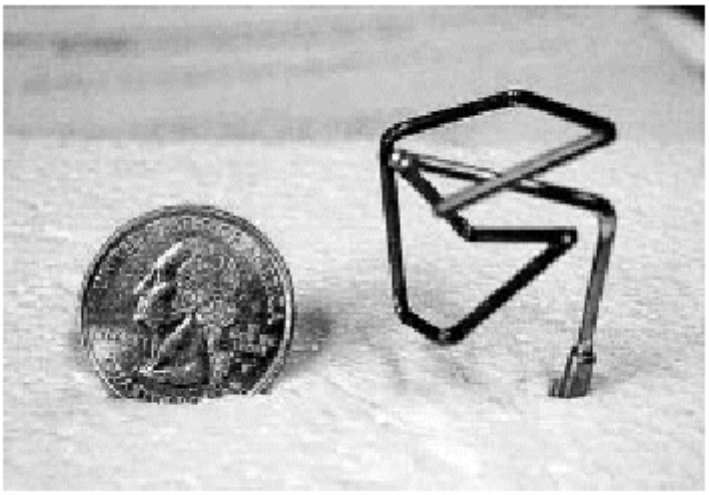

Figure 2-6 A ten-segment self-resonant small wire antenna (after Altshuler *et al*, 2000).

2.5 Desirable Characteristics for Mobile Terminal Antennas

The parameters and considerations described below play a dominant role in specifying as well as elucidating the performance aspects of practical mobile terminal antennas.

The bandwidth of an antenna is defined as the range of frequencies within which the performance of the antenna, with respect to some characteristics, conforms to a specified standard. In practise, the voltage standing wave ratio (VSWR) should be less than 2 for the range of frequencies over the impedance bandwidth of interest. In general, this is a crucial performance consideration of antennas. The bandwidth of operation of a mobile antenna should be sufficient for the system in which it is to be

used, including a margin for production tolerances. Table 2-1 lists the bandwidth specifications of some present-day mobile cellular communication systems.

Table 2-1 Bandwidth specifications of present-day mobile cellular communication systems

System	Frequency range (MHz)	Minimum antenna bandwidth (MHz)
GSM	890-960	70
DCS	1710-1880	170
Personal Communication System (PCS)	1850-1990	140
Universal Mobile Telecommunication System (UMTS)	1920-2170	250
Wireless Local Area Network (WLAN)	2400-2484	84
	5150-5350	200

Antenna efficiency accounts for the losses within the structure of the antenna, including conductor and dielectric losses. A mobile antenna should have a high radiation efficiency, which will ensure that the maximum amount of power is actually radiated. This enables either a greater communication range or longer battery life by minimising the transmitter power needed.

A radiation pattern shows a plot of the power radiated from an antenna in a specified plane as a function of the angle. The two orthogonal planes commonly measured and published in antenna specifications are the vertical (elevation) and horizontal (azimuthal) planes. Mobile antennas should have nearly omnidirectional radiation patterns in the azimuthal plane, however, a reduction in gain in the direction of the

operator may be desirable for a low specific absorption ratio (SAR). This not only ensures that the user absorbs a lower amount of radiated power but in addition their proximity has less effects on the radiation pattern (Fujimoto *et al*, 1994).

A mobile antenna should also have adequate and equal sensitivity to both horizontally polarised signals and vertically polarised signals. This is important for reception, because of the unavoidable random orientation of the transceiver in use and also the low polarisation purity of the received signals when used in urban mobile radio environments (Taga *et al*, 1987).

The natural input impedance of a mobile antenna should be designed to be as close as possible to 50 Ohm resistive. Using this standard value permits antenna and transmitter / receiver design and measurement to be nearly independent of each other. If the antenna impedance is very different from this value, a matching circuit between the feed wire and the antenna is necessary. Resistive losses in the components of this matching circuit will give rise to unavoidable signal loss on both transmit and receive.

A mobile antenna should be a small, low profile structure and occupy a minimum volume. A simple and robust mechanical design is highly desirable. This also helps with low cost volume manufacturing,

CHAPTER THREE

3. LITERATURE REVIEW

3.1 Introduction

The antennas commonly employed in mobile radio terminals include the monopole, the sleeve dipole, and the normal mode helix (Fujimoto *et al*, 1994). Planar antennas, such as the printed line antenna, microstrip patch antenna, PIFA and MLA, which have recently come into use due to the attractive features of small size and low profile, are promising candidates for miniaturisation design consideration. For mobile communications, such antennas must possess a bandwidth of approximately 10 % with uniform coverage over the horizontal plane. An outline of these leading low profile small antenna structures is given below.

3.1.1 Printed line antennas

Printed line antennas are an extension of the monopole. They can be easily fabricated by etching a copper strip 1/2- or 1/4-wavelength long onto the radio circuit board. Such antennas are inexpensive to make and can be analysed using the transmission line model (Lebbar *et al*, 1992).

3.1.2 Microstrip patch antenna

Microstrip patch antennas are a good choice for a system that requires a beam pattern focused in a certain direction. Patches are fabricated as square or round copper areas on the top surface of a circuit board. The radiation beam of these patch antennas is normal to the surface of the board. Performance analysis of patch antennas can be done using the transmission line model and cavity model (Hirasawa *et al*, 1992; Sainati, 1996).

3.1.3 PIFA (Planar inverted-F antenna)

One antenna type that has become increasingly popular is the PIFA (Taga *et al*, 1987). The PIFA literally looks like the letter 'F' lying on its side with the two shorter sections providing feed and ground points and the 'tail' providing the radiating surface. The PIFA has a low profile structure, so that it can easily be incorporated into mobile terminals as an embedded antenna. Also, it exhibits a somewhat omnidirectional pattern. In addition, the PIFA needs a ground plane, which generally takes the form of the printed circuit board (PCB) of the mobile device. More specific details of the PIFA are reviewed in section 3.2.

3.1.4 MLA (Meander line antenna)

The MLA is a new type of radiating element, made from a combination of a loop antenna and frequency tuned meander lines. The electrical length of the MLA is made up mostly by the delay characteristic of the meander line rather than the length of the radiating structure itself. Seale (Seale, 1993) has presented a Modified Transmission Line Antenna (MTLA) based on this principle in an attempt to achieve a reduction in antenna size. Also, the wire structure of an MLA can be embedded in a dielectric structure to further reduce the antenna size (Wong, 2002).

3.2 PIFA as an Internal Mobile Terminal Antenna

A monopole is a dipole that has been divided in half at its centre feed point and fed against a ground plane as shown in Figure 3-1 (a). Its height is often a quarter of the wavelength. When it is bent like the structure shown in Figure 3-1 (b), the antenna is called an Inverted-L Antenna (ILA). An ILA consists of a short monopole as a vertical element and a horizontal element attached at the end of the monopole.

The ILA is basically a low profile structure, because the height of the vertical element is usually constrained to a small fraction of the wavelength. The horizontal element is not necessarily very short, and usually has a length of a quarter wavelength. Thus the ILA

may essentially be considered as a vertical short monopole loaded with a long horizontal wire at the end of the monopole. As a consequence, its input impedance nearly equals that of the short monopole plus the reactance of the horizontal wire closely placed to the ground (Fujimoto *et al*, 1987). This impedance is very low (often around a few Ohms) and therefore the simple ILA is not really practical. To increase the input impedance, another inverted L–shaped element is attached at the end of the vertical element, thus forms an Inverted-F Antenna (IFA) as shown in Figure 3-1 (c). This modification is significant because the input impedance of the IFA can be arranged to have an appropriate value by changing the length d_f of the attached element to match the load impedance, without using any matching network between the antenna and the load (Fujimoto *et al*, 1987). By utilising this feature, the IFA, rather than the ILA, has been used in practice as a low profile antenna.

One drawback of an IFA implemented from thin wires is its narrow bandwidth, typically only one percent or less, of the centre frequency. To get broad bandwidth while still maintain a low profile structure, another modification to the IFA can be made by replacing the wire element by a metal strip, as shown in Figure 3-2. The resulting antenna is called the PIFA (Fujimoto *et al*, 1987).

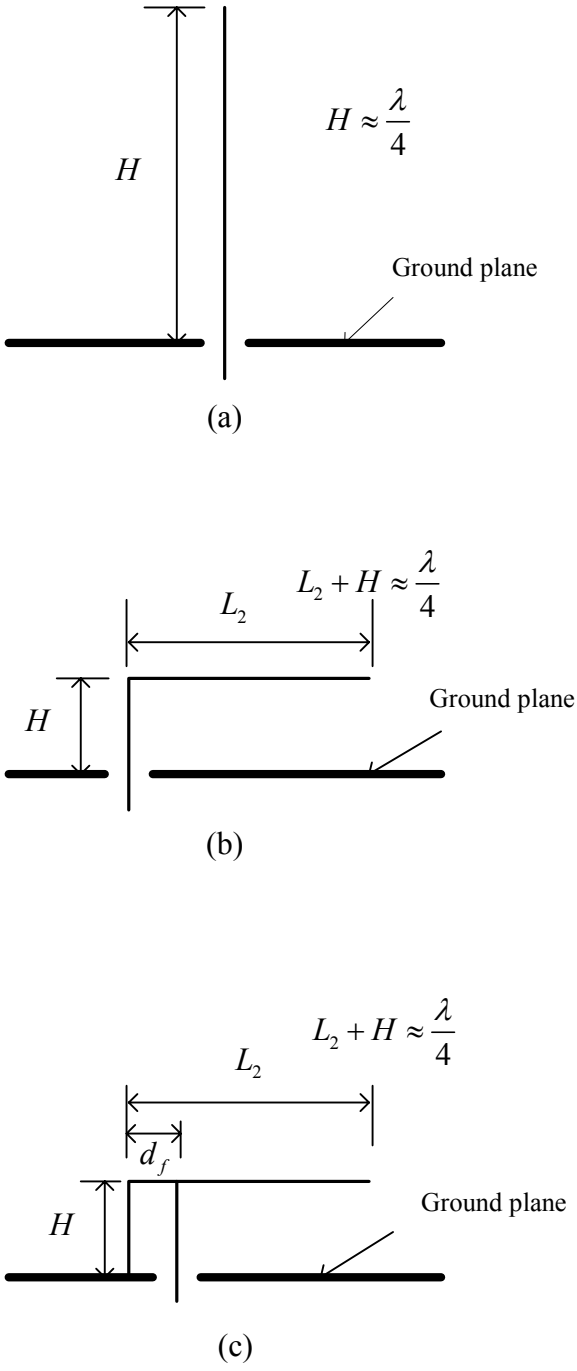

Figure 3-1 (a) A monopole; (b) an inverted-L antenna (ILA); (c) an inverted-F antenna (IFA).

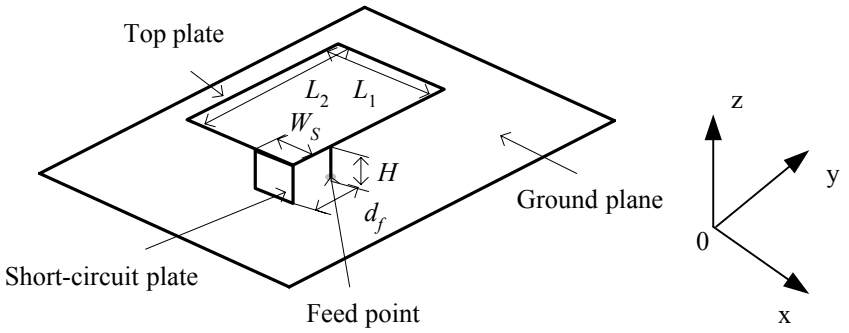

Figure 3-2 Configuration of a PIFA.

Harrison (Harrison, 1958) investigated the ILA as a special case of the transmission line loaded antenna. He used an infinite load impedance, and in effect created an antenna with open-ended transmission line loading. King (King *et al*., 1960) extended this work to include ILAs fed against a ground plane, using shunt drive. This arrangement is called the IFA. In their study, the IFA has been analysed in terms of an approximately equivalent circuit that consists of a shunt-driven transmission line terminated in a reactor at each end. The radiation resistance of the IFA has been found to be dependent on two factors: the height of the transmission line above the ground plane, and the propagation constant of the transmission line. The reactance can be obtained from transmission-line formulae. Based on the input impedance, which consists of the radiation resistance (if loss resistance is neglected) and reactance, the resonant frequency and bandwidth of the antenna may be calculated. However, the height of the antenna is limited to not more than 0.1λ in order to obtain an accurate radiation resistance. This is because of the conditions of transmission-line theory and the assumption that the currents in the shunt elements have uniform amplitudes, are not well satisfied when the height of the antenna is more than 0.1λ. Guertler (Guertler, 1977) continued King *et al*'s work. He has analysed the radiation patterns of a quarter wavelength long IFA. His analytical result shows that the IFA radiates uniformly in the half-space above an infinite ground plane.

The PIFA was first proposed by T. Taga and K. Tsunekawa in 1987 (Taga *et al*, 1987). Taga computed the characteristics of a PIFA on an infinite ground plane using the Spatial Network Method (SNM) (Hirasawa *et al*, 1992). In the analysis, the

distributions of the electric field between the planar element and the ground plane have been presented with respect to the short-circuit plate width. These results clearly show that the dominant component of the electric field $\vec{E}_z$ (see in Figure 3-2) is equal to zero in the position of the short-circuit plate. The surface current distributions have also been presented. It is found that when the width of the short-circuit plate is narrowed, the current distribution varies, and the effective length of the current flow on the short-circuit plate and planar element becomes longer. Consequently, the resonant frequency will be lowered, and the PIFAs become smaller than the short-circuit microstrip antennas. Moreover, it is found that the bandwidth increases when the antenna height *H* is raised. This increase in bandwidth also occurs when the planar element ratio of length to width, or the short-circuit plate width is increased. Furthermore, the PIFA exhibits sensitivity to both vertically and horizontally polarised radio waves.

Performance analysis of most of these antennas has been done assuming an infinite ground plane. For these cases, simple and closed form analytical formulae are available for evaluating the antenna performance, such as resonant frequency, radiation patterns and gain (Stutzman *et al*, 1981; Sainati, 1996). For example, a monopole antenna on an infinite ground plane may be modelled by image theory as a dipole with one-half of the input impedance and double the peak directivity of the dipole (Stutzman *et al*, 1981). However, in practice antennas are often mounted on a finite ground plane. Due to the small size of the ground plane, its edges act as scatterers which diffract the incident field. The diffraction from the edges modifies the current on the ground plane and alters the radiation pattern, causing scalloping (Williams *et al*, 1990) or nulls (Long, *et al*, 1987) in the forward radiation, giving rise to back radiation or radiation behind the ground plane (Weiner, 1987), and higher cross polarisation levels (Long *et al*, 1987). Other parameters such as input impedance may also be affected (Bhattacharyya, 1991).

When antennas are mounted on the conducting box of a device, the conducting box will also act as a radiating element. Alternatively, the conducting box may be considered as a finite ground plane. A monopole antenna mounted on a conducting box has been studied in (Long *et al*, 1987) and (Bhattacharya *et al*, 1987). It has been shown that as the monopole antenna is moved from the centre of the top surface towards the edge or a corner, the magnitude of the conductance decreases by 50%, the resonant frequency

increases by a few percent, and deep nulls are produced in the radiation pattern. For a helical antenna, when the ground plane radius is reduced to approximately the radius of the helix, a transition from forward to backfire radiation will occur (Nakano *et al*, 1988). Taga *et al* (Taga *et al*, 1987) analysed the characteristics of the PIFA mounted on a conducting box using both the pattern averaging gain estimation method and wire-grid mode. It is found that the antenna bandwidth approximately doubles when the PIFA is mounted on a conducting box, instead of an infinite ground plane. This bandwidth can further be widened by selecting appropriate dimensions for the conducting box. Also, it is found that the gain of the PIFA changes not only with the size and shape of the conducting box, but also is a function of its position and orientation on the box. These results were confirmed by experiments. This indicates that the conducting box becomes an integral part of the antenna system, and it must be considered in the design in order to achieve an overall good performance for such a PIFA system.

The characteristics of a number of MTLAs mounted on a conducting box were presented in (Seale *et al*, 1992; Seale, 1993). The "loop" part of the antenna is folded several times in an attempt to achieve a low profile structure, as shown in Figure 3-3. Most of these antennas are designed to be limited to (60 x 25 x 20) mm at a resonant frequency of approximately 1000 MHz. From their study, it is found that the bandwidth of such an antenna is largely determined by the antenna height, but is also dependent on the horizontal winding and the dimensions of the conducting box.

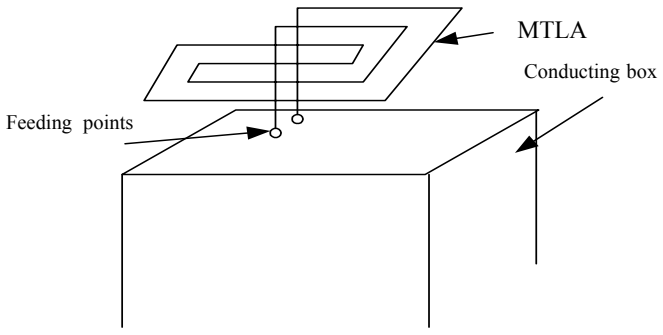

Figure 3-3 A MTLA on a conducting box.

In (He, 2000), a Strip Inverted-F Antenna (SIFA), as shown in Figure 3-4, was proposed for use in a notebook computer. A strip is used instead of the horizontal wire of an IFA in an attempt to achieve a wider bandwidth. The screen and keyboard parts of the computer were considered as a finite ground plane. Such an IFA is a low profile structure (18 mm high) and operates in the 820-970 MHz band with a return loss of less than -10 dB (VSWR $\leq$ 2). Such a bandwidth covers most mobile applications in the 800/900 MHz frequency bands. The input impedance at resonance is close to 50 Ohm. The antenna gain is 3.0 dBi at 881 MHz. The radiation patterns of this antenna system are similar to those of an asymmetric dipole.

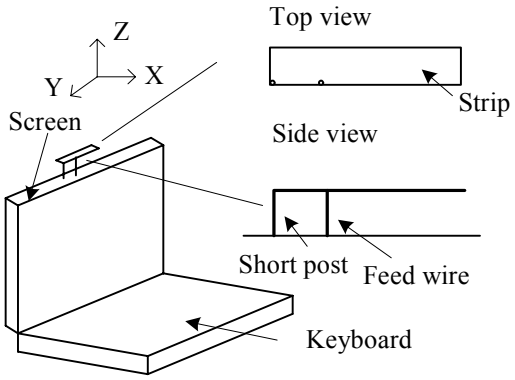

Figure 3-4 A SIFA mounted on a laptop computer.

More recently, a new trend in antenna development is towards integrated antennas for mobile terminals, that is by embedding a small antenna into the mobile radio dielectric casing. This kind of concealed antenna is attractive for ergonomic reasons and is less likely to be damaged, compared with the conventional whip or rod antennas. For these reasons, they are becoming very popular for use in portable phone units. Now, the low profile of a PIFA makes it attractive for consideration as a concealed antenna. An integral part of the PIFA is the ground plane, which needs to be sufficiently small in

order to fit into a mobile terminal. An in-depth study based on FDTD and MOM to enhance the bandwidth of a PIFA is presented in (Virga *et al*, 1997). In this study, the influence of the different antenna component parts on the performance of a PIFA mounted on a small finite ground plane is investigated. It has been found that a PIFA with a short-circuit wire has strong antiresonance characteristics. The impedance at the antiresonance has a sharp peak in the resistance and a sharp swing in the reactance from highly inductive to highly capacitive. The resistance for the antenna without the short-circuit wire is very low. To control the characteristics of the antiresonance, the short-circuit wire is replaced by a short-circuit plate. Both the length of the top plate and the location of the feed wire with respect to the short-circuit plate determine the resonant frequency and the overall bandwidth of the PIFA. The largest bandwidth obtained by this PIFA is reported to be 9.61%. Moreover, it has been found that the PIFA is linearly polarised with an omnidirectional radiation pattern. Furthermore, the effect of narrowing or shortening the ground plane has been examined. In this case, it found that narrowing the ground plane has a greater effect on the input impedance than shortening the ground plane.

A so-called Dual Inverted-L Antenna is also presented in (Virga *et al*, 1997). This antenna is basically a PIFA with an additional second element consisting of a top plate and short-circuit plate. The second element is capacitively coupled, rather than directly fed, to the main antenna element. These two elements are arranged in parallel with a narrow slot in between them. The Dual L antenna can be designed to have two different resonant frequencies. The dimensions of the main-fed element are designed to resonate at one frequency, while the dimensions of the composite structure including the second element are designed to resonate at another frequency. Now by moving the two resonant frequencies closer to each other, a larger of bandwidth of 16% at 900 MHz can be achieved for such a Dual L antenna having a height of 12.9 mm. The simulation results have been validated by measurements. The main advantage of this design is that it can achieve a wider bandwidth of 16% compared to the 9.6% obtained by a single element PIFA. However, this is achieved by having to double the volume of the antenna.

The performance of antennas in handheld radios operating in close proximity to a human hand or head is also affected by them, as the body may be considered to consist of heterogeneous lossy dielectric materials. The interaction between a handheld mobile radio unit and user has recently been investigated by several researchers (Pedersen *et al*, 1994; Jensen *et al*, 1994; Okoniewski *et al*, 1996; Li *et al*, 1997). One of the interesting findings coming from this research is that a Full Short circuit PIFA (FS-PIFA), mounted on the back side of the hand-held mobile radio unit, can have a spatial peak specific absorption rate (SAR) that is one tenth of the level indicated in the present safety standards (Pedersen *et al*, 1994). This is because the PIFA tends to have smaller backward radiation in the direct of the user due to the presence of the ground plane, which takes the form of the conducting box in this case.

Furthermore, there is a trend for a handheld phone to be able to be operated on more than one frequency band, or multi-band operation. As a result, this leads to a variety of novel PIFA designs, most of which are capable of dual-band operation (Wong *et al*, 1998; Lo *et al*, 1998, Rowell *et al*, 1997; Liu *et al*, 1996; Rowell *et al*, 1998; Chen *et al*, 2003). There are two major concepts involved in dual-band antenna designs: one uses two different resonant paths to produce two separate resonant modes for dual-frequency operation, and the other uses the first two resonant frequencies of a single resonant path for dual-frequency operation. A dual-band antenna, based on a PIFA, for applications in handheld cellular radio telephones is presented in (Liu *et al*, 1996). This dual-band antenna consists of two PIFAs, one operating at 900 MHz low band and the other operating at 1760 MHz high band, as shown in Figure 3-5. The higher frequency PIFA is inserted at the corner of the main PIFA with an L shaped slot between them. Both PIFA's have the same height. The two short-circuit pins are placed back to back to reduce the mutual coupling between the two feed ports. This dual-band antenna which is mounted on the side of a conducting box of dimensions 132 mm (H) x 62 mm (W) x 30 mm (D), was analysed using an FDTD method. The results of these simulations have been validated by measurements. The bandwidths obtained for this dual-band PIFA are 7% at 900 MHz and 6.3% at 1760 MHz for VSWR ≤ 2. Measurements show that the radiation patterns in the azimuth plane are approximately omnidirectional for both the two resonant frequencies. The main advantage of this design is that the dual-band antenna occupies almost the same volume, about 52 mm (L) x 30 mm (W) x 9 mm (H),

as the PIFA operating at the lower band. However, this dual-band design uses two feed ports, which is a major drawback, even though the mutual coupling between them is less than –17 dB.

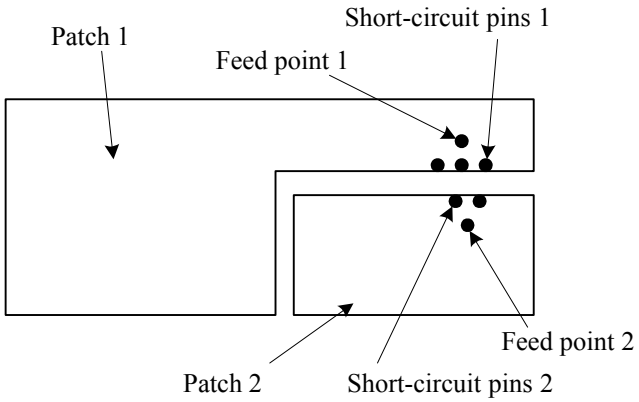

Figure 3-5 A probe direct feed dual-band PIFA – Top view.

A capacitively loaded PIFA with a capacitive feed, as shown in

Figure 3-6, has been proposed in (Rowell *et al*, 1997). The capacitive load is formed by folding the open end of the PIFA towards the ground plane and adding a plate (parallel to the ground plane) to produce a parallel plate capacitor for the load. The capacitive feed is constructed by terminating the inner conductor of a coaxial cable with a conducting plate, parallel to the top plate. The capacitive load reduces the resonant length of the PIFA from $\lambda/4$ to less than $\lambda/8$. Two such capacitively loaded and capacitive-fed PIFAs have been used to produce a dual-band antenna operating at 900 MHz and 1800 MHz (Rowell *et al*, 1998). This dual-band antenna also requires two separate feeds, as shown in Figure 3-7. The use of capacitive loads has reduced the overall size of this dual-band PIFA, compared with the PIFA presented in (Liu *et al*, 1996). The bandwidths achieved are 5% at 900 MHz, and 8% at 1800 MHz. Again the FDTD method has been used for numerical analysis, with the results verified by experimental measurements.

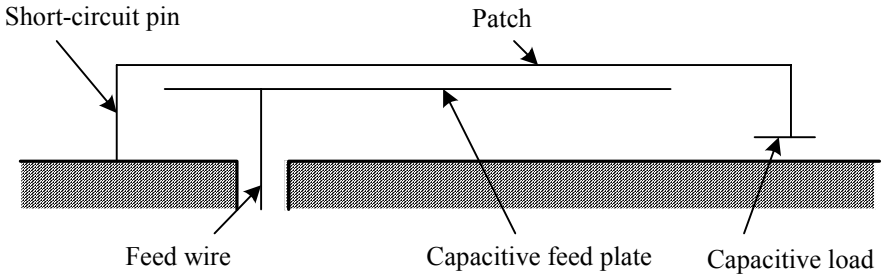

(a) Side view

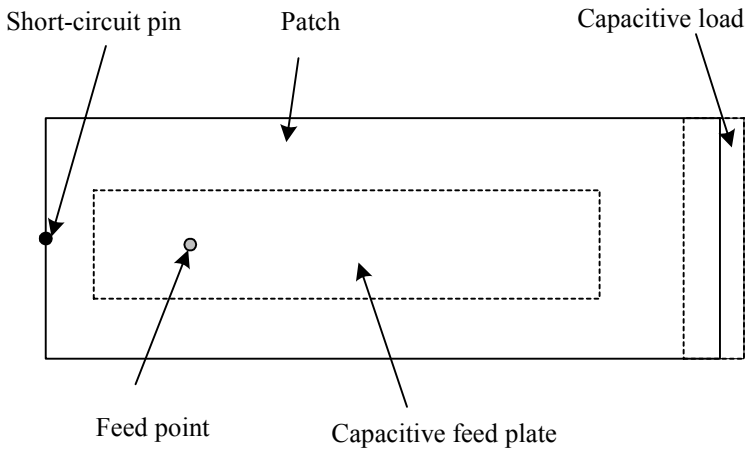

(b) Top view

Figure 3-6 A capacitively loaded PIFA with a capacitive feed.

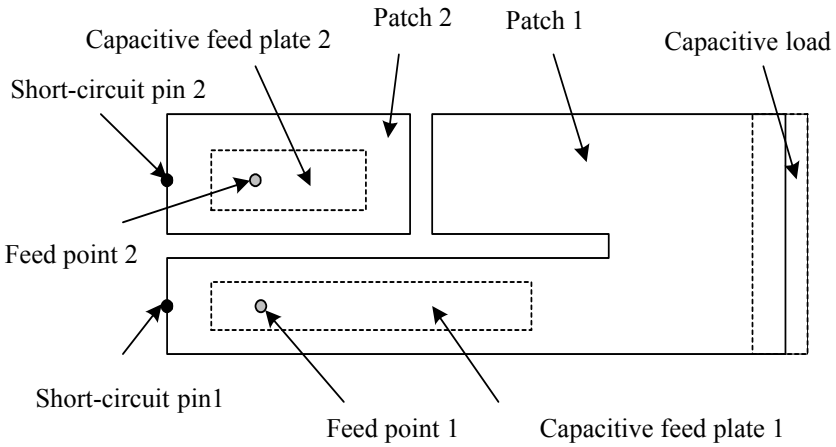

Figure 3-7 A capacitive feed dual-band PIFA - Top view.

Recently, a meandered and folded dual-band PIFA has been proposed for use in GSM 900 and DCS 1800 (Chen *et al*, 2003). A meandered patch is deposited on one side of a dielectric substrate, which is supported at a distance *H* above a ground plane, as shown in Figure 3-8. In this figure, the folded bottom patch is separated from the substrate in order to show its geometry. In practice, the folded bottom patch should attach to the bottom of the substrate and also connect to the top meandered patch. The antenna dimensions are 24 mm x 10 mm x 7.2 mm, giving a small volume. The frequency ratio of the first two resonant frequencies of this antenna can be tuned by removing a part of the top patch in the form of a rectangle of a given aspect ratio (*b/a*) near the feed position.

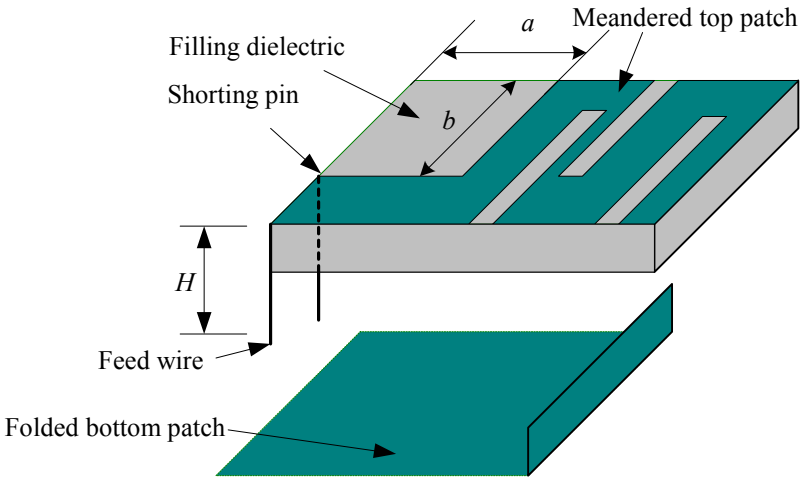

Figure 3-8 A meandered and folded dual-band PIFA.

3.3 Numerical Techniques for Analysing Antenna Systems

Computer techniques have revolutionised the way in which electromagnetic problems are analysed. Electrical engineers can now rely on efficient, accurate and well-tested computer models to analyse and evaluate the electromagnetic behaviour of antennas.

Although most electromagnetic problems ultimately involve solving only one or two partial differential equations, which are subject to boundary constraints, very few practical problems can be solved without resorting to computer-based methods. Computational electromagnetics involves the development of numerical algorithms for the solution of Maxwell's equations. These numerical techniques attempt to solve the fundamental field equations directly, subject to the boundary constraints posed by the geometry (Hubing, 1991). This avoids the need to make assumption about the geometry of the problem as in the analytical approach, which aims at arriving at a closed-form solution.

Nowadays, advanced computer software packages are available for accurate analysis involving antennas of complicated shapes. Most of these electromagnetic simulation packages are based either on the MOM or the FDTD or the FEM.

The MOM is a technique for solving complex integral equations by reducing them to a system of simpler linear equations for obtaining the current density on the conducting surfaces of antennas. It is generally applied to configurations consisting of only the conductor, or only the homogeneous dielectrics, or of very specific conductor-dielectric geometries, such as printed antennas in multilayer dielectric media of infinite extent. In addition, it is also the method of choice for the modelling and analysis of wire antennas or wires attached to large conductive surfaces. However, it is not so efficient when modelling arbitrary structures of complex geometry or inhomogeneous dielectrics.

On the other hand, the FDTD method is a volume-based solution to Maxwell's differential equations. With this method, Maxwell's equations are converted to central difference equations and solved directly in the time domain. Since the FDTD method provides a time-domain solution, a wide band frequency-domain result may be obtained from a single simulation run followed by a Fast Fourier Transform (FFT). It can handle any arbitrary combination of conducting and dielectric materials. As the FDTD technique is a volume-based solution, the absorbing boundary condition (ABC) must be electrically remote from the source and all radiation sources of the model. It is well suited for analysis of structural models containing enclosed volumes of metal, dielectric, and air. However, this technique is not well suited to modelling wires or other long, thin structures, as the computational area overhead increases very rapidly

with this type of structure. In general, the computation time increases with the size of the structural model.

Another volume-based technique is the FEM. It numerically solves Maxwell's partial-differential equations in the frequency domain. In general, this solution process is very time consuming and requires a large amount of computer memory. With FEM, the electrical and geometrical properties of each element of a given structure can be individually specified. For this reason, the FEM is appropriate for modelling complex geometrical configurations with numerous arbitrarily shaped dielectric regions. However, as stated above, computation will be time consuming and requires a large amount of memory.

Among the three numerical techniques, the MOM has been, by far, the most popular method for modelling and analysis of antennas since it was first introduced by Harrington (Harrington, 1993). It basically starts with an integral equation for the current density on a conductor surface that forms part of an antenna structure. The current density is found by converting the integral equation for the current to a matrix equation, and then solving the latter for the unknown current. Once the current density on the surface of an antenna is known, its radiation pattern, directivity, and gain can then be calculated using a far-field transformation. Other important antenna parameters, such as input impedance, VSWR, and scattering parameters may also be computed using post processing (Chang *et al*, 1992). A general procedure for the MOM is given in Appendix A.

The MOM is particularly efficient for the analysis of wire antennas or other resonant conducting surfaces. The Numerical Electromagnetic Code (NEC), developed by Lawrence Livermore Laboratory, has been the most widely used MOM-based simulation code (Burke *et al*, 1981). The numerical integral equation technique adopted in NEC uses the free space Green's function; thus it is not appropriate for modeling microstrip or other printed antennas, which are becoming increasingly popular in mobile radio communications, because of their low profile, light weight and ability to conform to different shapes. As a result, the so-called mixed potential integral equation (MPIE) has been proposed for analysing multilayered planar antennas of arbitrary shapes (Mosig, 1988; Chang, *et al*, 1992). To solve this MPIE numerically for

unknown current densities, one typically uses GaIerkin's method (see Appendix A). In (Mosig, 1988), a microstrip structure is divided into a set of rectangular cells. Then a special form of linear "roof-top" basis functions is used to approximate the current distributions. This method is obviously most appropriate when the structure under investigation can be divided into rectangular cells. However, it would not be as efficient when the rectangular cell size cannot be fitted into the boundaries of a given structure. This shortcoming may be overcome by a combination of rectangular and triangular cells (Chang *et al*, 1992). This enhancement has been adopted in the electromagnetic simulator, IE3D from Zeland (Zeland, 1996). It should be noted that the MPIE does not account for the effect of surface-wave reflection and diffraction at the edges of a truncated layer. Such effects may be ignored for an electrically thin layer. The above so-called two-and one-half dimensional (2.5 D) techniques can be extended to the 3D conducting surfaces, albeit still with infinite magnetodielectric layers, by including the vertical current Green's function in the MPIE.

To apply MOM for full 3-D modelling of conducting and dielectric objects, one can resort to the use of a surface integral equation (SIE) approach with a surface formulation. With this approach, the electromagnetic field inside a homogeneous isotropic and linear region is expressed in terms of an impressed field so that the equivalent electric and magnetic currents are distributed over its boundary surface. The SIEs are usually solved by the MOM. Moreover, there are only a few methods that can handle structures of arbitrary shape (Sarkar *et al*, 1989; Rao *et al*; 1991). These methods often make use of sub-domain basis functions of triangular forms. This will lead to a very large number of unknown currents to be solved, even in cases with the simplest structure. To reduce the number of unknowns, Kolundzija proposed a new, general and efficient MOM method for analysing arbitrary composite structures consisting of conducting and dielectric materials (Kolundzija, 1999). This proposed method is still based on SIEs, but uses polynomial entire-domain expansions defined over isoparametric surfaces, which automatically satisfy the continuity equation, assuming that there are no line charges along multiple conducting and /or dielectric junctions. As a result, it requires about five times fewer unknowns than other general methods based on the MOM solution of SIEs. Such an approach is used in the electromagnetic simulation software, WIPL-D (Kolundzija *et al*, 2000).

While a sophisticated numerical approach is useful for accurately predicting antenna performance with complex configurations, its use for optimising the design parameters is often hampered by the large computing time required. Therefore, from this point of view, approximate analytical approaches such as the transmission line model and cavity model analysis could be rather attractive for deriving initial estimates of the design parameters (Hirasawa *et al*, 1992; Sainati, 1996).

3.4 Concluding Remarks

This literature review presents the state of knowledge in research on low profile antennas for mobile radio terminals. The antenna trend for this type of application is towards the use of internal antennas concealed within the dielectric casing or radome of the terminals. To keep the terminal as compact as possible, many researchers focus on antenna miniaturisation techniques, which are becoming the art of compromise when designing the smallest possible antenna that will still meet the input and radiation characteristics for a given application. However, the author has not been able to uncover any published papers regarding design considerations for concealed antennas operating within a dielectric casing or radome of the mobile terminal. In practice, a concealed antenna tends to be electrically small with a high Q for maintaining efficiency. In this case, the influence of the dielectric casing on the operating performance of the antenna is significant and needs to be accounted for in the overall design of the antenna system. For this reason, this research sets out to investigate this influence and to find ways for enhancing the operating performance of such a concealed antenna.

This review also identifies the PIFA as one attractive candidate for application in mobile radio terminals. The PIFA has a small low profile structure and it can also achieve reasonably wide bandwidth with an almost omnidirectional pattern in the azimuthal plane. These features make it an attractive choice for this research. Moreover, the operation of a PIFA requires a ground plane, which in practice may often be the main PCB in the mobile terminal. The location where a PIFA is mounted on a small ground plane could have a significant impact on its performance due to diffraction

around the ground edges. There is a paucity of reports on the study of this aspect. Thus, a study on the performance of PIFA on the finite ground plane due to the mounting location is also conducted.

A fast and accurate analytical approach will form a useful tool in the design cycle of an antenna. Among the many approaches, the TLM is one of the most efficient analytical techniques to analyse rectangular or square patch antennas. The TLM has also been applied to a PIFA for determining the value of the capacitance of the capacitive load (Rowell *et al*, 1997). However, this previous study only provides a loose approximate relationship between the physical parameters of the antenna and the antenna resonant frequency. In this study, a more accurate and efficient TLM has been derived for analysing the input characteristics of a PIFA. The effect of the dielectric cover layer has also been included in this new model.

Dual-band antennas are likely to be the next generation antennas for mobile radio applications. Several novel dual-band PIFA designs have been reviewed in this chapter. Most of these dual-band antennas required dual feed points. Such antennas are less attractive as they require additional switches and diplexers in the RF front-end circuit for proper operation. The additional losses due to these switches and diplexers can have a significant effect on both receive and transmit performance of the radio; hence, the obvious way of avoiding their use is to have a single feed antenna. One such novel dual-band antenna is proposed in Chapter 7.

Numerical approaches are necessary for accurate analysis of concealed mobile antennas operating in the proximity of a dielectric casing or radome. As pointed out in section 3.3 of this review, the FDFD and FEM are both volume-based techniques, which can be used to model arbitrary shaped structures constructed from material of different electrical properties. However, the cell size is determined by the highest frequency of interest and the smallest physical dimensions to be considered. Consequently, the number of cells required for accurate modelling will become very large when the FDTD and FEM are applied to thin structures. On the other hand, the MOM is a surface-based technique so it is suitable for modelling thin structures. The MOM, likes FEM, is a frequency-domain based technique. When compared with a time-domain based technique such as FDTD, it needs a separate simulation run for each desired frequency.

This shortcoming of the MOM may be overcome by using sophisticated interpolation techniques to fill in the missing frequency values (Miller, February 1998, April 1998 and June 1998; Schlagenhaufer, *et al*., 2001). In this research, the dielectric casing is considered to be a thin planar structure with respect to the operating wavelength. Therefore, the MOM is considered the most appropriate analysis method for the applications under consideration in this research.

CHAPTER FOUR

4. PERFORMANCE ANALYSIS OF PIFA MOUNTED ON A FINITE GROUND PLANE AND IN CLOSE PROXIMITY TO DIELECTRIC LAYER

4.1 Introduction

As discussed in Chapter 3, PIFAs have attracted much interest due to their potential small size, low profile structure, ease of impedance matching and appreciable bandwidth, making them promising candidates for use within the casings of portable radio transceivers. In such applications, the PIFA, as an internal part of the electronic hardware, needs to be mounted on a small finite ground plane, which is usually the PCB for the electronic circuit of the radio transceiver. In this case, diffraction of the ground edges could alter the current distribution on the surface of the antenna. Also, for a compact design, the dielectric casing of the portable device is often closely located within the reactive field area of the PIFA, and this could have a strong impact on the operation of the antenna.

In this chapter, the effects of the positions of both the short-circuit plate and the feed wire on the input characteristics of a PIFA, such as resonant frequency and bandwidth, are examined. Then the effect of the location where the PIFA is mounted on a finite ground plane is investigated. Based on the above observations, a PIFA is designed to operate at about 900 MHz. Finally, a study of the effect of a dielectric cover layer on the operating performance of this PIFA follows. This includes the influence due to both the electrical parameters and physical configurations of the dielectric cover layer. In this study, the MOM based electromagnetic simulator, IE3D, is used and the simulated results are validated by measurements.

4.2 MOM Modelling for Multilayered Planar Antennas

With the availability of high-speed computers and appropriate software simulation packages, full-wave electromagnetic analysis is becoming more and more common for analysing and modelling antenna systems. MOM has been by far the most popular numerical technique for modelling and analysis of antennas since it was introduced by Harrington (Harrington, 1993). As described in section 3.3, the NEC, a MOM based computer simulation package that uses the free space Green's function, is not suitable for modelling planar antennas with multilayered surfaces. Thus the so-called MPIE technique has been developed for modelling and analysing these multilayered planar antennas of arbitrary shapes. This MPIE technique has been applied in several popular MOM based electromagnetic simulation tools such as IE3D. The details of the MPIE formulation for arbitrarily shaped conducting objects in layered media and the derivation of the Green's function are given in (Michalski *et al*, 1990). Here, a brief description in the formulation used in the IE3D is given.

An integral equation formulation for a general scatter problem can be derived based on the following principle. When an incident wave from a source impinges on a metallic structure, this gives rise to a current distribution, as shown in Figure 4-1. The excited current creates a secondary field to maintain the boundary condition on the metallic structure, or for $\mathbf{r} \in S$, the total tangential field, $\mathbf{E}(\mathbf{r})$, on the surface is given by

$$\mathbf{E}(\mathbf{r}) = \mathbf{E}_{inc}(\mathbf{r}) + \mathbf{E}_s(\mathbf{r}) = Z_s(\mathbf{r})\mathbf{J}(\mathbf{r}) \tag{4.1}$$

where S is the conducting surface; $\mathbf{r}$ is the vector position of the field point; $\mathbf{E}_{inc}(\mathbf{r})$ is the incident field; $\mathbf{E}_s(\mathbf{r})$ is the secondary field created by $\mathbf{J}(\mathbf{r})$, which is the current distribution on the surface; and $Z_s(\mathbf{r})$ is the surface impedance of the conductor.

$\mathbf{E}_s(\mathbf{r})$ can be written in terms of the Green's function as

$$\mathbf{E}_s(\mathbf{r}) = \int_S \mathbf{G}(\mathbf{r} \mid \mathbf{r}') \cdot J(\mathbf{r}') ds' \tag{4.2}$$

where $\mathbf{G}(\mathbf{r}\,|\,\mathbf{r}')$ is the dyadic Green's function of the structure and $\mathbf{r}'$ is the vector position of the source point. The Green's function $\mathbf{G}(\mathbf{r}\,|\,\mathbf{r}')$ satisfies the boundary condition in the layered medium. The only boundary condition not imposed on the Green's function is the boundary condition on the metallic structure.

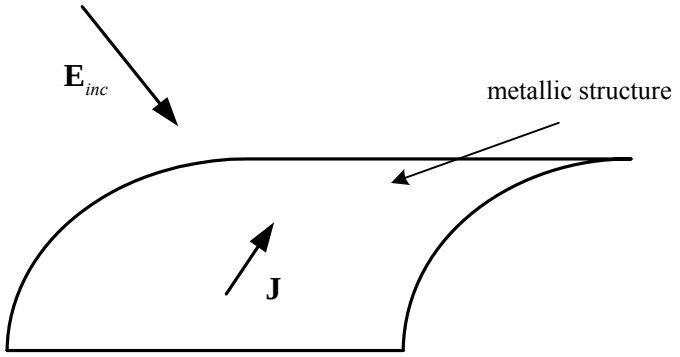

Figure 4-1 An incident field is applied to a metallic structure.

To solve equation (4.1) numerically for the unknown current, the Galerkin's method is used (see Appendix A). In this method, the unknowns are first expanded using a set of basis functions, then the integral equation is weighted with a set of testing functions chosen to be the same as the expansion basis functions.

By approximating the current distribution by a set of basis functions, and combining equations (4.1) and (4.2), the following can be obtained:

$$Z_s(\mathbf{r})\sum_n I_n\mathbf{B}_n(\mathbf{r}) = \mathbf{E}_{inc}(\mathbf{r}) + \sum_n I_n\int_S \mathbf{G}(\mathbf{r}\,|\,\mathbf{r}')\cdot\mathbf{B}_n(\mathbf{r}')ds' \tag{4.3}$$

where

$$\mathbf{J}(\mathbf{r}) = \sum_n I_n\mathbf{B}_n(\mathbf{r}),\ \ n = 1,2,... \tag{4.4}$$

and $\mathbf{B}_n(\mathbf{r})$ are the basis functions and I_n are the current distribution coefficients.

From Galerkin's procedure, equation (4.3) is converted into

$$\sum_m \int_S ds \mathbf{E}_{inc}(\mathbf{r}) \cdot \mathbf{B}_m(\mathbf{r})$$

$$= \sum_m \sum_n I_n \left\{ \int_S ds Z_S(\mathbf{r}) \mathbf{B}_m(\mathbf{r}) \cdot \mathbf{B}_n(\mathbf{r}) - \int_S ds \int_S ds' Z_S(\mathbf{r}) \mathbf{B}_m(\mathbf{r}) \cdot \mathbf{G}(\mathbf{r} \mid \mathbf{r}') \cdot \mathbf{B}_n(\mathbf{r}) \right\} \tag{4.5}$$

This process is enforcing equation (4.3) with a complete set of test functions. A complete basis function set consists of an infinite number of terms. Mathematically, equation (4.5) is an infinite dimensional problem and cannot usually be solved exactly. A projection of the infinite dimensions into a finite M-dimensions in mathematic terminology is necessary for a numerical solution of equation (4.5). After the projection, equation (4.5) becomes an M by N matrix equation, such that

$$[Z_{mn}][I_n] = [V_m] \tag{4.6}$$

where

$$Z_{mn} = \int_S ds Z_S(\mathbf{r}) \mathbf{B}_m(\mathbf{r}) \cdot \mathbf{B}_n(\mathbf{r}) - \int_S ds \int_S ds' Z_S(\mathbf{r}) \mathbf{B}_m(\mathbf{r}) \cdot \mathbf{G}(\mathbf{r} \mid \mathbf{r}') \cdot \mathbf{B}_n(\mathbf{r}) \tag{4.7}$$

and $$V_m = \int_S ds \mathbf{E}_{inc}(\mathbf{r}) \cdot \mathbf{B}_m(\mathbf{r}) \tag{4.8}$$

The solution of equation (4.6) is the current distribution coefficients. After the current distribution is solved, the s-parameters and radiation patterns are calculated. It needs to be mentioned here that the formulation based on the MPIE can also express a magnetic current representing the field distribution on a metallic aperture. The magnetic current can be similarly set up.

All MOM formulations, no matter whether simple or complex, take the form of equation (4.6). The differences are only via the choice of basis functions and the Green's function, which are the two important factors required for obtaining an accurate solution. In the IE3D, a proprietary Green's function formula for a 3D metallic structure in multi-dielectric layers and a roof-top basis function for handling arbitrarily shaped and oriented 3D structures are used (Zheng, 1994). For example, a

discretisation of the surface currents using rooftop basis functions is shown in Figure 4-2. From this figure, it can be noted that each rooftop is associated with one edge of the mesh and represents a current with constant density flowing through that edge. The advantage of such a roof-top basis function is that triangular cells can be used in a consistent manner with the rectangular cells to efficiently partition a given geometry.

Execution time and computer storage requirements are two factors that tend to limit the size of antenna structures that may be analysed with MOM. The solution time for the above MOM approach mainly consists of the CPU time required for computation of the Green's function, the calculation and filling of the matrix elements Z_{mn} in equation (4.7) and the inversion of this matrix in equation (4.6). The numerical computation of the Green's function is usually a small percentage of the overall solution time.

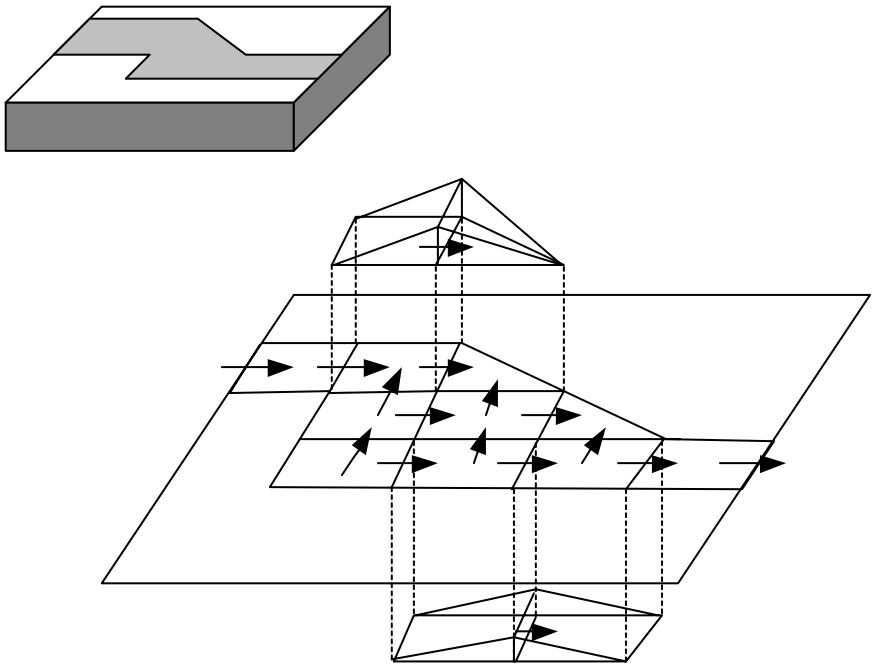

Figure 4-2 Discretisation of the surface currents using rooftop basis functions.

4.3 PIFA on a Finite Ground Plane

4.3.1 Structure

The PIFA under investigation is shown in Figure 4-3. The PIFA consists of a finite ground plane, a top plate element parallel to the ground plane, a feed wire attached between the ground plane and the top plate, and a short-circuit plate which connects the top plate to the ground plane. The top plate has dimensions of width L_1 and length L_2. It is placed at a height H above the finite ground plane having dimensions of width W_g and length L_g. The width of the short-circuit plate is W_s. As shown in Figure 4-3, the lower corner of the ground plane is used as the reference with coordinates (*0,0,0*). The corner edge of the short-circuit plate is located at the coordinates (D_S, g_s,, *0*), and the feed point is located at the coordinates ($D_S + d_f$, g_f, *0*).

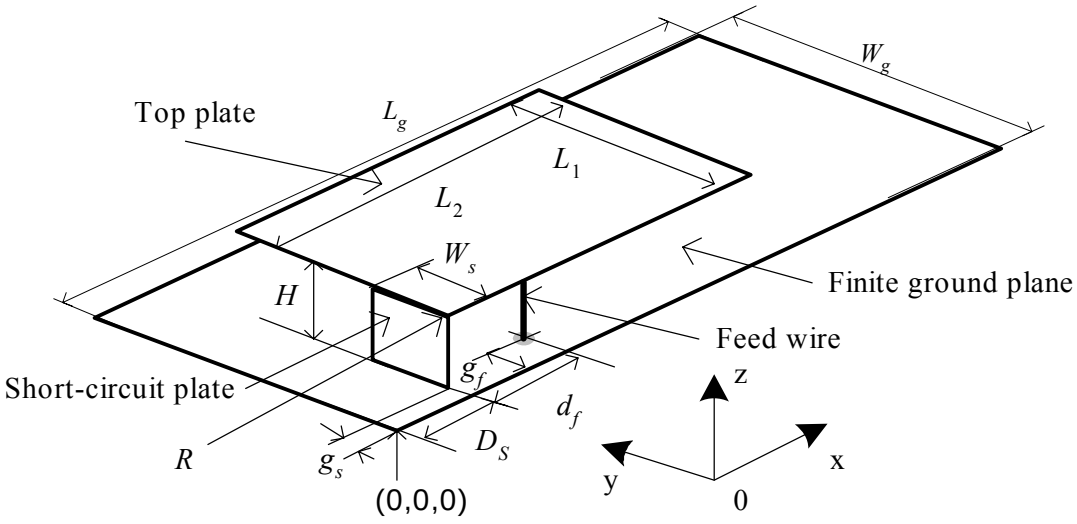

Figure 4-3 The structure of a PIFA on a finite ground plane.

4.3.2 PIFA on an infinite ground plane

The characteristics of a PIFA on an infinite ground plane have been computed by an analysis method called the spatial network method (SNM) (Hirasawa *et al*, 1992). In this analysis, the distributions of the electric fields between the planar element and the

ground plane, and the surface current distributions have been presented with respect to the short-circuit plate width. Also, it relates the resonant frequency, and bandwidth to the physical parameters of the antenna, such as the short-circuit plate width and the antenna height. These observations are useful in understanding the behaviour of radiation characteristics in PIFAs.

Now, referring to Figure 4-3, but assuming the size of the ground plane is infinite, the resonant frequency f_0 of such a PIFA can be expressed as follows (Hirasawa *et al*, 1992):

For

$$\frac{L_1}{L_2} \leq 1,\ f_0 = r \cdot f_1 + (1-r) \cdot f_2 \tag{4.9}$$

where $r = W_s / L_1$ and f_1 is related to wavelength λ_1, such that $f_1 = \frac{c}{\lambda_1}$, where c is the wave propagation velocity, around $3\text{x}10^8$ m/s, and

$$\lambda_1 = 4*(L_2 + H) \tag{4.10}$$

Similarly, f_2 is related to λ_2, which is given by

$$\lambda_2 = 4*(L_1 + L_2 + H - W_s) \tag{4.11}$$

The above two relationships are applied to two special cases:

(i) The width of the short-circuit plate is equal to that of the top plate of the antenna, i.e., $W_s = L_1$. In this case, the PIFA becomes a standard $\lambda/4$ short-circuit patch antenna and has a maximum resonant frequency, given by

$$f_{\max} = \frac{c}{4(L_2 + H)} \tag{4.12}$$

(ii) When $W_s = 0$, and so the short-circuit plate takes the form of a short-circuit pin. Under this condition, the antenna has a minimum resonant frequency, given by

$$f_{\min} = \frac{c}{4(L_1 + L_2 + H)} \tag{4.13}$$

This shows that it is possible to obtain a resonant frequency for a given PIFA that falls between f_{min} and f_{max} by appropriately adjusting the width of the short-circuit plate.

Now, equation (4.9) may be used to provide an initial estimate of the dimensions for a PIFA operating at a given resonant frequency. However, equation (4.9) also indicates that the operation of the PIFA is influenced by the dimensions of various elements of the antenna. This then means that a number of iterations will normally be required to adjust the antenna elements in order to finally achieve the specified requirements. This laborious adjustment process could often be aided by considering the following guidelines:

- An increase in H widens the bandwidth.
- Reducing W_s, such that $W_s < L_1$, reduces the bandwidth.
- Varying L_2 allows frequency tuning.
- Every modification will require a change in the position of the feed point for impedance matching.

Based on the above observations, the initial dimensions for a PIFA operating in the 900 MHz frequency band have been chosen as follows:

- The dimensions of the radiating top plate are (L_1, L_2) = (30 mm, 56.5 mm).
- The height H is 13.3 mm.
- The width of the short-circuit plate W_s is 10 mm.
- A finite ground plane with a length of 110 mm and a width of 50 mm is used.

- The feed point and the lower edge of the short-circuit plate are located at the coordinates (d_f, g_f) = (12 mm, 10 mm), and (D_S, g_s) = (6 mm, 10 mm), respectively.

This antenna is used in this study for investigating several factors which could further influence the operation of the PIFA but have not previously been considered in the literature.

4.3.3 MOM model

Earlier studies have demonstrated that IE3D is an accurate and efficient 3D electromagnetic simulator for the modelling and analysis of multilayered planar antennas of arbitrary shapes (Zeland, 1996). This simulator is used to study the operation of a PIFA in a finite ground plane and in close proximity to a dielectric cover layer. Figure 4-4 shows the MOM model of this PIFA. In this model, the highest frequency has been set at 1.2 GHz with 20 cells per wavelength discretisation. Edge meshing has been adopted to achieve accurate computation of the current distribution. This model consists of 259 cells with 435 unknown currents.

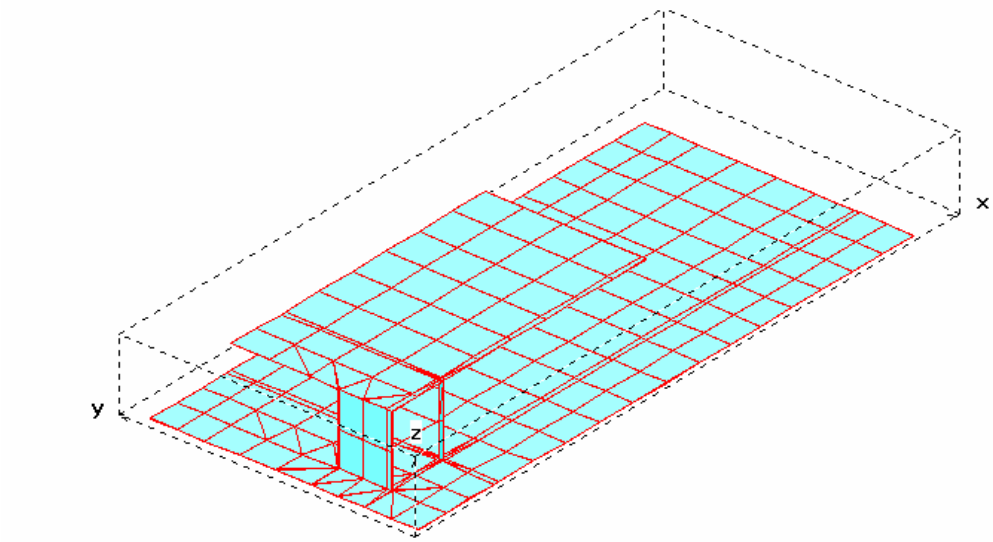

Figure 4-4 A MOM model of the PIFA on a finite ground plane.

As IE3D is based on the MOM, which is a frequency-domain analysis algorithm, each computational run will provide results for only one frequency. This means that many simulation runs would be required to predict the antenna performance over a wide range of frequencies. In this study, an interpolation technique based on a rational function is used to significantly reduce the simulation run times (Schlagenhaufer *et al*, 2001). With this method, the impedances for several relatively widely spaced frequencies are computed using IE3D and stored. The other impedances at intermediate frequencies can then be computed by interpolating the pre-calculated and stored impedance values. The formulae used for this interpolation process are given in Appendix B.

4.3.4 Effect of the location of the short-circuit plate

In this section, the influence of the position of the short-circuit plate on the resonant frequency and bandwidth of the PIFA is studied. Figure 4-5 (red dotted line) and Figure 4-6 (red dotted line) show how the resonant frequency and bandwidth change with the location of the short-circuit plate along the y-axis. In this case, the top plate and feed point are fixed at their initial positions. From these two curves, it is noted that both the resonant frequency and the bandwidth of the antenna increase when the short-circuit plate moves along the y-axis away from the feed wire. When the plate moves from one end of the top patch to the other, the resonant frequency and bandwidth increase by more than 9.5 % and 92 %, respectively.

4.3.5 Position of the feed wire

The influence on the resonant frequency and bandwidth caused by changing the location of the feed point of the PIFA has also been investigated. In this case, the short-circuit plate is fixed at the initial corner position, i.e., at the coordinates (6 mm, 10 mm, 0). The variations in resonant frequency and bandwidth of the antenna, with respect to the feed point location along the y-axis, are shown in Figure 4-5 (green solid line) and Figure 4-6 (green solid line), respectively. From these two curves, it is noted that the resonant frequency and the bandwidth of the antenna increase when the feed wire

moves along the y-axis away from the short-circuit plate. Now, with the feed wire moving from one end of the top patch to the other, the resonant frequency and bandwidth increase by more than 7.8 % and 98 %, respectively.

Comparing these two cases (the short-circuit plate case and the feed wire case), it is observed that the short-circuit plate "movement" has a stronger effect on the resonant frequency than the feed wire "movement". On the other hand, the effect of the feed point "movement" produces a slighter increase in bandwidth change than the short-circuit plate. Since a larger PIFA is associated with a lower operating frequency, these observations suggest that for an antenna design to have a minimum volume, both the feed wire and the short-circuit plate should be located on the same edge of the top patch. However, such a design would suffer from a minimum achievable bandwidth. Now, since the feed wire "movement" has a significantly larger influence on the bandwidth than the resonant frequency, it may be a good design compromise to consider fixing the short-circuit plate at the edge of the top plate while moving the feed point away from the edge to obtain the required bandwidth.

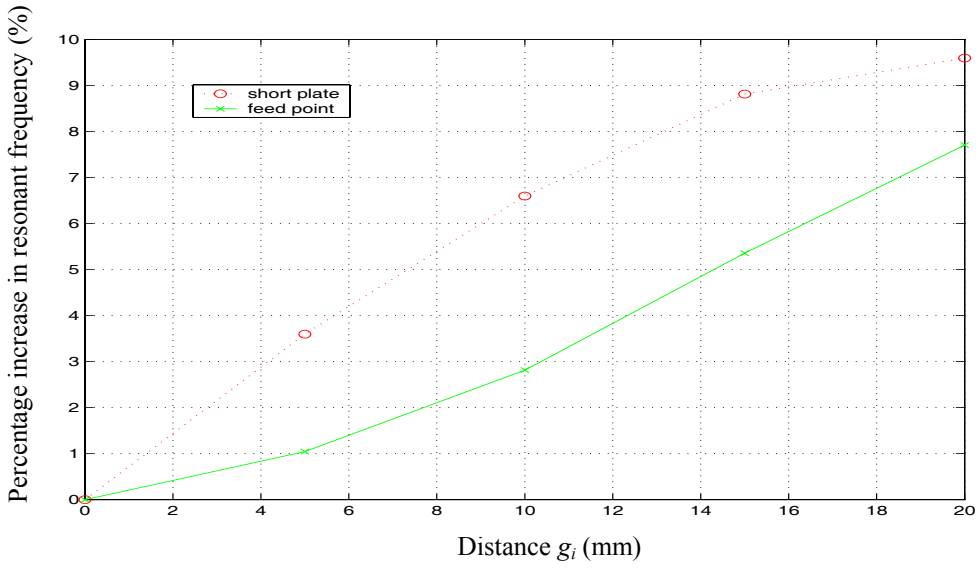

Figure 4-5 Resonant frequency change against the position of the short-circuit plate or feed wire. (The distance g_i is with respect to the initial position of the short-circuit plate, g_s, and that of the feed wire, g_f. In this case, the values of both g_s and g_f are initially set at 10 mm.)

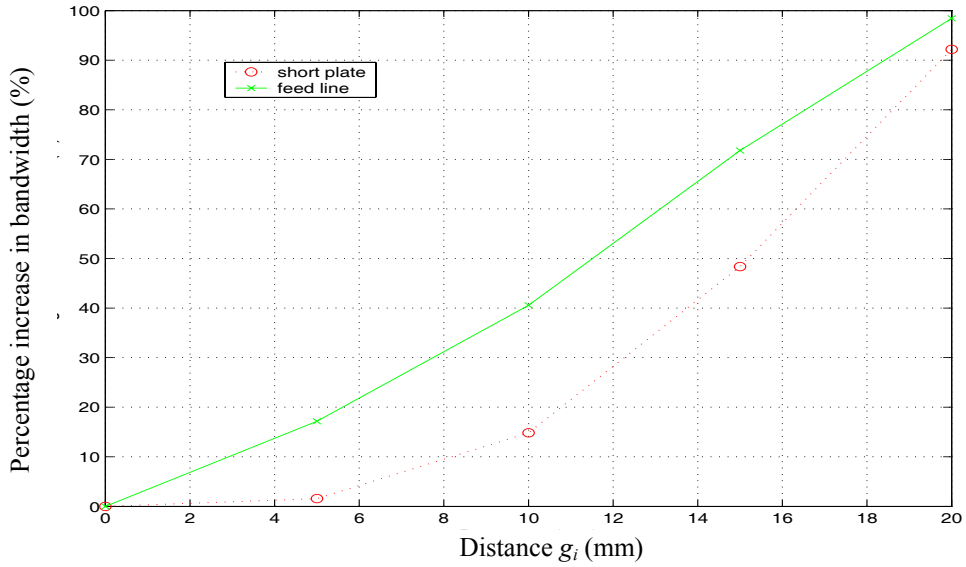

Figure 4-6 Bandwidth change against the position of the short-circuit plate or feed wire. (The distance g_i is with respect to the initial position of the short-circuit plate, g_s, and that of the feed wire, g_f. In this case, the values of both g_s and g_f are initially set at 10 mm.)

Next, with the short-circuit plate and the feed point set at their initial positions, the variations in the input impedance of the antenna when the feed wire is moved from the short-circuited end of the top patch toward the open end along the x-axis, are plotted in Figure 4-7. It is observed that the resistance of the antenna at resonance increases when the feed wire is moved away from the short-circuit plate along the x-axis. This particular characteristic of the PIFA provides a convenient way for antenna impedance matching.

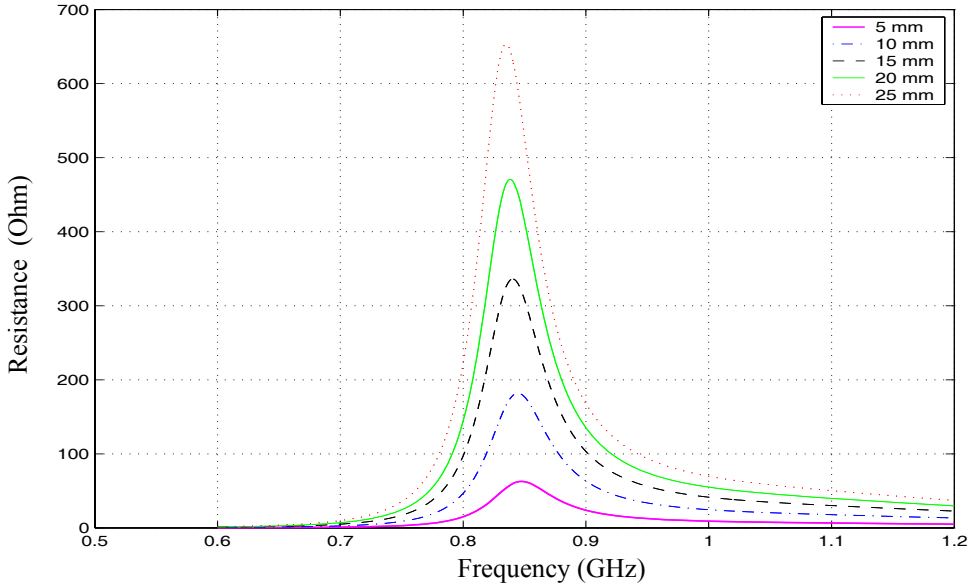

(a)

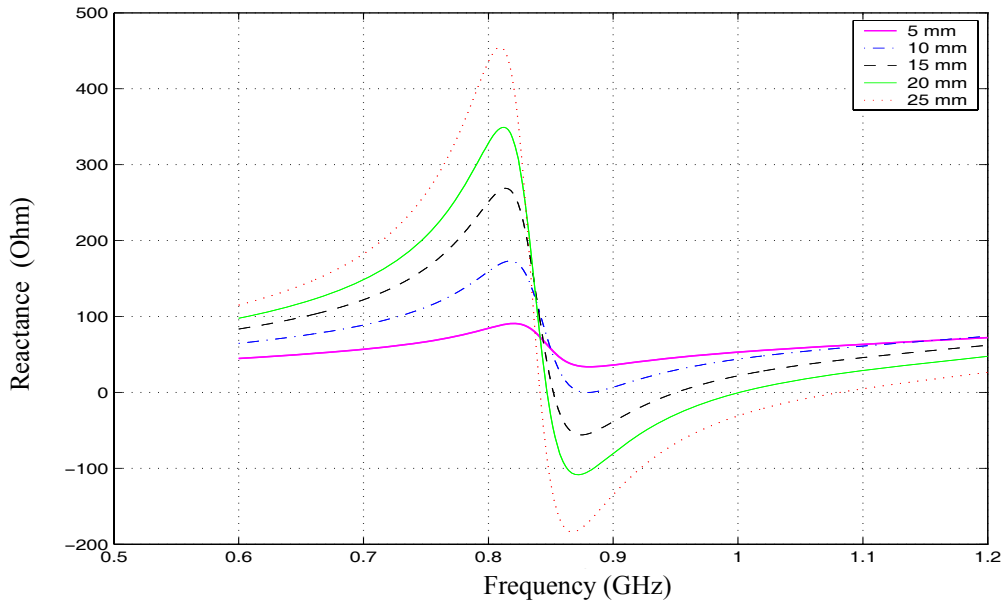

(b)

Figure 4-7 Input impedance of the PIFA with different positions of the feed wire, i.e., g_f varies from 5 mm to 25 mm along the x axis: (a) resistance; (b) reactance.

4.3.6 Location of PIFA on a finite ground plane

The effects on the resonant frequency and bandwidth due to where the top plate assembly of the PIFA is mounted on the finite ground plane has also been investigated in this study. Such effects have not previously been published. In this case, the short-circuit plate and the feed point remain fixed at their initial positions with respect to the top patch. The placement of the top patch assembly is represented by the coordinates of the corner point between the top patch and the short-circuit plate as shown in Figure 4-3.

The PIFA input impedance and VSWR for a 50 Ohm match for the different locations along the x-axis are plotted in Figure 4-8 and Figure 4-9, respectively. It can be observed that as the distance D_S decreases along the x axis, i.e., the top plate is moved closer to the left hand edge of the ground plane, the antenna resonant frequency decreases while its bandwidth increases. With D_S set to 6 mm for this PIFA (green thin solid lines), a maximum bandwidth of 8.5 % for a $\text{VSWR} \leq 2$ is achieved at the resonant frequency of 909.5 MHz.

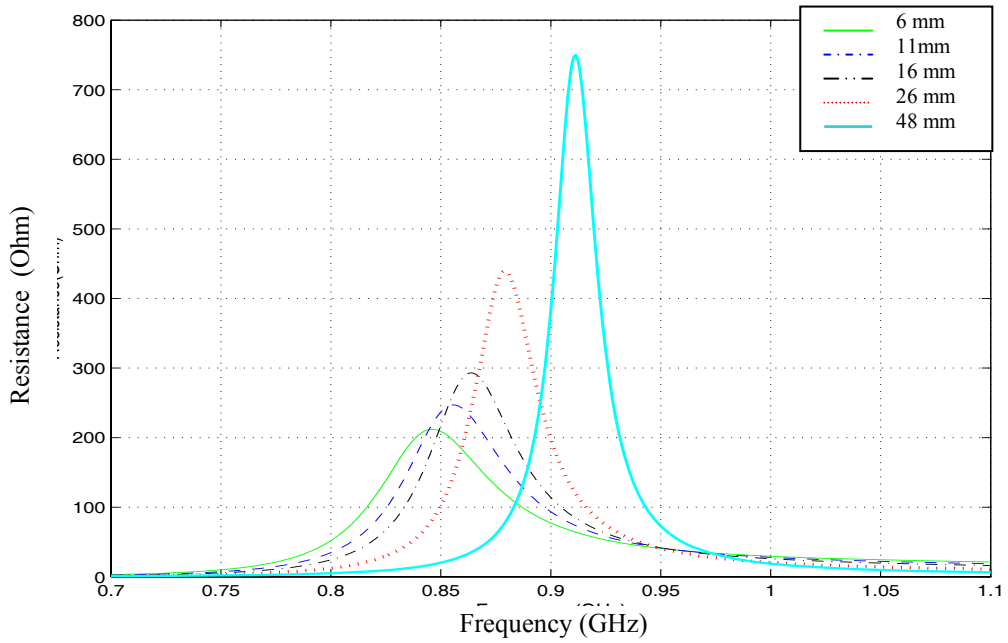

(a)

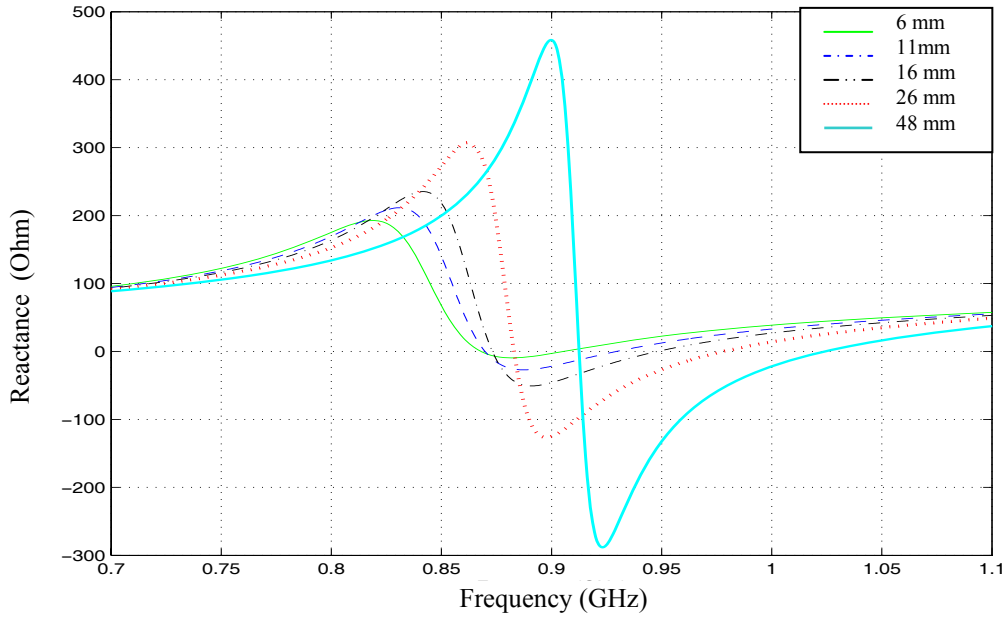

(b)

Figure 4-8 Input impedance for a PIFA mounted at different values of D_s: (a) resistance; (b) reactance.

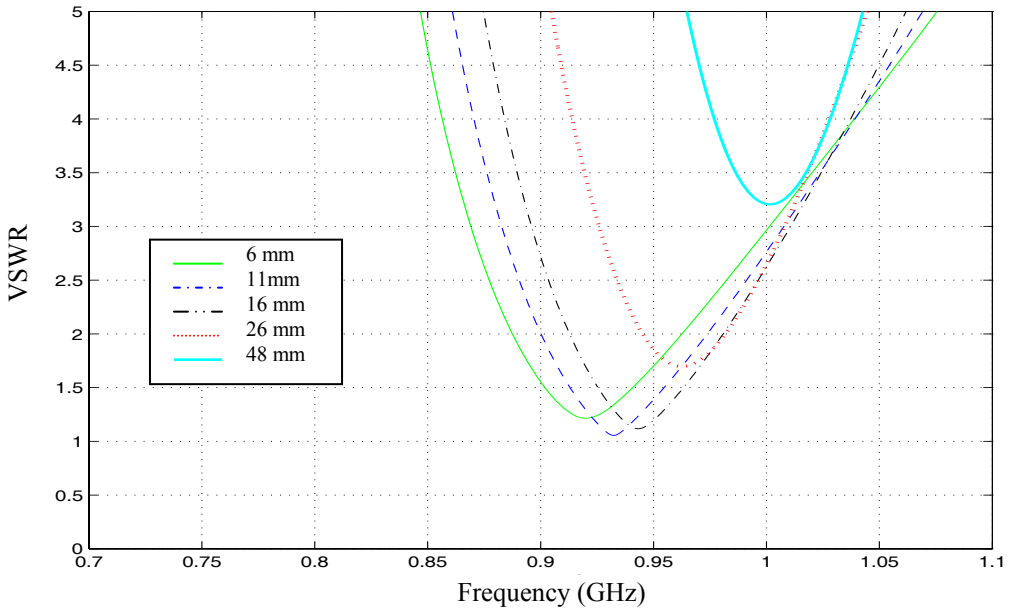

Figure 4-9 VSWR (for a 50 Ohm match) as a function of frequency with the PIFA mounted at different values of D_s.

Also, the resultant resonant frequencies and bandwidths as a function of the locations of the top-patch assembly with respect to the finite ground plane are shown in Figure 4-10 and Figure 4-11, respectively. The ratio of the bandwidth to resonant frequency as a function of the location of the top patch assembly with respect to the finite ground plane is plotted in Figure 4-12. It is noted that the PIFA fails to resonate when point R of the PIFA assembly is moved beyond the x, y coordinates as indicated in these figures, i.e., with x > 25 mm and y > 20 mm.

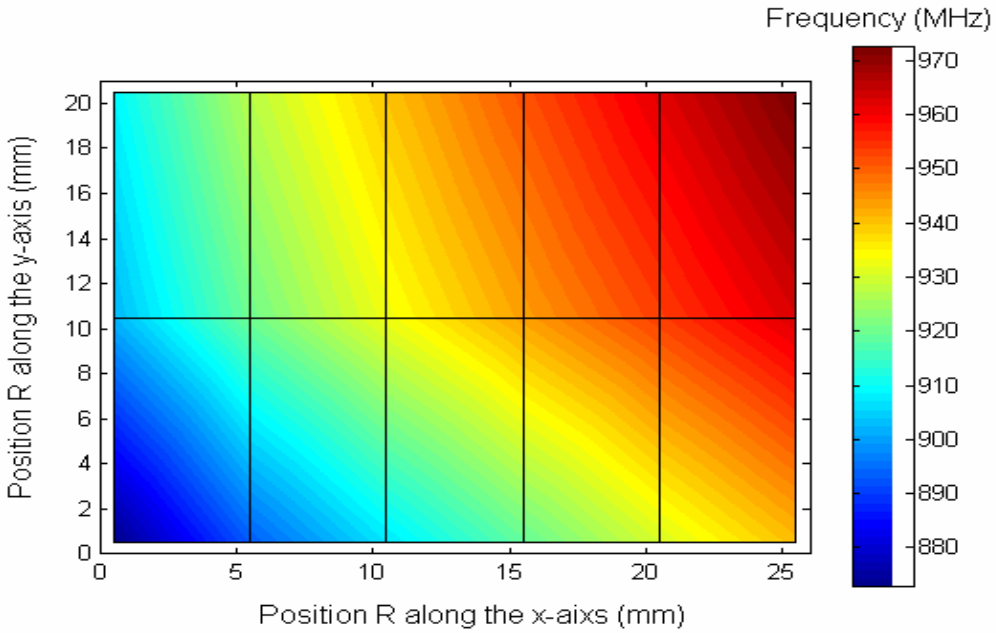

Figure 4-10 Resonant frequency as a function of the position of the antenna on the ground plane.

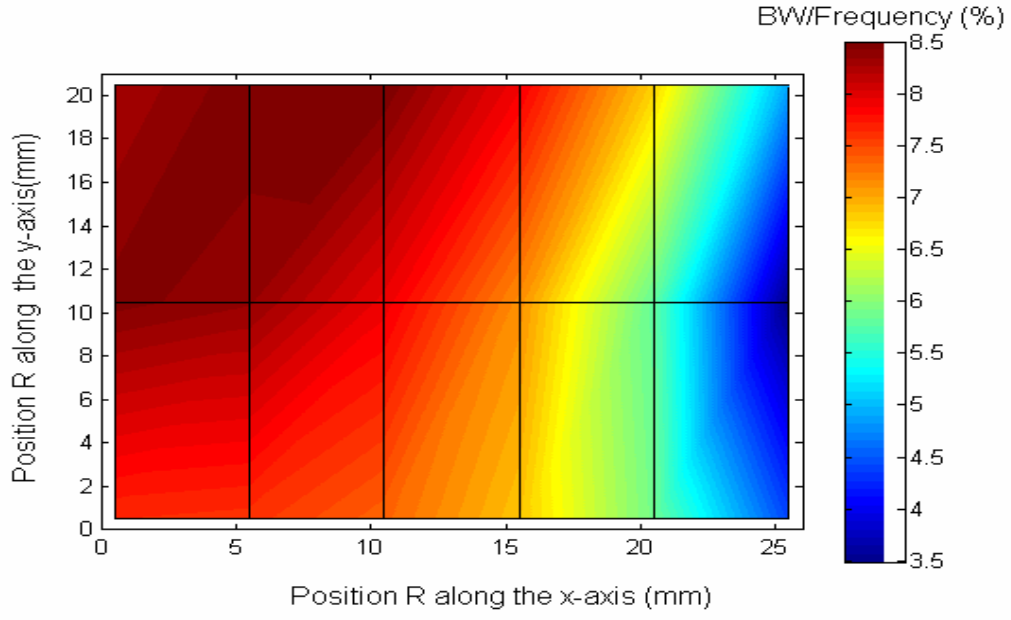

Figure 4-11 Bandwidth as a function of the position of the antenna on the ground plane.

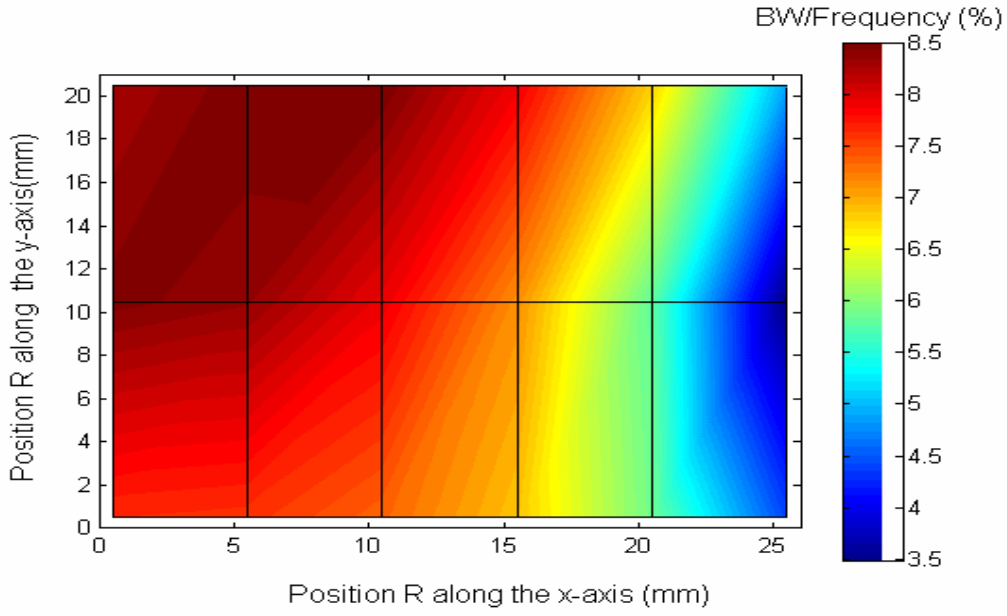

Figure 4-12 The ratio of bandwidth to resonant frequency as a function of the position of the antenna on the ground plane.

These results indicate that the position where the PIFA is located on the finite ground plane could have a significant impact on its input characteristics. It is known that the design variables of a PIFA, on an infinite ground plane are the height, width and length of the top plate, the width of the short-circuit plate and the location of the feed point wire. However, from this study, it has been found that one more variable that has to be considered is the location where the PIFA is mounted on the finite ground plane.

From Figure 4-10, it is noted that the lowest resonant frequency of the antenna is achieved when the point R is located at the edge of the ground plane, i.e., $(x, y = 0, 0)$. This observation suggests that for a given resonant frequency, the size of a PIFA can be made smaller if it is located at the edge of the ground plane. On the other hand, it is observed from Figure 4-11 that a larger bandwidth could be obtained when the point R is located within the area of the ground plane bounded by $2.5mm \le x \le 12.5mm$ and $10mm \le y \le 20mm$. This means that if it is desired to have a larger ratio of the bandwidth to resonant frequency, then the PIFA has to be located in the middle of the ground plane or having the point R located within the area bounded by $0 \le x \le 10mm$

and $10mm \le y \le 20mm$, as shown in Figure 4-12. These two seemingly contradicting requirements for small size and wide bandwidth call for some form of compromise in the actual PIFA implementation. An example of a compromised design with a bandwidth of 8.5% (VSWR $\le$ 2) at the resonant frequency of 909.5 MHz for the test PIFA is to have the coordinates (*x, y*) of the point *R* of the top patch assembly, the short-circuit plate and the feed point set to (6 mm, 10 mm), (6 mm, 10 mm), and (18 mm, 10 mm), respectively.

4.4 Effect of Dielectric Cover Layer

In this section, the influence of a dielectric cover sheet in close proximity to the top plate on the input characteristics of the PIFA is investigated using IE3D. For the computer modelling, the dielectric cover sheet is assumed to be of infinite extent. As a result, the surface-wave reflection and diffraction at the edge of a truncated layer are not taken into account. However, they are negligible for an electrically thin layer.

Two configurations are considered in this study. In the first one, the top plate of the PIFA is directly attached to the underside of the dielectric layer as shown in Figure 4-13 (a). In the second one, an air gap *g* is kept between the top plate of the PIFA and the dielectric cover layer, as shown in Figure 4-13 (b). In both cases, the dielectric layers can be considered to be part of a radome used for protecting the antenna. The thickness of the dielectric layer is indicated as *d* in the figures.

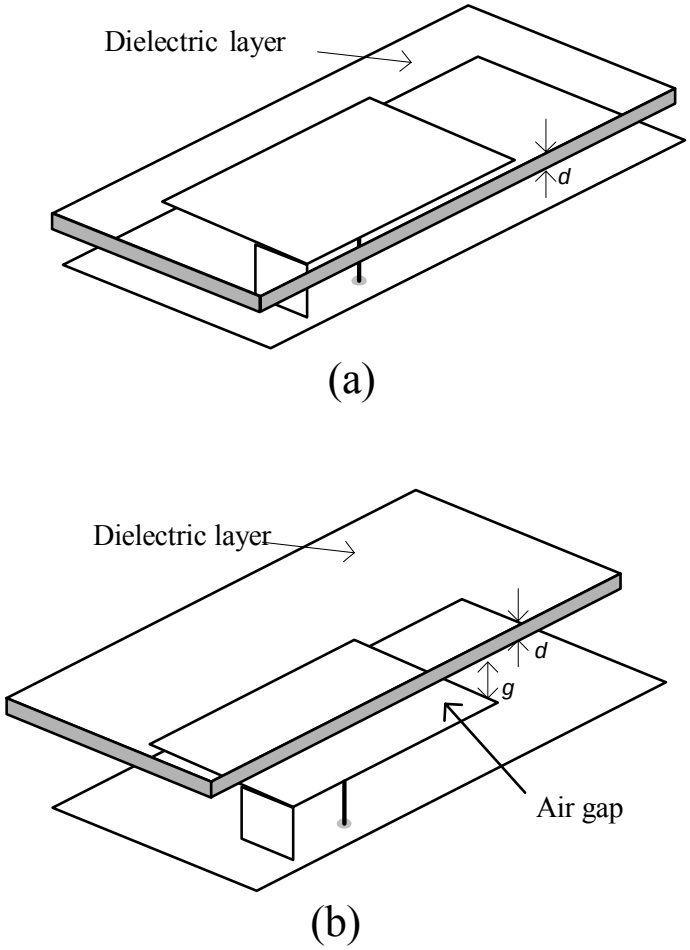

Figure 4-13 Antenna-dielectric cover layer structures under investigation: (a) dielectric-covered PIFA without an air gap; (b) dielectric-covered PIFA with an air gap.

4.4.1 Dielectric covered PIFA without a gap

When the PIFA is covered by a dielectric layer without an air gap as shown in Figure 4-13 (a), its input impedance, bandwidth and efficiency are affected by the dielectric constant, loss tangent and thickness of the layer. For these tests, two different dielectric materials have been considered: one with low loss having a dielectric constant of 3.38 and a loss tangent of 0.0027, while the other is lossy with a dielectric constant of 4.4 and a loss tangent of 0.007. The first material corresponds to the substrate material used in the R4003 series of low loss PCB manufactured by Roger and the second to the common FR-4 fibreglass PCB. Two different thickness values of 0.8 mm and 1.6 mm for each material are considered. Both the R4003 low loss material and FR-4 have been used in the experimental set up for validating the simulated results, as will be discussed in section 4.5.

The simulated input impedance and return loss of the PIFA with its top plate in contact with a low loss dielectric cover layer are shown in Figure 4-14 and Figure 4-15, respectively. For comparison, the results obtained with no cover, as well as with a lossless dielectric material, are also plotted as references. The corresponding simulated results for the case with a lossy dielectric material, such as FR-4 PCB, are shown in Figure 4-16 and Figure 4-17. The corresponding values of the resonant frequency, bandwidth, input impedance and the efficiency of the antenna for the two dielectric materials used are tabulated in Table 4-1.

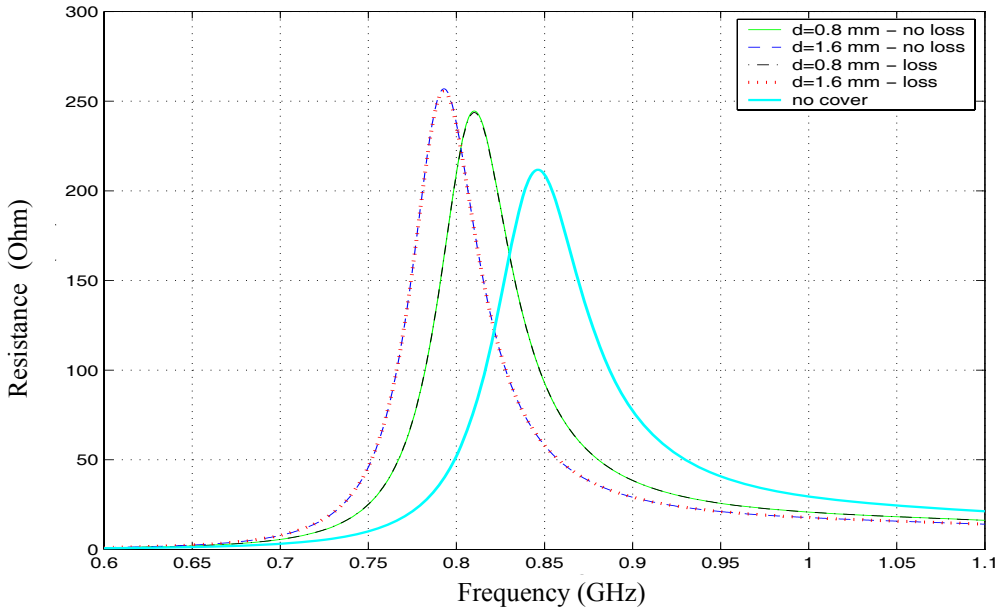

(a)

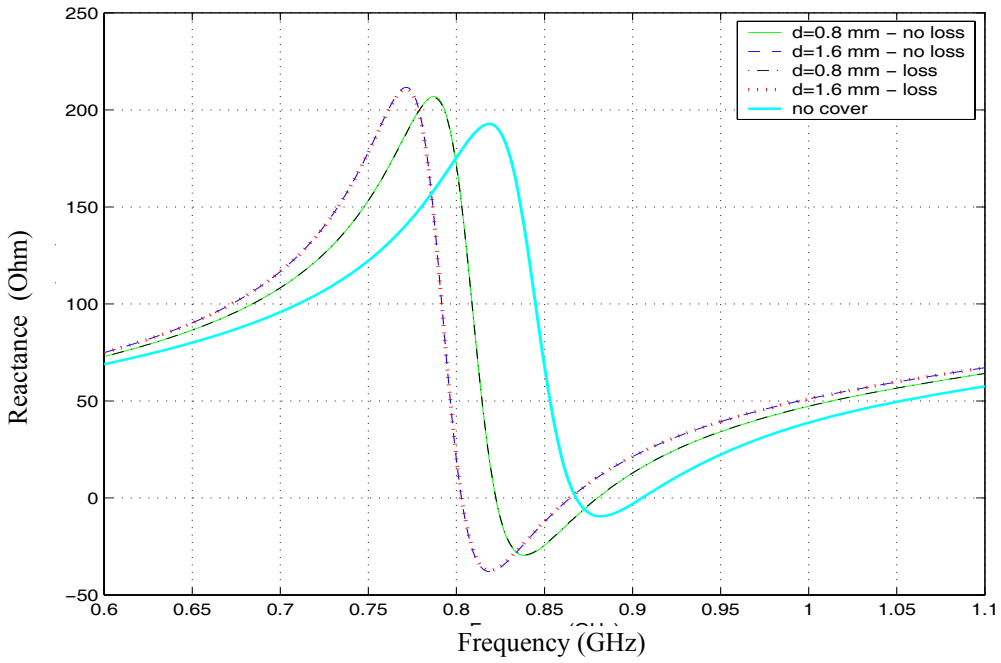

(b)

Figure 4-14 Input impedance of the PIFA covered with a Rogers R4003 material: (a) resistance; (b) reactance. Note that the label of "no loss" represents that the loss tangent of the dielectric material is assumed to be zero.

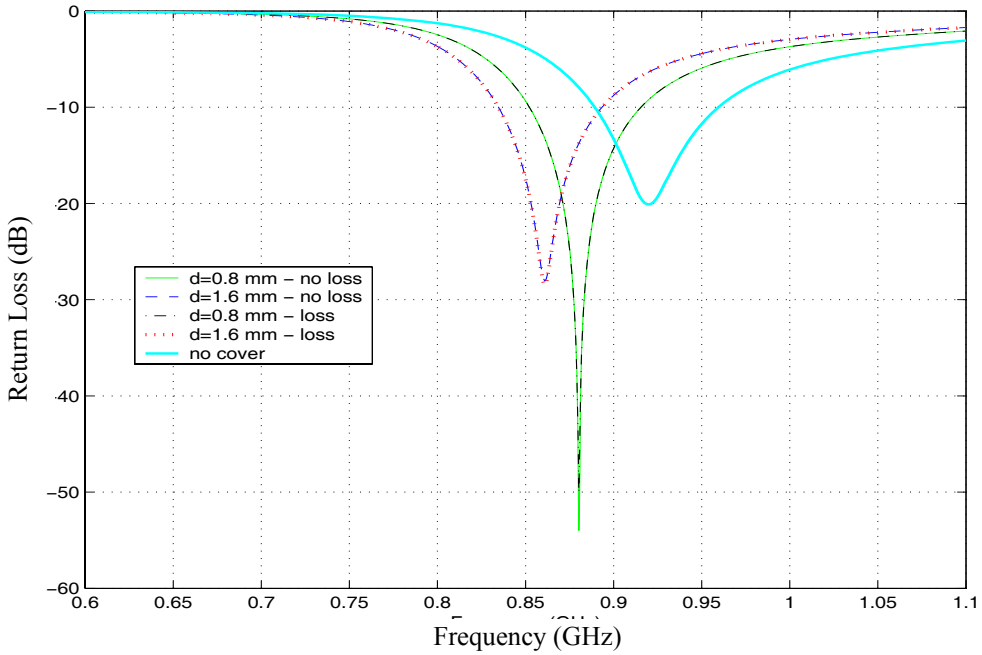

Figure 4-15 Return loss of the PIFA covered with a Rogers R4003 material.

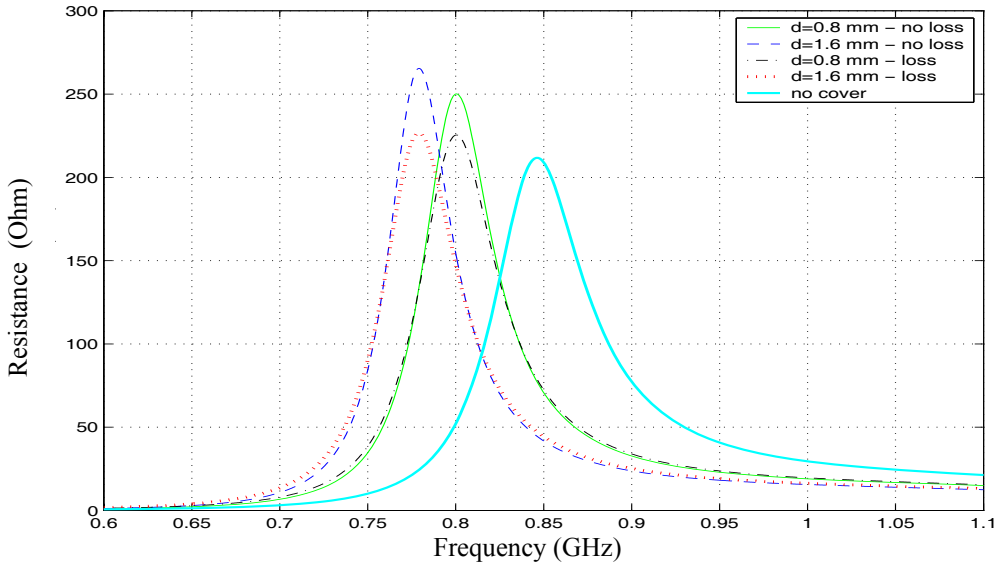

(a)

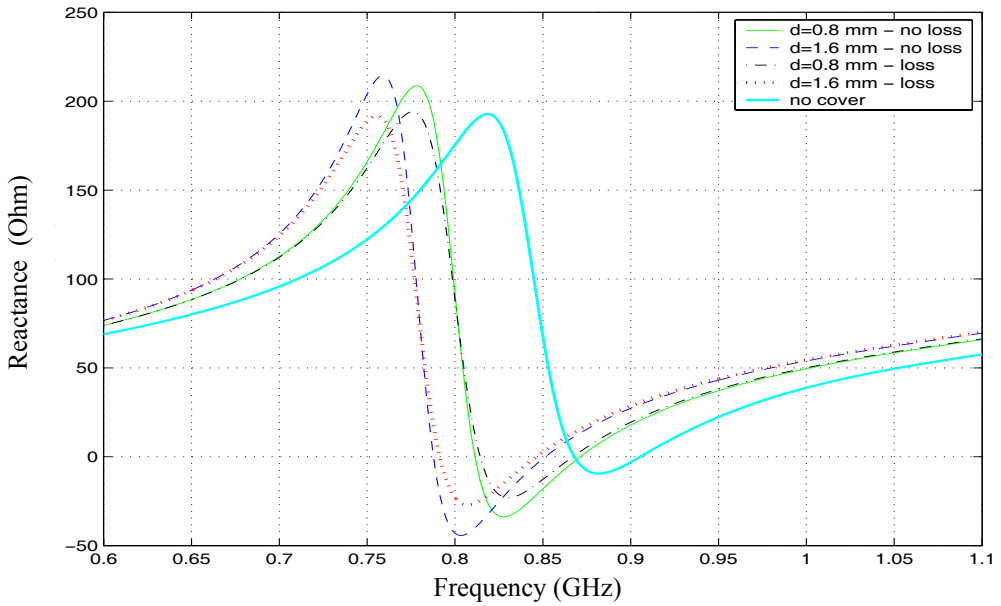

(b)

Figure 4-16 Input impedance of the PIFA covered with a FR-4 material: (a) resistance; (b) reactance.

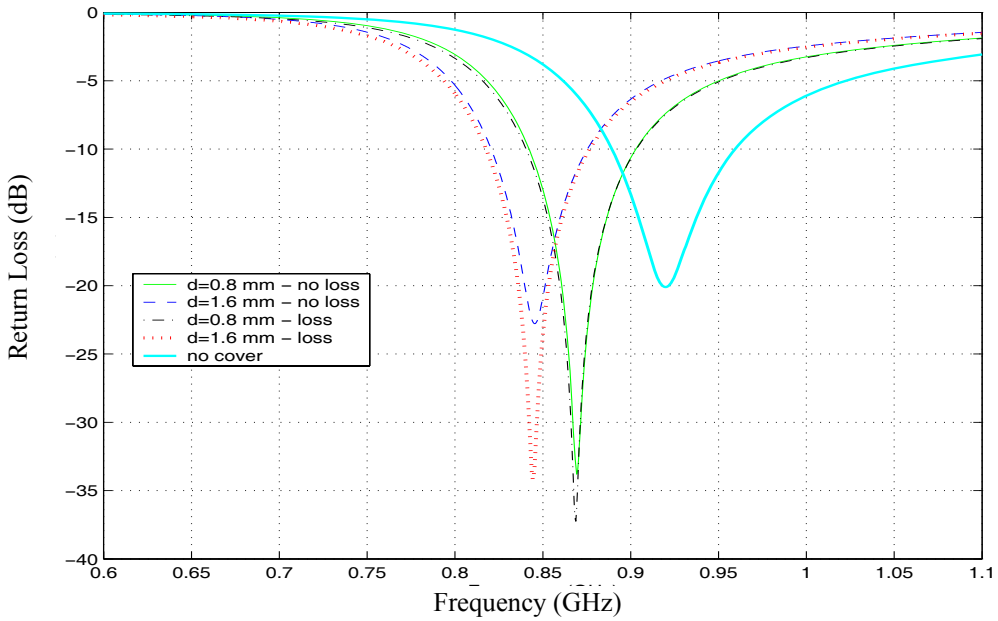

Figure 4-17 Return loss of the PIFA covered with a FR-4 material.

From Figure 4-14 and Figure 4-15, it is observed that the resonant frequency of the PIFA is shifted to a lower frequency in the presence of the dielectric cover layer. This becomes even more noticeable as the dielectric constant increases or a thicker dielectric layer is used. This is because the electromagnetic wave propagation is slower in a dielectric medium as compared to free space. This effect becomes more significant as the dielectric constant increases. Also, for a thicker dielectric layer the relative dielectric constant of the dielectric-air interface also becomes larger, thus slowing the wave propagation. Moreover, it is noted that for a low loss dielectric material the effect on the input impedance characteristics of the antenna is quite insignificant. Nonetheless, Figure 4-15 shows that the bandwidth of the PIFA decreases somewhat in the presence of the dielectric layer.

Similar effects on the input impedance and return loss of the PIFA are also observed for the case of the dielectric material of a larger loss, as shown in Figure 4-16 and Figure

4-17. However, the peak values of the input impedance become smaller as compared with the case of no dielectric layer. This larger loss dielectric material gives rise to a drop in the efficiency of the antenna as shown in Table 4-1.

Table 4-1 Simulated results of the effect of the dielectric cover on the performance of the PIFA

Contion			Resonant Frequency (MHz)	Bandwidth (MHz)	Impedance (Ohm)	Efficiency (%)
d (mm)	ε_r	$\tan\delta$				
1.6	4.4	0	851.5	59	41	86.1
0.8	4.4	0	875.5	64	47	87.4
1.6	4.4	0.07	846.5	62	47	76.3
0.8	4.4	0.07	867	66	52.5	81
1.6	3.38	0	864.5	62	45	87.3
0.8	3.38	0	880	67	51	88.2
1.6	3.38	0.0027	864	62	45.5	87
0.8	3.38	0.0027	880	66.5	51	87.9

4.4.2 **Dielectric covered PIFA with a gap**

It has been shown in the previous section that the operation of a PIFA could be affected by the presence of a lossy dielectric layer in contact with the top plate of the antenna. In an attempt to minimise the effect of the dielectric layer, an air gap, g, has been introduced between the top plate of the PIFA and the dielectric cover layer, as shown in Figure 4-13 (b). Figure 4-18, Figure 4-19 and Figure 4-20, respectively, give the input impedance, resonant frequency and bandwidth of the dielectric covered PIFA as a function of the air gap, g, when the thickness and electrical properties of the dielectric cover layer are fixed. In these simulations, the electrical properties of a Rogers R4003 PCB substrate sheet with a thickness of 1.6 mm are used. From these figures, it can be observed that the input impedance, resonant frequency and bandwidth of the antenna all decrease drastically when the air gap decreases to less than 10 mm. When the air gap increases beyond 10 mm, the input impedance increases gradually, however, the resonant frequency initially increases gradually to reach a peak value at g = 50 mm. From there on, it decreases gradually with increase in the air gap. At the same time, the bandwidth reaches the peak when g = 10 mm. After that, it gradually decreases before

it turns around at g = 50 mm. These results indicate that the dielectric layer has a significant impact on the input impedance, resonant frequency and bandwidth of the PIFA if it is in close proximately to the top plate, i.e., for $g \leq 10$ mm. For an air gap g larger than 10 mm, the effect of the dielectric layer becomes weaker.

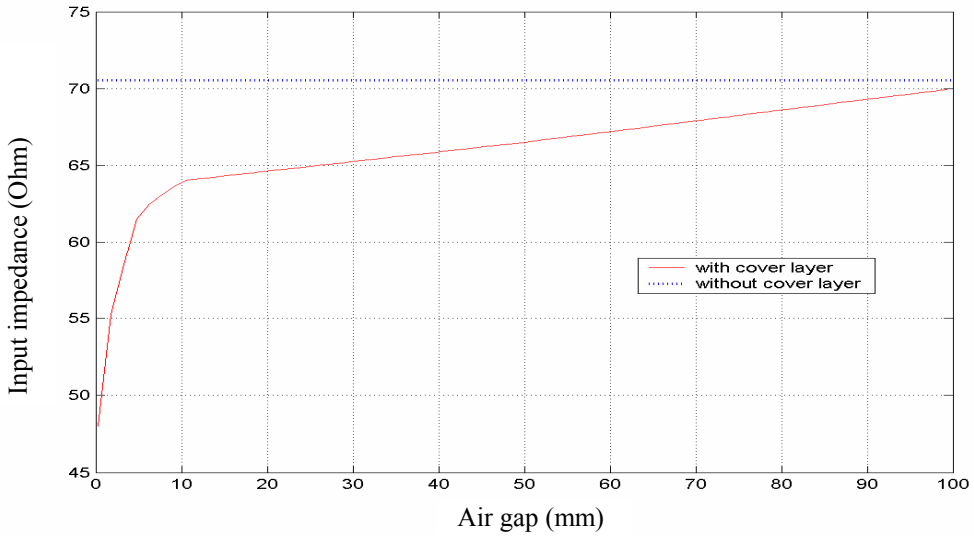

Figure 4-18 Input impedance of the dielectric-covered PIFA as a function of the air gap g.

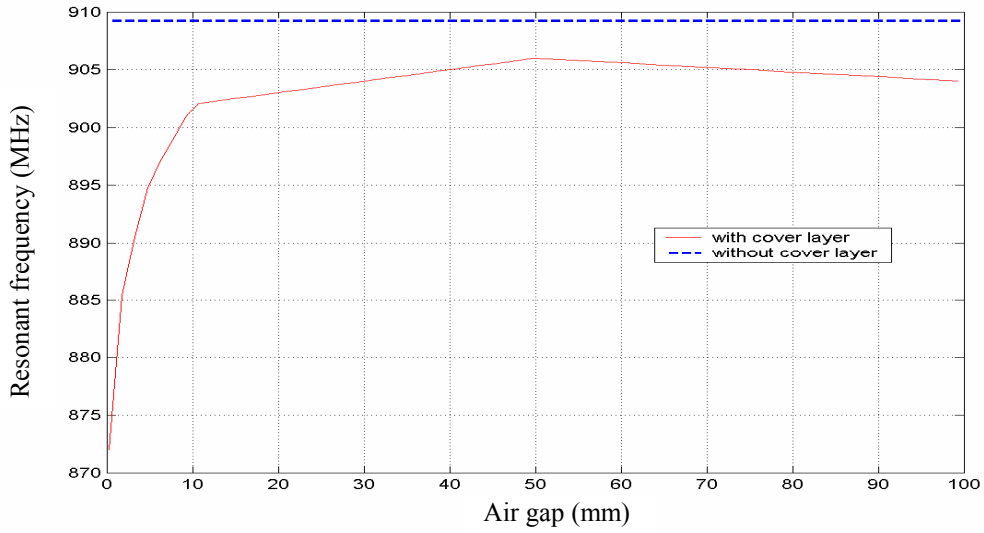

Figure 4-19 Resonant frequency of the dielectric-covered PIFA as a function of the air gap g.

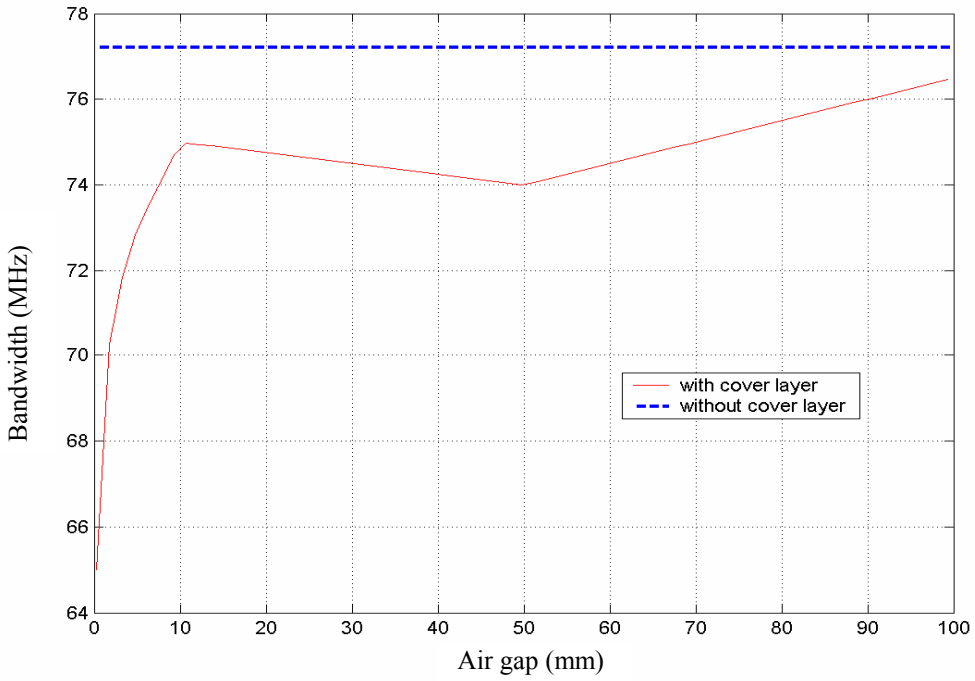

Figure 4-20 Bandwidth of the dielectric-covered PIFA as a function of the air gap *g*.

4.4.3 Distribution of surface current on the radiating patch

The distributions of surface currents at resonance for the PIFA with different cover layer configurations are shown in Figure 4-21(a)-(d). Figure 4-21(a) shows the surface current of the PIFA alone at resonant frequency 909.5 MHz. The current flows in the x direction on the top patch from the short-circuit plate edge to the opposite open-end edge. At the open-end edge, the displacement current may be on the ground plane; hence, the current flows back to the short-circuit plate on the ground plane. This current flow corresponds to the current distribution of the TM_{100} resonant mode of the rectangular short-circuit MSA. The maximum current intensity and gain are 13.1 A/m, and 2.7 dBi, respectively.

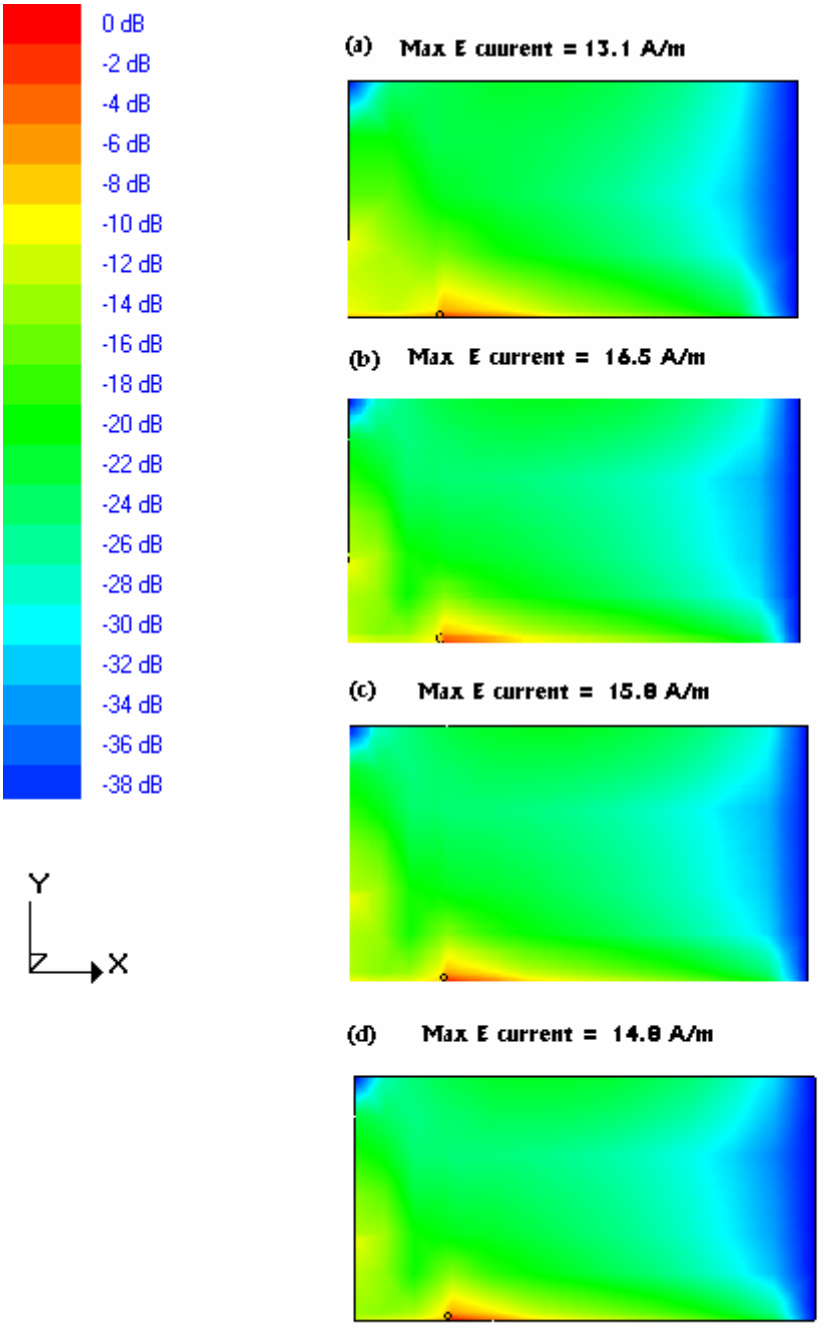

Figure 4-21 Distributions of surface current at resonance on the top patch: (a) the PIFA alone; (b) the lossless dielectric covered PIFA without a gap; (c) the lossy dielectric covered PIFA without a gap; (d) the lossy dielectric covered PIFA with an air gap of 2 mm.

When a lossless dielectric layer having a relative dielectric constant of 4.4 and a thickness of 1.6 mm is located on the top patch, the effective length of the current flow on the patch becomes longer. Consequently, the resonant frequency is lowered to 846.5 MHz. Also, the current distribution varies noticeably as shown in Figure 4-21 (b) though it corresponds to the TM_{100} mode. Moreover, the maximum current intensity is increased to 16.5 A/m and the gain is reduced to 2.47 dBi.

When this dielectric cover layer is considered to be lossy, the surface current magnitude is shown in Fig. 4-21(c), the effective length of the current flow on the patch is identical to the one in Figure 4-21 (b). However, the maximum current intensity and gain are reduced to 15.8 A/m and 1.97 dBi, respectively.

When this lossy dielectric cover layer is separated 2 mm away from the top patch, the resonant frequency is back to 889.5 MHz. This is because the effective wavelength becomes shorter. The distribution of the surface current at this resonant frequency is shown in Figure 4-21 (d), which is similar to those in Figure 4-21 (b) and (c). The maximum current intensity becomes 14.8 A/m and the gain is back to 2.44 dBi.

These results confirm the type of behaviour exhibited in the study of input impedance. When a dielectric cover layer is located close to the PIFA, the resonant frequency of the antenna is shifted to a lower frequency because the effective length of the current flow on the top patch becomes longer. Also, the distribution of the surface current magnitude on the patch varies noticeably even though it is still corresponding to the TM_{100} mode at resonant frequency. These changes are mainly determined by the dimensions, positions and dielectric constant of the cover layer. However, the loss tangent of the cover layer will have a significant impact on the gain of the antenna.

4.5 Measurement Validation

The test PIFA as described in section 4.3.1 and shown in Figure 4-3 has been fabricated. Figure 4-22 is a photo of the test antenna. It has been used to provide measurement results to validate the values obtained in section 4.4 from computer simulations.

Figure 4-22 A photo of the PIFA.

4.5.1 Measurement setup

Direct measurement of voltage and current (and hence impedance) is not practical at high frequencies when circuit elements become a significant fraction of the wavelength. Instead, quantities that are easier to measure are the reflection coefficient, a ratio of the incident and scattered waves. The relationships between input impedance, return loss, VSWR and the reflection coefficient are discussed in Appendix C.

In this study, the input impedance of the PIFA has been measured using a network analyser (NA) (HP8753C from HP) over a frequency range spanning from 600 MHz to 1200 MHz. For accurate measurements, great care has been taken to calibrate the network analyser with respect to the reference plane as shown in Figure 4-23.

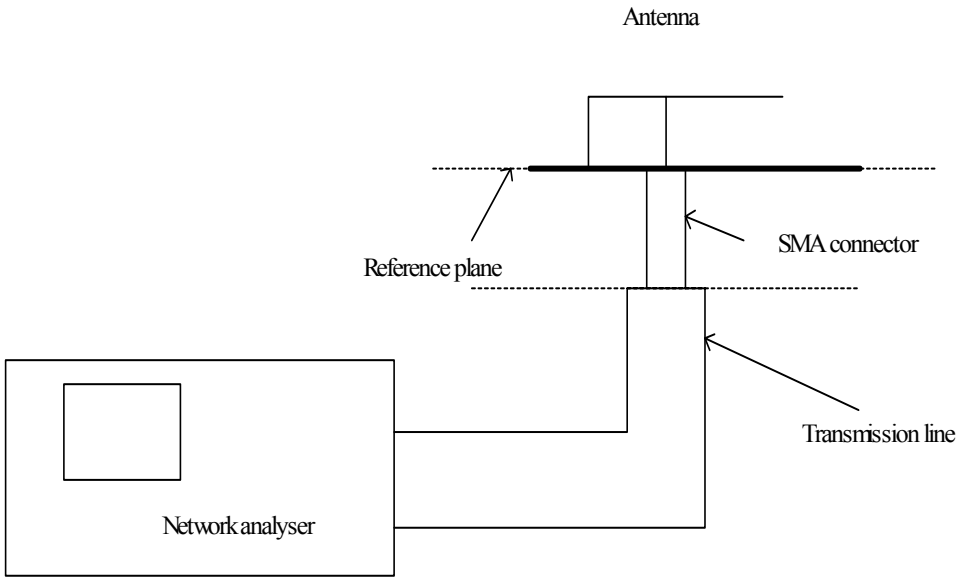

Figure 4-23 Experimental setup for measuring the antenna input impedance, return loss and VSWR**.**

4.5.2 Comparison of results

First, the input impedance and return loss of the test PIFA have been obtained from the measured S-parameters and are shown in Figure 4-24 and Figure 4-25, respectively. From these figures, it is observed that the measured results agree well with the simulated ones over the frequency range of 600 MHz to 1200 MHz.

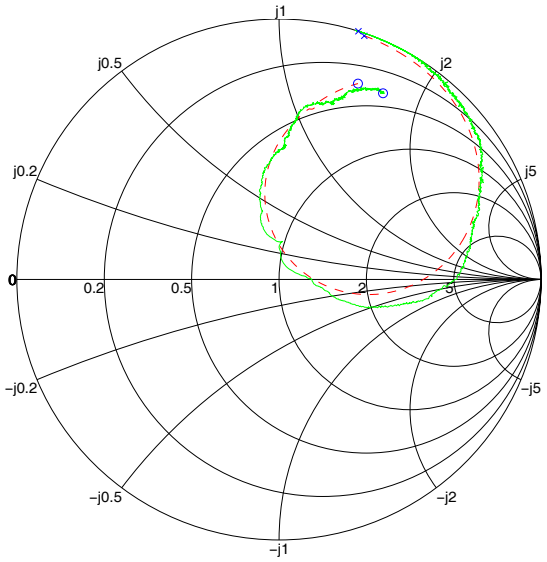

Smith Chart: 0.6 Ghz (blue "x") to 1.2 GHz (blue "o"); Z_0 = 50 Ohm

Figure 4-24 Comparison of the MOM simulated and measured input impedance for the test PIFA (red dot line – simulated, green solid line – measured; "x" - start frequency, "o"- stop frequency).

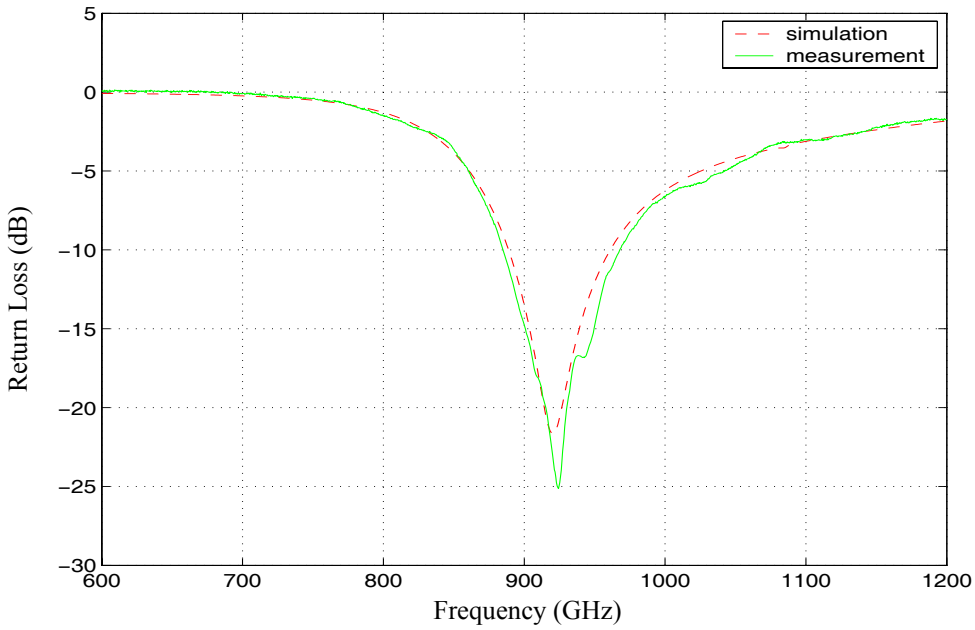

Figure 4-25 Comparison of the MOM simulated and measured return loss (for a 50 Ohm match) for the test PIFA (red dot line – simulated, green solid line – measured).

In the next experiment, a dielectric sheet was placed in contact with the top plate of the PIFA with the aid of a styrofoam block of relative permittivity $\varepsilon_r \cong 1.05$. The size of the dielectric sheet measuring 265mm x 80mm is much larger than the top plate of the antenna (55.5 mm x 30 mm). This experimental setup is to validate the simulated model of the PIFA covered by a dielectric layer without an air gap, as shown in Figure 4-13 (a). Both the simulated and measured results showing the percentage changes in the PIFA's resonant frequency and bandwidth for the two different dielectric materials are tabulated in Table 4-2. The measured results of Table 4-2 indicate that a larger dielectric constant or a thicker layer of the dielectric cover has a greater influence on the resonant frequency and bandwidth of the PIFA. This is the same observation as derived from the simulated results of Table 4-2. Furthermore, Table 4-2 shows that measured and simulated values of the changes in resonant frequency and bandwidth due to the presence of the dielectric cover layer are in reasonable agreement.

Table 4-2 Changes of the input characteristics of the dielectric-covered PIFA without an air gap (Figure 4-13 (a))

Dielectric Cover	ε_r	d (mm)	Resonant frequency change (%)		Bandwidth change (%)	
			Measured	Simulated	Measured	Simulated
Styrofoam	1.05	11.00	0.3	0.4	-0.3	-2.7
R4003	3.38	1.52	4.9	4.6	-12.3	-17.3
		3.05	7.8	7.3	-20.6	-26.7
FR-4	4.4	1.52	5.8	6.5	-15.5	-17.3
		3.05	8.9	9.9	-21.2	-25.3

For the third experiment, a styrofoam sheet with a thickness of 11 mm, having a dielectric constant very close to air, is inserted between the dielectric sheets and the top plate of the PIFA. This styrofoam sheet is used to emulate an air gap between the dielectric layer and the top plate of the antenna as shown in Figure 4-13 (b). Table 4-3 shows both the measured and simulated changes in the resonant frequency and bandwidth of the antenna in the presence of a 11 mm air gap. From this table, similar

findings to the ones found from Table 4-2 are obtained. A comparison of Table 4-2 and Table 4-3 shows that the influence of the dielectric cover layer can be reduced by introducing an air gap. Both tables show that the measured and simulated results agree fairly well. Comparing the above results, it is concluded that there is good agreement between the numerical and experimental values. This gives confidence in our MOM computational model.

Table 4-3 Changes of the input characteristics of the dielectric-covered PIFA with an air gap (Figure 4-13 (b))

Dielectric Cover	ε_r	d (mm)	Resonant frequency change (%)		Bandwidth change (%)	
			Measured	Simulated	Measured	Simulated
Styrofoam	1.05	11.00	0.3	0.4	-0.3	-0.9
R4003+ Styrofoam	3.38	1.52	1.3	0.9	-10.5	-11.0
		3.05	2.2	1.3	-14.6	-15.2
FR-4+ Styrofoam	4.4	1.52	1.5	1.1	-9.9	-10.5
		3.05	2.3	1.5	-15.1	-6.0

4.6 Summary

The influence on the input characteristics of a PIFA on a finite ground plane, due to the positions of the short-circuit plate and the feed wire, and whereabouts the PIFA is mounted on the ground plane has been investigated. It is found that the short-circuit plate "movement" has a stronger effect on the resonant frequency than "movement" of the feed wire. On the other hand, the effect of the feed point "movement" produces a slighter increase in bandwidth change than the short-circuit plate "movement" does. Also, when an antenna is designed to have a minimum volume, both the feed wire and the short-circuit plate should be located on the same edge of the top patch. However, such a design would suffer from a minimum achievable bandwidth. Since the feed wire "movement" has a significantly larger influence on the bandwidth than the resonant frequency, it may be a good design compromise to consider fixing the short-circuit plate

at the edge of the top plate while moving the feed point away from the edge to obtain the required bandwidth. In addition, it is observed that the resistance of the antenna at resonance increases when the feed wire is moved away from the short-circuit plate along the x-axis. This particular characteristic of the PIFA provides a convenient way for antenna impedance matching. Furthermore, it is observed that the position where the PIFA assembly is located on the finite ground plane could greatly alter the input characteristics of the antenna. For a PIFA to resonate at the lowest frequency, it should be located in the corner of the ground plane. This observation suggests that for a given resonant frequency, the size of a PIFA could be made smaller if it is located at the edge of the ground plane. However, for a PIFA to achieve a maximum bandwidth it is desirable to have it mounted in the middle of the ground plane. It is found that the ratio of the bandwidth to resonant frequency could be varied from 3.5 % to 8.5 % just by locating the PIFA at different locations on the ground plate. These two seemingly contradictory requirements for small size and wide bandwidth call for some form of compromise in the actual PIFA implementation. These results indicate that the location of the antenna on the finite ground plane must be taken into account in the design.

The effects of dielectric loading on the performance of PIFAs have also been investigated by computer simulations and experimental measurements. Both the simulated and experimental results, which have been found to be in fairly good agreement, show that the resonant frequency, input impedance and bandwidth of the PIFA are significantly affected when a thick sheet of high dielectric constant is attached to the top plate. For example, the resonant frequency could decrease by more than 9% from 909.5 MHz, when the PIFA is covered by a 3.048 mm thick dielectric sheet with a dielectric constant of 4.4. The simulated results of the distribution of the surface current on the top patch confirm the type of behaviour exhibited in the study of input impedance. When a dielectric cover layer is located close to the PIFA, the resonant frequency of the antenna is shifted to a lower frequency because the effective length of the current flow on the top patch becomes longer. Thus the distribution of the surface current magnitude on the patch varies noticeably even though it is still corresponding to the TM_{100} mode at a new resonant frequency. These changes are determined by the dimensions, positions and dielectric constant of the cover layer. These observations help to provide appropriate adjustments to the dimensions of the PIFA to account for

the influence of the dielectric layer in the design stage of such a dielectric-covered antenna. Moreover, as is expected, the efficiency of the antenna is lowered when a dielectric material with a large loss tangent is used, that is, the loss tangent of the cover layer will have a significant impact on the gain of the antenna. For example, a cover layer of FR-4 with a thickness of 1.6 mm resulted in the gain dropping more than 0.5 dB at 900 MHz band. However, there was almost no impact on the gain when a low loss tangent RG4003 was used. Furthermore, this study shows that if a sufficiently large air gap, such as 0.03λ, is introduced between the dielectric sheet and the top plate of the PIFA, the influence of the dielectric layer is reduced significantly.

CHAPTER FIVE

5. PERFORMANCE ANALYSIS OF PIFA ENCLOSED WITHIN A RECTANGULAR DIELECTRIC RADOME

5.1 Introduction

In chapter 4, the effect of a top dielectric cover layer on the performance of a 900 MHz PIFA has been investigated numerically and experimentally. The results show that such effects could cause the operating performance of the antenna to fall outside the design specifications. In the previous investigation, the side parts of the dielectric casing are assumed to be far away from the radiating element compared with that of the top part. This suggests that the dielectric radome can then be considered as a dielectric layer of infinite extent and the effects of the side parts of the radome may be ignored. Thus the MPIE based MOM technique that is used in the IE3D can be efficiently applied to modelling and analysing the problem at hand.

However, when a dielectric radome is used to protect an antenna from its environment, the spacings separating the antenna and the dielectric radome in all directions are usually small compared to the operating wavelength to keep the radome-antenna system low profile and compact. Under such a situation, the loading of the dielectric radome including the side parts will have to be accounted for in studying the radiation characteristics of the antenna system. Without proper design consideration, this may result in an antenna system with poor performance. As discussed in section 4.2, the IE3D using the MPIE based MOM technique is not able to deal with dielectric objects of arbitrary shapes, because the Green's function used can only satisfy the multi-layered environment.

In this chapter, the performance of a PIFA enclosed in a rectangular dielectric radome has been extensively studied using MOM to solve surface integral equations (SIEs) for electric and magnetic currents over dielectric boundary surfaces and perfect electric conductors (PECs). This technique, proposed by Kolundzija (Kolundzija, 1999), can be

used to model and analyse composite metallic and dielectric structures of arbitrary shapes. The input and radiation characteristics of this 900 MHz radome enclosed PIFA have been analysed, including a study of the effects introduced by each individual part of the radome. The study has also been extended to include the influence of a dielectric radome on a PIFA designed to operate at 2400 MHz, a popular frequency band used in Wi-Fi Wireless Local Area Network (WLAN).

5.2 Formulation of the Problem

Inhomogenous dielectrics may be modeled as part by part homogeneous dielectrics. Hence, any composite metallic and dielectric structure can be represented as the electromagnetic system consisting of a finite number of finite-size linear, homogenous, and isotropic regions, situated in an unbounded linear, homogeneous, and isotropic environment, as shown in Figure 5-1 (a) (Kolundzija *et al*, 1999). Often, this environment is a vacuum, but it can also be another medium (e.g., water).

Some of the regions can be Perfect Electric Conductors (PEC). In the interior of any such region, the electromagnetic field is always zero. Hence, all of them will collectively be denoted as region 0 and referred to as zero-field regions. Some special cases of zero-field regions are metallic wires and plates. Plate forming an open surface can be considered as a degenerated case of a zero-field region, where one dimension of the region, e.g. thickness, is considered to be zero.

Besides these zero-field regions, electromagnetic fields are generally existing in other regions. These regions will collectively be referred to as non-zero-field regions. The total number of such regions, is denoted by n. The medium filling out region i is assumed to be described by its complex permittivity, $\varepsilon^{(i)}$, and permeability, $\mu^{(i)}$, i = 1,…, n, which can include losses. In any of these regions, there may exist impressed electric and magnetic fields, $\mathbf{E}_{inc}^{(i)}$ and $\mathbf{H}_{inc}^{(i)}$, i = 1,…, n, whose angular frequency is ω.

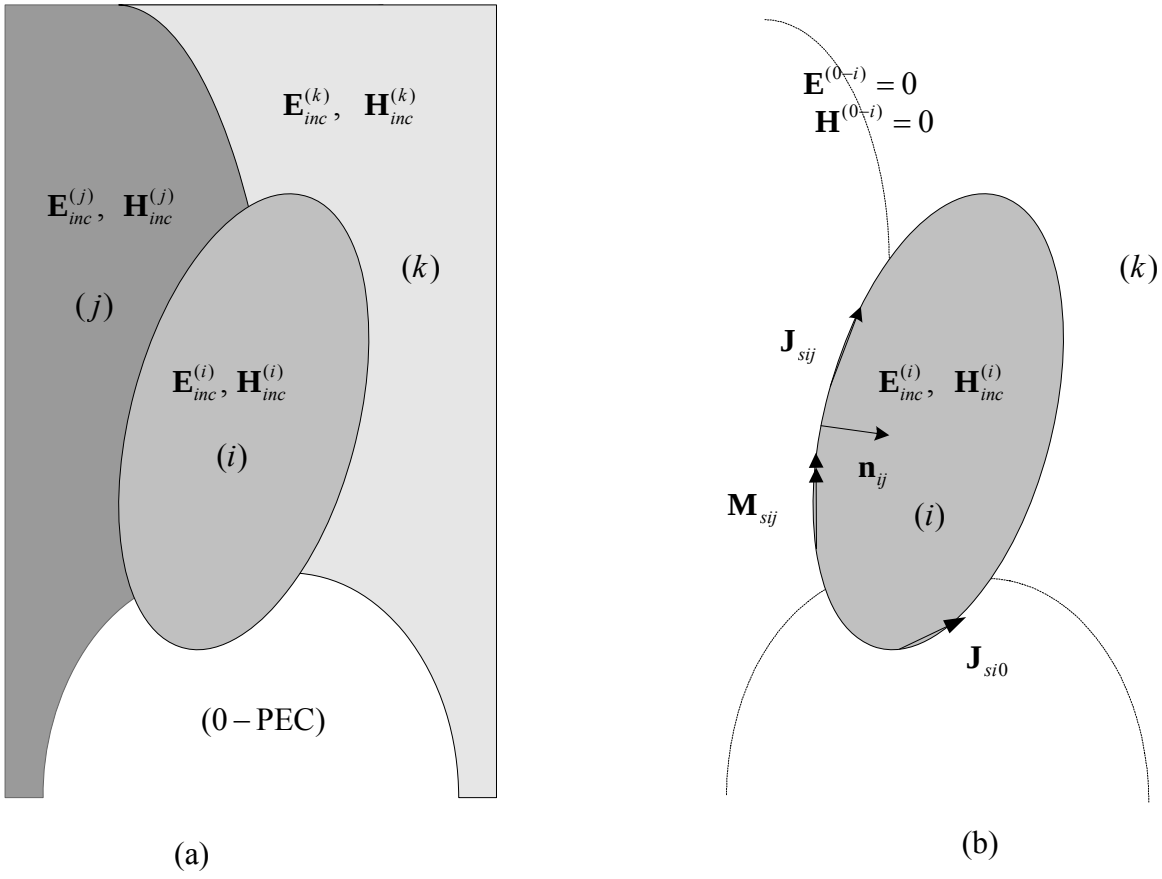

Figure 5-1 Decomposition of a multiple-region problem into single-region problem: (a) original Problem; b) equivalent Problem for Region *i*.

Kolundzija (Kolundzija *et al*, 1999) extends the MOM technique for analysing metallic and dielectric structures of arbitrary shapes using the Surface Equivalence Theorem (SET). According to the SET, the influence of all sources outside region *i* can be replaced by equivalent currents placed at the boundary surface of region *i*, in which case the field outside region *i* becomes zero, as shown in Figure 5-1 (b). Hence, the region outside region *i* is denoted as region 0-*i* (i.e., region 0 with respect to region *i*, in the equivalent problem for region *i*). Since the field outside region *i* is zero it can be homogenised with respect the region *i*, i.e., it can be filled by the same material as region *i*. Thus, a multiple-region problem, say n-regions, may be decomposed into *n* single-region problems.

The densities of equivalent currents at the boundary surface between region *i* and *j* are

$$\mathbf{J}_{sij} = \mathbf{n}_{ij} \times \mathbf{H}^{(i)} \tag{5.1a}$$

$$\mathbf{M}_{sij} = -\mathbf{n}_{ij} \times \mathbf{E}^{(i)} \tag{5.1b}$$

where $\mathbf{n}_{ij}$ is the unit normal directed from region *j* to region *i*, and $\mathbf{E}^{(i)}$ and $\mathbf{H}^{(i)}$ are the electric and magnetic fields at the boundary surface, just inside region *i*. If equivalent currents for region *j*, $\mathbf{J}_{sji}$ and $\mathbf{M}_{sji}$, are considered, they are evaluated according to equation (5,1), but with the indices *i* and *j* interchanged. That is

$$\mathbf{J}_{sji} = \mathbf{n}_{ji} \times \mathbf{H}^{(j)} \tag{5.2a}$$

$$\mathbf{M}_{sji} = -\mathbf{n}_{ji} \times \mathbf{E}^{(j)} \tag{5.2b}$$

Since there are no currents between region *i* and *j*, the fields $\mathbf{H}^{(i)}$ and $\mathbf{H}^{(j)}$, and the fields $\mathbf{E}^{(i)}$ and $\mathbf{E}^{(j)}$ satisfy the boundary conditions

$$\mathbf{n}_{ij} \times (\mathbf{H}^{(i)} - \mathbf{H}^{(j)}) = 0 \tag{5.3a}$$

$$\mathbf{n}_{ij} \times (\mathbf{E}^{(i)} - \mathbf{E}^{(j)}) = 0 \tag{5.3b}$$

After expressing the field vectors in terms of the equivalent currents according to equation (5.1) and (5.2), and using $\mathbf{n}_{ij} = -\mathbf{n}_{ji}$, the equivalent currents are related as

$$\mathbf{J}_{sij} = -\mathbf{J}_{sji} \tag{5.4a}$$

$$\mathbf{M}_{sij} = -\mathbf{M}_{sji} \tag{5.4b}$$

Thus, *n* single-region problems are mutually coupled through conditions (5.3) and (5.4). By satisfying these conditions, it is able to guarantee uniqueness of the solution for both sources and fields. In this case, the distributions of the equivalent electric and magnetic currents at the boundary surfaces of single-region problems, which satisfy conditions (5.3) and (5.4), are evaluated.

5.3 Field Integral Equation

The field integral equations are derived from the boundary conditions of equation (5.3). The total electric field in region *i* can be expressed as

$$\mathbf{E}^{(i)} = \sum_{k=0}^{n} \mathbf{E}^{(i)}(\mathbf{J}_{sik}, \mathbf{M}_{sik}) + \mathbf{E}_{inc}^{(i)} \tag{5.5}$$

where $\mathbf{E}_s^{(i)}(\mathbf{J}_{sik}, \mathbf{M}_{sik})$ represents the scattered field inside region *i*, produced by the currents placed on the boundary surface between regions *i* and *k*. $\mathbf{E}_{inc}^{(i)}$ is the corresponding incident field. The scattered field, just inside region *i*, due to the currents placed on the boundary surface of regions *i* and *k*, is

$$\mathbf{E}^{(i)}(\mathbf{J}_{sik}, \mathbf{M}_{sik}) = -Z^{(i)} L^{(i)}(\mathbf{J}_{sik}) + K^{(i)}(\mathbf{M}_{sik}) \tag{5.6}$$

where $Z^{(i)}$ is the intrinsic impedance of the medium filling region *i*, and $L^{(i)}$ and $K^{(i)}$ are operators defined by

$$L^{(i)}(\mathbf{J}_{sik}) = \gamma \int_{S_{ik}} \left[\mathbf{J}_{sik}(\mathbf{r}'_{ik}) G^{(i)}(\mathbf{r} \mid \mathbf{r}') - \frac{1}{\left[r^{(i)} \right]^2} \nabla_{sik} \bullet \mathbf{J}_{sik}(\mathbf{r}''_{ik}) \nabla G^{(i)}(\mathbf{r} \mid \mathbf{r}') \right] dS'_{ik}$$

(5.7)

and $$K^{(i)}(\mathbf{M}_{sik}) = \int_{S_{ik}} \mathbf{J}_{sik}(\mathbf{r}''_{ik}) \times \nabla G^{(i)}(\mathbf{r} \mid \mathbf{r}') dS'_{ik} \tag{5.8}$$

where $G^{(i)}(\mathbf{r} \mid \mathbf{r}')$ is the Green function in region *i*, given by

$$G^{(i)}(\mathbf{r} \mid \mathbf{r}') = \frac{e^{-\gamma^{(i)} r}}{4\pi r}, \quad r = \left| \mathbf{r} - \mathbf{r}'_{ik} \right|, \quad \gamma^{(i)} = j\omega\sqrt{\varepsilon^{(i)} \mu^{(i)}} \tag{5.9}$$

$\mathbf{r}'_{ik}$ is the position vector of the source point and $\mathbf{r}$ is the position vector of the field point. ∇_{sik} acts on $\mathbf{r}'_{ik}$, which is inside surface S_{ik}, and ∇ acts on $\mathbf{r}$. γ and $\gamma^{(i)}$ are the complex propagation constants in free space and region *i*, respectively. Finally,

after replacing (5.5) and (5.6) for regions i and j into (5.3a), the integral equation is obtained in the form of

$$\mathbf{n}_{ij} \times \left\{ \sum_{\substack{k=0 \\ k \neq i}}^{n} \left[Z^{(i)} L^{(i)}(\mathbf{J}_{sik}) - K^{(i)}(\mathbf{M}_{sik}) \right] - \sum_{\substack{k=0 \\ k \neq j}}^{n} \left[Z^{(j)} L^{(j)}(\mathbf{J}_{sjk}) - K^{(j)}(\mathbf{M}_{sjk}) \right] \right\}$$

$$= \mathbf{n}_{ij} \times (\mathbf{E}_{inc}^{(i)} - \mathbf{E}_{inc}^{(j)}) \qquad (5.10)$$

In a similar way, the integral equation from the magnetic field boundary condition (5.3b) can also be obtained, which is dual to integral equation (5.10).

Note that in the case when one of the two regions having a common boundary surface is a PEC, the magnetic currents at the boundary surface are equal to zero. As a result, equation (5.10) degenerates into the EFIE.

Thus, a set of SIEs for the unknown electric and magnetic currents is obtained. This set can then be solved by the MOM.

5.4 Radome-enclosed PIFA Configuration

The antenna system under investigation in this chapter consists of a PIFA enclosed by a rectangular dielectric radome as shown in Figure 5-2. In an attempt to reduce the computation time, it is assumed that the PIFA is located on an infinite ground plane and the short-circuit plate occurs in the middle of the edge of the top patch. This results in the geometry of the radome-antenna system being symmetrical in the xz plane. Consequently, only half of the geometry needs to be considered in the computer model, giving rise to a saving in the computation time due to halving the unknown elements.

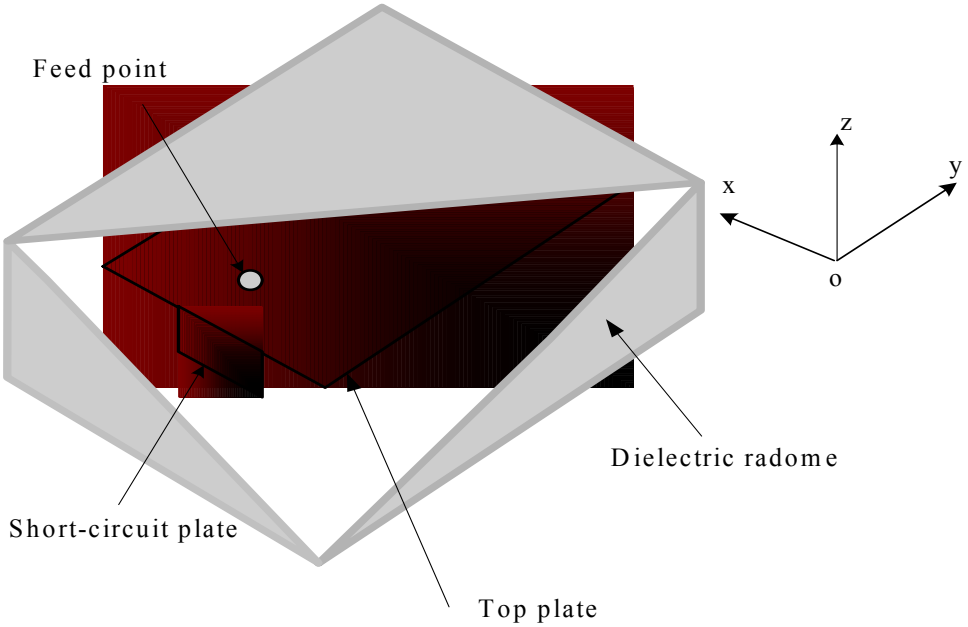

Figure 5-2 A PIFA enclosed by a rectangular dielectric radome.

Figure 5-3 shows the cross sectional (a) and top (b) views of this radome-enclosed PIFA. The top radiating patch parallel to the ground plane measures L_2 by L_1 with a height of H. It is fed by a probe located d_f away from the short-circuit plate, which has a width of W_s and the same height as the top radiating patch. The thickness of the dielectric radome is d. The relative dielectric constant and loss tangent of this dielectric are ε_r and $\tan\delta$, respectively. The radome is maintained at a distance d_{top} from the top patch, a distance d_{side} from the side edges of the top patch, a distance d_{open} from the open end of the top patch, and a distance d_{short} from the short-circuit plate.

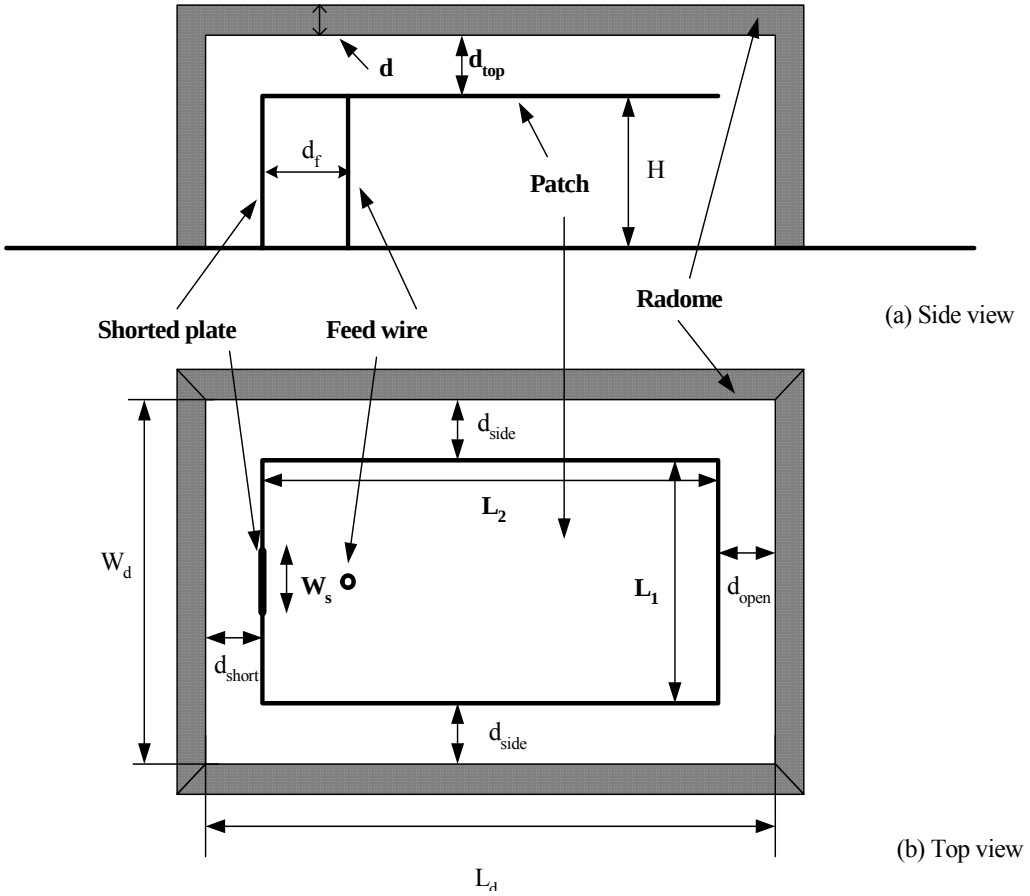

Figure 5-3 A PlFA enclosed by a rectangular dielectric radome: (a) cross-sectional view; (b) top view.

5.5 MOM Modelling

The configuration of the radome-enclosed PIFA, shown in Figure 5-2, has been modelled using a MOM based electromagnetic simulator, WIPL-D (Kolundzija *et al*, 2000). The basis for this code is given in sections 5.2 and 5.3. This simulator makes use of the SIEs and is able to model composite metallic and dielectric structures of arbitrary shapes. The SIEs in the WIPL-D are solved by using the Galerkin's method, which is the same method as that used in the IE3D.

5.5.1 PIFA

A PIFA has been designed to operate without a radome at a 900 MHz band. This antenna is considered to be the reference for comparing the results presented later in this chapter. The geometry of this antenna is shown in Figure 5-4, with dimensions chosen to be L_2 = 55 mm, L_1 = 35 mm, H = 15 mm, W_s = 15 mm, and d_f = 12 mm.

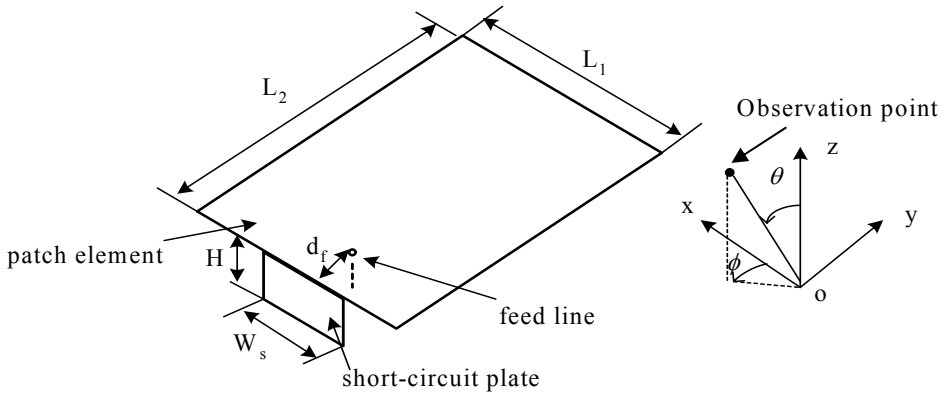

Figure 5-4 The geometry of the reference PIFA.

Often, the fast variations of the electromagnetic field in the vicinity of the metallic patch edges makes it difficult for low-order polynomial expansions to be properly approximated. However, computations for this model of the PIFA converge very slowly with increasing orders of current expansions. Consequently, the edges of the

patch plate have been modelled as separate narrow strips, as shown in Figure 5-5, to account for such edge effects. In this case, the total number of unknown currents is 26 at the maximum frequency of 1200 MHz for the simulation.

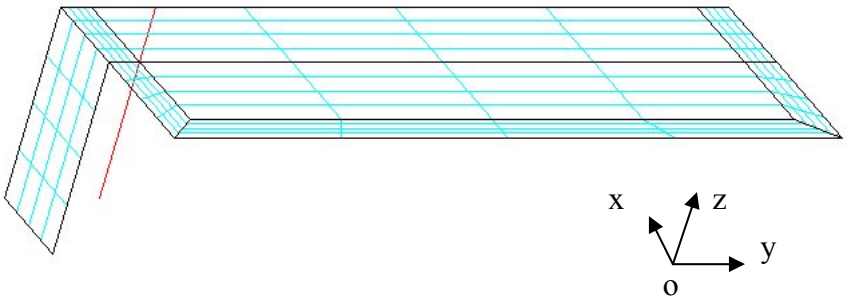

Figure 5-5 The MOM computer model of the PIFA.

The simulated input impedance, and return loss of the PIFA alone are shown as red dashed curves in Figure 5-6, and Figure 5-7, respectively. Also, the radiating 2D polar azimuth and elevation gain patterns of the antenna are shown as red dashed curves in Figure 5-8 and Figure 5-9, respectively. Figure 5-10 shows its 3D gain patterns. Note that the radiation patterns have been normalised to the maximum gain of the antenna.

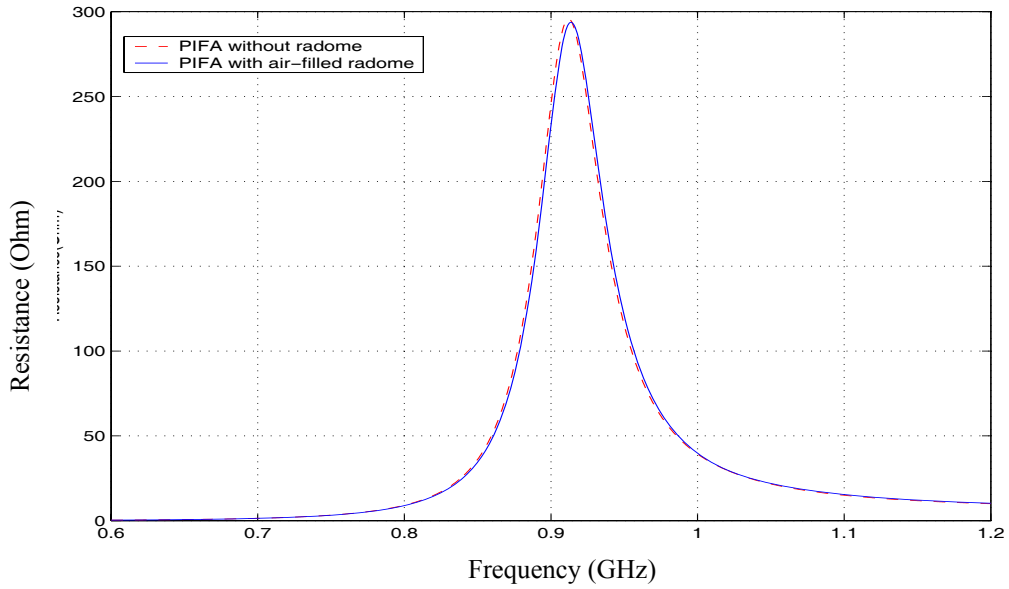

(a)

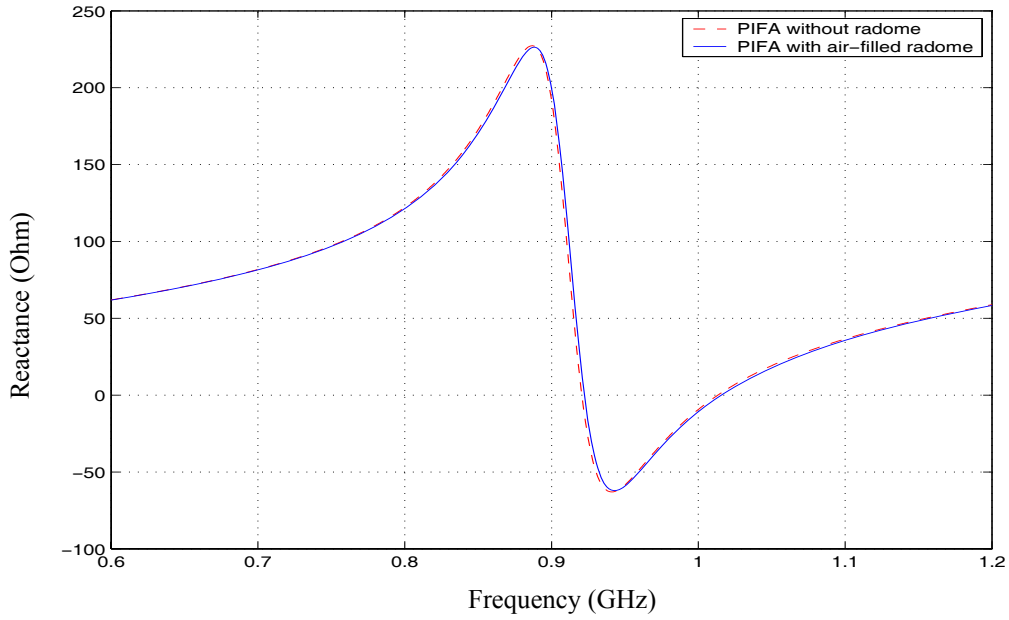

(b)

Figure 5-6 The simulated input impedances for the PIFA alone, and with an air-filled radome: (a) resistance; (b) reactance.

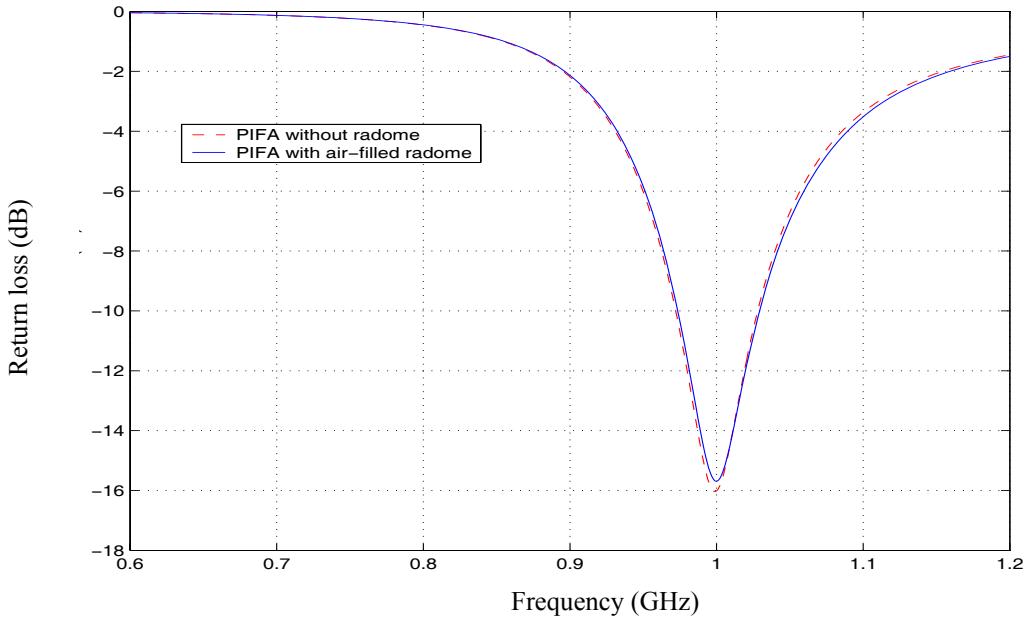

Figure 5-7 The simulated return loss results of the PIFA alone, and with an air-filled radome.

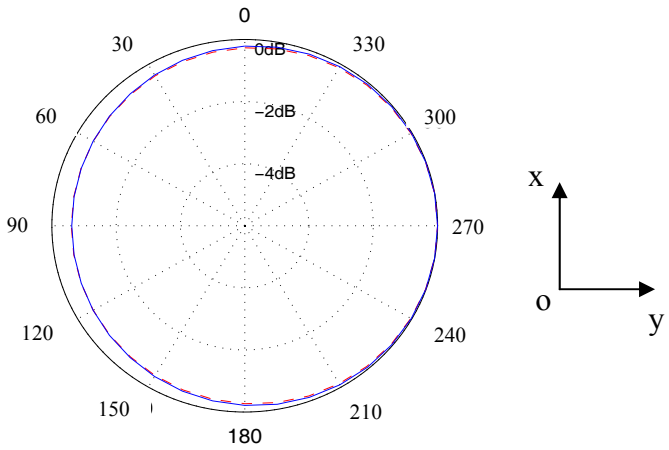

Figure 5-8 The 2D polar azimuth patterns of the PIFA alone, and with an air-filled radome.

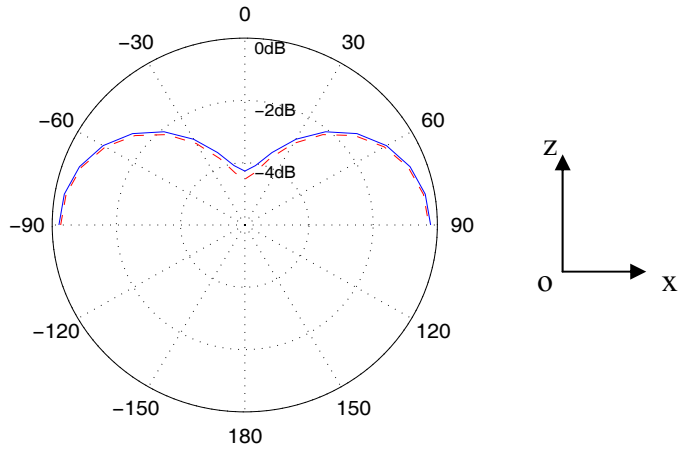

Figure 5-9 The 2D polar elevation patterns of PIFA alone, and with an air-filled radome.

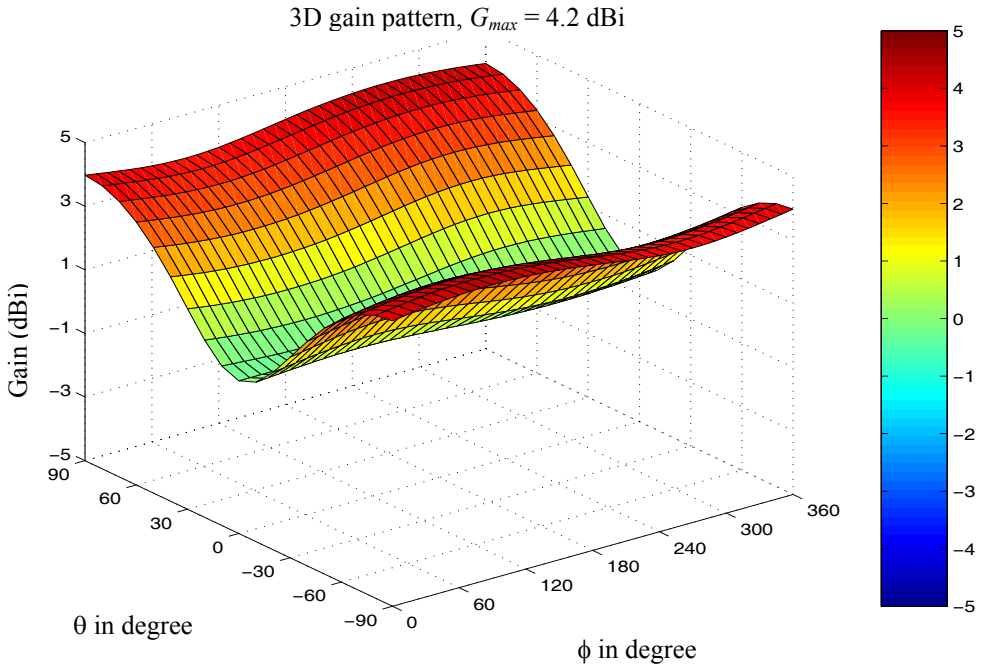

(a)

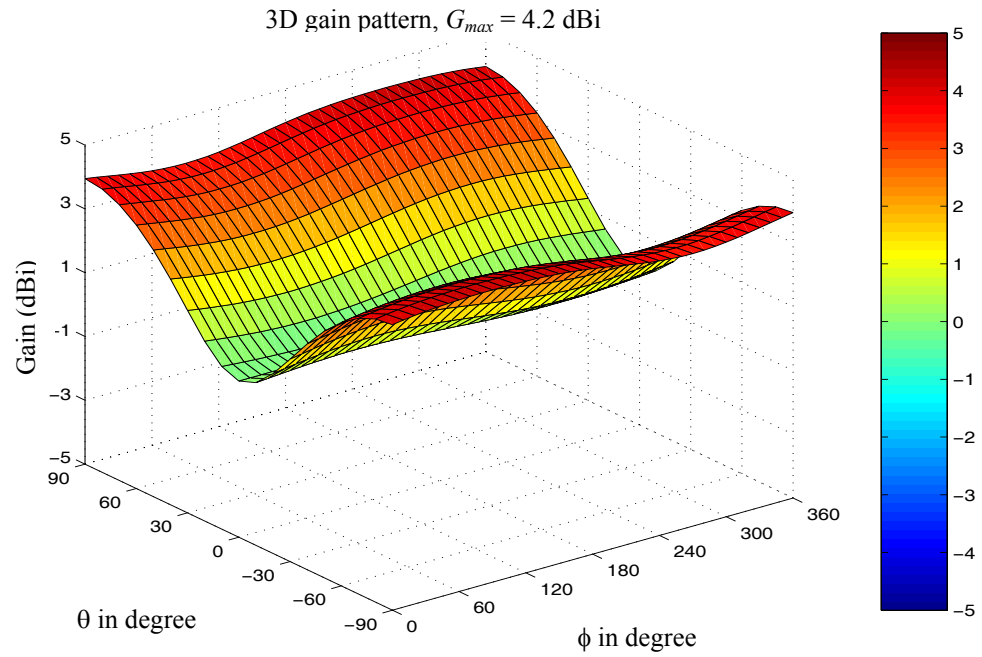

(b)

Figure 5-10 The 3D gain pattern of the PIFA: (a) without the radome; (b) with an air-filled rdaome.

From Figure 5-6 and Figure 5-7, it is found that the antenna resonates at 1013.2 MHz with a return loss of less than –15 dB and the bandwidth of the impedance of the antenna for VSWR $\leq$ 2 is around 59.46 MHz. From Figure 5-8, Figure 5-9 and Figure 5-10, it can be noted that the PIFA has an almost omni-directional radiation pattern in the xy plane but the gain in the – y direction and in the $\pm$ x directions are around 0.5 dB and 0.2 dB less than the maximum gain, respectively. The maximum gain, which occurs at the x direction, is 4.2 dBi. In the yz plane, the PIFA has a null in the z direction, where the gain is more than 4 dB but lower than the maximum gain. This shows that the top patch is not the main radiating plate.

5.5.2 Modelling of a rectangular dielectric radome

A model for the PIFA alone has been established in section 5.5.1. In this section, the PIFA with a rectangular dielectric radome is modelled. Figure 5-11 shows the model of the PIFA combined with its rectangular dielectric radome. In this figure, the plates with the cyan grid lines represent the metallic plates, which are immersed in one domain only. They are accompanied by a single electric current sheet. The plates with the red grid lines represent the boundary surfaces between two dielectric domains, i.e., air and radome dielectric material. They are accompanied by equivalent electric and magnetic current sheets. In this configuration, the geometry of the PIFA is the same as the one given in section 5.4. The internal dimensions of the dielectric radome, as shown in Figure 5-3, are $L_d = L_2 + 0.017\lambda_0$, and $W_d = L_1 + 0.017\lambda_0$, where λ_0 is the free space wavelength at the resonant frequency of the PIFA. In this model, the total number of unknowns to be solved is 186 at the maximum frequency of 1200 MHz, including 106 electrical currents and 80 magnetic currents. Compared with the model of the PIFA alone, the unknowns of 160 have increased due to the presence of the dielectric radome.

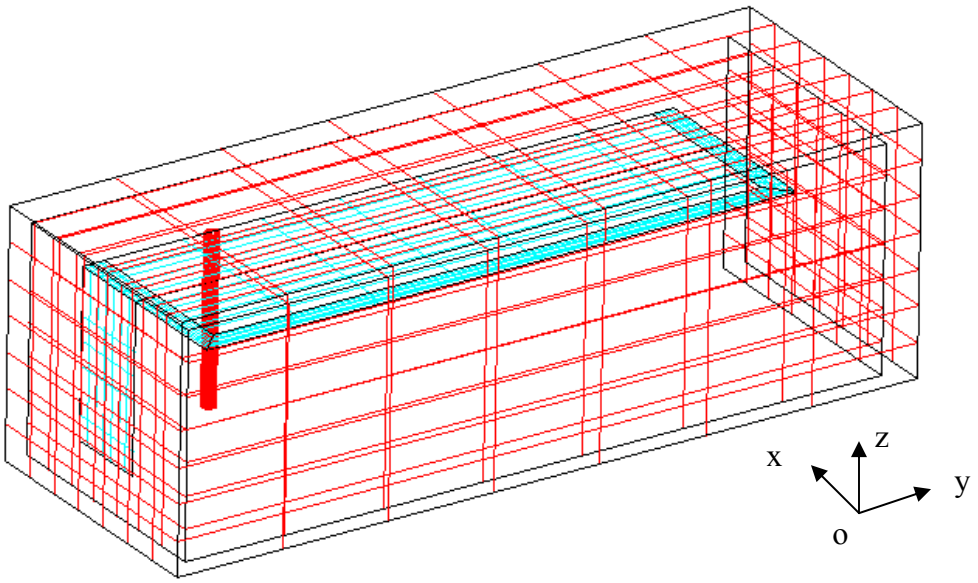

Figure 5-11 The MOM computer model of the PIFA with a rectangular dielectric radome.

5.5.3 Validation of the MOM model

5.5.3.1 Model of PIFA with an air–filled radome

The accuracy of the proposed radome-antenna model has been verified by simulations carried out by specifying that the relative dielectric constant of the radome dielectric is equal to 1, that is, the material of the radome is air. The results including input impedance, return loss, and 2D radiation patterns for this air-filled radome-PIFA model are also shown in Figure 5-6 to Figure 5-9, as blue solid lines. The 3D gain radiation pattern for this model is shown in Figure 5-10 (b). From these figures, it can be noted that the PIFA with an air-filled radome gives the same results as obtained without a radome, both in input and radiation characteristics. This has validated the use of this radome-antenna model.

5.5.3.2 Power balance check

The accuracy and reliability of the simulations have also been validated through the power balance check.

In this case, the power applied to the antenna, P_{gen}, is expended as radiation, P_{rad} and loss, P_{loss}, such that

$$P_{gen} = P_{rad} + P_{loss} \tag{5.11}$$

The error currents dJ and dM representing the differences between the approximate currents estimated by WIPL-D and their exact values, are considered as impressed currents. To arrive at a solution, WIPL-D forces the power generated by such impressed currents to be zero. However, related to the analysis method, these error currents radiate into virtual outer spaces of bounded domains (second, third, etc), P_{rad} (2), P_{rad} (3), and so forth. In this case, the total radiated power is given by

$$P_{rad} = P_{rad}(1) + P_{rad}(2) + \ldots \tag{5.12}$$

Often, P_{rad} (1) is close to P_{rad}, which means that the error currents are small and the solution is therefore satisfactory. If P_{rad} (1) is not close to P_{rad}, then the error currents are not small and the numerical solution would have to be improved upon. In order to improve the solution, the current expansion orders need to be increased or the geometrical model may need to be redefined.

When the integrals involved in WIPL-D analysis are calculated there remains some numerical error. This error results in either power generation or power loss, P_{num}. In the case of antennas, this power is determined by:

$$P_{num} = P_{gen} - P_{rad} - P_{loss} \tag{5.13}$$

When P_{gen} is close to (P_{rad} + P_{loss}), it means that P_{num} can be neglected. If P_{gen} is not close to (P_{rad} + P_{loss}), then the SIEs involved in the analysis are not accurately evaluated and the solution is not satisfactory. The accuracy of these SIEs can be improved by increasing the order of the numerical integration formulas. However, the CPU time needed for integration will necessarily increase.

To evaluate whether the model adopted is accurate or not, an internal check of the power balance has been conducted. The power balances associated with the PIFA alone and the PIFA enclosed by an air-filled radome are given in Table 5-1 and Table 5-2, respectively. For both of these models, it is assumed there is no loss, so that P_{loss} is zero. From these two tables, it is observed that in both cases the power due to numerical errors may be neglected. The absolute maximum ratio of P_{num} to P_{rad} is less than 2.3 %, over the frequency range of from 600 MHz to 1200 MHz, which points to a very good solution.

Table 5-1 The power balance associated with a PIFA alone

Freuquency (GHz)	0.60	0.67	0.73	0.80	0.87	0.93	1.00	1.07	1.13	1.20
Prad (1) (mW)	4.0757E-02	7.5176E-02	1.4522E-01	3.0420E-01	7.3833E-01	2.3898E+00	1.2052E+01	9.2207E+00	2.8710E+00	1.4044E+00
Prad (mW)	4.0688E-02	7.5176E-02	1.4522E-01	3.0420E-01	7.3833E-01	2.3898E+00	1.2052E+01	9.2207E+00	2.8710E+00	1.4044E+00
Prad(1)/Prad (%)	100.168	100.000	100.000	100.000	100.000	100.000	100.000	100.000	100.000	100.000
Pgen (mW)	4.0757E-02	7.5326E-02	1.4549E-01	3.0495E-01	7.4035E-01	2.3969E+00	1.2091E+01	9.2530E+00	2.8819E+00	1.4101E+00
Pgen/Prad (%)	100.168	100.200	100.183	100.249	100.273	100.298	100.324	100.351	100.379	100.408
Pnum/Prad (%)	-0.168	-0.200	-0.183	-0.249	-0.273	-0.298	-0.324	-0.351	-0.379	-0.408

Table 5-2 The power balance of a PIFA with an air-filled radome

Freuquency (GHz)	0.60	0.67	0.73	0.80	0.87	0.93	1.00	1.07	1.13	1.20
Prad (1) (mW)	4.0397E-02	7.4457E-02	1.4365E-01	3.0030E-01	7.2548E-01	2.3226E+00	1.1719E+01	9.8870E+00	3.0241E+00	1.4633E+00
Prad (2) (mW)	4.8700E-05	4.5500E-05	4.4000E-05	4.8000E-05	6.2000E-05	1.2000E-04	4.0000E-04	4.1000E-04	1.4000E-04	8.0000E-05
Prad (mW)	4.0445E-02	7.4502E-02	1.4369E-01	3.0035E-01	7.2554E-01	2.3228E+00	1.1719E+01	9.8874E+00	3.0242E+00	1.4634E+00
Prad (1)/Prad (%)	99.880	99.939	99.969	99.984	99.991	99.995	99.997	99.996	99.995	99.995
Prad (2)/Prad (%)	0.120	0.061	0.031	0.016	0.009	0.005	0.003	0.004	0.005	0.005
Pgen (mW)	3.9535E-02	7.3061E-02	1.4111E-01	2.9509E-01	7.1291E-01	2.2822E+00	1.1513E+01	9.7129E+00	2.9708E+00	1.4376E+00
Pgen/Prad (%)	97.749	98.065	98.199	98.249	98.258	98.253	98.243	98.235	98.233	98.238
Pnum/Prad (%)	2.251	1.935	1.801	1.751	1.742	1.747	1.757	1.765	1.767	1.762

5.6 Performance of Radome-enclosed PIFA Operating at 900 MHz

In this section, the effects of a rectangular dielectric radome on the input and radiation characteristics of a PIFA operating in the 900 MHz band are studied. Then, the effects due to each of the individual parts of this radome are examined to gain a better understanding on the interactions between the antenna and the radome. Furthermore, a series of investigations have been carried out to determine the effects of the radome on the various parameters of the PIFA, such as resonant frequency, bandwidth, radiation pattern and gain, due to different thickness of the radome, the separation between the radome and the antenna patch, and the dielectric constant and the loss tangent of the radome material used.

5.6.1 Effect of a rectangular dielectric radome

The PIFA described in section 5.5.1 is adopted as a reference for this study. In this section, the influence of a rectangular dielectric radome on the performance of the PIFA has been investigated. The material of the radome is considered to have a relative dielectric constant of 4.66, which is typical of the dielectric constant used in FR-4 printed circuit board. The internal-dimensions of the radome are 59 mm long x 39 mm wide x 17 mm high. The thickness of the radome is 2 mm.

Figure 5-12 shows the input impedances of the radome-PIFA with (green dotted curve) and without (blue solid curve) considering the radome material loss. The lossy radome material has a loss tangent of 0.155. Also, as a reference, the input impedance of this PIFA without a radome is plotted as a red dashed curve in Figure 5-12. The return loss curves, which are used to determine the bandwidth of the antennas, are plotted in Figure 5-13. For this study, the bandwidth is calculated based on a VSWR of not more than 2.

- 94 -

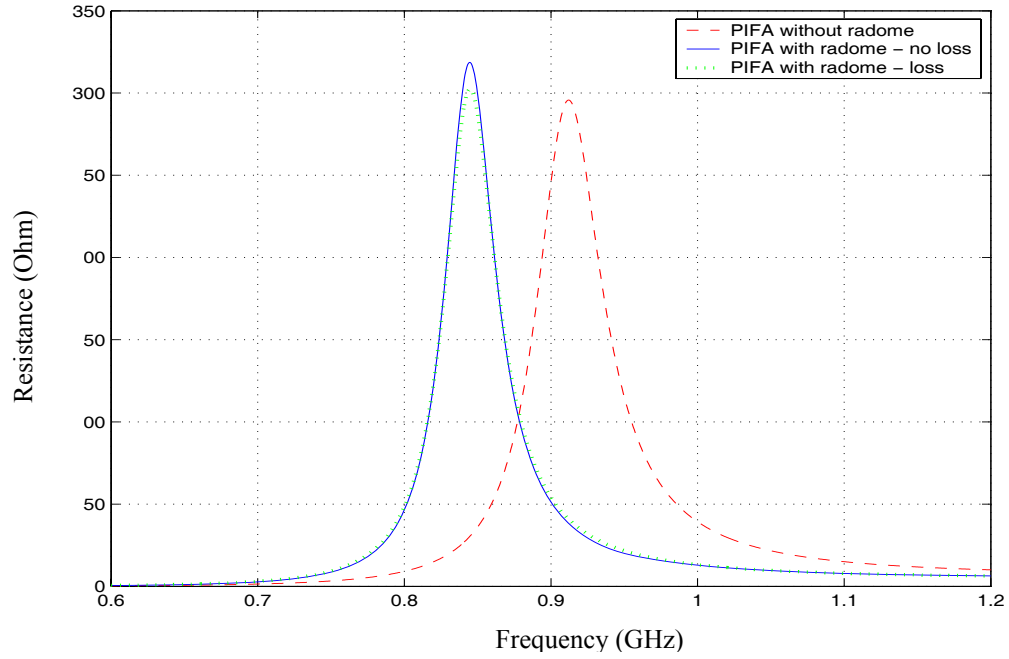

(a)

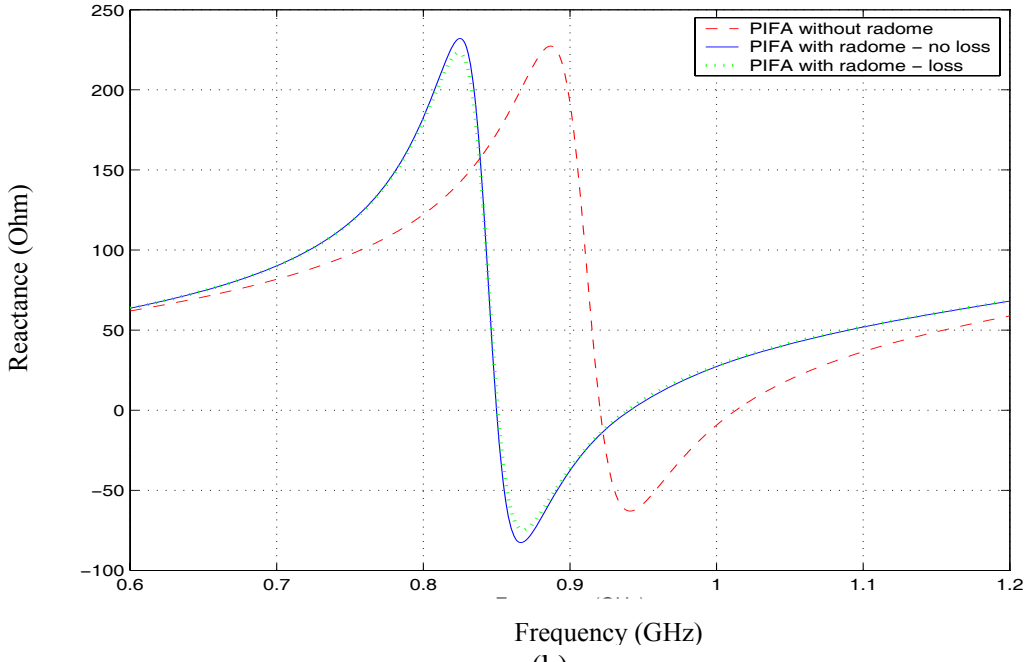

(b)

Figure 5-12 Comparison of the input impedance of a PIFA when it is enclosed by a rectangular dielectric radome with different electrical properties: (a) resistance; (b) reactance.

- 95 -

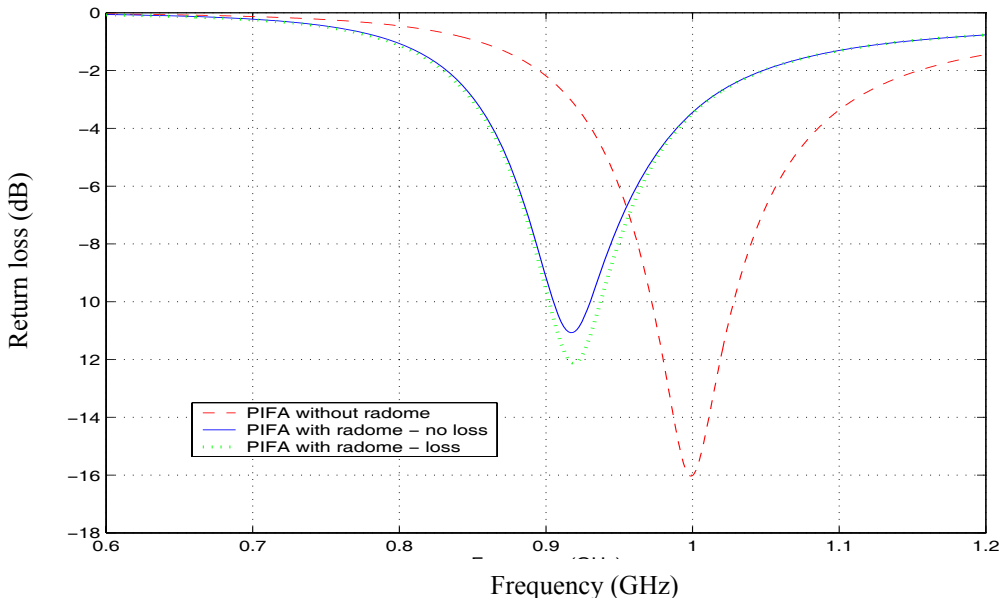

Figure 5-13 The return loss of the PIFA when it is enclosed by a rectangular dielectric radome with and without loss.

It can be noted in Figure 5-12 that in the presence of a radome, the frequency responses of both the resistance and the reactance of the antenna are shifted to a lower frequency. Moreover, it is observed that the loss tangent of the radome material affects only slightly this shift in frequency, but it does reduce the peak value of the resonance of the input impedance due to the lower Q. Compared to the case without a radome, the resonant frequency is shifted from 1015.6 MHz to 941.1 MHz (zero loss tangent) and to 939.6 MHz (with loss tangent of 0.155). Furthermore, it is observed from Figure 5-13 that the bandwidth of the antenna has been reduced from 59.5 MHz to 30.6 MHz (zero loss tangent) and to 39 MHz (with loss tangent of 0.155). Table 5-3 lists the electrical parameters associated with these three different operating conditions of the PIFA.

- 96 -

Table 5-3 The influence of rectangular dielectric radome on the resonant frequency, input impedance and bandwidth of a PIFA.

Dielectric parameters	Resonance frequency (MHz)	Input impedance (Ohm)		Bandwidth (MHz)
		Real part	Imaginary part	
1-j0	1015.6	31.6	-0.03	59.5
4.66-j0	941.1	22.5	0.08	30.6
4.66-j0.155	939.3	25.2	-0.11	39.0

For comparison, the percentage changes in resonant frequency and bandwidth with reference to the PIFA without the radome are tabulated in Table 5-4.

Table 5-4 The percentage changes of resonant frequency, and bandwidth of a PIFA enclosed in a rectangular dielectric radome.

Dielectric parameters	Resonant frequency change (%)	Bandwidth change (%)
4.66-j0	-7.3	-48.5
4.66-j0.0155	-7.3	-45.5
4.66-j0.155	-7.5	-34.3

Also, the influence of a radome on the radiation pattern of the PIFA has been investigated. Figure 5-14 and Figure 5-15 depict the polar azimuth pattern with $\theta = 90^o$, and the elevation pattern with $\phi = 0^o$, respectively, of the PIFA enclosed in a radome. The blue solid line is associated with a radome material of no loss, while the red dotted curve represents the case without a radome. The radiation pattern has been normalised against the maximum magnitudes obtained in each case. Compared with no radome, Figure 5-14 shows that the gain of the PIFA at $\theta = 90^o$ is reduced by 0.2 dB in both the + and - x directions in the presence of the radome. However, no noticeable change has been observed in both the + and - y directions when the PIFA is enclosed in the rectangular dielectric radome. From Figure 5-15, it can be seen that the magnitude in the yz plane at $\phi = 0^o$ is reduced. For example, the radiation magnitude is reduced by up to 0.5 dB at the z direction and by 0.3 dB at both of the + and - y directions.

- 97 -

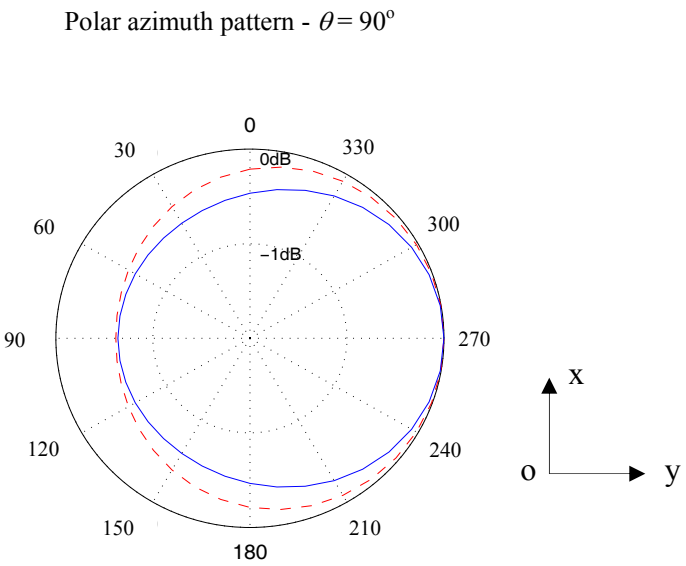

Figure 5-14 The 2D polar azimuth gain patterns of an PIFA without (red) and with dielectric radome of no loss (blue).

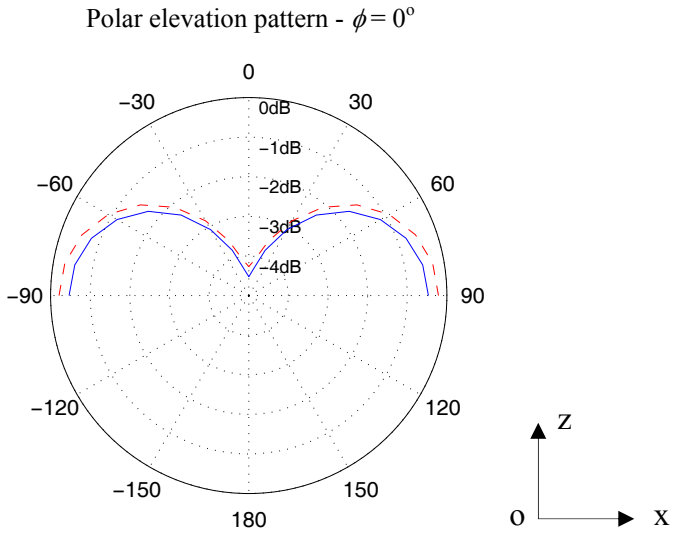

Figure 5-15 The 2D polar elevation gain patterns of an PIFA without (red) and with dielectric radome of no loss (blue).

- 98 -

The radiation patterns for the antenna enclosed in the lossy radome are plotted as green dotted lines in Figure 5-16 and Figure 5-17. For comparison, the azimuth and elevation patterns for the case with a radome of no loss are also plotted on the same figures as red dashed lines. From Figure 5-16 and Figure 5-17, it can be noted that there is almost no change in the radiation patterns for the two cases considered.

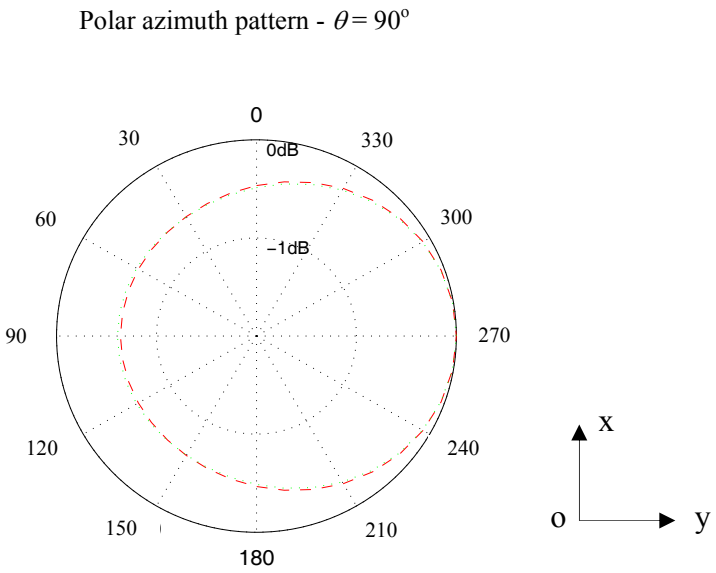

Figure 5-16 The 2D polar azimuth gain patterns of a rectangular dielectric radome enclosed PIFA without (red) and with (green) considering the dielectric loss.

- 99 -

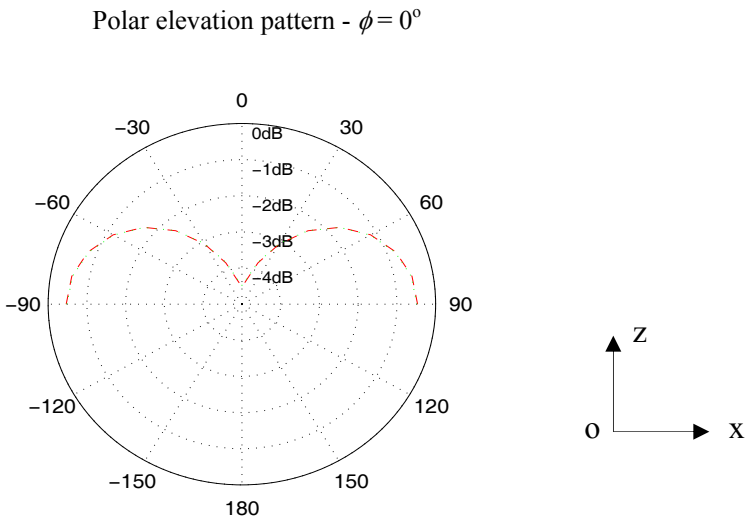

Figure 5-17 The of 2D polar elevation gain patterns of a rectangular dielectric radome enclosed PIFA without (red) and with (green) considering the dielectric loss.

Figure 5-18 and Figure 5-19 show the 3D gain patterns for the antenna enclosed in a radome of no loss and a radome with loss, respectively. It can be observed that the shapes of the patterns for both of these two cases are similar, except that the average gain for the lossy case is lower than the one of the lossless case. The maximum gains obtained for these two cases are listed in Table 5-5. For comparison, the maximum gain of this antenna without a radome is also tabulated. It is observed that the maximum gain of the antenna is only slightly affected by the dielectric constant of the radome material. However, the loss tangent of the radome material is a dominant factor in reducing the maximum gain of the antenna, as shown in Table 5-6.

The above observations can be explained by referring to the distributions of the surface currents of the antenna in those cases, as discussed in section 4.4.3. Due to the presence of the radome, the current density has been changed even though the current flow on the patch still corresponds to the current distribution of the TM_{100} resonant mode at its new resonant frequency. The distribution of the surface current on the patch is mainly determined by the dimensions and positions and dielectric constant of the radome,

- 100

rather than the loss tangent of the radome material, which determines the surface current magnitude.

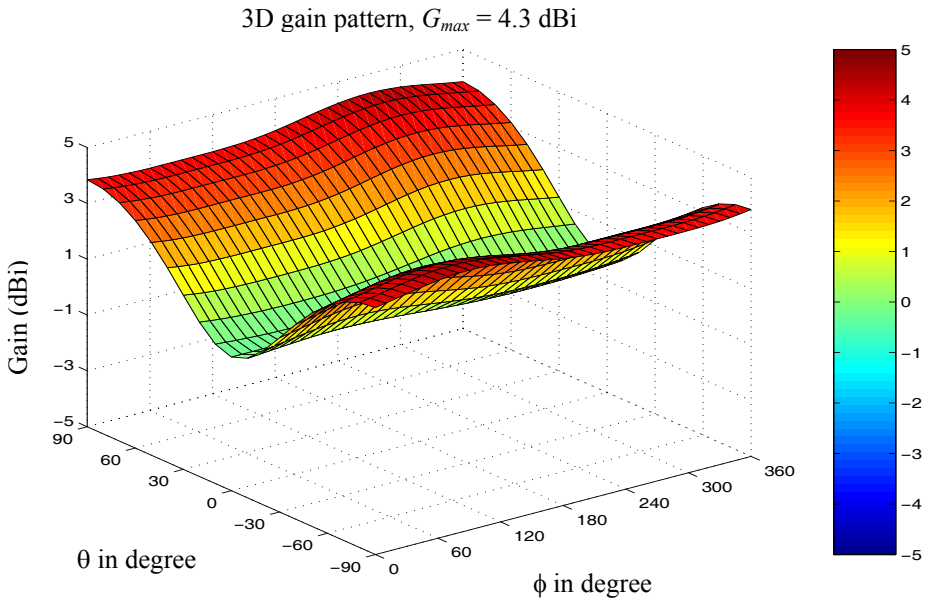

Figure 5-18 The 3D gain pattern of a rectangular dielectric radome–PIFA without considering the dielectric loss.

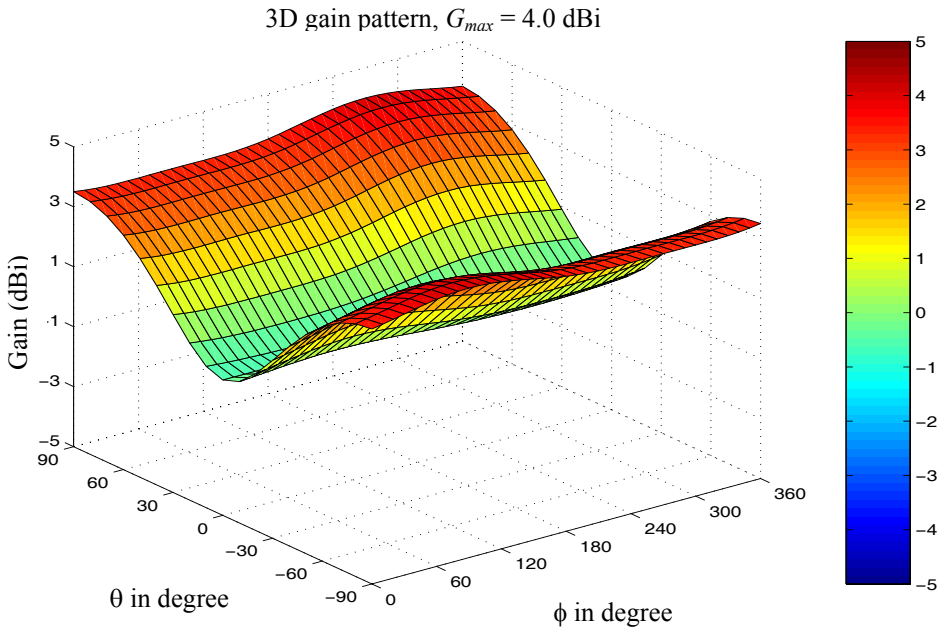

Figure 5-19 The 3D gain pattern of a rectangular dielectric radome-PIFA with considering the dielectric loss.

- 101

Table 5-5 Gains achieved with PIFA only, PIFA with radome of no loss, and PIFA with a lossy radome

PIFA	Dielectric parameters	Gain (dBi)
No radome	1-j0	4.2
With lossless radome	4.66-j0	4.3
With lossy radome	4.66-j0.155	4.0

Table 5-6 Percentage changes of gain of a PIFA with a radome of different lossy materials.

Dielectric parameters	Gain change (%)
4.66-j0	0.2
4.66-j0.0155	-0.2
4.66-j0.155	-4.5

5.6.2 Effect of each individual part of a radome

In this section, the effect on the performance of the PIFA caused by the presence of an individual component of the radome is investigated. This is an attempt to determine the most desirable placement of the PIFA within a given radome. For this study, the rectangular dielectric radome is considered to be made up of five composite parts, i.e., the one parallel to the top patch of the PIFA is referred to as the "top"; the one parallel to the short-circuit plate of the PIFA is referred to as the "short"; the one located at the open end of the PIFA is referred to as the "open"; and the two others located respectively at the both sides of the PIFA are referred to as the "side".

Figure 5-20 shows the input impedance of the PIFA, in terms of resistance (a) and reactance (b), due to the presence of one of these individual radome parts. For comparison, the input resistance and reactance associated with the PIFA without the radome (referred to as the "no"), and with the complete rectangular radome (referred to as the "whole") are also shown. The values of the input impedance, and the values of the return loss associated with each individual radome components are plotted in Figure 5-21.

- 102

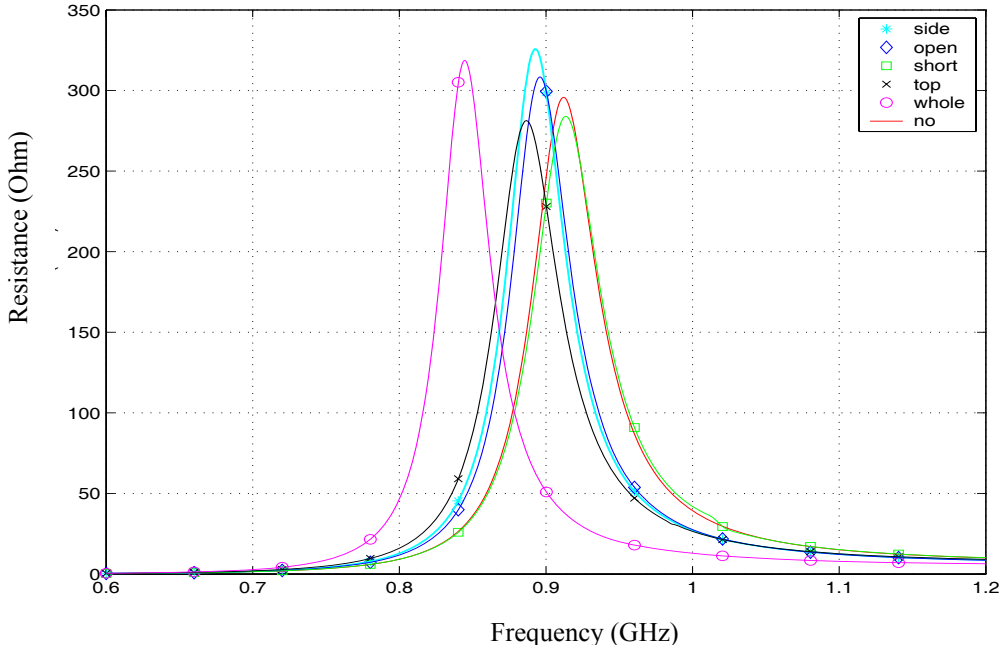

(a)

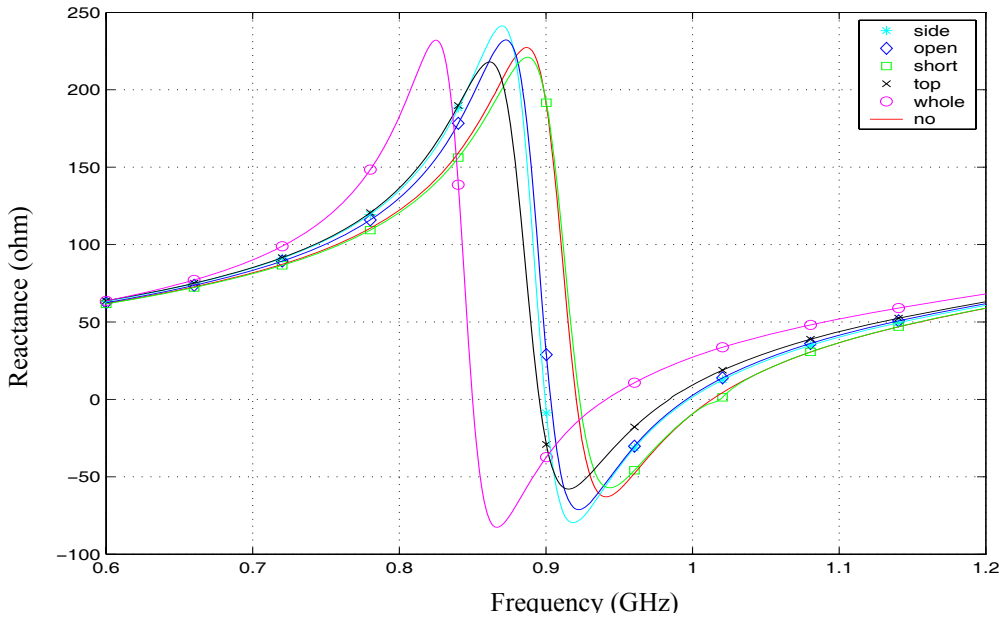

(b)

Figure 5-20 Comparison of the input impedances of the PIFA with the individual radome parts: (a) resistance; (b) reactance.

- 103

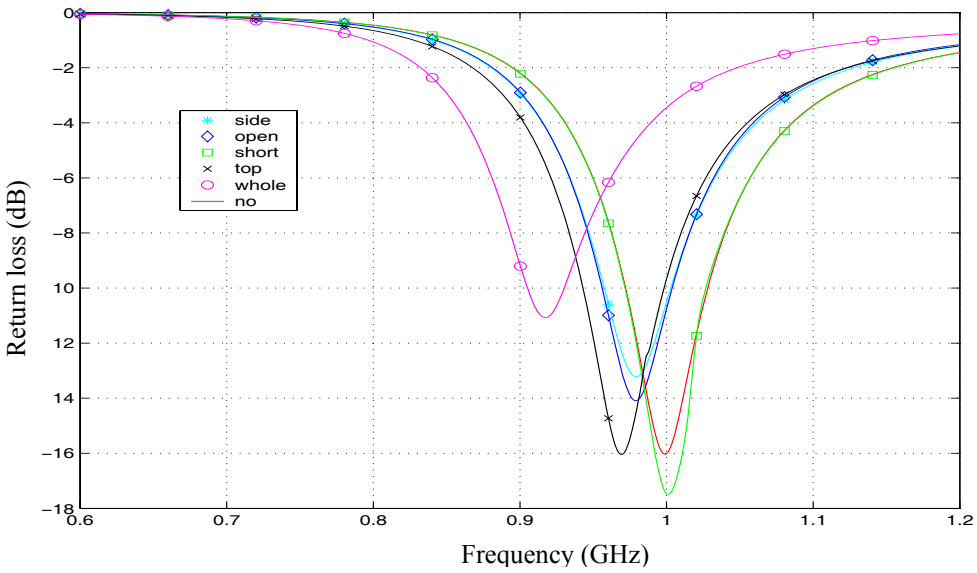

Figure 5-21 Influence of each individual radome part on the return loss of the PIFA.

The resonant frequency, input impedance and bandwidth at the resonant frequency for each of the six cases are tabulated in Table 5-7. Also, the percentage change of these PIFA input parameters obtained with each of the individual radome configurations, in comparison with the respective values obtained without a radome, are also shown Table 5-7. As a result, the following conclusions may be drawn:

1. The effect of each individual part of the radome on the input impedance characteristic of the PIFA is quite different. The "top" part has the strongest influence on the input impedance of the antenna, followed by the "side" and the "open", respectively. The "short" part has the weakest effect. This is to be expected as the fringe field around the short-circuit plate is minimum. Because the fringe fields along all the four edges of the radiating patch interact with the "top" part, this results in the strongest coupling between the "top" part and the antenna. The "side" part has a lesser influence than the "top" part, since it interacts with only the two edges of the radiating patch. However, the "side" part has a greater influence than the "open" part. This is because the side edge of the radiating patch is longer than the open edge and so the coupling between

- 104

the "side" part and the patch becomes larger than that between the "open" and the patch.

2. The presence of each radome part causes the frequency response of the input impedance of the PIFA to shift to a lower frequency except for the "short", which shows minimal change in the resonant frequency, as shown in Table 5-7.

3. Each radome part could cause the bandwidth of the PIFA to alter differently. As observed from Table 5-7, the bandwidth of the PIFA is reduced by the presence of any individual radome part except the "top".

Table 5-7 The input and radiation parameters of the PIFA with individual radome configurations

	Resonant frequency (MHz)	Resonant frequency change (%)	Input impedance at resoance (Ohm)	Input impedance change (%)	Bandwidth (MHz)	Bandwidth change (%)	Gain (dBi)
side	997.6	1.54	27.9	14.2	49.85	16.16	4.3
open	995.8	1.72	29.2	10.1	51.65	13.13	4.34
short	1011.2	0.20	31.0	4.7	58.86	1.01	4.32
top	984.4	2.85	31.7	2.5	59.46	0.00	4.41
whole	941.1	7.11	22.5	30.8	30.63	48.48	4.31
no	1013.2	0.00	32.5	0.0	59.46	0.00	4.16

To study the influence of each individual radome part on the radiation pattern of the antenna, the azimuth and elevation planes due to the presence of a radome part have been obtained and plotted as shown in Figure 5-22 and Figure 5-23, respectively. For comparison purpose, the patterns for the antenna without the radome ("no"), and with the whole radome ("whole") are also shown in these figures. From Figure 5-22, it can be observed that in the xy plane, the "short" part of the radome has a minimum impact on its radiation pattern, that is, there is almost no change in the y-axis of the antenna but only a slight change in the direction normal to the x-axis of the antenna. The "open"

- 105

part has the greatest impact on the patterns among the six radome parts, and its influence is almost the same as that attributed to the "whole" radome. The effect of the "top" on the patterns is less than the "open'' but larger than the "short". The effect of the "side' is quite similar to that of the "top" but also results in a 30 degree rotation counter-clockwise both in the maximum and minimum. It can be noted that the maximum electric field change of the pattern is 0.2 dB.

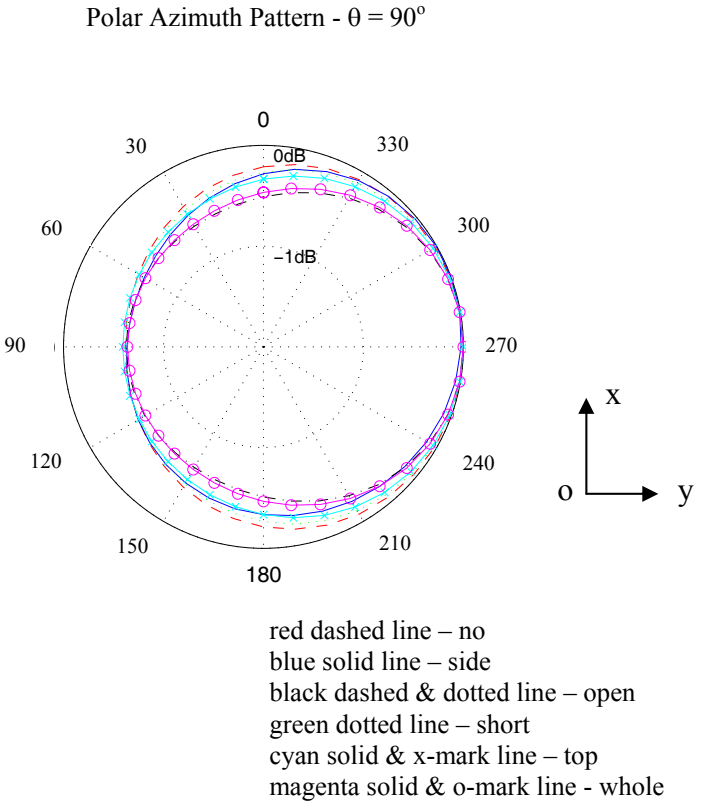

Figure 5-22 The radiation patterns of the PIFA obtained in the presence of an individual radome part as a function of the azimuth angle.

- 106

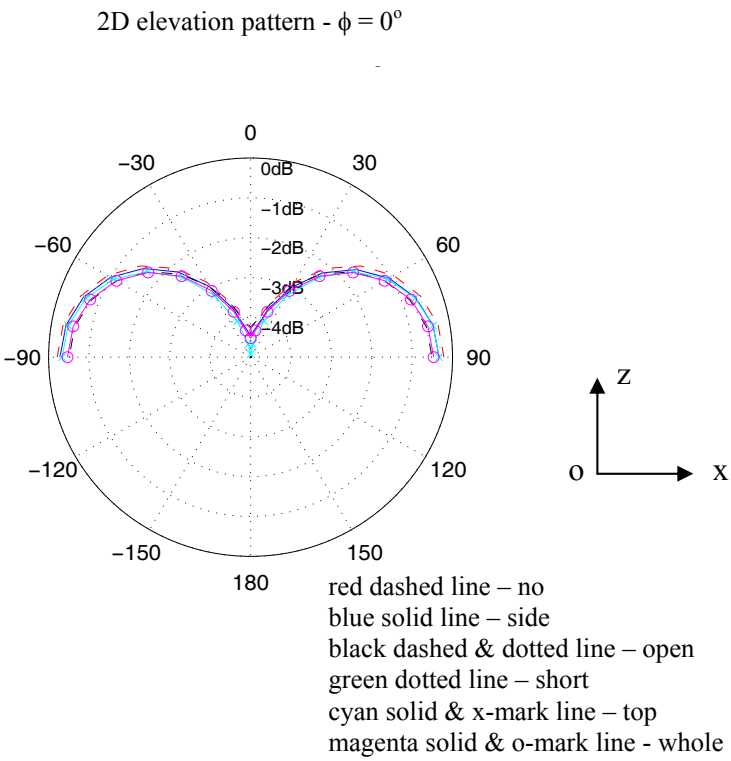

Figure 5-23 The radiation patterns of the PIFA obtained in the presence of an individual radome part as a function of the elevation angle.

From Figure 5-23, it can be observed that in the xz plane, the "open" part has the largest impact on the radiation pattern, causing a gain reduction of about 0.3 dB when observed at the elevation θ of $\pm 90^{o}$. This is followed by the "top", "side" and "short". However, when θ is 0^{o}, the "top" has the dominant influence causing a 0.7 dB decrease in the gain, followed by the "short" and the "side". The "open" seems to make no impact on the pattern in this direction.

Figure 5-24 to Figure 5-27 show the 3D gain patterns of this PIFA in the presence of the "side"", "open", "short" and "top" of the radome, respectively. The corresponding patterns obtained for the no radome and the radome have also been plotted in Figure 5-10 (a) and Figure 5-18, respectively. The maximum gains from these six patterns together with their input parameters are tabulated in Table 5-7. From the table, it may be observed that the presence of any given part of the dielectric radome results in the resonant frequency of the antenna shifting to a lower frequency. This is because when a dielectric object is in close proximity to the antenna, it reduces the effective electrical

- 107

length of the antenna. However, it may be noted that the bandwidth of the antenna is not always reduced due to the presence of such a radome. This depends on the electrical properties, location and dimensions of the radome. For instance, the presence of the "top" causes the resonant frequency to be reduced by 2.85% but the bandwidth stays the same. This observation suggests that it could be possible to design a PIFA system having a smaller size but without any loss of performance, such as bandwidth, through the use of a well-designed radome. In addition, it may be noted that the variation of the maximum gain due to the presence of an individual radome part is less than 0.1 dB for the case when the radome material is lossless.

- 108

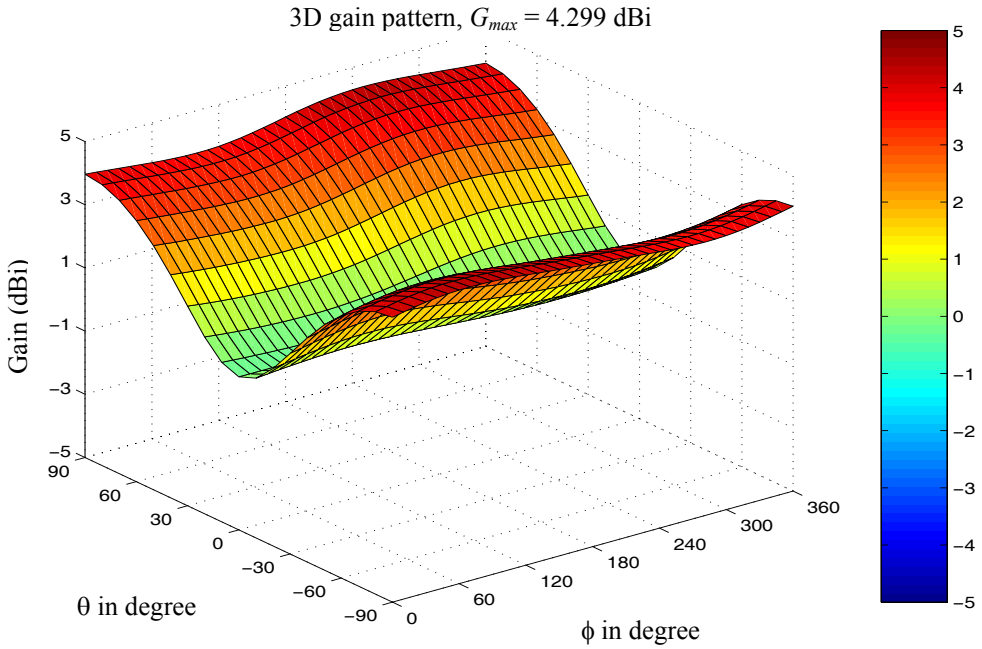

Figure 5-24 The 3D gain pattern of the PIFA with the "side" of the radome.

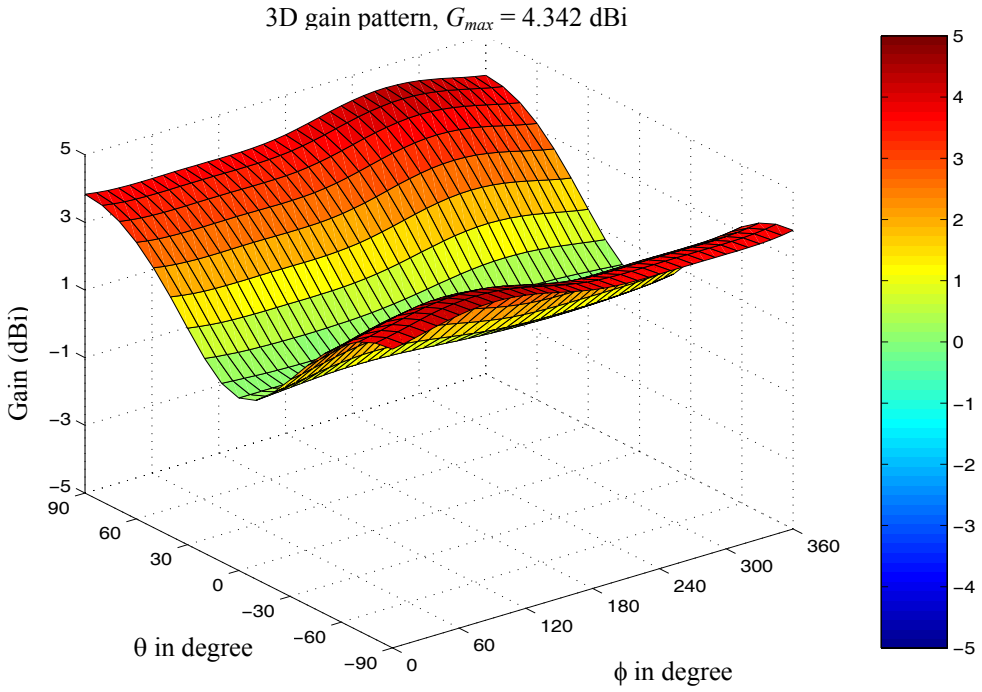

Figure 5-25 The 3D gain pattern of the PIFA with the "open" of the radome.

- 109

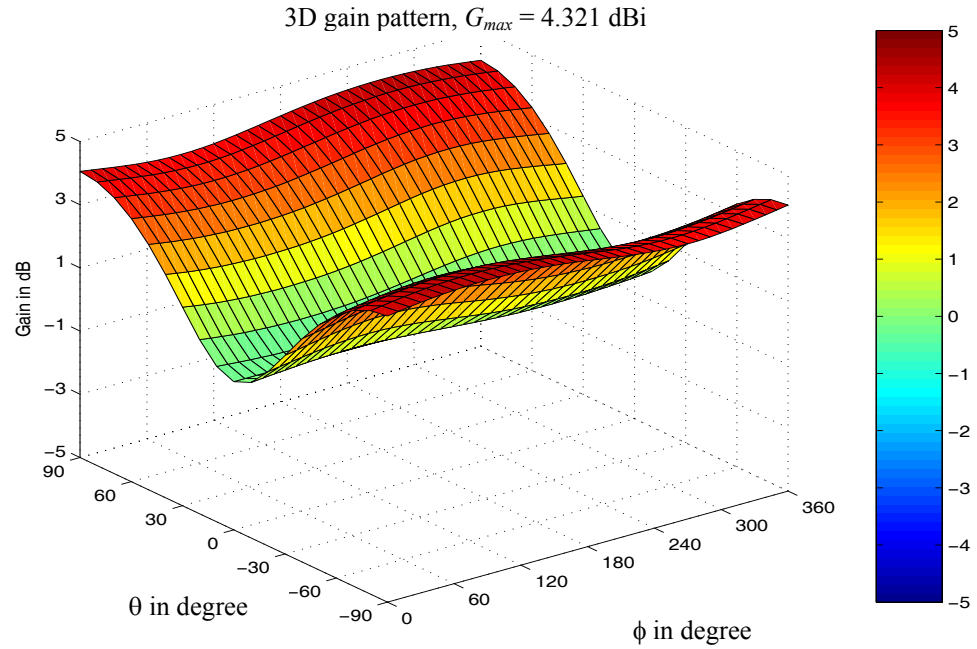

Figure 5-26 The 3D gain pattern of the PIFA with the "short" of the radome.

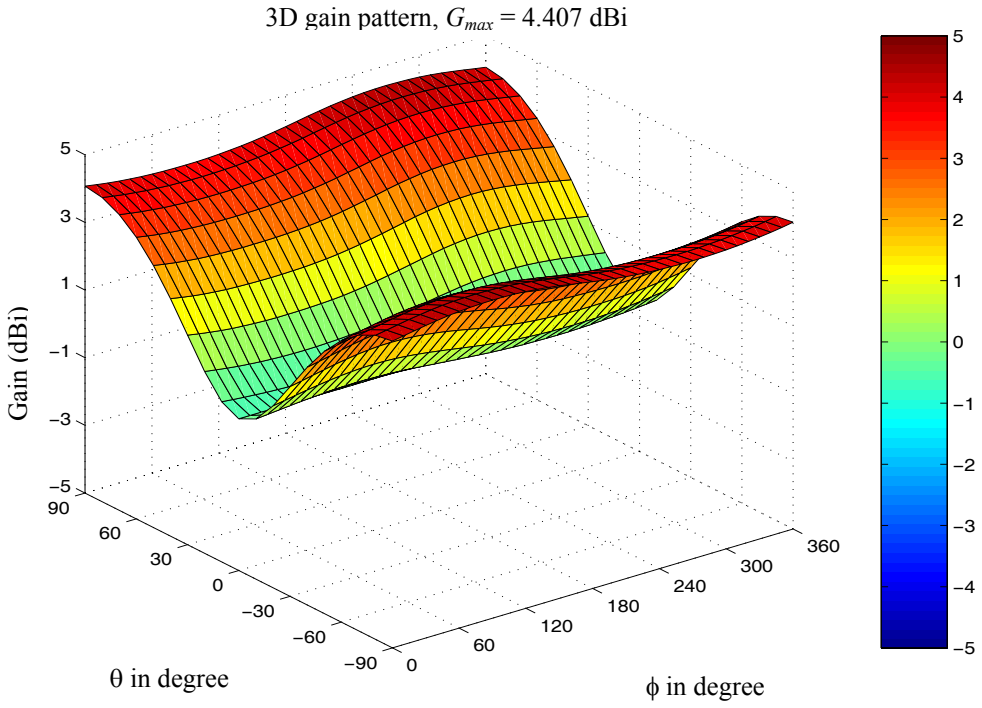

Figure 5-27 The 3D gain pattern of the PIFA with the "top" of the radome.

- 110

5.6.3 Influence of the separation between radome and antenna

In this section, the influence of the separation between the radome and the antenna on the resonant frequency and bandwidth has been studied. To reduce the unknown elements in the simulation model, only the top part of the radome, which has the largest influence on the operation of the PIFA, has been considered. The radome material used is assumed to have a relative dielectric constant of 4.66 with no loss. The dimensions of the top radome plate are 0.21λ (62 mm) long x 0.16λ (49 mm) wide with a thickness of 0.007λ (2 mm). Table 5-8 lists the resonant frequency, input impedance and bandwidth obtained as a function of the distance, d_{top}, between the top radome plate and the antenna patch. Again the PIFA without a radome is used as the reference for performance comparison. Figure 5-28 shows the changes in resonant frequency and bandwidth against the distance. From Figure 5-28, it can be observed that when the distance d_{top} decreases to about 0.3λ (88.5 mm), the resonant frequency gradually decreases to a lower value. This decrease in frequency becomes more rapid when the distance d_{top} is reduced to less than 0.05λ (15 mm). As for the bandwidth, this starts to increase as the distance d_{top} falls below 0.4λ (118 mm) and a peak appears at $d_{top} \approx$ 0.05λ - 0.1λ (14.3 mm - 29.5 mm), where the bandwidth is around 3% wider than that achieved without the radome. As the distance d_{top} continues to decrease, the bandwidth falls off rapidly. For example, when the distance d_{top} is equal to about 0.005λ (1.5 mm), where the radome is almost touching the antenna patch, the bandwidth is observed to reduce by more than 3% while the resonant frequency has shifted lower by over 4% compared to the PIFA without the radome. The most interesting observation from this study is the possibility of the bandwidth of the antenna being increased through the introduction of an appropriately placed dielectric radome top plate. This is because the radome will act as a load and affect the frequency response of the input impedance of the antenna while it is close to the near field of the antenna. The change of the frequency response of the input impedance is likely to give rise to a new bandwidth. This bandwidth may vary with the dimensions of the antenna and the radome as well as the separation between them. This bandwidth could either increase or decrease, meaning that the value of the new bandwidth depends on where the new resonant point occurs. The occurrence of this resonance is a non-linear function of the radome size and its separation from the antenna.

- 111

Table 5-8 The resonant frequency, input impedance, and bandwidth of the PIFA obtained with the presence of a radome top part as a function of the separation between the antenna element and the radome

Distance/Wavelength	Resonance frequency (MHz)	Input impedance (Ohm)		Bandwidth (MHz)
		Real part	Imaginary part	
0.005	970.0	33.7	-0.17	57.66
0.01	980.5	247.0	-0.06	58.86
0.02	991.0	33.0	-0.11	60.06
0.05	1004.8	33.4	-0.12	61.26
0.1	1010.8	33.1	0.05	61.26
0.2	1012.6	32.9	-0.12	60.66
0.3	1013.2	32.6	-0.04	60.06
0.4	1013.2	32.5	-0.03	59.46
0.5	1013.2	32.5	-0.08	59.46
0.6	1013.2	32.5	-0.03	59.46
0.7	1013.2	32.5	-0.02	59.46
0.8	1013.2	32.5	-0.03	59.46
0.9	1013.2	32.5	-0.05	59.46
1	1013.2	32.5	-0.05	59.46

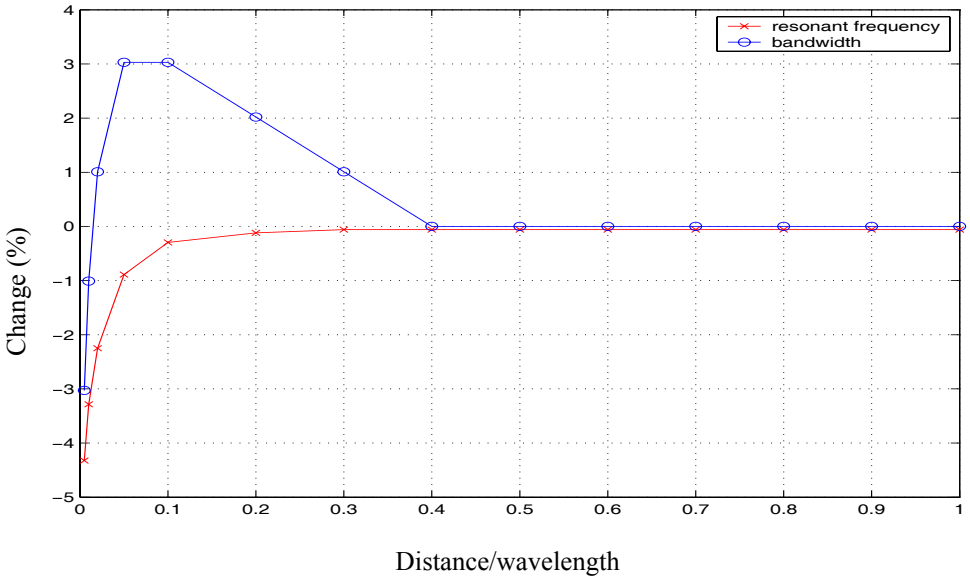

Figure 5-28 The percentage variations of the resonant frequency and bandwidth of the PIFA against the separation between the radome top and the antenna top patch.

- 112

5.6.4 Effect of the thickness of a radome

In this section, the change in input characteristics as a function of the thickness of a top radome plate is examined. In this case, the same top radome plate, as specified in section 5.6.3, has been used with the distance d_{top} between the radome and the antenna patch kept constant. Table 5-9 lists the resonant frequency, input impedance and bandwidth against the thickness of the radome, while the distance, d_{top}, is maintained at 0.0068λ (2 mm). Figure 5-29 shows both the changes in resonant frequency and bandwidth against the thickness of the radome. The input characteristics of the PIFA only (without the radome) are used as the reference. From this figure, it can be observed that as the thickness increases, the resonant frequency decreases exponentially. When the thickness $d = 0.1\lambda$ (29.5 mm), the resonant frequency decreases by more than 25% as compared to a PIFA without a radome. On the other hand, as the thickness of the radome increases, the bandwidth changes in a varied manner. The bandwidth initially decreases until the thickness reaches 0.01λ (3.0 mm), then it remains constant till the thickness is 0.02λ (6 mm). When the thickness is between 0.02λ to 0.03λ (9 mm), the bandwidth increases again. When the thickness is further increased to over 0.03λ, the bandwidth decreases again by up to around 6% narrower than the PIFA without the radome with $d = 0.05\lambda$ (15 mm). Beyond d = 0.05λ, the antenna gain continues to increase and reaches the same value as that without the radome at $d = 0.1\lambda$ (29.5 mm). When the thickness of the radome top plate increases beyond a certain value, such as 0.2λ, the antenna stops resonating.

Table 5-9 The resonant frequency, input impedance and bandwidth of the PIFA with the radome top as a function of its thickness

Ratio of thickness to wavelength	Resonance frequency (MHz)	Input impedance (Ohm)		Bandwidth (MHz)
		Real part	Imaginary part	
0.005	982.6	32.7	0.15	58.90
0.01	958.0	33.3	-0.04	57.66
0.02	914.7	32.1	-0.16	57.66
0.03	884.1	32.7	-0.15	58.86
0.04	858.9	40.1	0.05	57.66
0.05	828.8	46.5	-0.19	55.86
0.1	759.8	64.5	9.84	59.46

- 113

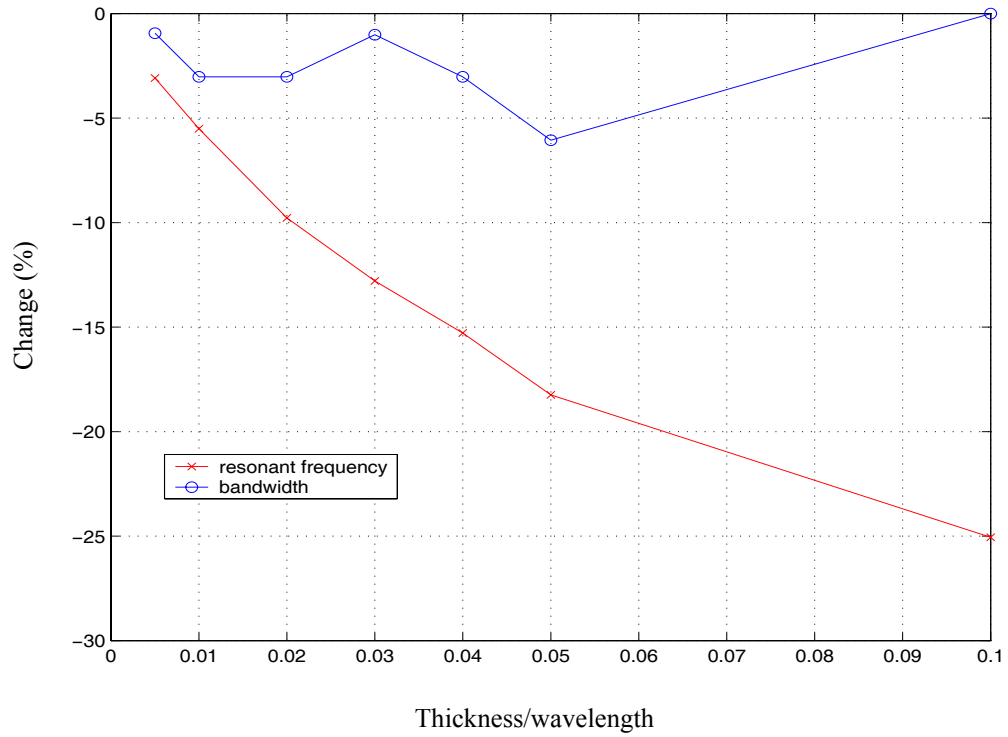

Figure 5-29 The percentage changes in the resonant frequency and bandwidth of the PIFA against the thickness of the radome top.

5.6.5 Effect of the dielectric constant of a radome material

In this section, the effects of the radome having different dielectric constants on the input characteristics of the antenna are investigated. In this case, the radome is again considered to consist of only the top plate with the same separation of 0.0068λ (2 mm) from the antenna patch as specified in section 5.6.3. Table 5-10 lists the resonant frequency, input impedance and bandwidth of the radome antenna as a function of the relative dielectric constant. Figure 5-30 plots the changes in both resonant frequency and bandwidth against the dielectric constant of the radome material. The PIFA without the radome is the reference for comparison. From Figure 5-30 it can be observed that as the relative dielectric constant increases to a value of 3, the resonant frequency decreases by more than 3% while the bandwidth remains almost unchanged. As the relative dielectric constant increases beyond a value of 3, both the bandwidth and resonant frequency continue to decease. When the dielectric constant of the radome is

- 114

as high as 30, the resonant frequency of the antenna system is lowered by more than 10% and the bandwidth decreases to nearly 20% of the one without a radome.

Table 5-10 The resonant frequency, input impedance and bandwidth of the PIFA with the radome top as a function of its dielectric constant

Dielectric constant	Resonance frequency (MHz)	Input impedance (Ohm)		Bandwidth (MHz)
		Real part	Imaginary part	
1	1022.8	33.3	0.06	60.06
2	1002.4	33.8	0.12	60.07
3	991.0	33.8	0.11	60.06
4	977.8	33.1	0.08	58.26
5	971.8	32.9	0.05	57.66
6	967.0	32.6	0.19	57.06
8	958.6	32.3	-0.04	55.86
10	952.0	32.0	-0.15	55.26
15	935.1	29.5	0.05	52.25
20	926.7	29.3	-0.13	51.05
25	920.7	28.9	-0.09	50.45
30	913.5	28.7	0.03	48.65

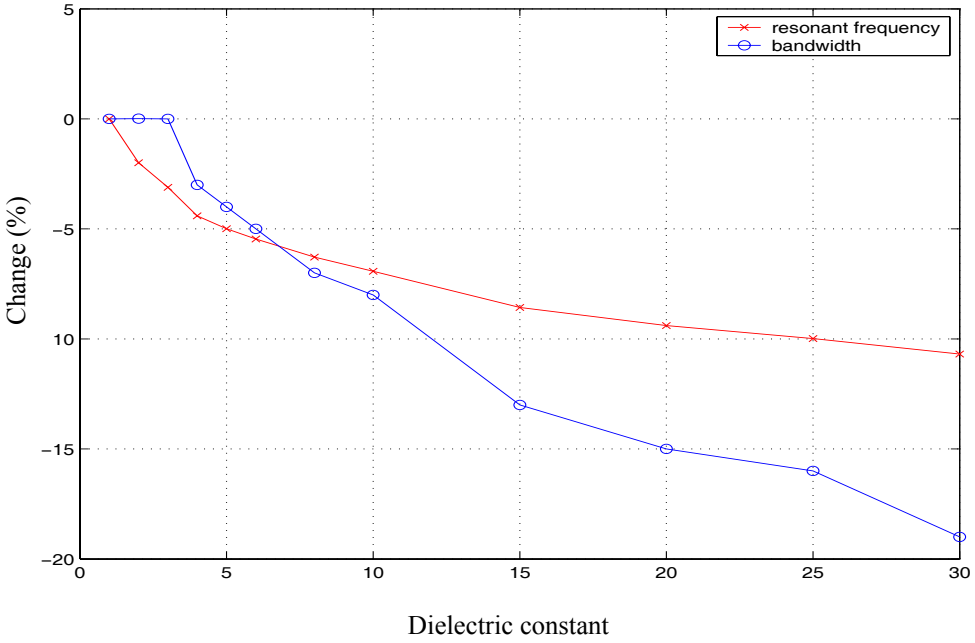

Figure 5-30 The percentage changes in the resonant frequency and the bandwidth of the PIFA with a radome top as a function of the its dielectric constant.

- 115

5.6.6 Effect of the loss tangent of the radome material

The influence on the input and the radiation characteristics of the PIFA due to the presence of a lossy radome has also been studied. The study considered five different values of loss tangent for the radome material ranging from 0 to 1, and with a relative dielectric constant of unity. Also, the same radome as that specified in section 5.6.3 is used. Table 5-11 tabulates some of the simulation results obtained for the input characteristic parameters.

Figure 5-31 plots the changes in both resonant frequency and bandwidth with reference to the antenna only (without radome). Figure 5-32 (a) to (e) shows the 3D-gain radiation patterns simulated using the five different lossy materials. The maximum values of the gain obtained for these five cases are also tabulated in Table 5-11. From these results, it can be observed that a small loss tangent of the radome material has little impact on the bandwidth and the resonant frequency of the antenna, but it does reduce the gain slightly. However, a radome with a large loss tangent of more than 0.01 could significantly affect both the input and the radiation characteristics of the antenna. For example, when the loss tangent is unity, the gain of the PIFA system is reduced by amount 1.75 dB, thus making the antenna unattractive.

Table 5-11 The resonant frequency, input impedance and bandwidth of the PIFA with the radome top against its loss tangent

Loss tangent	Resonance frequency (MHz)	Input impedance (Ohm)		Bandwidth (MHz)	Gain (dBi)
		Real part	Imaginary part		
0	1022.8	33.3	0.06	60.1	4.21
0.001	1002.4	33.8	0.12	60.7	4.21
0.01	1022.8	33.9	0.19	61.3	4.18
0.1	1019.8	39.4	-0.10	64.9	3.93
1	967.6	138.2	0.76	39.6	2.46

- 116

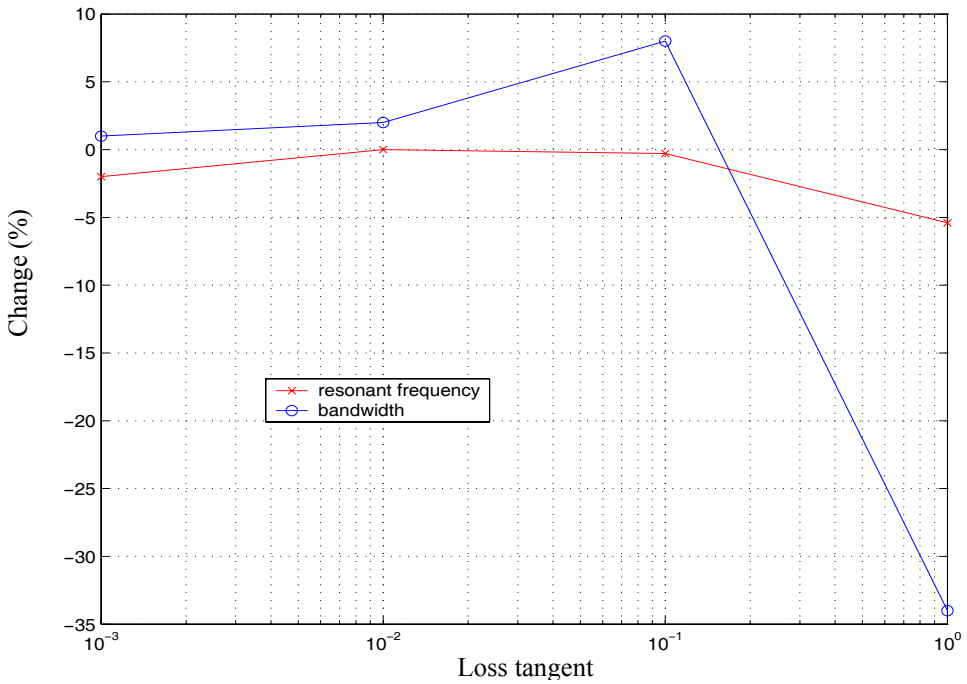

Figure 5-31 The percentage changes in the resonant frequency and the bandwidth of the PIFA with the radome top as a function of the loss tangent of the radome material.

- 117

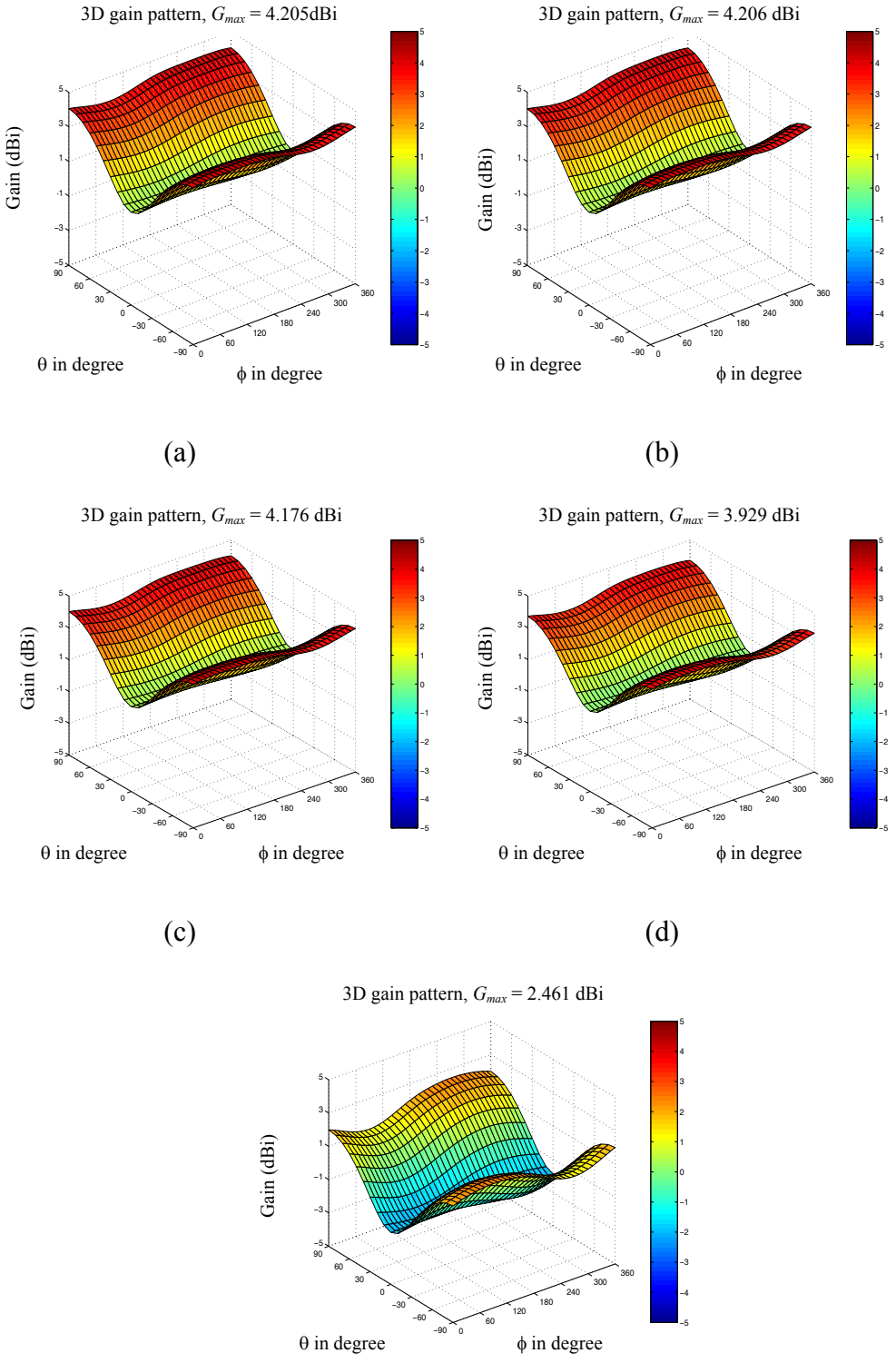

Figure 5-32 The 3D gain patterns of the PIFA enclosed by a radome having different values of loss tangent: (a) $\tan\delta = 0$; (b) $\tan\delta = 0.001$; (c) $\tan\delta = 0.01$; (d) $\tan\delta = 0.1$; (e) $\tan\delta = 1$.

- 118

5.6.7 Influence of different parts of the radome in terms of the separation between radome and antenna

The influence of the separation between the "top" part of the radome and the antenna on the resonant frequency and bandwidth has been described in section 5.6.3. In this section, the input characteristics of the PIFA have been investigated when it is covered by either the "short", or the "open" or the "side" parts of the radome. In the case of the "side", the PIFA is covered in both the "left-side' and "right-side". The dimensions of the "short", "open" and "left-side" or "right-side" parts are 45 mm x 22 mm x 2 mm, 45 mm x 22 mm x 2 mm and 62 mm x 22 mm x 2 mm, respectively.

Figure 5-33 and Figure 5-34 show the variations in resonant frequency and bandwidth of the PIFA in terms of the separation between the antenna and each individual part of the radome, that is the "top", the "short", the "open", and the "side". Again, the PIFA without a radome is used as a reference. From these two figures, it can be observed that each of the four different parts of the radome has a different effect on the input characteristics of the PIFA. For all these cases if the distance separation is less than 0.3λ, the resonant frequency is observed to decrease when the separation is reduced. As the radome is almost touching the antenna patch, for example, when the distance separation equals to 0.005λ, the resonant frequency decreases by 0.2% for the "short", 1.4% for the "open", 2% for the "side" and 4.4% for the "top" when compared to the PIFA without a radome. It is also clear that the "short" has the least effect on the bandwidth among the four individual random parts considered. When the radome is placed close to the antenna, say by less than 0.01λ, both the "open" and "side" cause the bandwidth to decrease by more than 10%. As for the effect of the "top", which has been discussed in section 5.6.3, it is interesting to note that the use of the dielectric radome could increase the bandwidth the antenna system if an appropriate consideration is taken during the design stage.

- 119

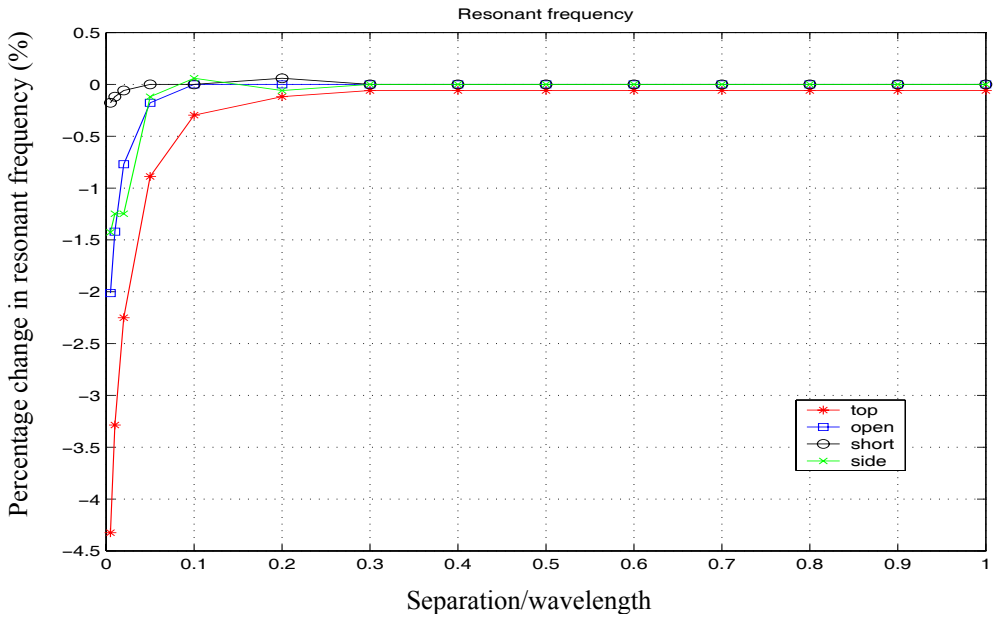

Figure 5-33 The percentage changes in the resonant frequency of the PIFA against the distance between the individual radome part and the antenna.

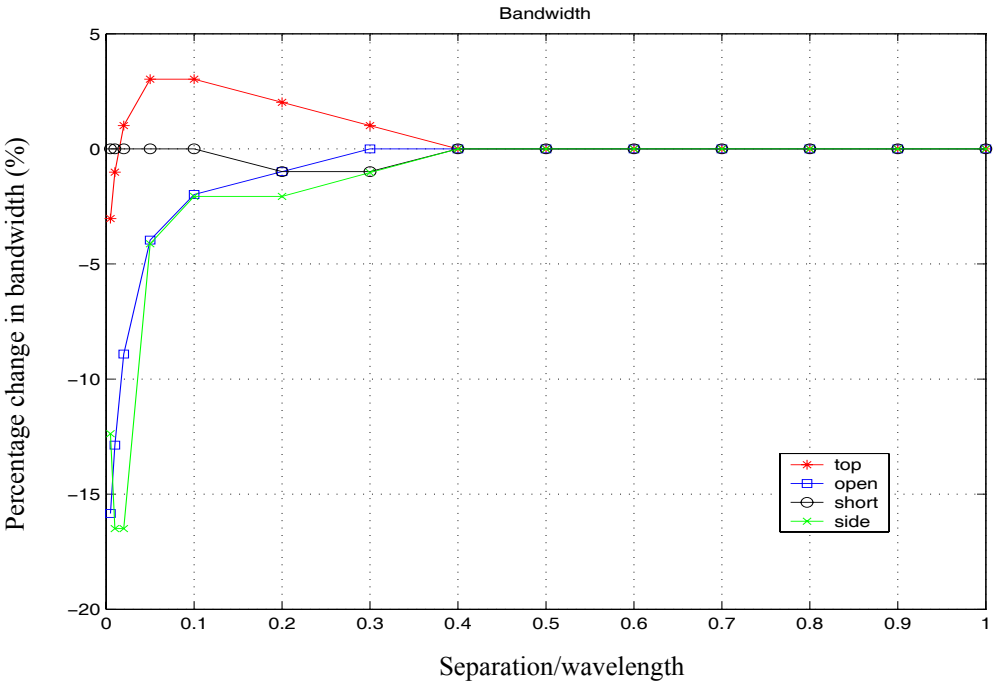

Figure 5-34 The percentage changes in the bandwidth of the PIFA against the distance between the individual radome part and the antenna.

- 120

5.7 Influence of a Dielectric Radome on PIFA Operating at 2400 MHz

5.7.1 Introduction

The use of the 2.4 GHz ISM band is becoming very popular in wireless data communications, for example, Wi-Fi WLAN, Bluetooth (Yeh et al., 2003) and Zigbee (Evans-Pughe, 2003). It is envisaged that an enormous number of potential applications based on these technologies are likely to evolve in the near future (Fenk, 2003). Moreover, for operation at such a frequency, it is expected that the interaction between the radiation elements of a PIFA and its dielectric radome is likely to be even greater than for 900 MHz. In this section, the influence of the radome on the input and the radiation characteristics of a PIFA operating in the 2400 MHz band is investigated by conducting a series of simulations. The simulation methodology adopted in this section is consistent with that of section 5.6.

5.7.2 Parameters for simulation

The configuration of the radome-PIFA under investigation here is the same as in Figure 5-2 and Figure 5-3. However, the dimensions of the PIFA have been modified for operation at 2400 MHz and these are: L_2 = 20.5 mm, L_1= 16 mm, H = 6 mm, W_s = 6 mm, d_f = 3 mm. Table 5-12 tabulates the parameters adopted for simulating the various antenna-radome models studied in this section.

- 121

Table 5-12 Parameters used for simulating a 2400 MHz radome-PIFA system

Antenna-radome model		Radome geometry (mm)			Radome eletrical parameters	
		Distance separation		Thickness		
		d_{top}	$d_{side} = d_{short} = d_{open}$	d	ε_r	$\tan\delta$
Group A	1	2	2	2	1	0
	2				4.66	0
	3				4.66	0.0155
	4				4.66	0.155
Group B	1	0.8	2	2	1	0
	2				4.66	0
	3				4.66	0.0155
	4				4.66	0.155
Group C	1	0.8	2	0.8	1	0
	2				4.66	0
	3				4.66	0.0155
	4				4.66	0.155

5.7.3 Group A radome-PIFA systems

5.7.3.1 Input characteristics

For Group A, the 2400 MHz PIFA is enclosed by a rectangular dielectric radome with a thickness of $d = 2$ mm. The separation between the radiation element and each of the five sides of the radome is kept at 2 mm, as listed in Table 5-12. Altogether four different antenna setups in Group A have been used to investigate the effects of such a radome on the input and radiation performance of the PIFA as a result of adopting a different radome material. The radome is assumed to be made of a dielectric material having a permittivity of either unity (air), or 4.66-j0 (no loss), or 4.66 - j0.0155 (small loss), or 4.66 – j0.155 (big loss).

Figure 5-35 shows the input impedances associated with the four antenna models over a frequency range of 1800 MHz to 2800 MHz. Also, the respective plots of their return loss are shown in Figure 5-36. From Figure 5-35, it can be noted that the frequency response of the input impedance of the PIFA is shifted to lower frequencies when it is enclosed by the dielectric radome, irrespective whether the dielectric material of the radome is lossy or not. However, the dielectric material that has a big value of loss tangent may result in the reduction of the peak value of the impedance. Also, it can be

- 122

observed that the dielectric radome causes a noticeably narrower resonant frequency response. From Figure 5-36, it can be observed that the bandwidth becomes smaller when the PIFA is enclosed by a dielectric radome. Table 5-13 lists the input characteristics of the four PIFA configurations. In addition, the percentage changes in the input characteristics of a PIFA enclosed by radomes of different dielectric properties compared with the one having an air filled radome, which acts as the reference, are given in Table 5-14.

Comparison of Table 5-14 with Table 5-4 clearly demonstrates that the influence of the radome on the resonant frequency of the antenna is more significant at 2400 MHz than at 900 MHz, when the radome has the same thickness and the distance separation between the radome and the antenna is kept the same.

- 123

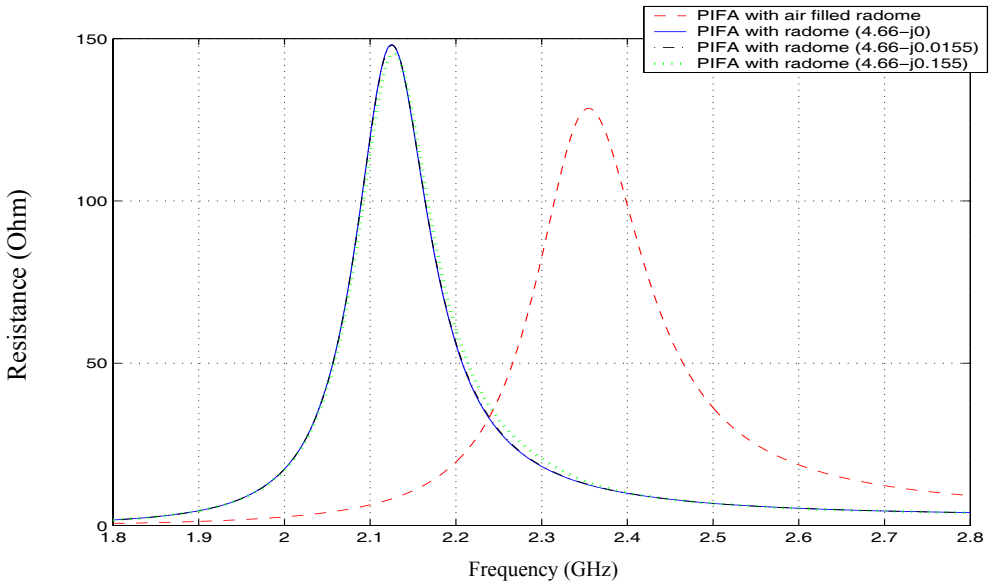

(a)

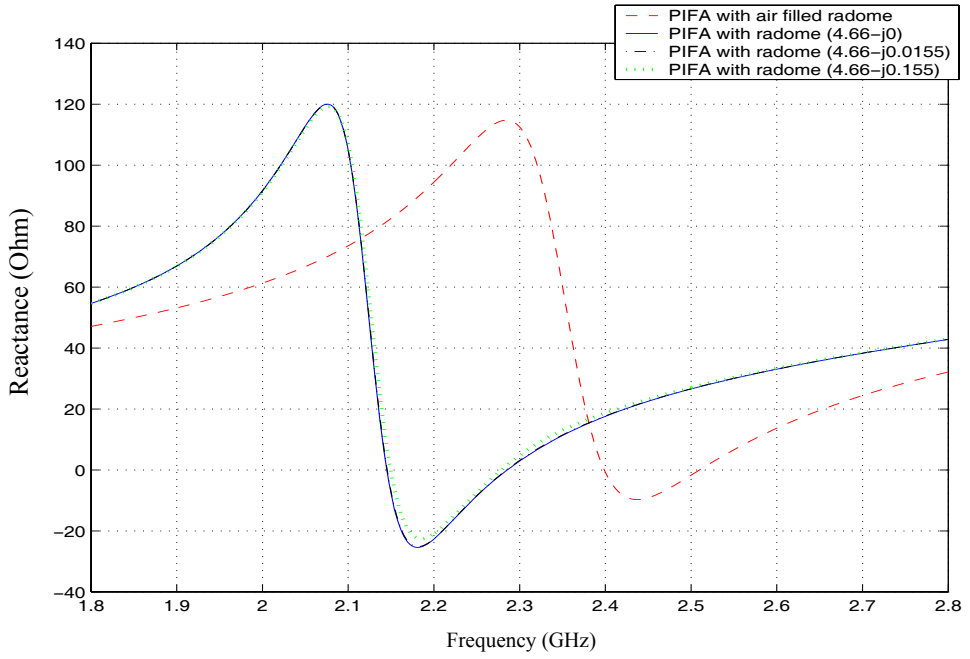

(b)

Figure 5-35 The input impedance due to different electrical parameters of the radome at 2400 MHz: (a) resistance; (b) reactance.

- 124

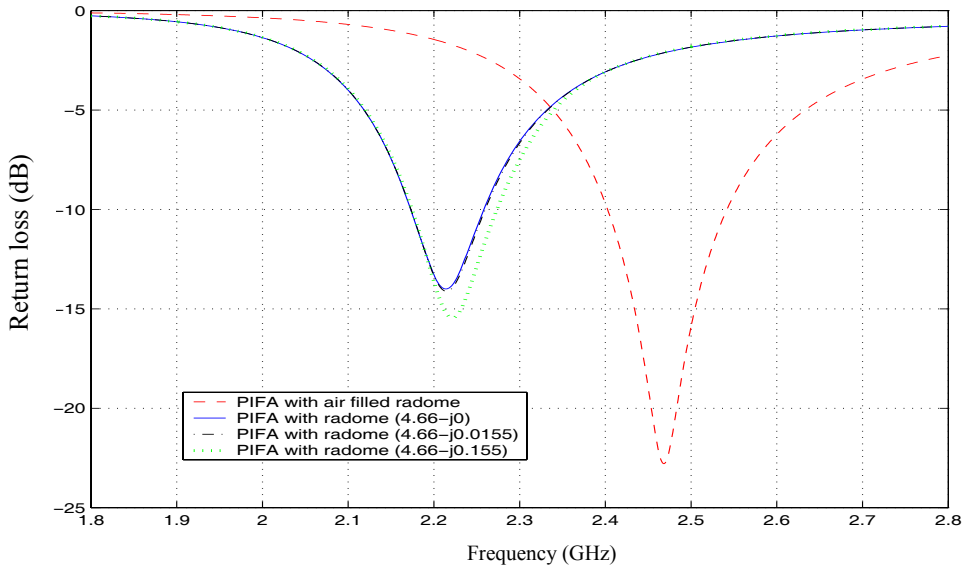

Figure 5-36 The return loss due to different electrical parameters of the radome at 2400 MHz.

Table 5-13 The input and radiation characteristics of the PIFA enclosed by a radome with different electrical parameters at 2400 MHz

Dielectric parameters	Resonant frequency (MHz)	Input impedance (Ohm)		Bandwidth (MHz)	Gain (dBi)
		Real part	Imaginary		
1-j0	2510.7	33.2	0.14	147.1	4.32
4.66-j0	2286.5	20.3	0.19	93.1	4.61
4.66-j0.0155	2285.5	20.7	0.14	93.1	4.60
4.66-j0.155	2279.5	24.6	0.14	106.1	4.22

Table 5-14 Changes in input and radiation characteristics of the PIFA enclosed by a radome with different electrical parameters at 2400 MHz

Dielectric parameters	Change in resonant frequency (%)	Change in bandwidth (%)	Change in gain (%)
4.66-j0	-8.9	-36.7	6.8
4.66-j0.0155	-9.0	-36.7	6.5
4.66-j0.155	-9.2	-27.9	-2.4

- 125

5.7.3.2 Radiation patterns

The 2D polar radiation patterns in the xy and xz planes are plotted in Figure 5-37 and Figure 5-38, respectively, for the four cases considered in Group A. From Figure 5-37, it can be observed that the maximum gain of the PIFA remains along the y direction, i.e., the open side of the PIFA, when it is enclosed by the radome. However, the gains obtained for the other directions of the xy plane have been reduced by up to 0.5 dB in comparison with the corresponding values achieved by the antenna without a radome (red dashed curve). From Figure 5-38, it can be noted that the radiation in the xz plane has been reduced in all directions, from a small but noticeable change in the z direction to more than 0.5 dB reduction in both the $\pm$ x directions, compared to those without a radome (red dashed curve). It is also worth noting from both of these figures that the loss tangent of the radome material has little effect on the radiation pattern.

The 3D gain patterns for the four cases in Group A are plotted in Figure 5-39 to Figure 5-42. From these figures, it can be observed that the dielectric constant of the radome material can influence the radiation patterns while the loss tangent can reduce the gain of the antenna significantly. For instance, compared with an antenna without a radome, a reduction in maximum gain of 0.39 dB is observed when the loss tangent of the radome material is 0.15. The maximum gains obtained for the four cases are listed in Table 5-13, and their percentage changes with respect to the corresponding value obtained for an air filled radome case, are tabulated in Table 5-14.

By comparing the polar radiation patterns of Figure 5-37 and Figure 5-38 with those of Figure 5-14 to Figure 5-17, and the changes in maximum gain as tabulated in Table 5-16 with those in Table 5-6, it can be observed that the radiation patterns are affected to a greater extend at 2400 MHz than 900 MHz by the presence of a dielectric radome.

- 126

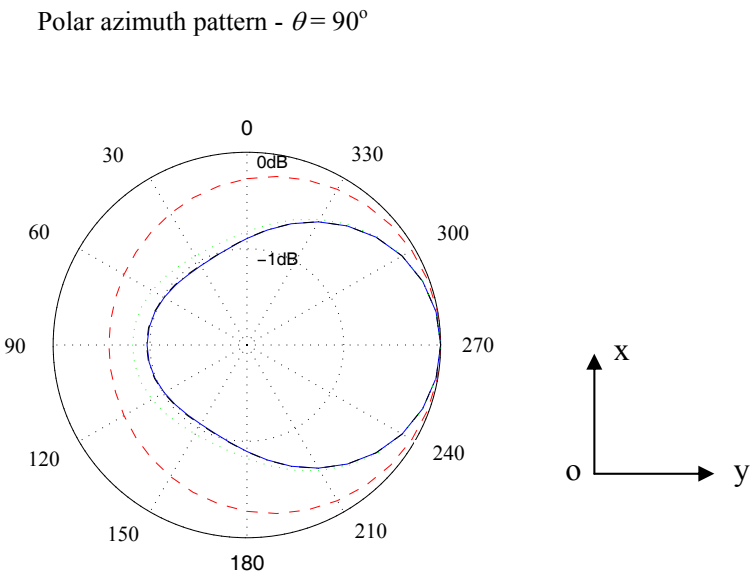

Figure 5-37 The radiation patterns in the xy plane associated with the four antenna systems in Group A.

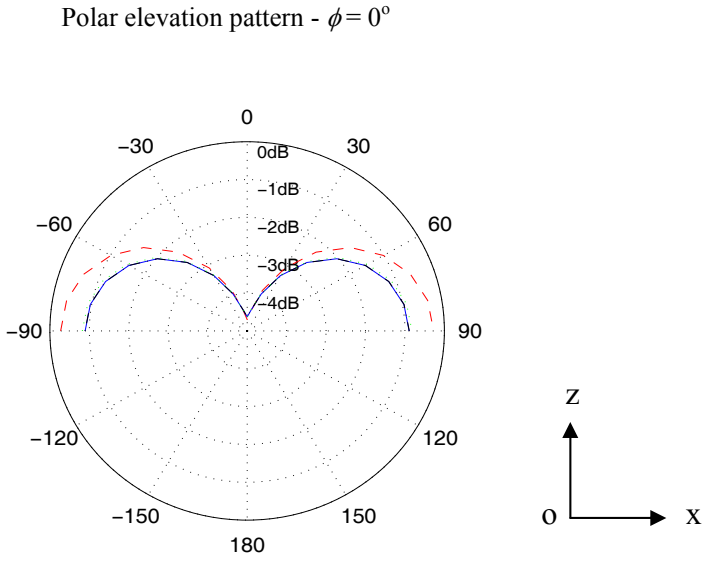

Figure 5-38 The radiation patterns in the xz plane associated with the four antenna systems in Group A.

- 127

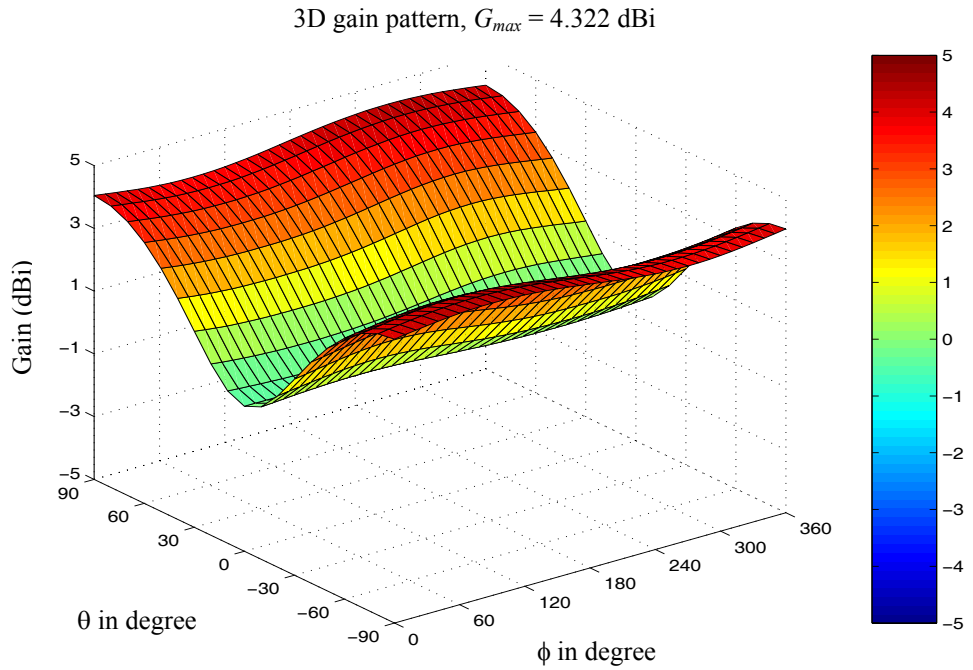

Figure 5-39 The 3D gain pattern for the PIFA with an air filled radome.

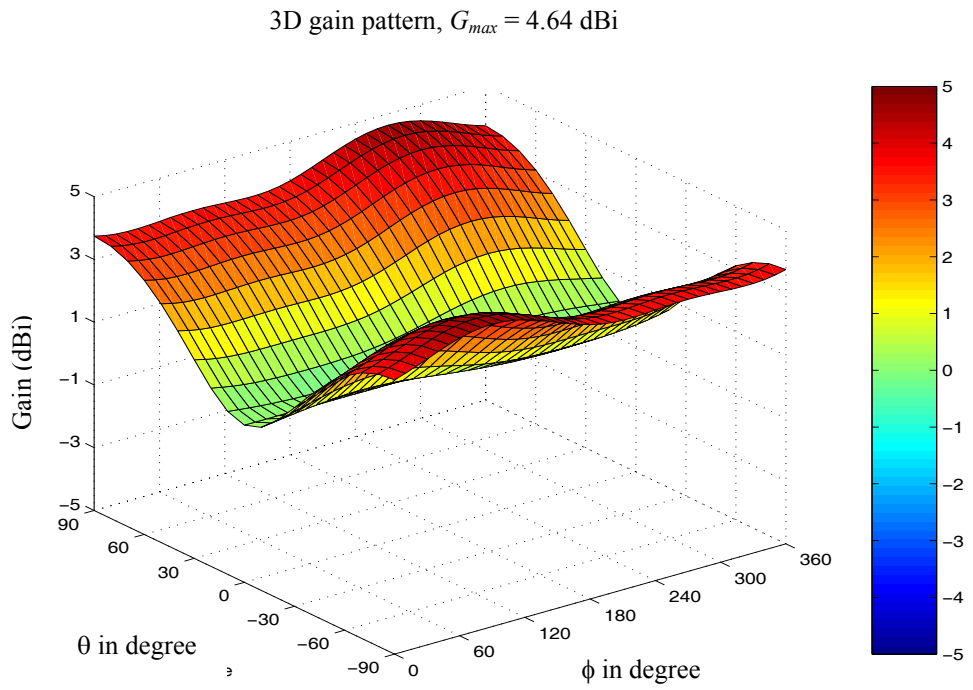

Figure 5-40 The 3D gain pattern for the PIFA with a dielectric radome (4.66-j0).

- 128

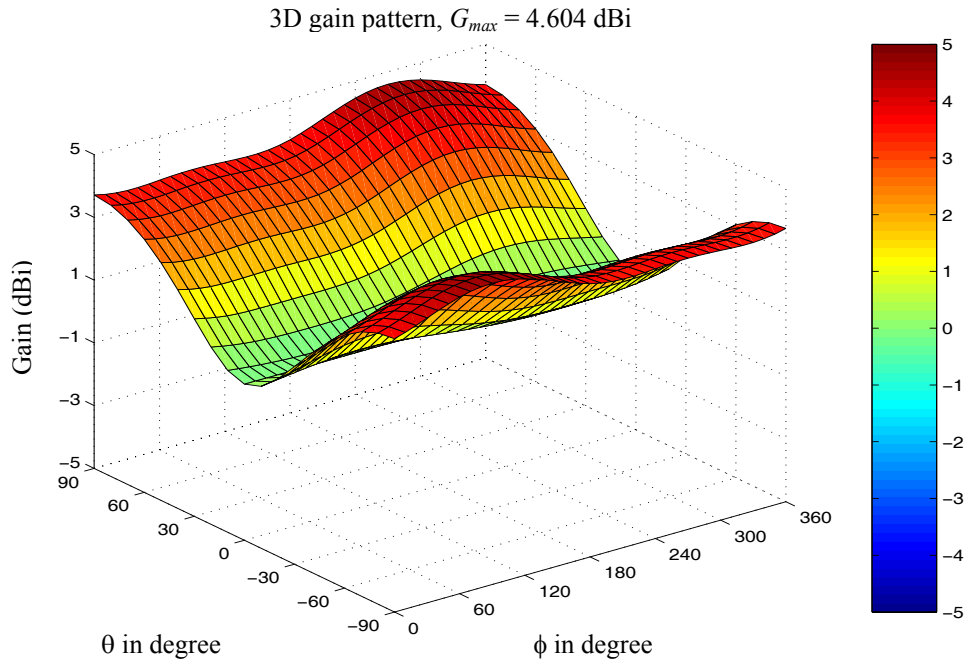

Figure 5-41 The 3D gain pattern for PIFA with a dielectric radome (4.66-j0.0155).

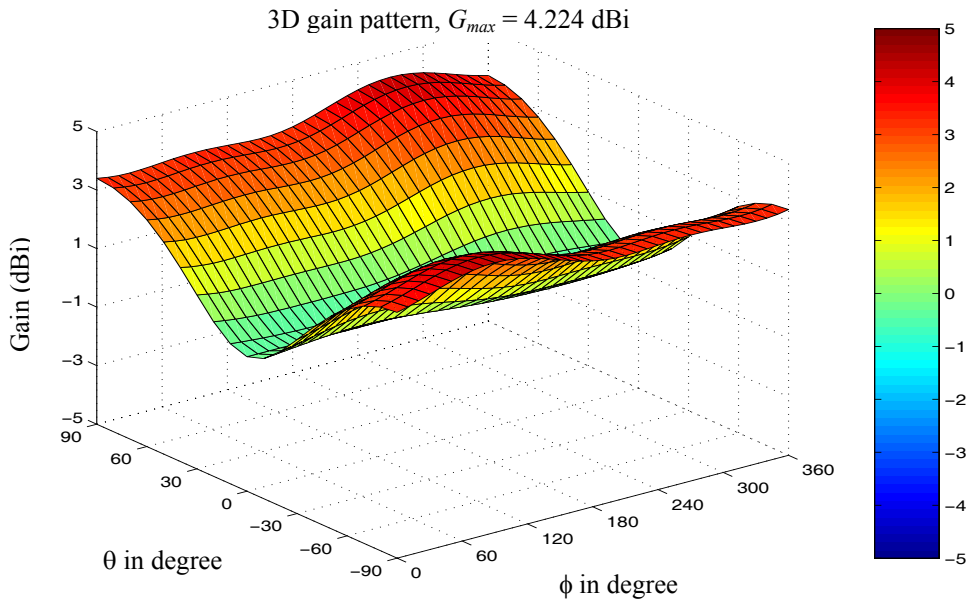

Figure 5-42 The 3D gain pattern for the PIFA with a dielectric radome (4.66-j0.155).

- 129

5.7.4 Group B radome-PIFA systems

The four antenna configurations in Group B are similar to those in Group A except for the separation between the radiating element and the radome, d_{top}, being reduced to 0.8 mm, which is approximately equal to 0.0068λ. The input and the radiation characteristics of these four radome-enclosed PIFA systems obtained by simulations are tabulated in Table 5-15. The percentage changes in resonant frequency, bandwidth and gain with respect to the values obtained from the PIFA enclosed by an air-filled radome are tabulated in Table 5-16. By comparing Table 5-16 with Table 5-14, it is noted that the influence on the PIFA due to the presence of a radome is greater when the separation between them decreases.

Table 5-15 The input and radiation parameters for the case with d = 2 mm, and d_{top} = 0.8 mm

Dielectric parameters	Resonant frequency (MHz)	Input impedance (Ohm)		Bandwidth (MHz)	Gain (dBi)
		Real part	Imaginary		
1-j0	2509.7	49.5	0.07	136.1	4.39
4.66-j0	2209.4	20.9	0.23	86.1	4.49
4.66-j0.0155	2208.4	21.6	0.16	88.1	4.43
4.66-j0.155	2197.4	29.3	0.21	101.1	3.97

Table 5-16 Changes in the input and radiation parameters for the case with d = 2 mm and d_{top} = 0.8 mm

Dielectric parameters	Change in resonant frequency (%)	Change in bandwidth (%)	Change in gain (%)
4.66-j0	-12.0	-36.8	2.3
4.66-j0.0155	-12.0	-35.3	0.8
4.66-j0.155	-12.4	-25.7	-9.7

- 130

5.7.5 Group C radome-PIFA systems

For the four antenna systems in Group C, the thickness of the radome material, d, has also been reduced to 0.8 mm. The input and the radiation characteristics of these four antenna configurations are listed in Table 5-17. Again, the antenna with an air-filled radome is used as the reference for examining the changes in the input and radiation characteristics as a result of changes in the electrical properties of the radome material used. The percentage changes in resonant frequency, input impedance and gain are tabulated in Table 5-18. Comparing the results of Table 5-18 with those of Table 5-14 and Table 5-16, it can be observed that the effect of the radome becomes weaker when the thickness of the radome material is reduced.

Table 5-17 The input and radiation parameters for the case with d = 0.8 mm but d_{top} = 0.8 mm

Dielectric parameters	Resonance frequency (MHz)	Input impedance (Ohm)		Bandwidth (MHz)	Gain (dBi)
		Real part	Imaginary		
1-j0	2507.7	40.3	0.12	141.1	4.39
4.66-j0	2346.5	24.2	0.28	107.1	4.51
4.66-j0.0155	2345.5	24.6	0.18	108.1	4.48
4.66-j0.155	2338.5	28.9	0.13	116.1	4.20

Table 5-18 Changes in the input and radiation parameters for the case with d = 0.8 mm and d_{top} = 0.8 mm

Dielectric parameters	Change in resonant frequency (%)	Change in bandwidth (%)	Change in gain (%)
4.66-j0	-6.4	-24.1	2.7
4.66-j0.0155	-6.5	-23.4	2.0
4.66-j0.155	-6.7	-17.7	-4.3

- 131

5.8 Summary

In this chapter, a radome-PIFA model has been established for computer simulations using a MOM based electromagnetic simulator, WIPL-D. Through the introduction of the SET, the geometry of a dielectric radome can be modelled in the same way as for a metallic structure. Theoretically, it is possible to adopt this method to model and analyse any arbitrary shape radome-antenna structures. This simulation model has been validated in two different ways. First, the results for the input and the radiation characteristics of the PIFA with an air-filled radome have been validated with the corresponding values obtained for the same PIFA but without a radome. Secondly, the quality of the numerical solution has been checked by the power balance involving the above two antenna configurations. Thus the two verifications of results ensure that the methodologies adopted in this study are reliable and accurate.

Using the radome-antenna model developed in this chapter, the performance of a PIFA operating at 900 MHz in the presence of a rectangular dielectric radome has been analysed. It has been found that the resonant frequency of the PIFA is significantly shifted to a lower frequency whenever it is enclosed within a dielectric radome. This is mainly due to the dielectric constant of the radome directly influencing the impedance and electrical length of the antenna. Also, it has been found that the presence of the dielectric radome can alter the radiation patterns of the antenna. However, the loss tangent associated with a radome material does not seem to affect the radiation patterns but can significantly reduce the gain of the antenna system.

The investigation was then extended to examine the influence of each individual part of the rectangular radome on the performance of the antenna system. It has been observed that each individual part has a different degree of effect on both the input and the radiation characteristics of the PIFA. The observed effects on the input characteristics are in the following order from the strongest to the weakest: “top”, “side”, “open” and “short”. These results suggest that the short-circuit plate of the PIFA could be located as close as possible to the radome in order to minimise the overall size of the antenna. Also, it has been found that the radiation patterns are altered differently by each individual part of the radome. For instance, considering the effect on the radiation

- 132

pattern, the “open” is dominant and the “short” has the least effect. These factors have to be taken into account in the early design stages.

Next, the effects of the radome on the input impedance of the PIFA due to the separation between radome and antenna, the thickness and the electrical properties of the radome have been studied. It is found that the resonant frequency, bandwidth and gain of the antenna are affected by these radome parameters. Based on these observations, it is possible to improve the bandwidth while minimising the size of a radome-PIFA through appropriate choices for both the physical and electrical parameters of the radome.

Furthermore, the influence of each individual part of the rectangular radome on the resonant frequency and bandwidth of the radome-PIFA due to the separation between the radome and antenna element has been examined in comparison with the values obtained for the PIFA without the radome. This observation helps to further confirm the earlier statement that each individual part has a different degree of effect on the input characteristics of the PIFA.

Finally, the influence of a rectangular radome on the performance of a PIFA operating at the higher frequency of 2400 MHz has been investigated. The results clearly demonstrate that a radome has a greater impact on the operation of a PIFA at 2400 MHz than at 900 MHz. This is particularly true for the achievable gain but also the input and the radiation characteristics. This suggests that greater attention is needed in the design of such a radome–PIFA system operating at 2400 MHz.

- 133

CHAPTER SIX

6. TRANSMISSION LINE MODEL FOR A PIFA WITH DIELECTRIC COVER LAYER

6.1 Introduction

The influences of the dielectric cover layer and the dielectric radome on the input and the radiation characteristics of a PIFA have been investigated using the MOM in Chapter 4 and 5, respectively. These results show that the presence of the dielectric radome, particularly the top dielectric layer, has a strong impact on the performance of the PIFA when it is located close to the antenna. This effect can often change the antenna behaviour to such an extent that it operates outside its original design margin. Therefore, it is essential to account for such effects, caused by the presence of the radome, in the initial design. However, the numerical modelling of this effect often results in longer computing time. For this reason, a more efficient procedure, based on the transmission line model (TLM), is introduced in this chapter to be used as an engineering tool in the design of a PIFA-radome antenna system.

6.2 TLM for Patch Antennas

The TLM used for analysing a rectangular patch microstrip antenna (MSA) was introduced by Munson (Munson, 1974). It was later improved upon by Derneryd (Derneryd, 1978) and Pues *et al*. (Pues *et al*, 1984) by considering both the stored energy near the edges and the external mutual coupling between the radiating edges. Figure 6-1 shows a rectangular patch antenna of patch width L_1 and length L_2, where L_2 governs the fundamental resonance radiating mode. Figure 6-1 also shows four

- 134

imaginary radiating slots which form a useful model to calculate the radiation field of the antenna (Hammer, *et al*., 1979). These so-called equivalent slots consist of two main slots with a uniform electric field distribution and two side slots with a sinusoidal electric field distribution (Pues *et al*, 1984).

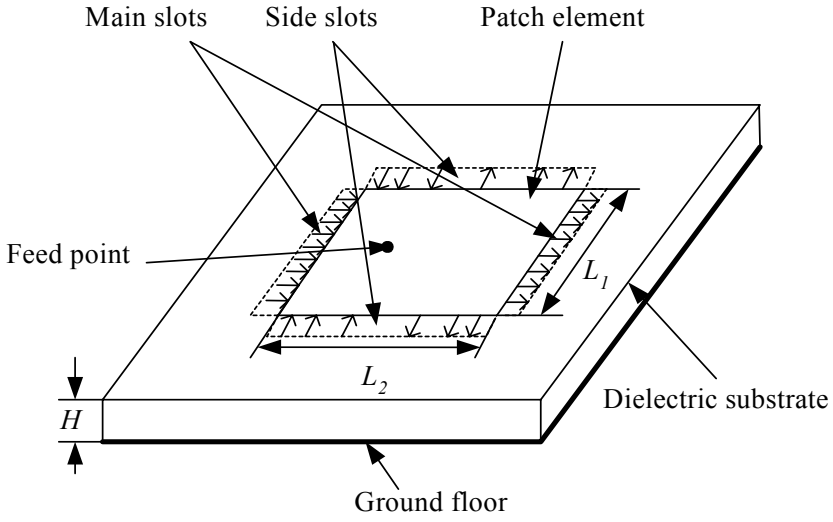

Figure 6-1 A microstrip patch antenna.

Figure 6-2 shows the equivalent circuit of the transmission-line model of the rectangular patch microstrip antenna with a feed point. In this case, the patch is modelled by a transmission line whose length, characteristic impedance, and propagation constant are L_2, Z_c and γ, respectively, with an admittance connected to each end of the transmission line. In Figure 6-2, G_s and G_r represent the surface-wave conductance and radiation conductance of the radiating edges. The susceptance B represents the stored energy near the edge, and the mutual admittance Y_m represents the external mutual coupling between the two radiating edges.

- 135

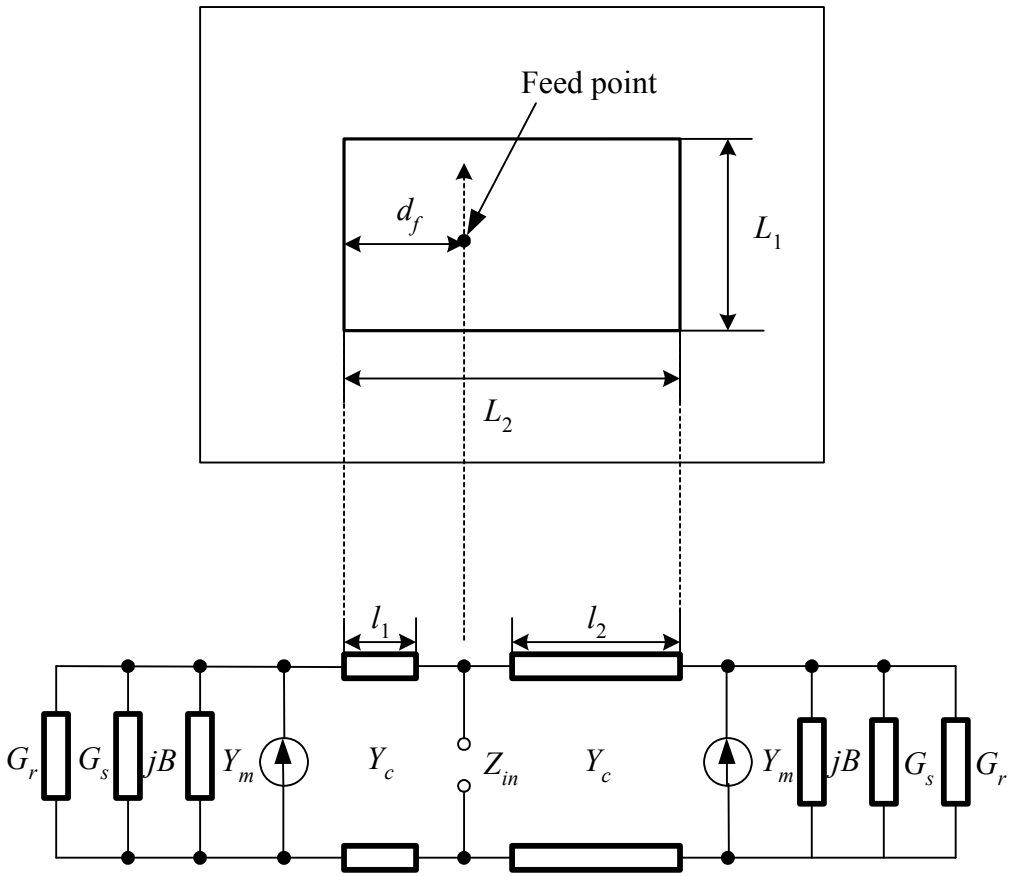

Figure 6-2 Transmission-line model of a patch microstrip antenna.

6.3 TLM Applied to PIFA

A rectangular microstrip antenna is designed to resonate in the TM_{100} dominant mode. The length of the rectangular element can be halved by placing a short-circuit plate between the radiator element and ground plane at the position where the electric field of the TM_{100} mode is zero. When the width of the short-circuit plate is set narrower than that of the planar element, the effective inductance of the antenna element increases, and the resonant frequency becomes lower than that of a conventional short-circuit patch microstrip antenna having the same sized planar element. As a result, the length of the short-circuit microstrip antenna can be further reduced. When the width of the short-circuit plate is narrowed, the final structure becomes the same as that of a PIFA.

- 136

To adopt this TLM, the PIFA is modelled as equivalent to two transmission lines of length l_1 and l_2, as shown in Figure 6-3 (b) where l_1 and l_2 are equal to d_f and L_2-d_f, respectively. One end of the PIFA is open while the other end is partly shorted. Consequently, the current is zero at the open end and in the shorted end it is a maximum.

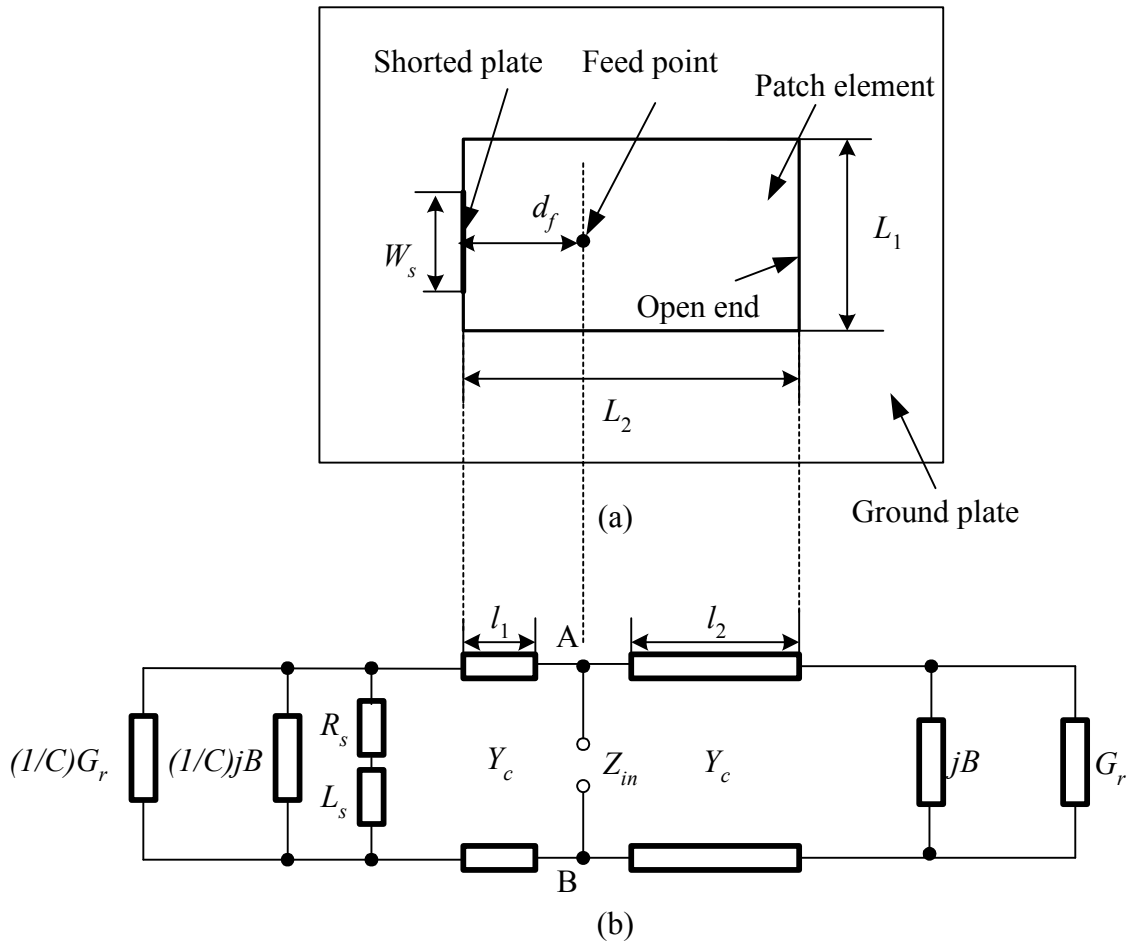

Figure 6-3 (a) An ideal transmission-line model of a PIFA; (b) equivalent lumped components to account for inductive and capacitive couplings.

Equivalent lumped components are introduced to account for the field coupling as shown in Figure 6-3 (b). The inductive coupling, due to the short-circuit plate, is modelled as a resistor R_s in series with an inductor L_s. The resistive part is assumed to be small and can normally be neglected. The inductive part is dependent on the width and height of the short circuit plate.

- 137

The capacitive coupling, due to the fringing fields at the open end of the PIFA is modelled as a capacitor $1/jB$ in parallel with a resistive load representing a radiation resistance $1/G_r$ as shown in Figure 6-3 (b). Now, due to the presence of the short-circuit plate, the fringing fields at this end of the top plate are much smaller than those at the open end. Therefore, the capacitive coupling at the short-circuit plate is reduced by a correction factor C, compared with one at the open end. Also, due to the presence of the short-circuit plate the mutual coupling between the open end and the short-circuit plate end of the PIFA is assumed to be small and is neglected. Moreover, because the air dielectric below the top plate is free from surface wave excitation, the surface-wave conductance G_s, normally presents in a patch microstrip antenna (see Figure 6-2), can be omitted here. However, the effect of the impedance of the coaxial probe feed on the input impedance of the PIFA needs to be considered, because the length of the feed wire in the case of the PIFA is longer than that in a patch microstrip antenna.

Using the transmission line theory (Owyang, 1989), the input impedance of the PIFA in Figure 6-3 (b) can be calculated as

$$Z_{in} = Z_f + \frac{Z_1 Z_2}{Z_1 + Z_2} \tag{6.1}$$

where Z_f represents the impedance of the coaxial feed wire; Z_1 represents the impedance across points A and B terminated by a short-circuit plate load Z_{sl} via a transmission line (l_1); and Z_2 represents the impedance across points A and B terminated by an open load Z_{ol} via another transmission line (l_2). Z_1 is given by

$$Z_1 = Z_c \frac{Z_{sl}\cosh(\gamma l_1) + jZ_{ol}\sinh(\gamma l_1)}{Z_{ol}\cosh(\gamma l_1) + jZ_{sl}\sinh(\gamma l_1)} \tag{6.2}$$

and Z_2 is given by

$$Z_2 = Z_c \frac{Z_{sl}\cosh(\gamma l_2) + jZ_{ol}\sinh(\gamma l_2)}{Z_{ol}\cosh(\gamma l_2) + jZ_{sl}\sinh(\gamma l_2)} \tag{6.3}$$

- 138

where Z_c is the characteristic impedance of the transmission line formed by the top plate; γ is the complex propagation constant of the line; and Z_{sl} and Z_{ol} are given respectively by

$$\frac{1}{Z_{sl}} = C \cdot G_r + C \cdot jB + \frac{1}{R_s + j2\pi f L_s} \tag{6.4}$$

and

$$\frac{1}{Z_{ol}} = G_r + jB \tag{6.5}$$

where f is the operating frequency in Hz.

6.4 Determination of the Model Parameters

The transmission-line model of Figure 6-3 (b) contains the following unknowns: the line parameters (Z_c, γ), the conductance of the radiating edge G_r, the edge susceptance B, the correction factor C, the feed wire impedance Z_f, the resistance R_s and the inductance L_s of the short-circuit plate.

6.4.1 Line parameters

The characteristic impedance Z_c of a transmission line can be computed using the relationship (Hammerstad *et al*, 1980),

$$Z_c = Z_0 \Big/ \sqrt{\varepsilon_{re}} \tag{6.6}$$

where Z_0 is the characteristic impedance of an identical air-filled transmission line and ε_{re} is the effective dielectric constant of the transmission line.

- 139

Z_0 is given by (Hammerstad *et al*, 1980) as

$$Z_0 = 60 \ln\left[\frac{q(u)}{u} + \sqrt{1 + \frac{4}{u^2}}\right] \tag{6.7}$$

with

$$q(u) = 6 + (2\pi - 6)\exp[-(30.666/u)^{0.7528}] \tag{6.8}$$

and

$$u = L_1 / H \tag{6.9}$$

where L_1 and H are respectively the width and the height of the top plate of the PIFA.

The effective dielectric constant ε_{re} of the TLM depends on the configuration of the PIFA. If a PIFA is not covered or filled by any dielectric materials, ε_{re} is equal to 1. The calculation of the ε_{re} when the PIFA is covered or filled by some dielectric materials will be discussed in section 6.4.4.

The complex propagation constant γ of the transmission line in the model is defined as

$$\gamma = \alpha + j\beta \tag{6.10}$$

where α represents the attenuation constant and β represents the phase constant. They may be expressed by (Kompa et, al, 1975)

$$\beta = k_0 \sqrt{\varepsilon_{re}} \tag{6.11}$$

$$\alpha = 0.5\beta \tan\delta_e \tag{6.12}$$

where $k_0 = 2\pi/\lambda_0$, the wave number in free space. λ_0 is the wavelength in free space and $\tan\delta_e$ is the effective loss tangent, which includes both the conductor and dielectric losses of the transmission line. In this study, these losses are not considered. For more detailed discussion of these losses refer to (Hammerstad *et al*, 1980).

- 140

6.4.2 Edge susceptance B and radiation conductance G_r

A rectangular patch capacitor can be considered to be a degenerated microstrip line as proposed by Wolff *et al* (Wolff *et al*, 1974). Based on this approach, the edge capacitance C_{L_1e} at the open end of the PIFA, as shown in Figure 6-3 (a), can be expressed as

$$C_{L_1e} = \frac{L_1}{2}\left(\frac{1}{v_{ph2L_2} \cdot Z_c(2L_2, H, \varepsilon_{re})} - \frac{\varepsilon_0 \varepsilon_r 2L_2}{H} \right) \tag{6.14}$$

where $Z_c(2L_2, H, \varepsilon_{re})$ is the characteristic impedance of the transmission line having a line width $2L_2$ and a line length L_1 with a height H. ε_{re} is the effective dielectric constant of the line. ε_r is the dielectric constant of the material filling the space between the top plate and the ground plane. v_{ph2L_2} is the phase velocity of a quasi-TEM mode in a transmission line of width $2L_2$, which is given by (Wolff *et al*, 1974)

$$v_{ph2L_2} = \frac{c \cdot Z_c(2L_2, H, \varepsilon_{re})}{Z_c(2L_2, H, \varepsilon_{re})} \tag{6.14}$$

It should be noted that the line impedance $Z_c(2L_2, H, \varepsilon_{re})$ can be calculated using equations (6.6) - (6.8) by putting $u = \frac{2L_2}{H}$.

Once the edge capacitance C_{L_1e} is known, the edge susceptance B shown in Figure 6-3 (b) can be computed in terms of the edge capacitance C_{L_1e} by

$$B = j\omega C_{L_1e} \tag{6.15}$$

- 141

The radiation conductance G_r is computed as a uniformly TE-excited slot radiator of length W_e and width Δl. W_e and Δl represent respectively the effective width and the end-effect extension of the open end of the transmission line. G_r is given by (Pues *et al*, 1984):

$$G_r = \frac{1}{\pi\eta_0}\left\{\left[pS_i(p) + \frac{\sin p}{p} + \cos p - 2\right]\left(1 - \frac{s_l^2}{24}\right) + \frac{s_l^2}{12}\left(\frac{1}{3} + \frac{\cos p}{p^2} - \frac{\sin p}{p^3}\right)\right\} \tag{6.16}$$

where $\eta_0 = \sqrt{\mu_0/\varepsilon_0}$ (6.17)

$$p = k_0 W_e \tag{6.18}$$

$$s_l = k_0 \Delta l \tag{6.19}$$

$$S_i = \int_0^w \frac{\sin x}{x} dx \tag{6.20}$$

and η_0 is the wave impedance of free space.

Using the planar waveguide model (Kompa *et, al,* 1975), the effective width of the transmission line can be expressed as

$$W_e = \frac{\eta_0}{\sqrt{\varepsilon_{re}}}\frac{H}{Z_c} \tag{6.21}$$

Since the dimensions of the patch are finite, the fields at the edge of the patch cannot drop off abruptly to zero, as they must obey the conservative nature of the electric field. The electric field lines extend outward into the region beyond the plates, as indicated in Figure 6-4.

- 142

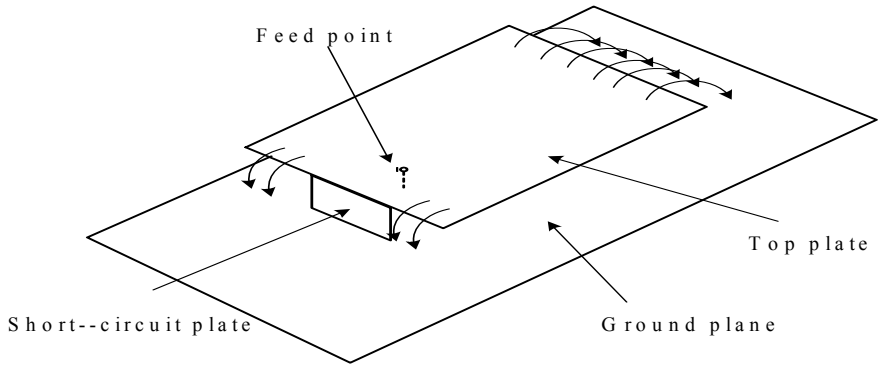

Figure 6-4 Radiating mechanism of PIFA.

The closed form expression for the end effect has been derived from a rigorous numerical hybrid mode solution of the microstrip open end problem (Kirschning *et al*, 1981). It describes the displacement Δl of the open circuit end of the hypothetical electric patch, with respect to the abrupt physical end of the strip. The displacement normalised by the height H is given by (Kirschning *et al*, 1981)

$$\Delta l / H = (\zeta_1 \zeta_3 \zeta_5 / \zeta_4) \tag{6.22}$$

with

$$\zeta_1 = 0.434907 \frac{\varepsilon_{re}^{0.81} + 0.26(L_1/H)^{0.8544} + 0.236}{\varepsilon_{re}^{0.81} - 0.189(L_1/H)^{0.8544} + 0.87} \tag{6.23}$$

$$\zeta_3 = 1 + \frac{0.5274 \tan^{-1}[0.084(L_1/H)^{1.94113/\zeta_2}]}{\varepsilon_{re}^{0.9236}} \tag{6.24}$$

where $\zeta_2 = 1 + \dfrac{(L_1/H)^{0.371}}{2.358\varepsilon_r + 1}$ (6.25)

$$\zeta_4 = 1 + 0.0377 \tan^{-1}[0.067(L_1/H)^{1.456}]\{6 - 5\exp[0.036(1-\varepsilon_r)]\} \tag{6.26}$$

$$\zeta_5 = 1 - 0.218\exp(-7.5 L_1/H) \tag{6.27}$$

- 143

The accuracy of equation (6.24) for a frequency of 1 GHz, as claimed in (Kirschning *et al*, 1981), is better than 2.5% for $0.01 \le L_1 / h \le 100$ and dielectric constants ε_r of less than 50.

6.4.2.1 Resistance R_s and inductance L_s of the short-circuit plate

The inductance L_s in nH and the resistance R_s in Ω of the short-circuit plate with the width W_s, the thickness t, and the height H are given by (Hoffmann, 1987)

$$L_s = 0.2H\left[\ln\left\{\frac{2H}{(W_s+t)}\right\} + 0.2235\left\{\frac{(W_s+t)}{H}\right\} + 5\right] \tag{6.28}$$

and

$$R_s = 1.3\times10^{-7}\frac{\sqrt{f\cdot\rho/\rho_{C_u}}}{W_s+t} \tag{6.29}$$

where f is the operating frequency in Hz, ρ is the specific resistance of the strip in $\Omega\cdot cm$. ρ_{C_u} is the specific resistance ρ of copper and is equal to $1.72\times10^{-6}\Omega\cdot cm$. The units for W_s, H and t are mm.

6.4.2.2 Coaxial feed wire impedance Z_f

The coaxial probe feed can be modelled as a coaxial stub in a parallel waveguide (Harrington, 1961). The formula for the probe input impedance is given by

$$Z_f = \frac{\eta_0}{4}k_0H\left(1 - j\frac{2}{\pi}\ln(1.781k_0r_f)\right) \tag{6.30}$$

where H represents the length of the probe and r_f is the probe radius in mm.

- 144

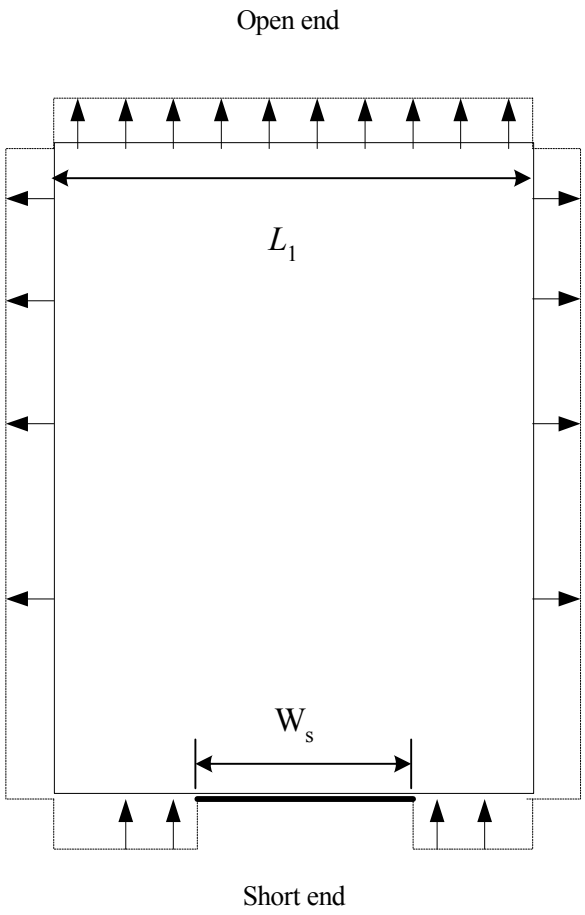

Figure 6-5 Equivalent radiating slots of PIFA – Top view.

6.4.3 Correction factor *C*

The edge of the top plate at the end with the short-circuit plate only radiates partially. Compared with the open end, the capacitive coupling is also reduced by a certain factor. A correction factor *C* is therefore introduced into the model (see Figure 6-3 (b)) and expressed by

$$C = \frac{L_1 - W_s}{L_1} \tag{6.31}$$

- 145

where L_1 and W_s are the widths of the top plate and short-circuit plate, respectively, as shown in Figure 6-5. From equation (6.31), it is observed that C is equal to 0 when the short-circuit plate has the same width as the top plate of the PIFA, and C is equal to 1 when there is no short-circuit plate. In the former case the termination is zero, i.e., a fully short-circuit plate, and in the latter case the termination is the same as the open end. Both of the cases are possible in practice.

6.4.4 Effect of a dielectric layer

A PIFA usually uses air or foam as its substrate in order to realise a wider bandwidth. Moreover, the top patch of the PIFA may be formed by etching a printed circuit board (PCB). Inverting the patch so that the PCB dielectric serves as the superstrate (cover), allows it to be fed by a coaxial probe, and so the substrate is still air or foam, as shown in Figure 6-6. In this case the top PCB substrate could form an external protection cover for the PIFA.

Now, for a PIFA covered or filled by a dielectric material, the effect of the dielectric layer is reflected in the line parameters of the equivalent transmission line, such as the effective dielectric constant ε_{re} and the line characteristic impedance Z_c.

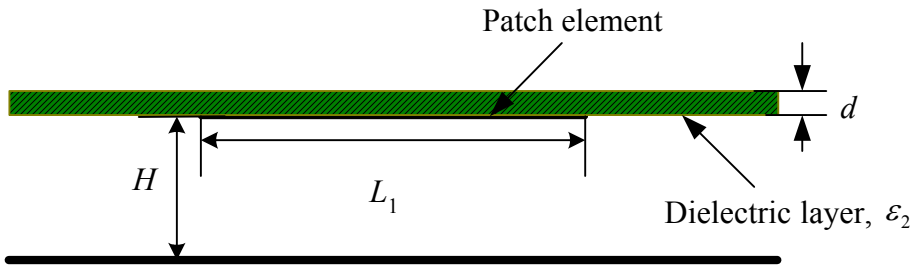

Figure 6-6 Cross section of an inverted microstrip.

As a result, a PIFA covered by a dielectric layer can be treated as an inverted microstrip line, as shown in Figure 6-6.

- 146

In an inverted microstrip, the dielectric layer above the patch changes the fringing electric fields between the patch and the ground plane. The effective dielectric constant can be obtained as (Tomar *et al*, 1987)

$$\sqrt{e_{re}} = 1 + F_1 F_2 \tag{6.32}$$

where

$$F_1 = \sqrt{e_r} - 1 \tag{6.33}$$

$$F_2^{-1} = \sum_{i=0}^{3} x_i (L_1 / H)^i \tag{6.34}$$

The function x_i in equation (6.34) is given by

$$x_i = \sum_{j=0}^{3} d_{ij} (H / d)^j \tag{6.35}$$

where the coefficients d_{ij} are known functions of ε_r (refer to Appendix D).

It is noted that this approximation is valid for ε_r up to 20. The stated error of the fit to the exact theoretical calculations is less than 0.6% for analysis and 1% for synthesis over the ranges $0.5 \le L_1 / H \le 10$ and $0.06 \le d / H \le 1.5$.

6.4.5 Air gap between dielectric cover and PIFA

When there is an air gap between the dielectric cover layer and the patch element of the PIFA, it can be treated as a multilayered microstrip line.

An approximate method for computing the equivalent dielectric constant ε_{eq} of the composite substrate having two layers is given by (Verma, 1995)

$$\varepsilon_{eq} = \frac{\varepsilon_{r1}\varepsilon_{r2}(d_1 + d_2)}{\varepsilon_{r1} d_2 + \varepsilon_{r2} d_1} \tag{6.36}$$

- 147

where ε_{r1} and ε_{r2} represent the dielectric constants of the two layers with a thickness of d_1 and d_2, respectively, as shown in Figure 6-7 (b).

For an air gap, ε_{eq} is obtained by letting ε_1=1 in equation (6.36). After that, the effective dielectric constant of the transmission line can also be computed using equations (6.32) to (6.35) but ε_r and d are replaced by ε_{eq} and ($d_1 + d_2$).

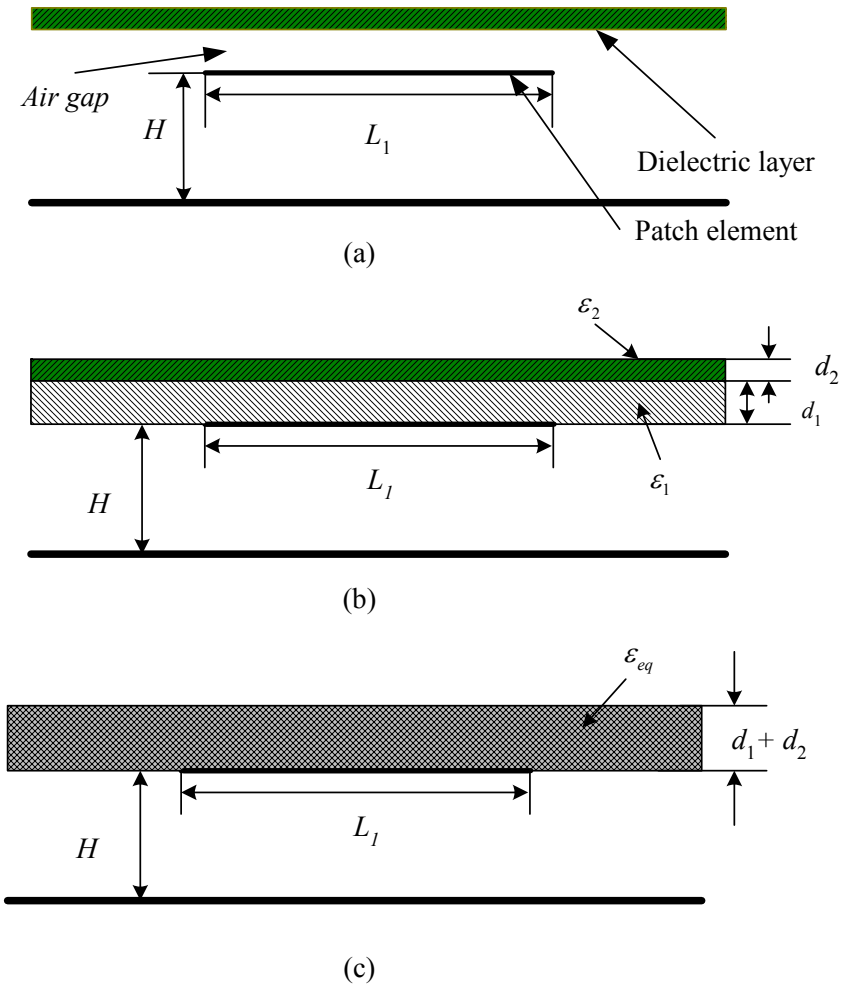

Figure 6-7 (a) Cross section of a PIFA with a dielectric layer having an air gap; (b) equivalent two-layer inverted microstrip line of (a); (c) equivalent one layer inverted microstrip line of (a).

- 148

6.5 Numerical Results

In this section, five examples with different configurations are presented to illustrate the use of the TLM described in section 6.3 and 6.4. Based on this model, a MATLAB (The Mathworks, 1984) program has been written to calculate the input impedance of the model.

6.5.1 PIFA with a fully short-circuit plate

Two PIFAs without a dielectric cover and referred to as case 1 and case 2 are considered. Their dimensions, as shown in Figure 6-3 (a), are tabulated in Table 6-1, where H and r_f represents the height and the probe radius of the antenna. In these two cases, we assume that the width of the short-circuit plate is the same as the width of the radiating patch, so that the correction factor C in equation (6.31) is set to zero. The results of the input impedance of the PIFAs based on the TLM are compared with the numerical results obtained using IE3D, an MOM based full wave electromagnetic simulation, as shown in Figure 6-8. From Figure 6-8, it can be observed that the TLM and MOM results have a reasonably good agreement except for the maximum and minimum values. It may also be noted that the resonant frequency in case 1 is more than 100 MHz lower than that for case 2. This is because the radiating patch in case 1 is bigger than the one in case 2. From this point of view, the TLM method reflects this change well.

Table 6-1 Physical parameters of PIFAs for TLM analysis

PIFA	L_2	L_1	H	W_s	d_f	r_f	Dielectric cover	Air gap
Case 1	70	40	5	40	20	0.75	no	no
Case 2	65	35	5	35	12	0.75	no	no
Case 3	65	35	5	35	12	0.75	yes	no
Case 4	65	35	5	35	12	0.75	yes	yes
Case 5	70	40	5	20	20	0.75	no	no

*All units in mm

- 149

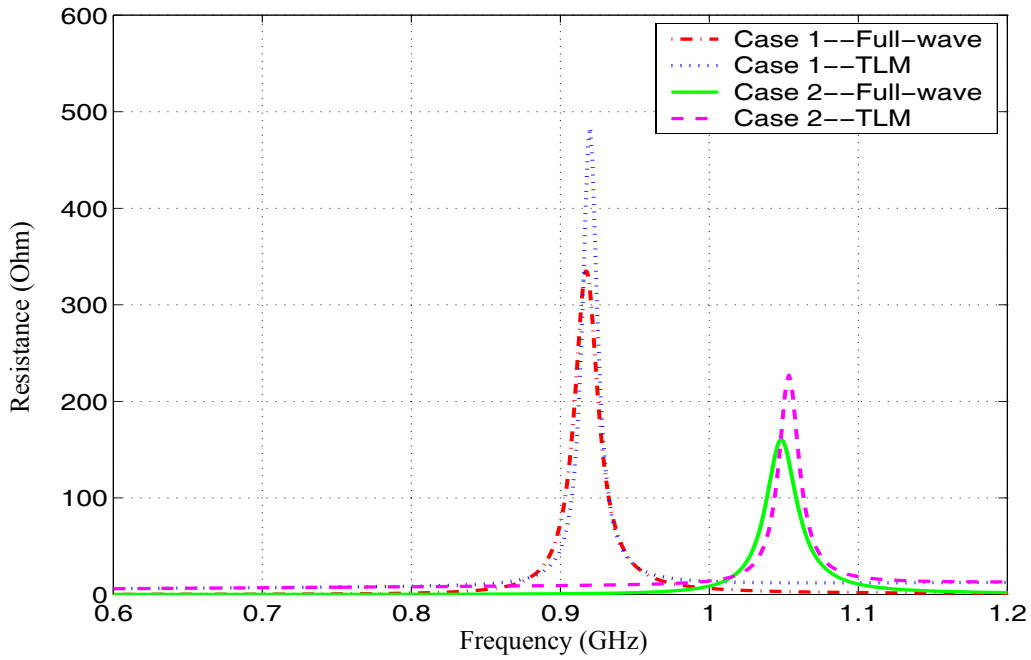

(a)

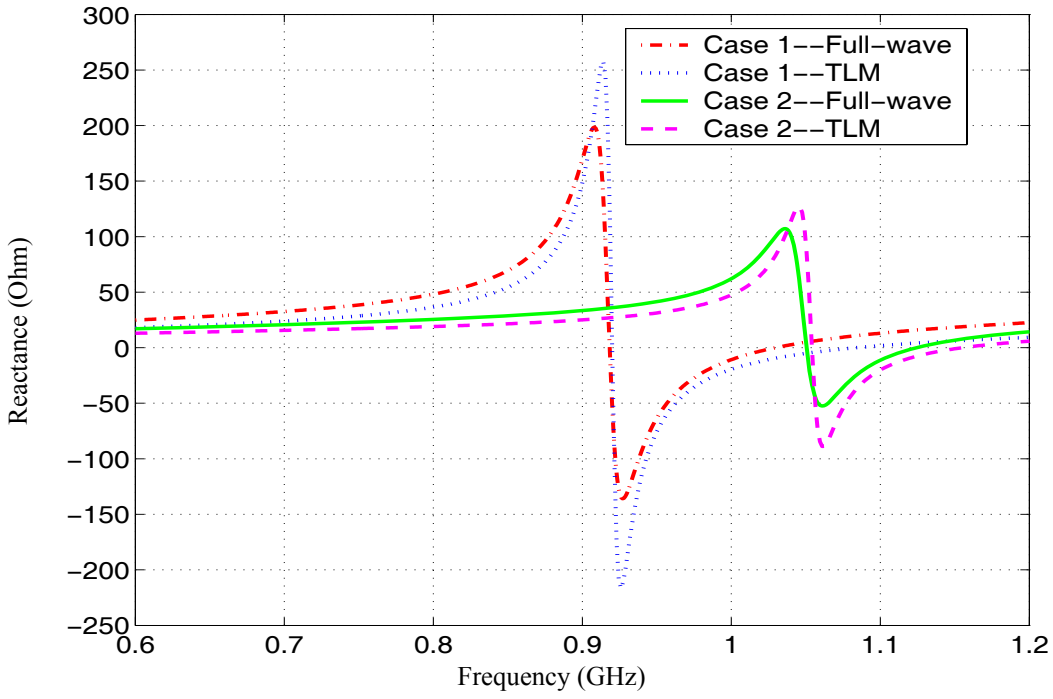

(b)

Figure 6-8 The input impedances of the PIFA for case 1 and 2: (a) resistance; (b) reactance.

- 150

6.5.2 PIFA with a dielectric cover

In this section, we consider the case of a PIFA with a dielectric cover. The dimensions of this PIFA, as given in case 3 of Table 6-1, are identical to those of case 2. The only difference is that the PIFA in case 3 is covered by a dielectric layer having a dielectric constant of 4.7 and a thickness of 1.6 mm. There is no air gap between the cover layer and the patch element. In this model, the transmission line is treated as an inverted microstrip line. The effect of the dielectric cover layer is included in both the effective dielectric constant ε_{re} of equation (6.36), and the characteristic impedance Z_c of equation (6.6) of the transmission line model. The input impedance of the PIFA, based on the TLM method for case 3, is compared with the computer simulated result of IE3D, as shown in Figure 6-9. From Figure 6-9, it can be observed that a reasonably good agreement is also achieved, except for the minimum and maximum values. In order to illustrate the effect of the dielectric cover layer, the input impedance of case 2 (without dielectric cover) is also shown in Figure 6-9. From these curves, it can be seen that the resonant frequency with a dielectric cover has shifted to a lower value. This is because the overall effective dielectric constant becomes larger due to the presence of the dielectric cover. For example, $\varepsilon_{re} = 1.0528$ for case 3, while $\varepsilon_{re} = 1$ for case 2. From these results, it can be observed that the TLM method reflects this change accurately.

- 151

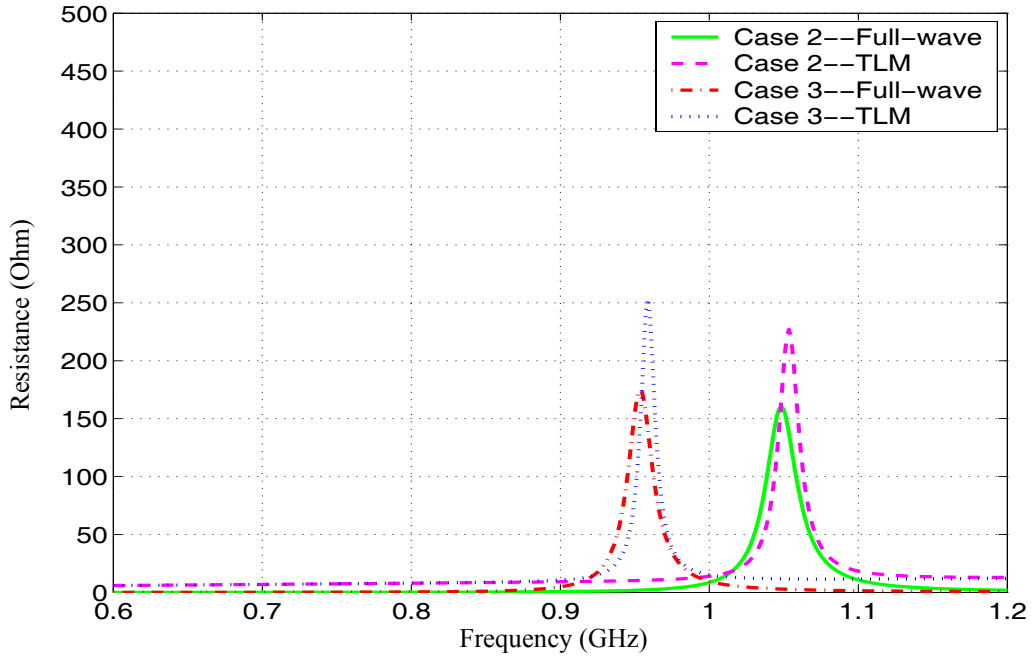

(a)

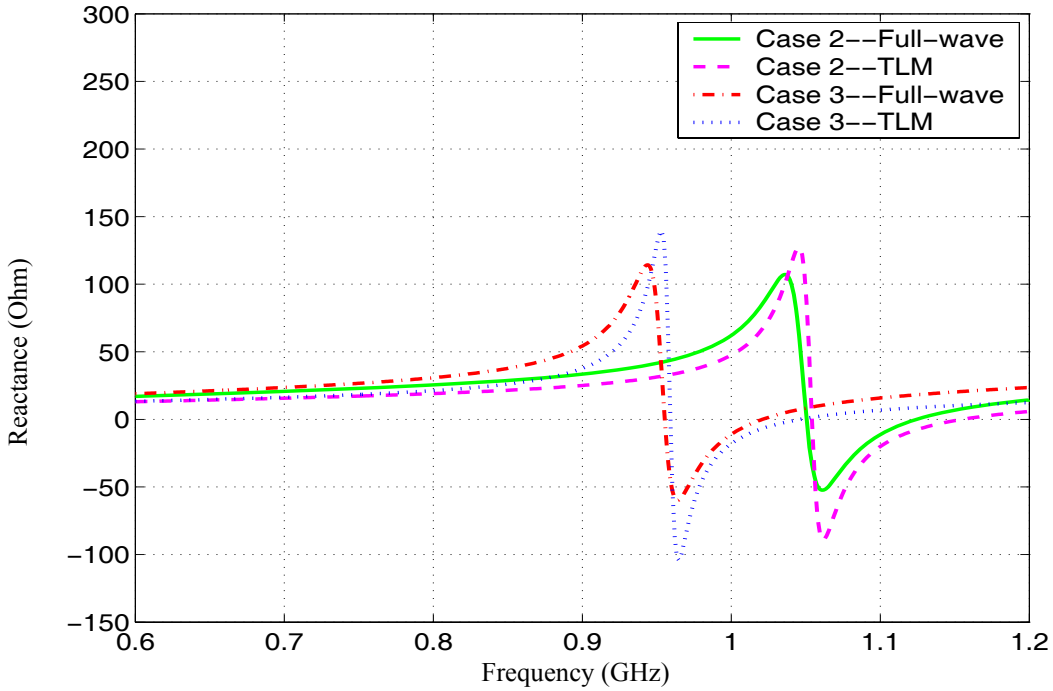

(b)

Figure 6-9 The input impedance of the PIFA for case 3: (a) resistance; (b) reactance.

- 152

6.5.3 PIFA with a dielectric cover having an air gap

Now, the case of a PIFA with a dielectric cover having an air gap, as given in case 4 of Table 6-1, is considered. The dimensions of the PIFA in both case 3 and case 4 are identical. The only difference is that in case 4 there is an air gap of 1.0 mm between the dielectric cover and the patch. In this model, an equivalent dielectric constant is first computed according to equation (6.36). Then the procedure to calculate the input impedance of the PIFA is the same as described in section 6.5.2. The input impedance of the PIFA of case 4, based on the TLM method, is compared with the computer simulated result from IE3D, as shown in Figure 6-10. From Figure 6-10, it can be observed that the TLM and MOM results have a reasonably good agreement again except for a slight frequency shift. In order to illustrate the effect of the air gap, the input impedances of case 3, based on both the TLM method and MOM, are also shown in Figure 6-10. From these curves, it can be observed that the resonant frequency in case 4 is shifted to a higher frequency, compared with case 3. This is because with an air gap the overall effective dielectric constant becomes smaller, compared to having no air gap. For example, $\varepsilon_{re} = 1.0236$ for this case.

- 153

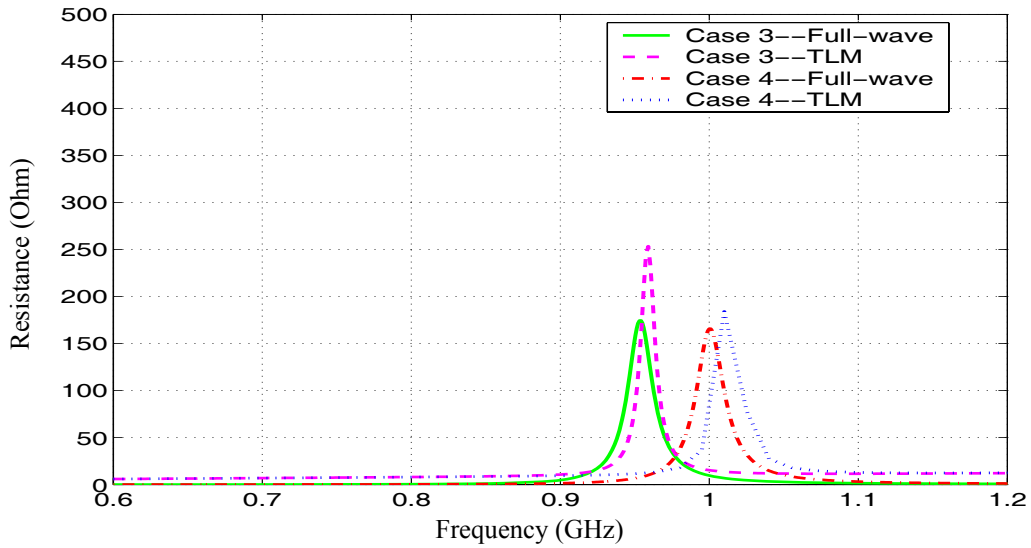

(a)

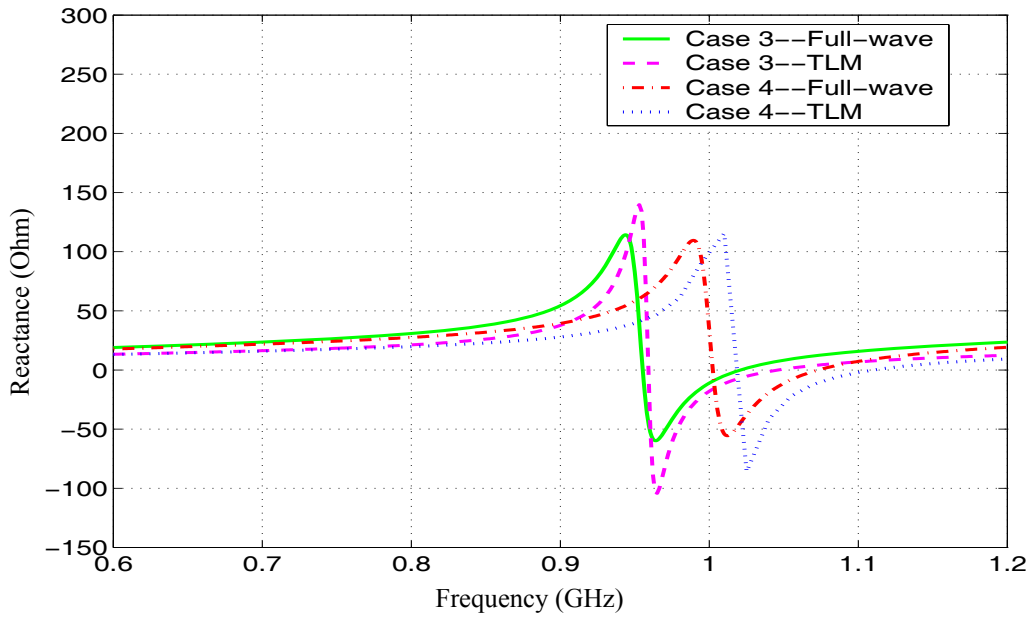

(b)

Figure 6-10 The input impedance of the PIFA for case 4: (a) resistance; (b) reactance.

- 154

6.5.4 PIFA with a partially short-circuit plate

Finally, the case is considered of a PIFA where the width of the short-circuit plate is less than that of the patch, as given in case 5 of Table 6-1. The dimensions of the PIFA in this case are the same as those in case 1, except that the width W_s of the short-circuit plate in case 5 is half of that in case 1. The correction factor C of equation (6.31) is therefore set to 0.5. In this case, not only the resistance and inductance of the short-circuit plate must be considered, but also the capacitance coupling and the radiation conductance at the edge of the short-circuit plate. Figure 6-11 shows the input impedances for this case, derived both by the TLM and the IE3D MOM methods. From Figure 6-11, it may be observed that reasonably good agreement (less than 1% error) is once again achieved between them, except for the minimum and maximum values. In order to illustrate the effect of the width of the short-circuit plate on the PIFA's resonant frequency, Figure 6-11 also shows the input impedance of case 1, where the width of the short-circuit plate W_s is equal to the width of the patch. From these graphs, it can be seen that the resonant frequency for case 5 is lower, compared to that of case 1, because the effective inductance of the PIFA increases when the width of the short-circuit plate is set narrower than that of the patch element. The TLM reflects this change accurately.

- 155

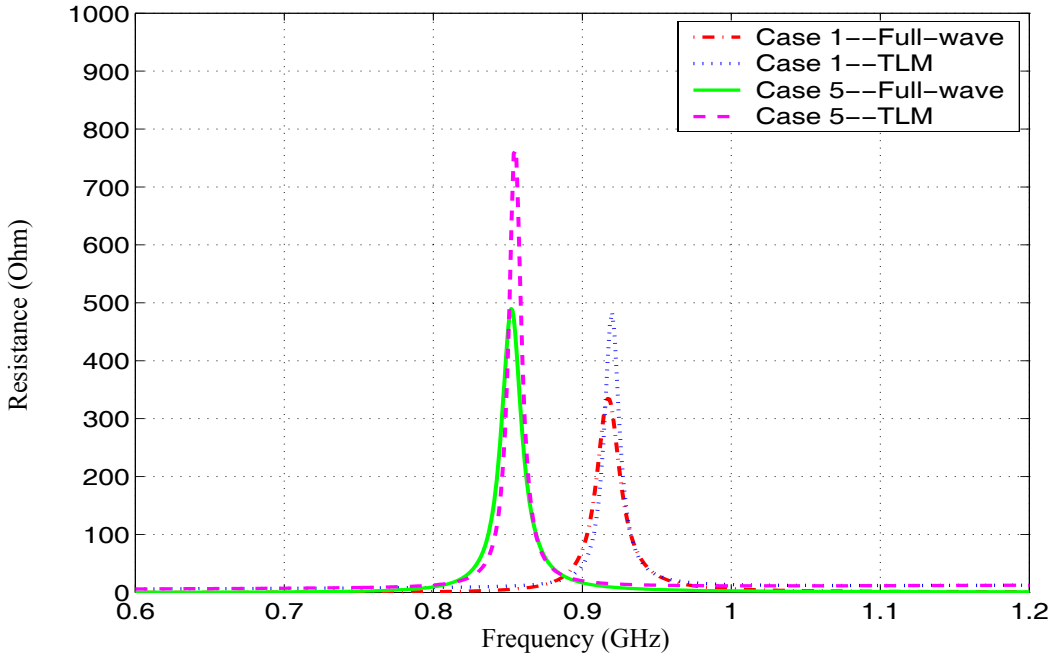

(a)

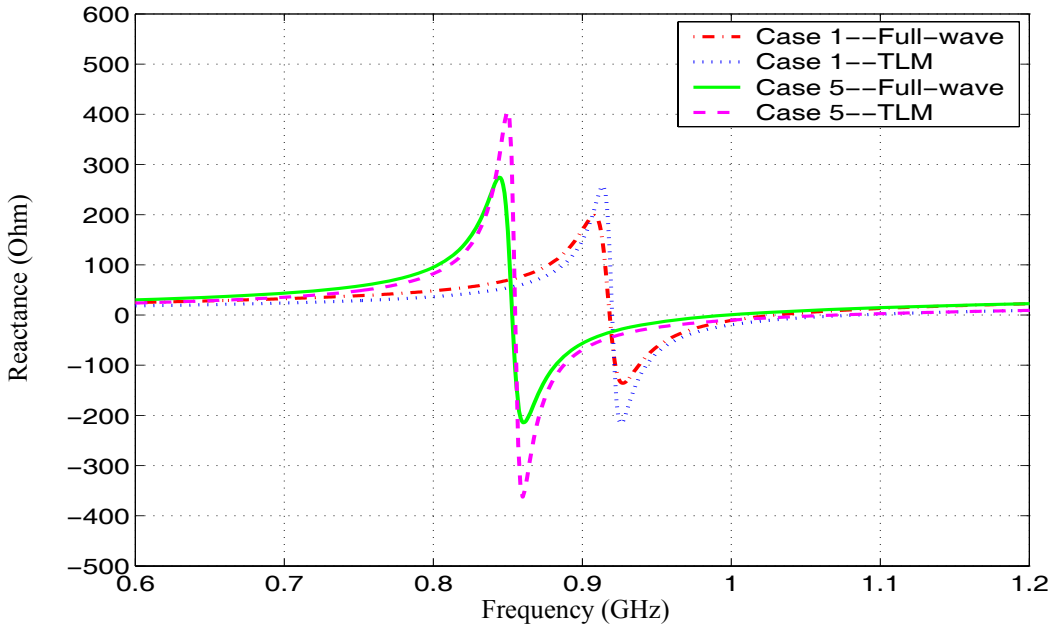

(b)

Figure 6-11 The input impedance of the PIFA for case 5: (a) resistance; (b) reactance.

- 156

6.6 Summary

This chapter presents a modified transmission-line model for computing the input impedance of a PIFA. The model incorporates the effects caused by the individual parts of the PIFA and any dielectric cover layers present. Comparison of the input impedances for different antenna configurations, computed using this modified TLM and the IE3D MOM simulation, shows a reasonably good agreement. However, the TLM only takes seconds to produce the antenna input impedance frequency response, compared with the hours needed by the IE3D method. This analytical approach for estimating the input impedance of a PIFA having a dielectric protective cover layer, can provide a cost-effective alternative to numerical methods. Alternatively it can validate a set of initial design parameters that can be used as the starting point for further numerical modelling, thus saving significant computing resources.

- 157

CHAPTER SEVEN

7. DESIGN OF A SINGLE-FEED DUAL-BAND PLANAR INVERTED-F ANTENNA AND THE EFFECT OF A DIELECTRIC COVER ON ITS PERFORMANCE

7.1 Introduction

The performance of a single band PIFA with dielectric radome operating as an internal mobile terminal antenna has been investigated in chapter 4 and 5. These investigations included relocation of the antenna on a small ground plane and the electromagnetic interaction between the antenna and the dielectric radome. In chapter 6, a modified TLM has been proposed to provide an initial design estimate for engineering the PIFA with a top dielectric cover layer. With the widespread use of mobile wireless communication systems and allocation of the second frequency band, there has been an increasing interest in developing dual-band antennas for mobile radio applications. It has also stimulated an increasing interest in understanding the effect of the dielectric casing on such a dual band antenna when used as an internal antenna within a mobile terminal.

In this chapter, a novel dual-band PIFA for wireless communications is presented. The proposed PIFA, driven by a single capacitive feed, consists of two separate co-located radiating elements. Such a dual-band PIFA is almost the same size as a single-band PIFA operating at the lower of the two resonant frequencies. As an example, the design of this novel dual-band antenna operating in the ISM frequency bands of 900 MHz and 2400 MHz is described. Computer simulations, based on the MOM, have been used to study the performance of the antenna. The simulated results have also been validated by measurement carried out on a fabricated antenna. After that, the effects of a dielectric cover on its input and radiation characteristics have been investigated.

- 158

7.2 Antenna Configuration

7.2.1 Radiating elements

The proposed dual-band PIFA consists of two separate radiating elements: a rectangular radiating element for the upper band and an L-shape radiating element for the lower band. One end of each radiating element is connected to the ground plane using a short-circuit plate. This is shown in Figure 7-1.

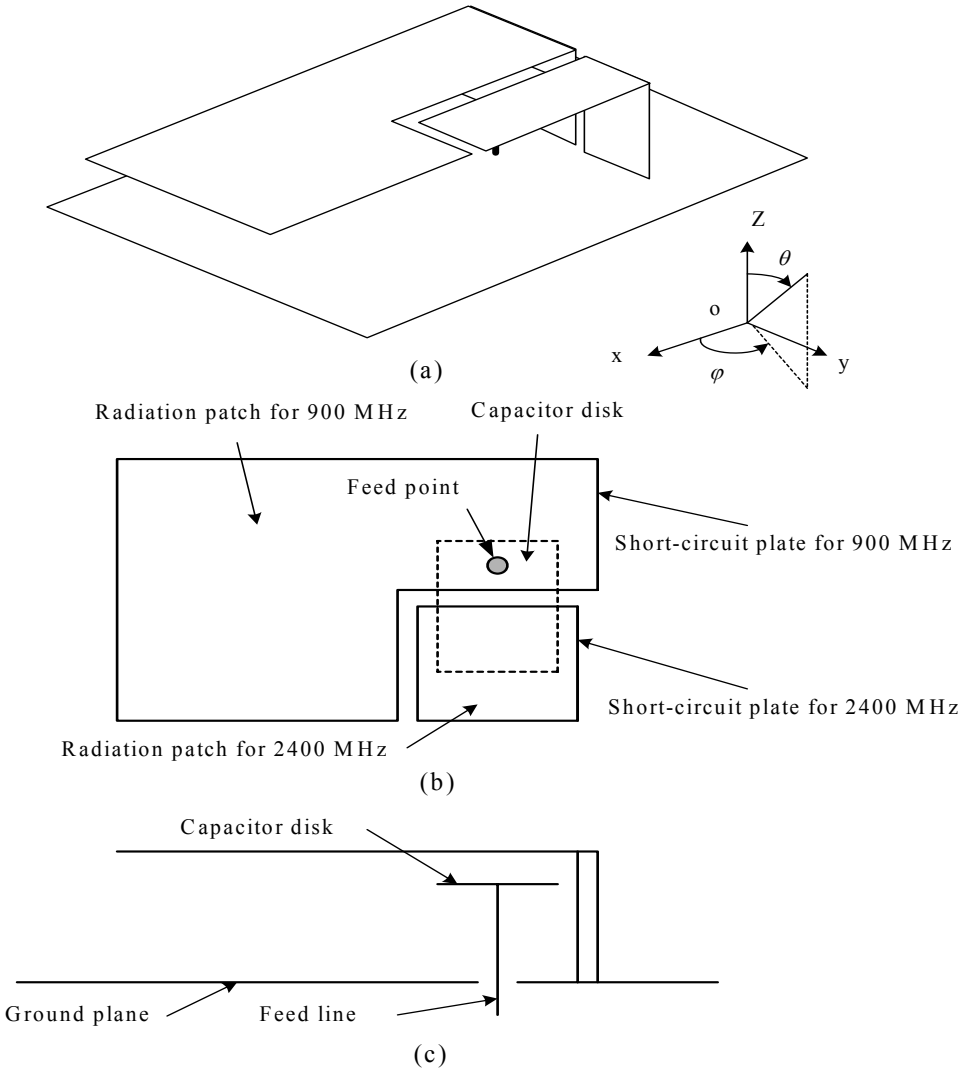

Figure 7-1 The proposed dual-band PIFA: (a) overview; (b) top view; (c) side view.

- 159

Consider the radiating element for the upper resonance to be that of a normal single-band standard PIFA. The initial dimensions of this element can be estimated using equations (4.9), (4.10) and (4.11). Although the radiating element for the lower resonant frequency has a different shape to the normal planar inverted-F antenna, both of them would have nearly the same current distribution. Therefore, its initial dimensions can also be approximately determined using the same equations.

7.2.2 Feed method

Patch antennas can be fed in a variety of ways. Among the widely used feed approaches are microstrip line and probe. Perhaps the simplest and most cost effective is a microstrip line feed connecting either at the patch edge or insetting into the patch. It can be implemented as a completely printed structure, but it suffers from potential feed radiation (Sainati, 1996). Such unwanted feed radiation may be avoided using the probe feed technique by connecting the centre conductor of a coaxial cable to a patch on the other side of the ground plane. A disadvantage of the coaxially fed configuration is the unavoidable mismatch, even at resonance, due to the inductance of the probe, particularly for a thick substrate. One possible solution, called capacitive feeding, is to cancel out the probe inductance by adding a capacitor in series. There are two ways of realising this series capacitor. For example, the capacitor can be formed within the patch itself by etching a rectangular or circular gap around the feed probe as shown in Figure 7-2 (a). The other way is to implement the capacitor by adding a disk to the end of the shorted probe, as shown in Figure 7-2 (b). The etched capacitor is more easily implemented, but predicting the capacitance so realised is more complex. On the other hand, the disk capacitor is a more complicated structure practically, but its capacitance can be more readily calculated. The latter method has been researched by Vandenbosch *et al* (Vandenbosch *et al*, 1994; Vandenbosch, 1995; Vandenbosch, 1999).

The capacitive feed technique was first adopted by Rowell for a single band PIFA in 1997 (Rowell *et al*, 1997). In dual-band or multi-band antenna design, a single feed is always attractive since it avoids the need for additional components, such as power switches or combiners, which are required to couple signals covering different frequency bands to the appropriate antenna inputs. Apart from the added complexity,

- 160

such components can introduce power losses as well as an increase in the volume, weight and cost of the antenna system. As reviewed in section 3.2, most of the dual-band PIFAs reported in the literature have two separate feeds. In this study, the capacitive feed is adopted to provide a single feed for the proposed dual-band PIFA.

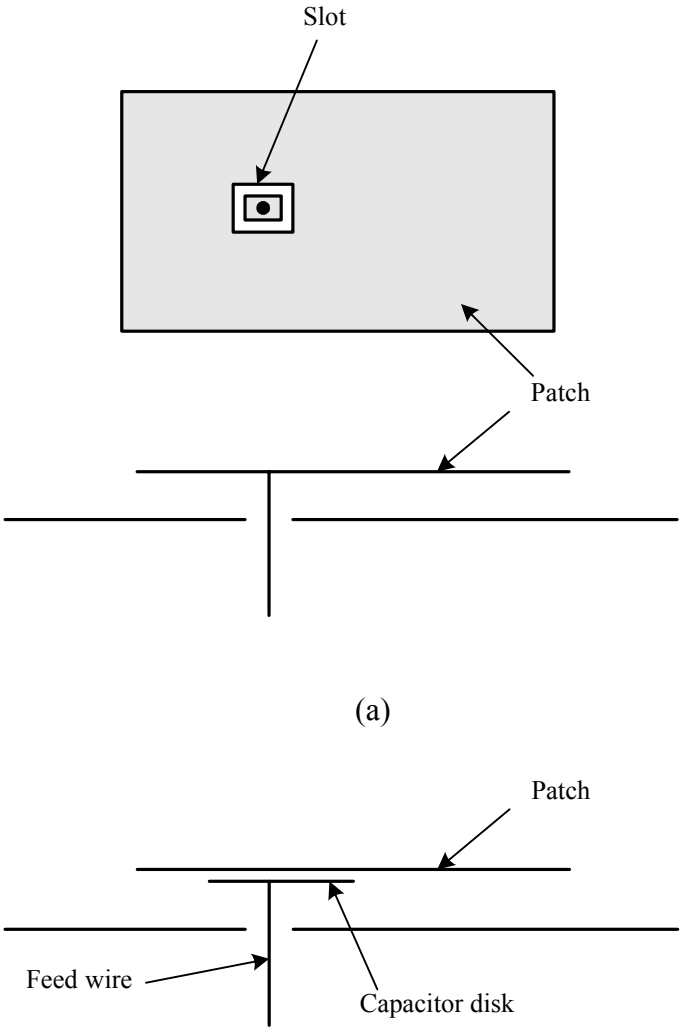

Figure 7-2 Configurations of capacitive feed: (a) etched capacitor; (b) disk capacitor.

- 161

7.3 Configuration Study

Computer simulations using IE3D have been performed to study different configurations of this proposed antenna over a large frequency range of 600 MHz to 2800 MHz, which includes both the 900 MHz and 2400 MHz ISM bands. In the simulations, the highest meshing frequency was set at 3 GHz, with 20 cells per wavelength discretisation, and edge meshing was adopted to achieve high accuracy in the calculation of the current distribution. Figure 7-3 shows the MOM simulation model of the dual-band PIFA.

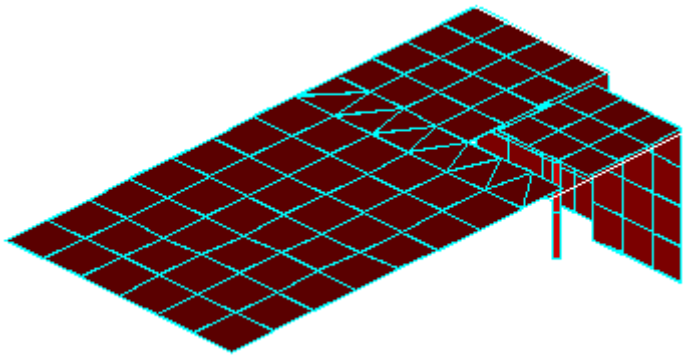

Figure 7-3 The MOM simulation model of the proposed dual-band PIFA.

7.3.1 Individual parts

In an attempt to identify the effect introduced by each individual part on the operating performance of the dual-band PIFA, a study of the PIFA in different stages of construction was first performed. The input impedance was computed for five different configurations as shown in Figure 7-4: (i) feed wire only, (ii) feed wire and capacitor disk, (iii) feed wire, capacitor disk and lower band element, (iv) feed wire, capacitor disk and upper band element, and (v) feed wire, capacitor disk and both lower and upper band elements. Figure 7-5 shows the dimensions of the various parts of this dual-band PIFA while their values are tabulated in Table 7-1.

- 162

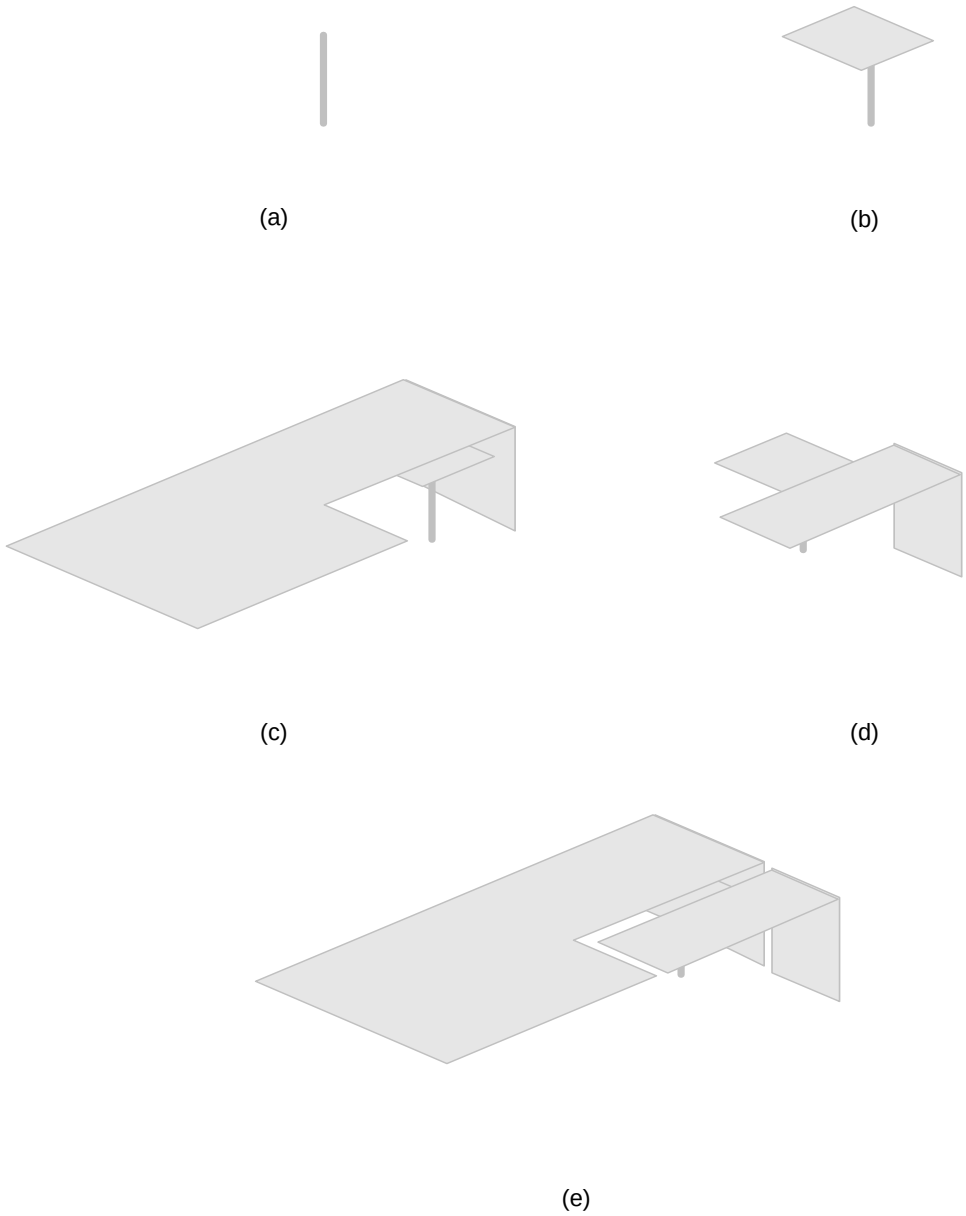

Figure 7-4 Configurations of a dual-band PIFA in different stages of construction: (a) feed wire only; (b) feed wire and capacitor disk; (c) feed wire and capacitor with the lower band patch; (d) feed wire and capacitor with the upper band patch; (e) feed wire and capacitor with the lower and upper band patches.

- 163

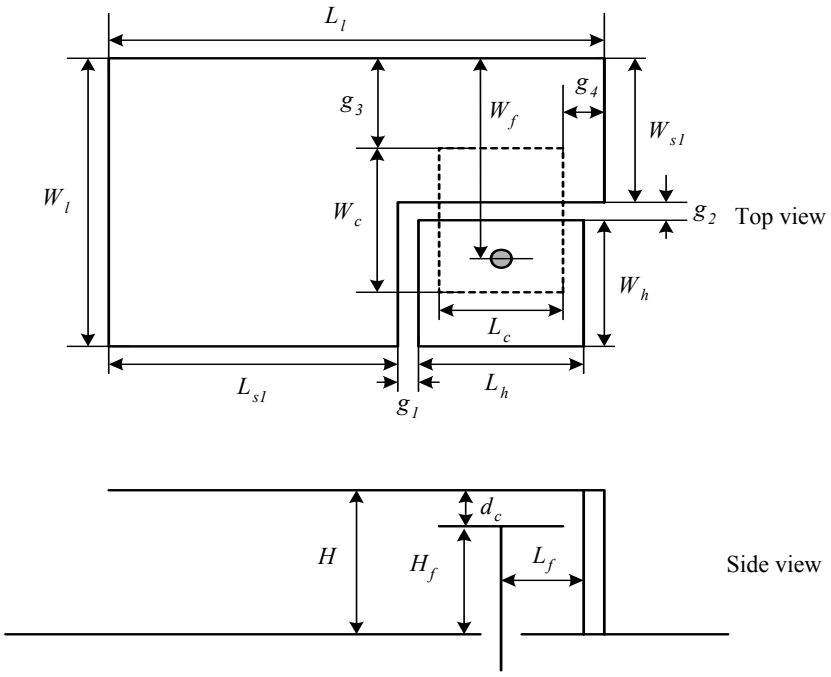

Figure 7-5 The dimensions of the different parts of the dual-band PIFA.

- 164

Table 7-1 A list of dimensions, in mm, for the dual-band PIFA

Lower band radiating patch	$L_l = 55$ $W_l = 36.5$ $L_{s1} = 39$ $W_{s1} = 25.5$ $H = 15$
Upper band radiating patch	$L_h = 11$ $W_h = 10.5$ $H = 15$
Capacitor disk	$L_c = 9$ $W_c = 12$ $H_f = 14$
Position parameters	$W_f = 16$ $L_f = 6.5$ $d_c = 1$ $g_1 = 3$ $g_2 = 0.5$ $g_3 = 5$ $g_4 = 2.5$

The input impedance corresponding to each of these different configurations is plotted in Figure 7-6. From Figure 7-6, it can be noted that the input resistance associated with the "feed wire only" is low and the reactance is strongly capacitive (green solid lines). This is the characteristic of an electrically small monopole. The input resistance of the "feed wire and capacitor disk combination" is much larger than the "feed and wire only" particularly at the higher frequencies, but the reactance is much less capacitive and becomes inductive when the operating frequency is greater than 2200 MHz (blue dashed lines). The "feed wire, capacitor disk and lower band element" configuration has a strong resonance characteristic in the 900 MHz band. The impedance at this resonance of 921 MHz has a sharp peak in the resistance of around 100 Ohm and a sharp swing in the reactance (black dashed and dotted lines). The resistance of the "feed wire, capacitor disk and upper band element" configuration is quite small, which is similar to that of the "feed wire only" structure and its reactance is slightly less

- 165

capacitive than that shown by the “feed wire and capacitor disk” combination (red dotted lines). For this configuration, no obvious resonance was observed in the upper band and both the resistance and inductive reactance tended to increase with increasing the operating frequency. The resistance of the “feed wire, capacitor disk and upper band patch with shorting plate” configuration is quite small, which is similar to the “feed wire only” structure and the reactance is slightly less capacitive than the “feed wire and capacitor disk” configuration (both red dotted lines). For the complete configuration of “feed wire, capacitor disk, and both lower and upper band elements”, the impedance not only shows a resonance at the lower band, very similar to the “feed wire, capacitor disk and lower band elements” configuration, but at the higher band also has another resonance, less sharp but having a relatively large peak value of over 210 Ohm in resistance. At the same time its reactance shows a less sharp swing from inductive to capacitive at the upper band (cyan solid lines). This suggests that for this dual-band PIFA, the lower band resonance is quite independent of the presence of the upper band radiating element. It follows that the dimensions of the lower band radiating element can be determined on their own, but that the upper band resonance is strongly impacted by the presence of the lower band element structure.

- 166

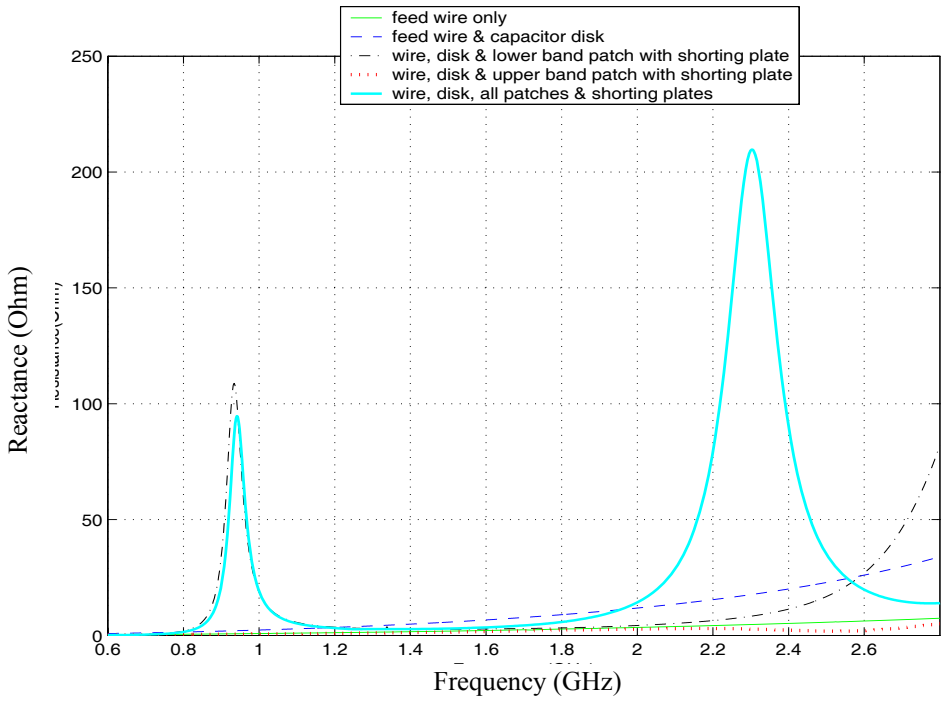

(a)

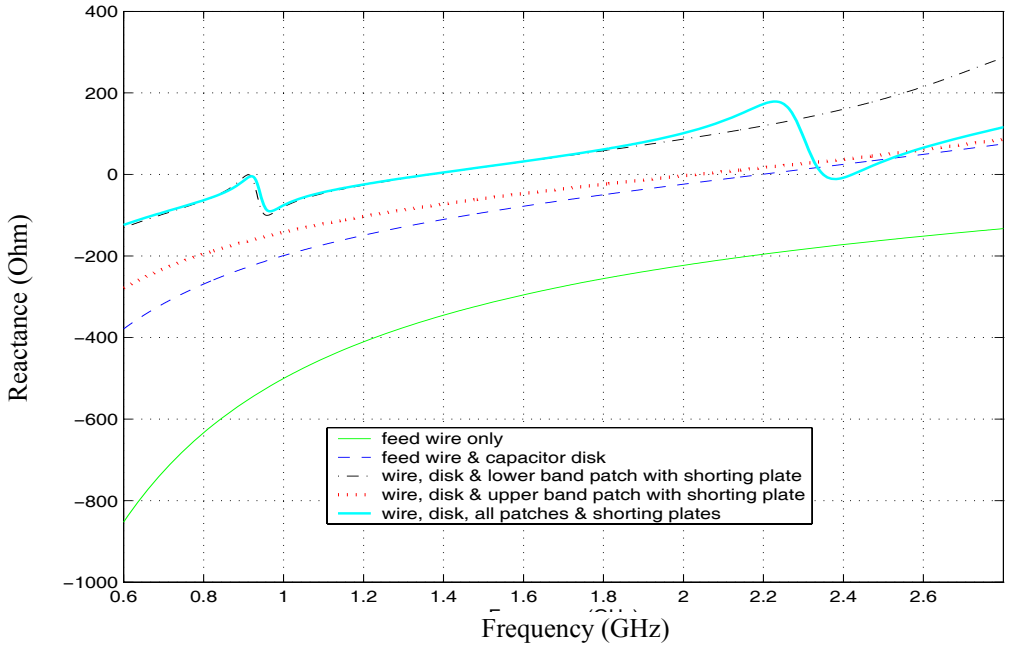

(b)

Figure 7-6 The impedance characteristics for the dual-band PIFA at different stages of construction: (a) resistance; (b) reactance.

- 167

7.3.2 Feed disk

In this section, the effect of the configuration of the feed disk on the input impedance of the proposed dual-band PIFA is examined. The different configurations of the feed disk are divided into the three groups. Each group has 5 cases. Group 1 uses a rectangular disk, as shown in Figure 7-7 (a). Group 2 and 3 uses a L shape disk, as shown in Figure 7-7 (b), except for case F and case K. The description of each case is listed in Table 7-2, Table 7-3 and Table 7-4. The simulated input impedance for each individual case in each group is shown in Figure 7-8, Figure 7-9 and Figure 7-10.

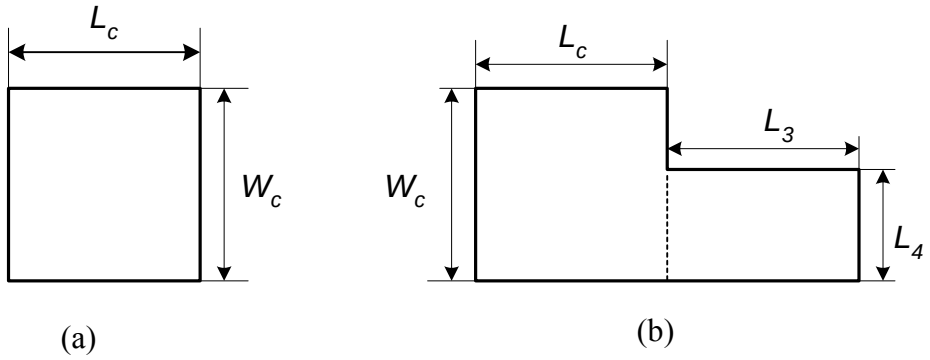

Figure 7-7 Geometry of the feed capacitor: (a) rectangular; (b) L shape.

Table 7-2 Parameters used for feed study in cases A to E of Group 1

Case	Geometry of the feed capacitor	Dimensions in mm
A	Rectangular	H_f = 14.5
B	Rectangular	H_f = 14
C	Rectangular	H_f = 13.5
D	Rectangular	H_f =14.75, L_l = 45
E	Rectangular	H_f =14, L_l = 45

Note: Except for H_f and L_l, all other parameters as shown in Table 7-1.

- 168

In the first group (Group 1), listed in Table 7-2, the input impedance characteristics of the antenna associated with different heights of the feed disk are examined. From Figure 7-8, it is found that the peak value of the resistive part increases for both the lower resonance and the upper resonance, when the height of the feed disk increases. For example consider the cases from C to B and to then case A. Looking next at the reactance of the input impedance, the whole curve is shifted up and at the same time the peak to peak value increases as the height of the feed disk increases. This is due to a larger resultant capacitance when the height of the feed increases. However, for both the resistance and reactance, the influence is much stronger in the upper band than that in the lower band. The frequency shift is obvious in the upper band but not so noticeable in the case of the lower band as the height increases. This is because the reactance contributed by the same value capacitance at a lower frequency is greater than that at a higher frequency. The results indicate that adjusting the height of the feed disk could alter both resonant frequencies (lower and upper) and the respective values of the input impedance at the same time but not independently. Comparing case B with E, it is found that the lower band resonant frequency is shifted to a higher value, but there is almost no change observed in the upper band when the length of the lower band antenna patch is decreased. This suggests that the length L_l can be used to control the resonant frequency of the lower band independently. The same findings are observed by comparing case D with E.

- 169

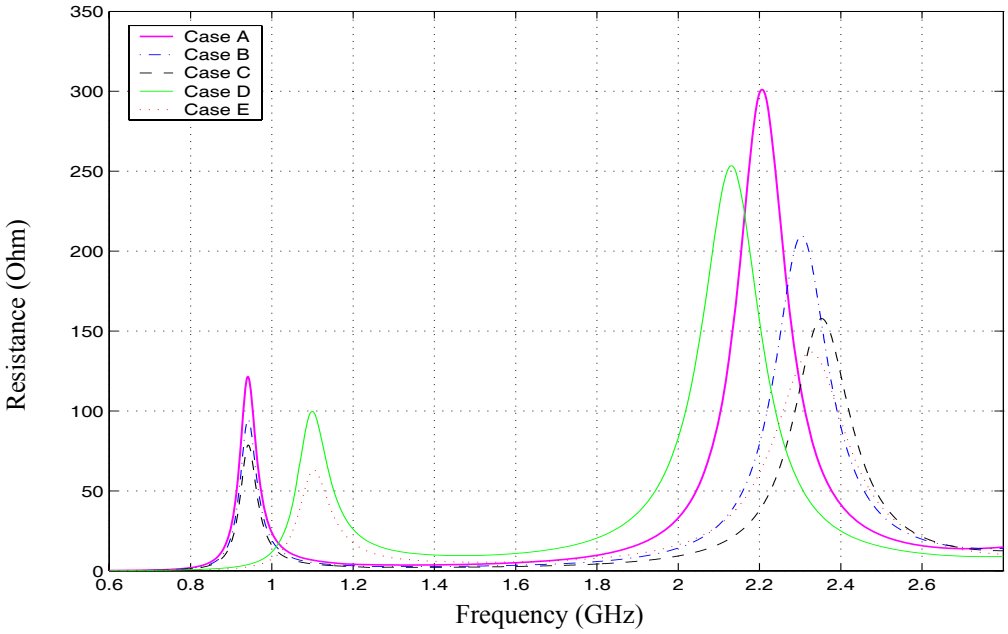

(a)

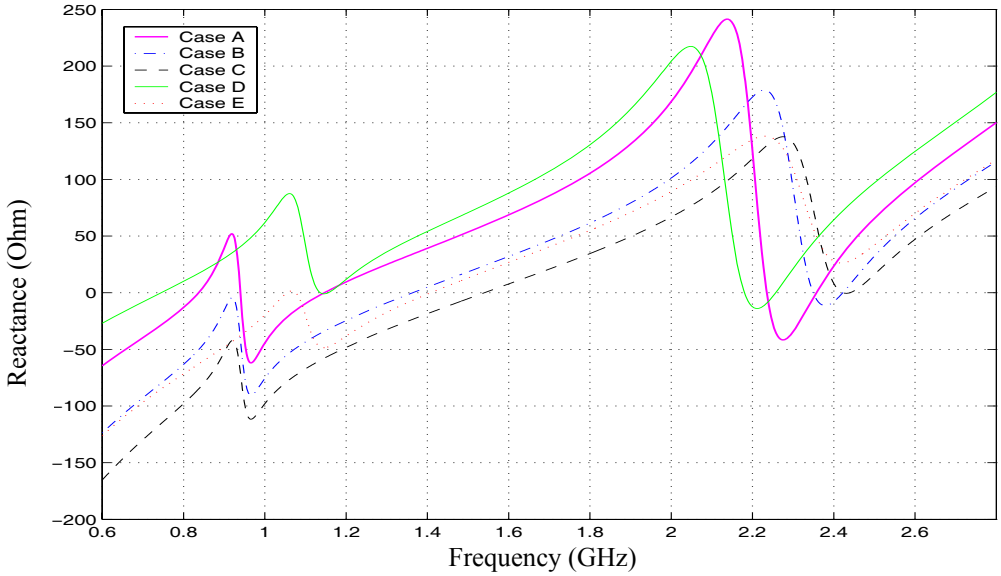

(b)

Figure 7-8 The input impedances of the dual-band PIFA for cases A to E of Group 1: (a) resistance; (b) reactance.

- 170

For the second group (Group 2), listed in Table 7-3, an "L" shape feed disk is used instead of the rectangular disk, in an attempt to achieve a stronger coupling with the lower band patch while reducing the effect at the higher band. Comparing the two curves of case F and G in Figure 7-9, it is found that the change to the L shape feed disk causes the input impedance to be affected not only in the lower band but also in the upper band. The variation in behaviour of the input impedance due to the change of this feed disk shape is almost the same as that caused by increasing the height of the feed disk. This is because the resulting capacitance of the feed disk increases for both of the cases. The failure to maintain the original input impedance of the upper band is because in this new dual-band configuration, the effects of the various constituent parts of the lower band antenna have a great impact on the behaviour of the upper band. This point has been outlined previously in section 7.3.1. In case H, the length L_3 of the feed disk (see Figure 7-7) increases so that the resulting capacitance of the feed disk is larger, compared with that of case G. In cases H, I and J, the same "L" disk is used but the length of the patch for the lower band is different. As expected, it is observed that the main difference in these three cases is the shift in the resonant frequency in the lower band.

Table 7-3 Parameters used for feed study in cases F to J of Group 2

Case	Geometry of the feed capacitor	Dimensions in mm
F	Rectangular	$H_f = 14$
G	L shape	$H_f = 14$, $L_3 = 30$, $L_4 = 9.5$
H	L shape	$H_f = 14$, $L_3 = 40$, $L_4 = 9.5$
I	L shape	$H_f = 14$, $L_3 = 40$, $L_4 = 9.5$, $L_l = 58.6$
J	L shape	$H_f = 14$, $L_3 = 40$, $L_4 = 9.5$, $L_l = 65$

Note: Except for H_f and L_l, all other parameters as shown in Table 7-1.

- 171

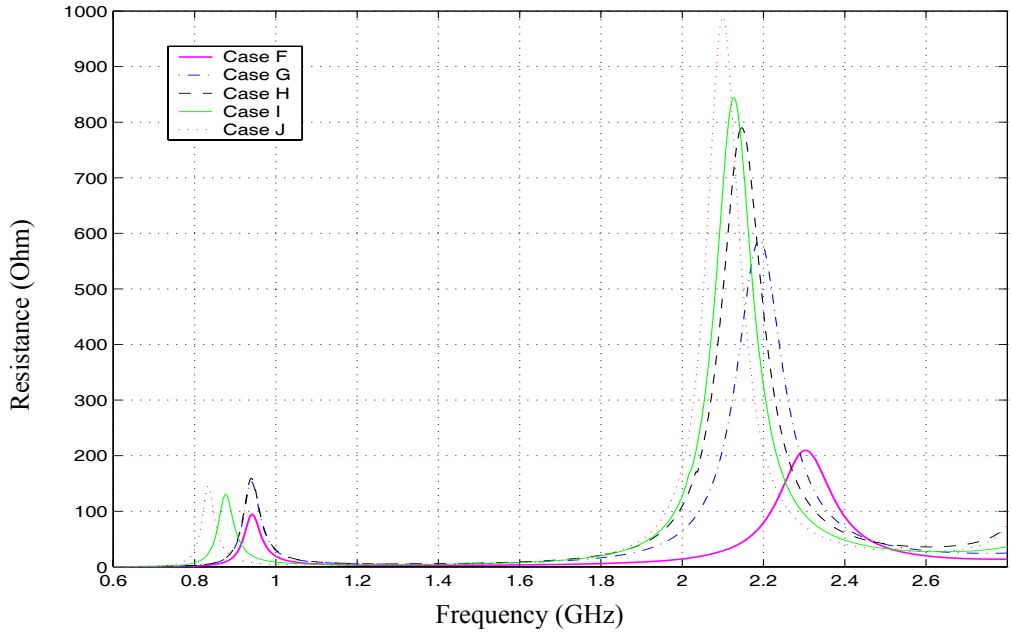

(a)

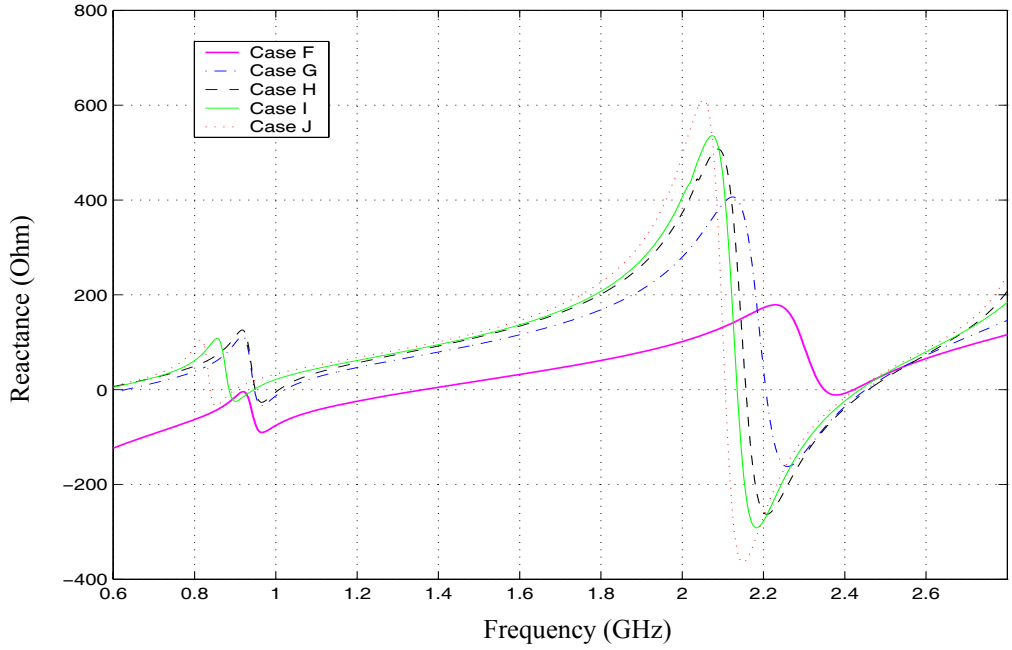

(b)

Figure 7-9 The input impedances of the dual-band PIFA for cases F to J of Group 2: (a) resistance; (b) reactance.

- 172

In the last group (Group 3), as listed in Table 7-3, the study is focused on how to control the performance of the upper band using the feed disk configuration. In this investigation, the physical parameters, W_c and L_c, are chosen to change. From Figure 7-10, it is found that when W_c increases (comparing case N with M), the resonant frequency of the upper band is shifted lower. This is because when W_c increases the area of the disk increases, that is, the capacitance of the feed disk increases in the upper band. However, the increase in W_c does not disturb the resonance of the lower band. This is because the upper band configuration of the antenna does not impact on the lower band performance, as discussed in section 7.3.1. When L_c decreases, as described in case O, the resonant frequency of the upper band is being pulled down, because in this case the area of the disk becomes smaller and the capacitance of the feed disk is reduced. As expected, the change in L_c does not affect the input impedance of the lower band.

In summary, all of these results indicate that the capacitive feed can provide a flexible way to control the two individual resonances and match the design specifications of the proposed dual-band PIFA.

Table 7-4 Parameters used for feed study in cases K to O of Group 3

Case	Geometry of the feed capacitor	Dimensions in mm
K	Rectangular	H_f = 14
L	L shape	H_f = 14, L_3 = 40, L_4 = 9.5
M	L shape	H_f = 14, L_3 = 40, L_4 = 9.5, L_l = 58.6
N	L shape	H_f = 14, L_3 = 40, L_4 = 9.5, L_l = 58.6, W_c = 13
O	L shape	H_f = 14, L_3 = 40, L_4 = 9.5, L_l = 65, W_c = 13, L_c = 8.9

Note: Except for H_f and L_l, all other parameters as shown in Table 7-1.

- 173

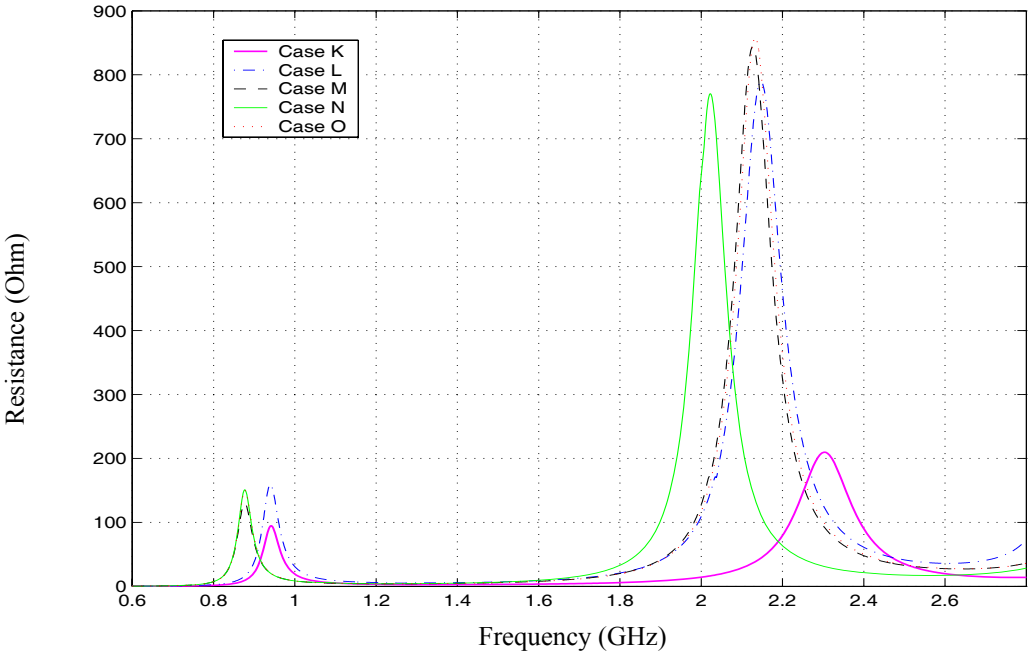

(a)

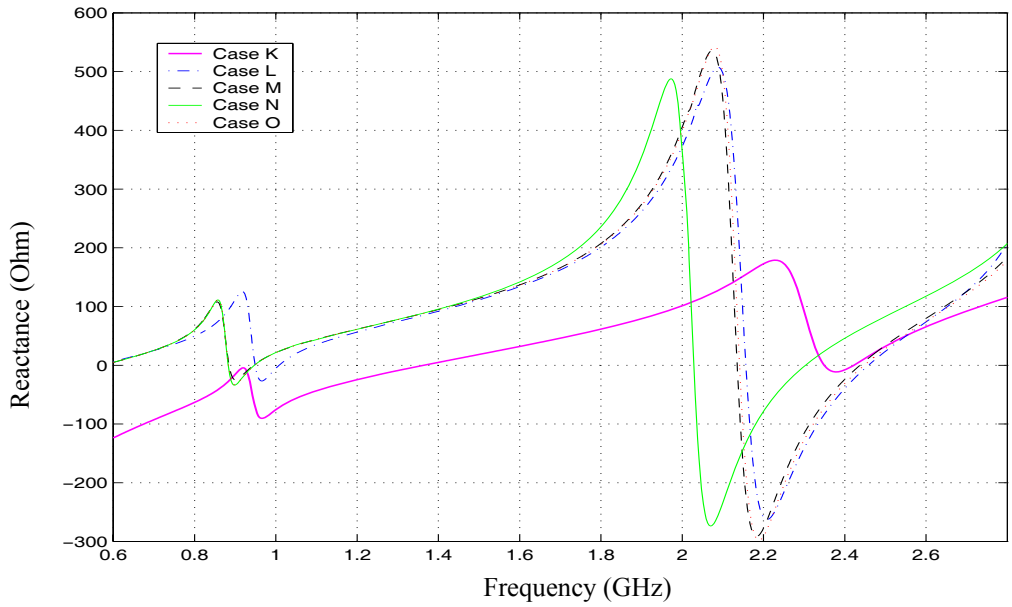

(b)

Figure 7-10 The input impedances of the dual-band PIFA for cases K to O of Group 3: (a) resistance; (b) reactance.

- 174

7.4 Numerical Results for the Dual-band PIFA

7.4.1 Return loss and bandwidth

The return loss over the frequency range of 600 MHz to 2800 MHz of the dual-band PIFA with the dimensions given in Table 7-1, is shown in Figure 7-11 . From this figure, the bandwidth of this PIFA, specified for a VSWR of ≤ 2, for the lower band, is found to be 29.4 MHz in the range from 902.7 MHz to 932.1 MHz. This bandwidth will fully cover the operating range for the ISM band at 900 MHz. Similarly, the bandwidth for the upper band is found to be 91 MHz in the range from 2395.8 MHz to 2486.8 MHz. Again this bandwidth will fully cover the ISM band at 2400 MHz. Figure 7-12 shows the VSWR of the antenna over the frequency range from 600 MHz to 2800 MHz.

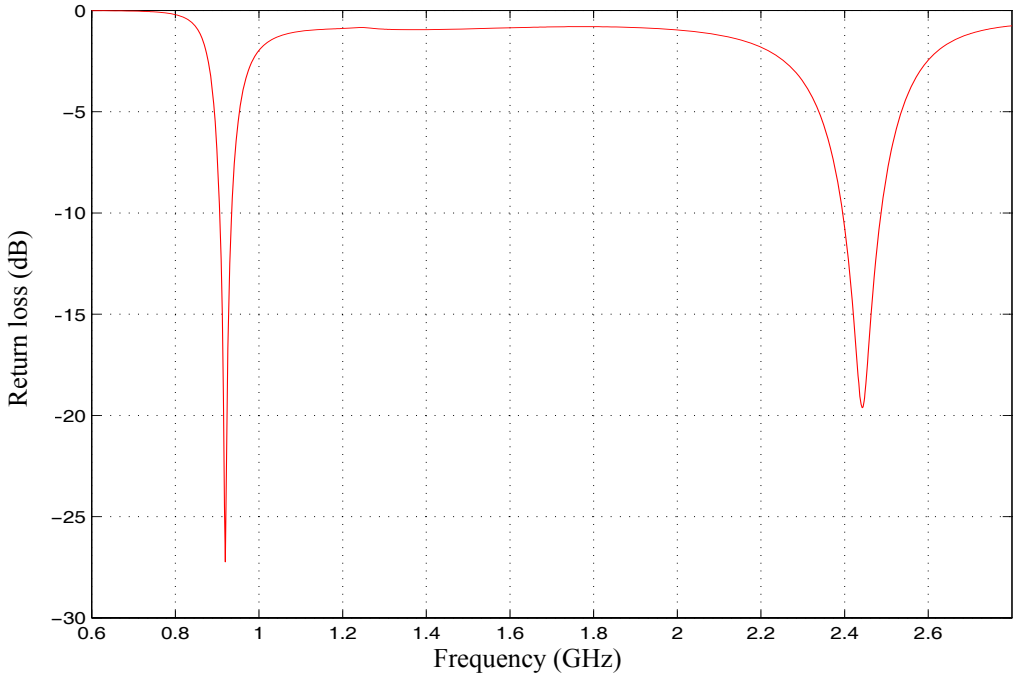

Figure 7-11 The return loss of the proposed dual-band PIFA.

- 175

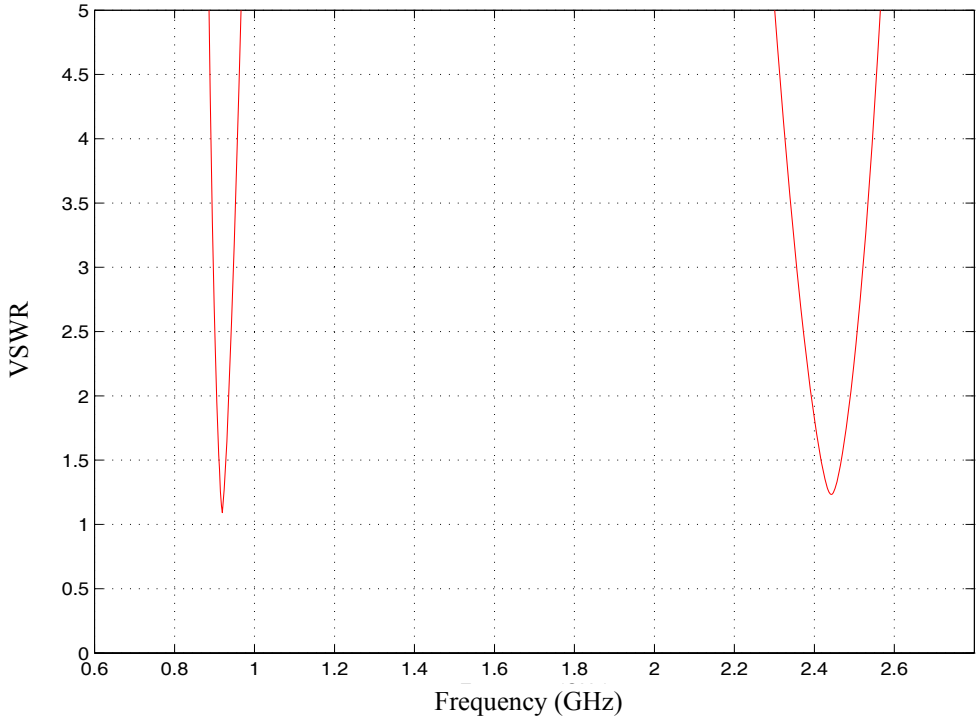

Figure 7-12 The VSWR of the proposed dual-band PIFA.

7.4.2 Surface current distributions

To gain an insight into the complex interactions between each individual part of the antenna, the currents flowing on the surfaces of each conductor have been examined.

Figure 7-13 (a) and (b) show the average current densities on the surface of the two top radiating plates of the dual PIFA at the two resonant frequencies of 920.4 MHz and 2423.4 MHz, respectively. A comparison of these two plots shows that the distribution of the surface current magnitude at 920.4 MHz has much larger values on the lower band radiating patch than it is on the upper band radiating patch. This is because at the lower band the surface currents are determined primarily by the dimensions of the lower band element. At 2423.4 MHz, the maximum current density can be observed to reside on the upper band radiating patch. However, it can also be seen that quite a large current density occurs around the area of the lower band radiating patch that is close to the upper band radiating patch. This is because at the higher band, the surface currents

- 176

are dominated not only by its own radiation element but also by the composite geometry of the dual-band PIFA. This confirms the type of behaviour exhibited in the study of the input impedance as described in section 7.3.

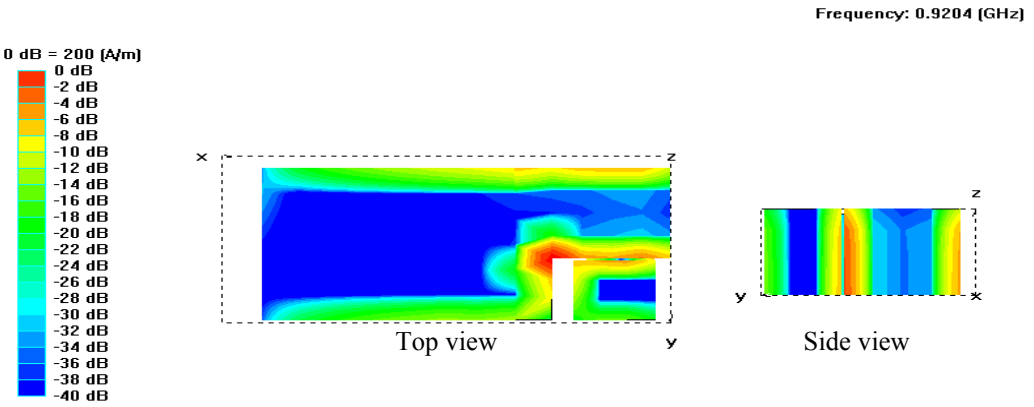

(a)

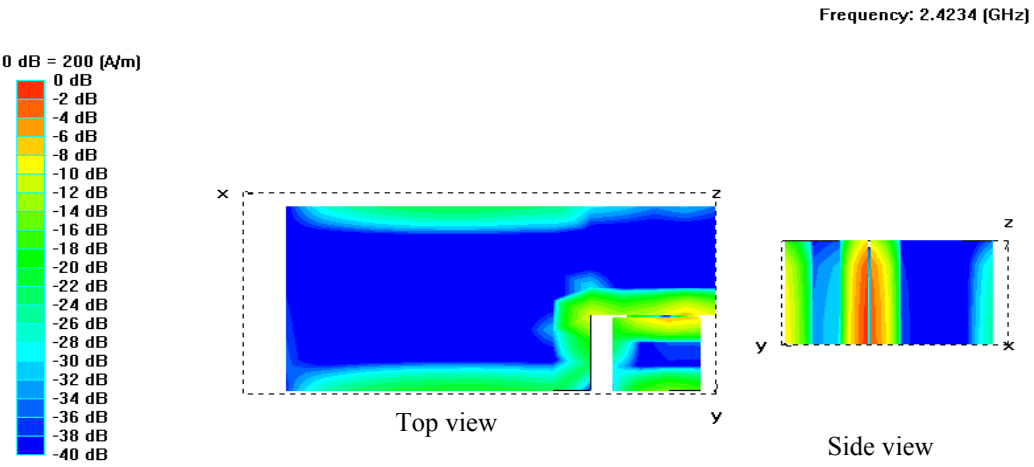

(b)

Figure 7-13 Average current densities on the surfaces of the top radiating plates of the proposed dual-band PIFA: (a) at 920.4 MHz; (b) at 2423.4 MHz.

- 177

7.4.3 Radiation parameters

Figure 7-14 illustrates the three-dimensional electric field radiation pattern at 920.4 MHz. The components E_θ and E_φ at the three principal orthogonal planes are depicted in Figure 7-15 (a) to (c). All the three radiation patterns shown have been normalised with respect to the maximum magnitude of the total electric field, so that the pattern has a maximum value of 0 dB. From Figure 7-15 (a), the antenna shows an omni-directional behaviour when operating at the lower band. From Figure 7-15 (b) and (c), it is noted that the polarisation of the antenna for this operating band is rather more elliptical than linear. This suggests that the antenna has the ability to receive both vertically and horizontally polarised electromagnetic waves.

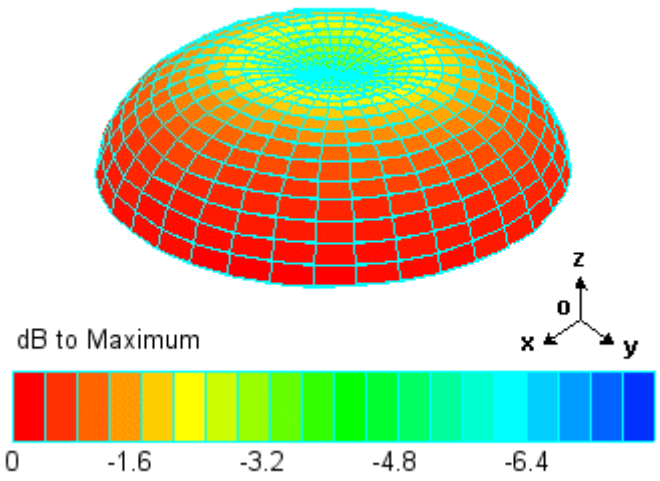

Figure 7-14 The 3D radiation field pattern of the proposed dual-band PIFA at 920.4 MHz.

- 178

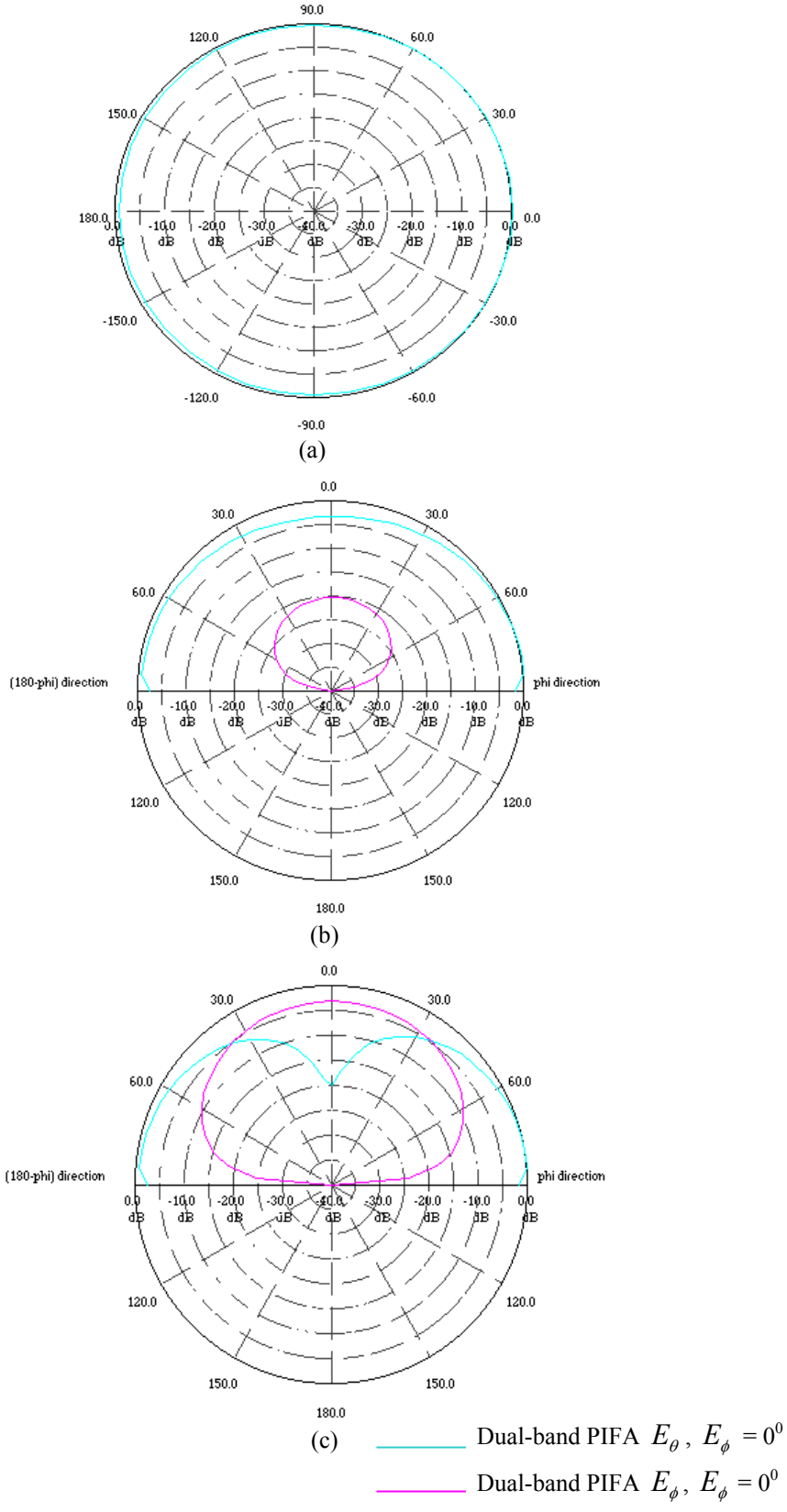

Figure 7-15 The 2D radiation patterns of the proposed dual-band PIFA at the lower band for components E_θ and E_φ: (a) xy plane; (b) xz plane; (c) yz plane.

- 179

The three-dimensional radiation field pattern of the antenna at 2423.4 MHz is shown in Figure 7-16. The components E_θ and E_φ in the three principal orthogonal planes are shown in Figure 7-17 (a) to (c). At the higher operating frequency of 2423.4 MHz, the antenna is less omni-directional and also there is a lobe in the direction perpendicular to the orientation of the antenna patch, as may be observed in Figure 7-17 (c). This is due to the influence of the adjacent lower band radiating element, which surrounds most of the radiating edges of this higher band radiating element. This effect can also be explained by the surface current distribution described in section 7.4.2. In addition, from Figure 7-17 (a) and (b), the antenna operating at the upper band shows a larger cross polarisation effect than its operation at the lower frequency.

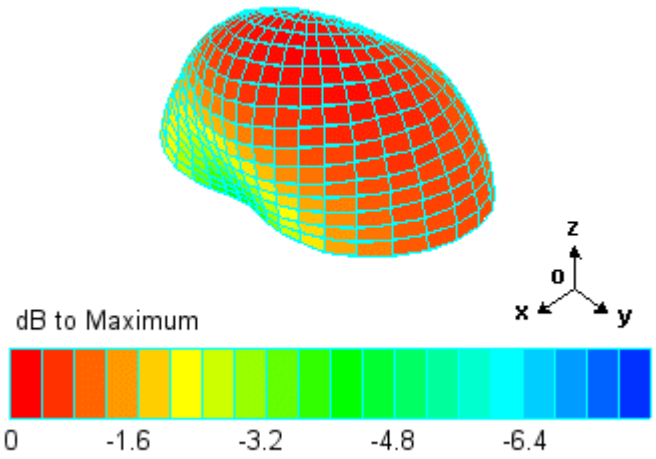

Figure 7-16 The 3D radiation field pattern of the proposed dual-band PIFA at 2423.4 MHz.

- 180

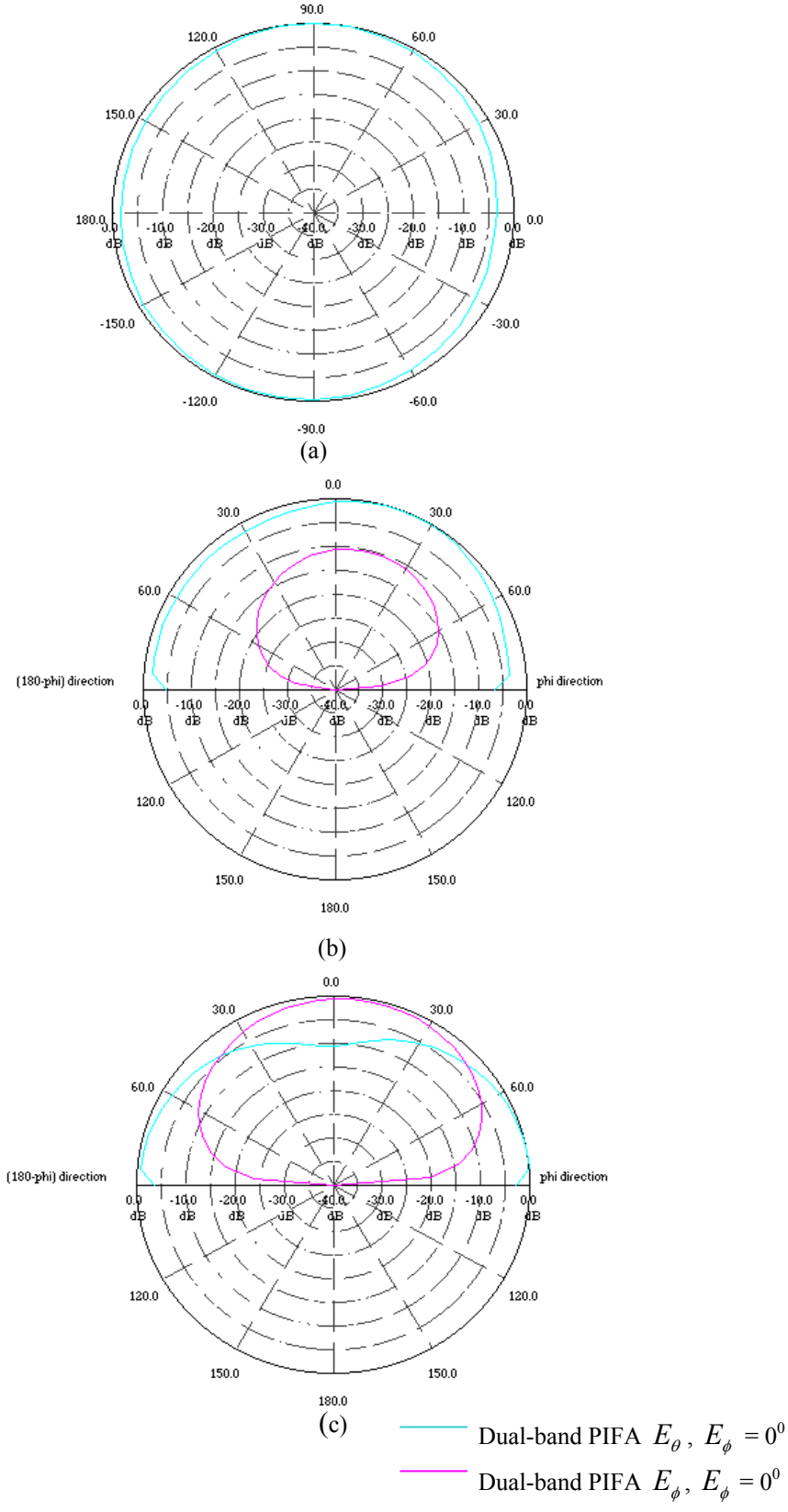

Figure 7-17 The 2D radiation patterns of the proposed dual-band PIFA at the upper band for components E_θ and E_φ: (a) xy plane; (b) xz plane; (c) yz plane.

- 181

Table 7-5 lists the values of θ and φ corresponding to the directions of maximum radiating field, the directivity, and the efficiency of the antenna at both resonant frequencies. From this table, it can be observed that the antenna does not have the same maximum radiation field direction for the two operating frequencies. The maximum radiation field direction at the lower operating frequency lies nearly on the ground plane. However, for the higher operating frequency the maximum radiating field direction is shifted close to the z axis. Moreover, the antenna has a higher directivity when operating at higher band frequencies. Also, the efficiency is slightly higher at the higher operating frequencies.

Table 7-5 The direction of maximum radiation, the directivity and efficiency of the dual-band antenna at both resonant frequencies

	PIFA only	
Radiation parameters	Lower resonance	Upper resonance
Maximum at (θ, φ)	(85^o, 30^o)	(25^o, 40^o)
Directivity (dBi)	4.13	4.49
Efficiency (%)	92.6	94.7
Gain (dBi)	3.82	4.25

7.5 Experimental Validation

To validate the simulated results, a dual-band PIFA based on the dimensions listed in Table 7-1 was fabricated. The PIFA was constructed by cutting out each part from thin copper sheets. The antenna was assembled by soldering the individual pieces together to form the final PIFA structure. A photo of the fabricated dual-band PIFA is shown in Figure 7-18. The return loss of the dual-band PIFA was measured with a HP 8753C network analyser using one port calibration. The measurement setup and calibration procedures are the same as those described in section 4.5.1 of Chapter 4. The measured return loss and VSWR are shown in Figure 7-19 and Figure 7-20, respectively. For comparison, the simulated results are also shown as the blue curve in these two figures.

- 182

From these figures, it can be seen that the return loss and VSWR computed using MOM agree reasonably well with measurements over the wide frequency range between 600 MHz and 2800 MHz.

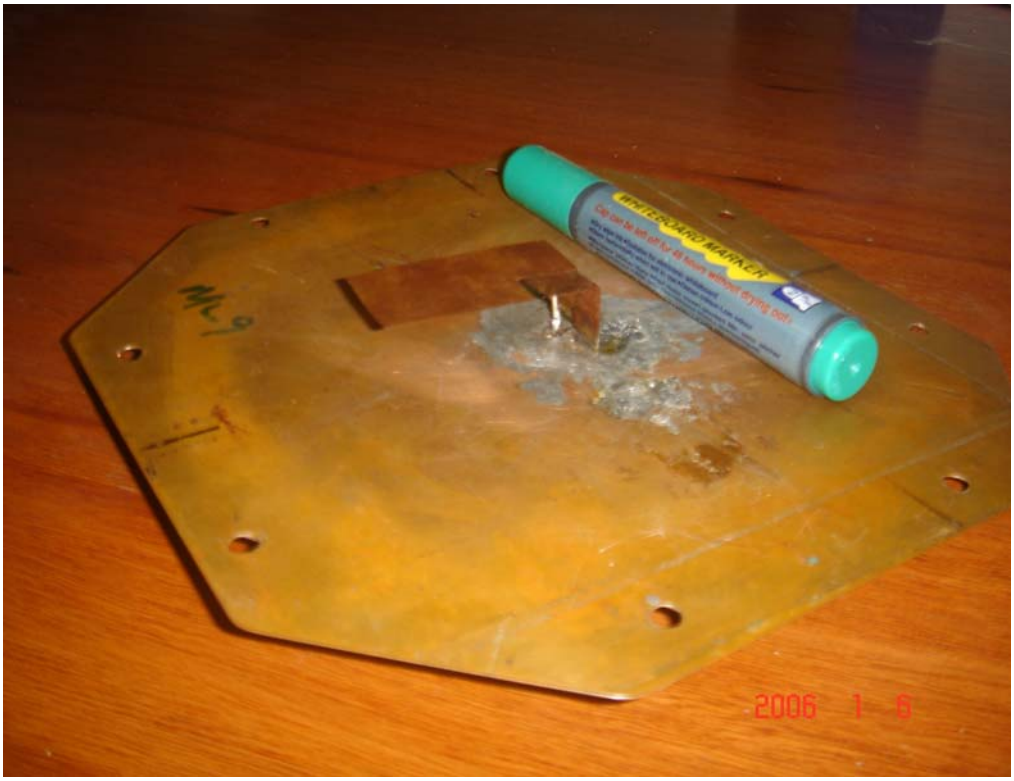

Figure 7-18 A photo of the fabricated dual-band PIFA.

- 183

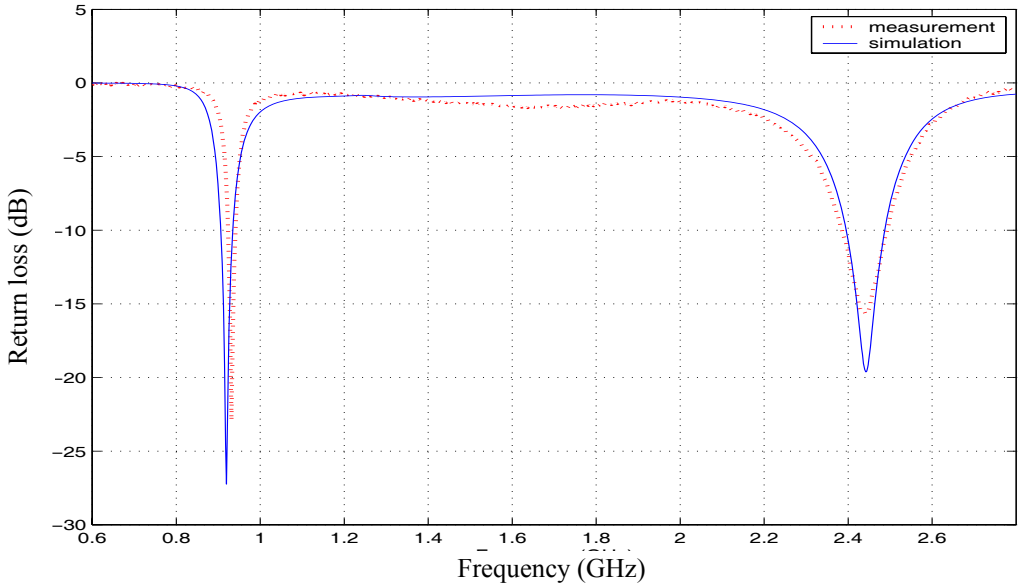

Figure 7-19 The return loss of the dual-band PIFA.

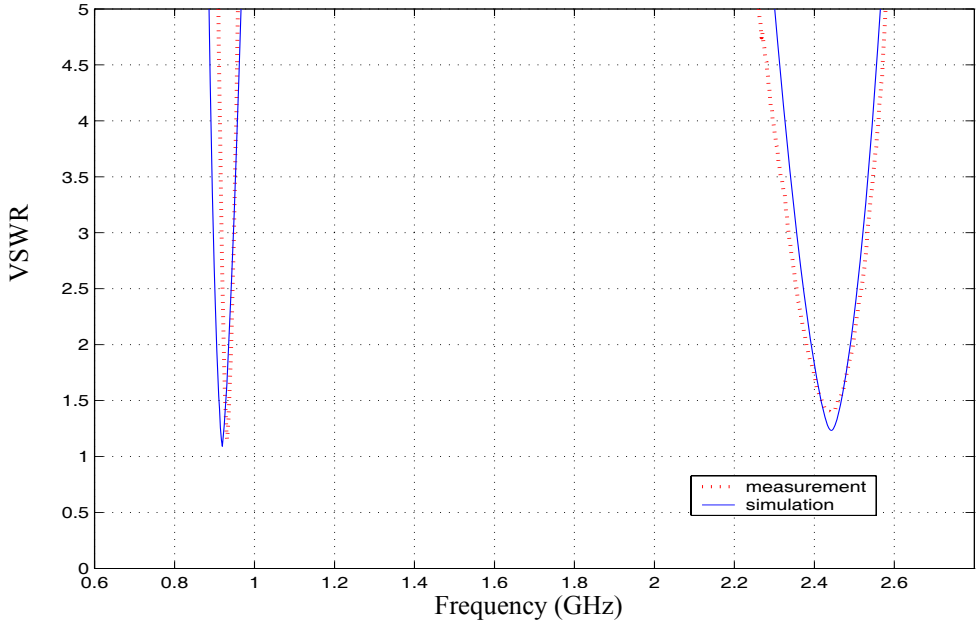

Figure 7-20 The VSWR of the dual-band PIFA.

- 184

7.6 Influence of the Dielectric Cover Layer on the Impedance and Radiation Characteristics of the Dual-band PIFA

In Chapter 4, the effect of a dielectric cover on the characteristics of a single-band PIFA has been investigated by simulation and experimental measurements. In this section, the influence of the dielectric cover on the impedance and radiation characteristics of a dual-band PIFA is analysed using the same MOM computer simulation package. The aim of this study is to help understand the impact of the dielectric properties and cover configurations on the performance of the dual-band PIFA and to aid the design of antenna systems that include such dielectric cover materials.

7.6.1 Geometry of a dielectric-covered dual-band PIFA

The side view of the configuration of the dielectric covered dual-band antenna is shown in Figure 7-21. The dielectric layer material with dielectric constant ε_r, loss tangent $\tan\delta$, and thickness d (mm) is placed above the antenna with an air gap g (mm). The dual-band PIFA proposed in section 7.3 is adopted here. Its dimensions are listed in Table 7-1.

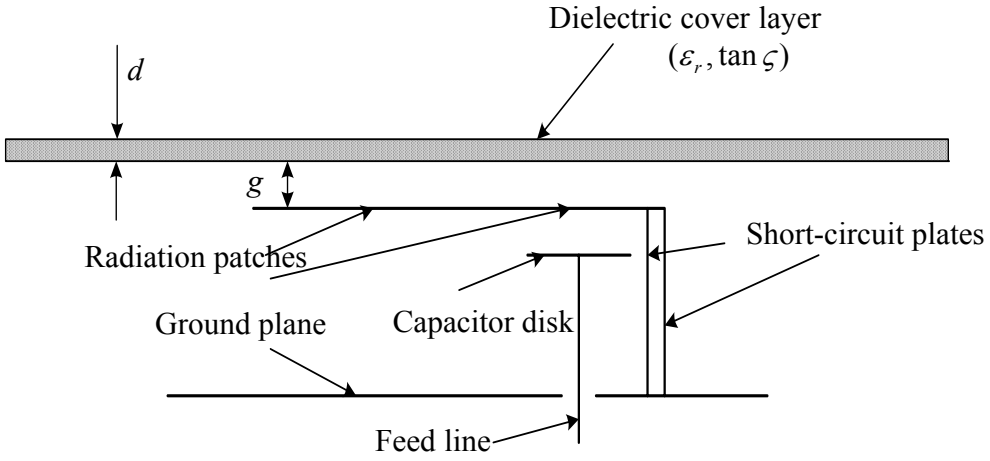

Figure 7-21 The side view of the configuration of a dielectric-covered dual-band PIFA.

- 185

7.6.2 Influence on impedance characteristics

The performance of this dual-band PIFA covered by a dielectric layer with or without an air gap, has been studied using computer simulations. The properties of the dielectric material are given in Table 7-6.

Table 7-6 Properties of the dielectric cover layer

Dieletric constant	Loss tangent	Thickness (mm)
4.66	0.0155	1.6

Figure 7-22 shows the input impedance of this dielectric covered antenna with or without an air gap. The blue dashed line is with a air gap of 1mm between cover layer and the radiating patch. The red dotted line is without an air gap. For comparison, the input impedance of the antenna without a cover is also shown as green solid. From Figure 7-22, it can be observed that when the dielectric cover layer is without an air gap, both resonant frequencies of the antenna are reduced but the change for the high band is larger than that for the low band. This is because the presence of the dielectric material affects the electrical length of the antenna and this is more significant at higher frequencies. Moreover, this resonant frequency shift becomes insignificant when a 1 mm air gap is introduced. This is because the presence of the air layer results in lowering the effective dielectric constant, thereby producing a lesser effect on the electrical length. The return loss and VSWR of the antenna for these three cases are plotted in Figure 7-23 and Figure 7-24, respectively. From these figures, it is noted that the bandwidths of the antenna associated with the two resonant frequencies have been noticeably altered. This is because the dielectric constant of the cover material affects the impedance characteristics, but this change may be positive or negative. Table 7-7 tabulates the resonant frequency and bandwidth of the dielectric covered dual-band PIFA achieved with or without an air gap. The resonant frequency and bandwidth without a dielectric cover are also listed in the table for comparison. Table 7-8 shows the percentage changes.

- 186

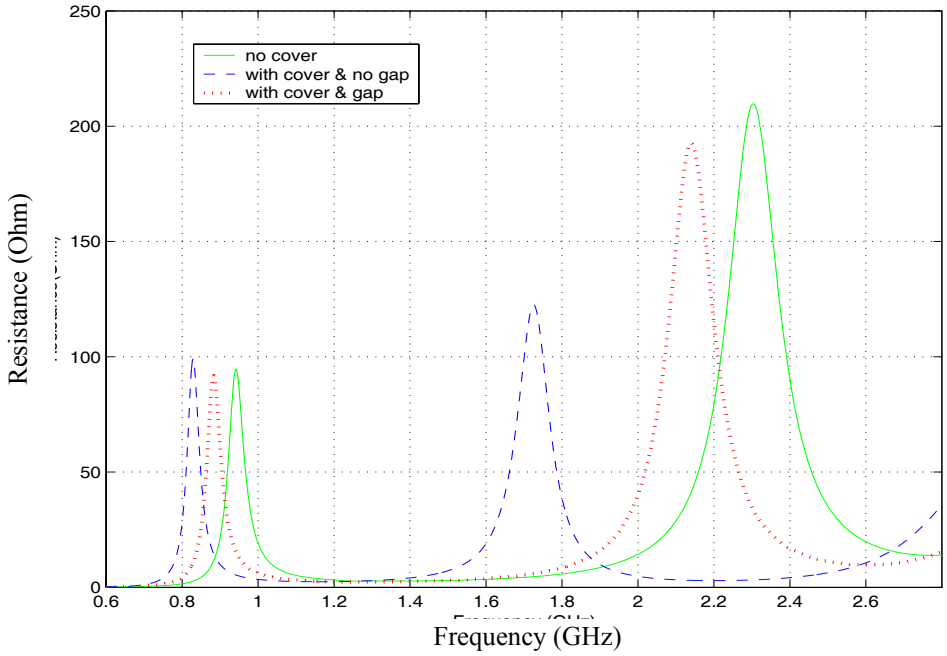

(a)

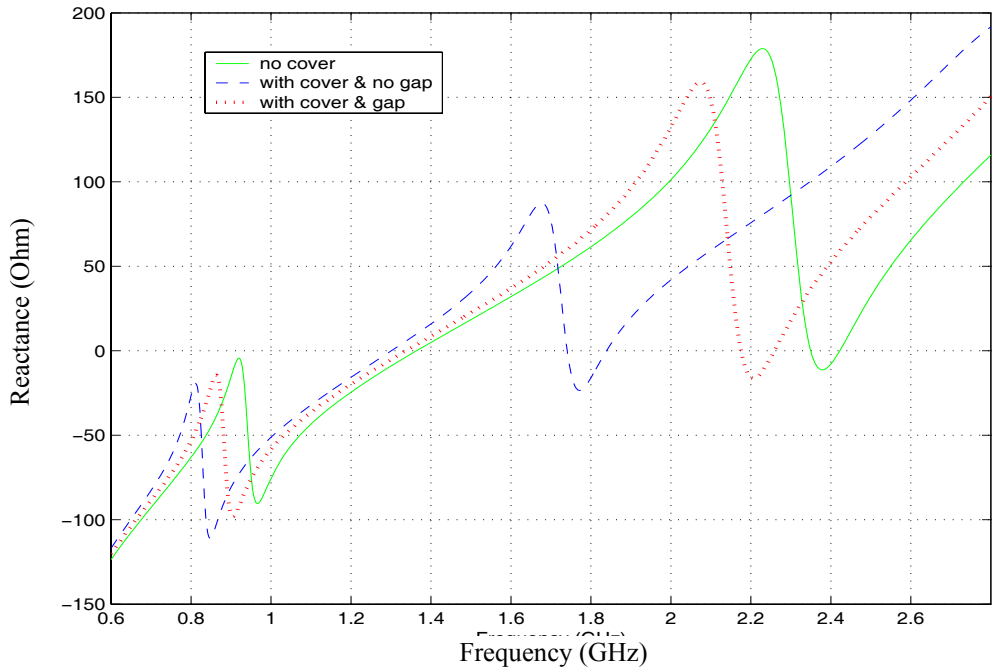

(b)

Figure 7-22 The input impedances of the dielectric covered dual-band PIFA with and without a 1mm air gap: (a) resistance; and (b) reactance.

- 187

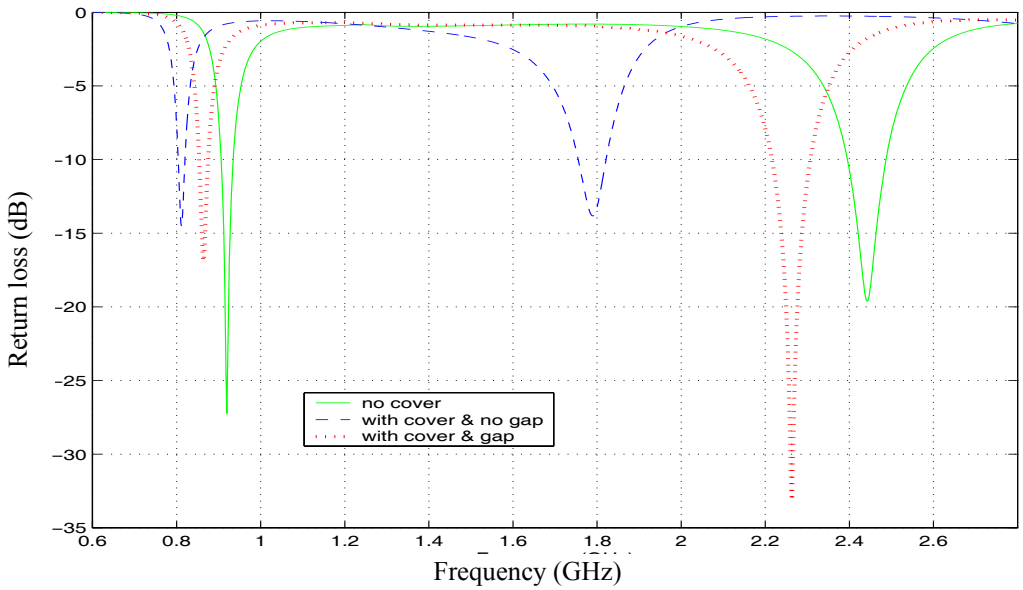

Figure 7-23 The return loss of the dielectric covered dual-band PIFA with and without a 1mm air gap.

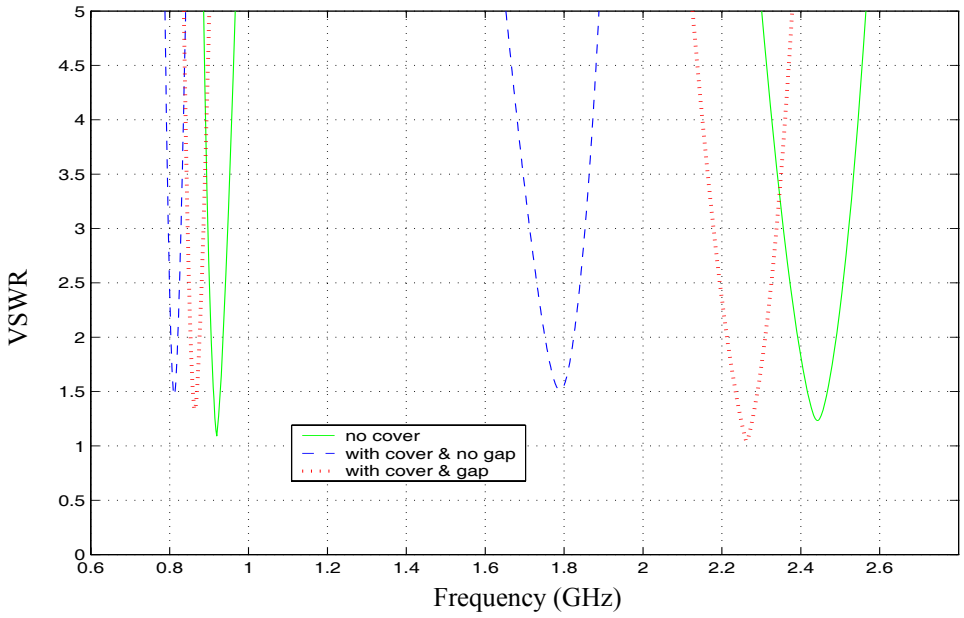

Figure 7-24 The VSWR of the dielectric covered dual-band PIFA with and without a 1mm air gap.

- 188

Table 7-7 The resonant frequency and bandwidth of the dielectric covered dual-band PIFA with and without a 1mm air gap. Note that the bandwidth is specified for an VSWR of 2.

	1st resonance		2nd resonance	
	Frequency (MHz)	Bandwidth (MHz)	Frequency (MHz)	Bandwidth (MHz)
no cover	920.4	28.6	2423.4	96.9
with cover & no gap	812.5	16.5	1839.4	71.6
with cover & gap	864.3	22	2258.8	95.8

Table 7-8 Percentage changes in resonant frequency and bandwidth of the dielectric covered dual-band PIFA with and without a 1mm air gap

	1st resonance		2nd resonance	
	Frequency change (%)	Bandwidth change (%)	Frequency change (%)	Bandwidth change (%)
with cover & no gap	-11.7	-42.3	-24.1	-26.1
with cover & gap	-6.1	-23.1	-6.8	-1.1

Next, the impedance characteristics of the dual-band PIFA covered by a dielectric layer with no loss and with finite loss are analysed. For the lossy case, a loss tangent of 0.0155 is used, which is a typical value for FR4 fibreglass laminate. The dielectric constant and thickness of the dielectric layer are assumed to be the same as those specified in Table 7-6.

Figure 7-25 shows the input impedances obtained for loss–free dielectric (red dotted curve) and for lossy dielectric (blue dashed curve). From Figure 7-25, it can be observed that the loss of the dielectric material makes almost no change in the resonant frequencies at both the low and high bands, but decreases the magnitude of the resonant peaks. The reduction of the resonant peak is greater for the higher resonant frequency. This is because the lossy dielectric material absorbs a part of the energy radiated from the antenna so damping its resonances, and the loss is higher at higher frequencies.

- 189

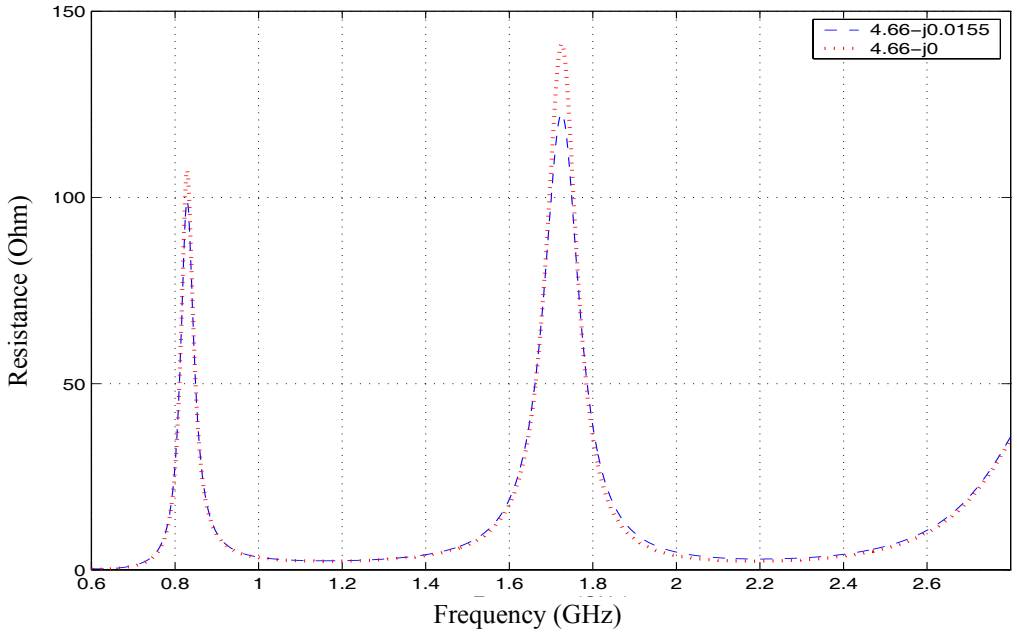

(a)

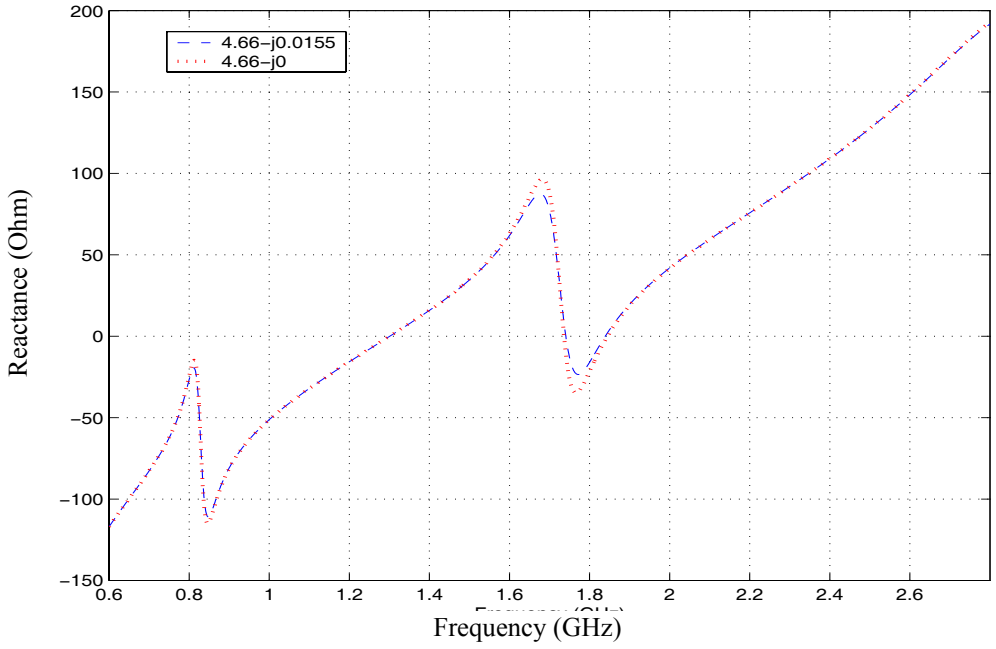

(b)

Figure 7-25 The input impedances of the dielectric covered dual-band PIFA with both zero (red) and finite dielectric loss (blue - loss tangent = 0.0155): (a) resistance; (b) reactance.

- 190

7.6.3 Influence on the radiation characteristics

The three-dimensional radiation field patterns of the dual-band PIFA covered by a lossy dielectric layer, with and without an air gap are shown in Figure 7-26 and Figure 7-27. Their main radiation parameters such as directivity, efficiency and gain are listed in Table 7-9. For comparison, the radiation parameters of this antenna without a cover are also included in this table. Compared with the 3D pattern in Figure 7-14, it is noted that the dielectric cover layer has a direct impact on the radiation pattern of the antenna, particularly in the case without an air gap. This impact is more significant for the high band. From Table 7-9, it can be observed that the position of the maximum field value is shifted by $55^o(\theta)$ and $200^o(\phi)$ in the high band, when the antenna is covered by a 1 mm thick dielectric layer of a dielectric constant of 4.66 and a loss tangent of 0.0155. It can also be seen that the directivity achieved with the dielectric cover for the low band and the high band are more than 0.8 dB and 1.7 dB, respectively, when compared with the value obtained without the cover,. However, the efficiency achieved with the presence of this cover decreases significantly for both of the bands, compared to that without the cover. Thus, its predicted gain is much lower than the antenna without a cover. In addition, it is worth noting that inserting an air gap between the cover layer and the radiating element may significantly reduce these influences.

Table 7-9 The radiation parameters of the dual-band PIFA and the lossy dielectric covered dual-band PIFA without and with an air gap

	PIFA only		PIFA with cover		PIFA with cover & gap	
Radiation parameters	Lower resonance	Upper resonance	Lower resonance	Upper resonance	Lower resonance	Upper resonance
Maximum at (θ, φ)	(85^o, 30^o)	(25^o, 40^o)	(80^o, 90^o)	(80^o, 240^o)	(80^o, 30^o)	(30^o, 50^o)
Directivity (dBi)	4.13	4.49	5.05	6.2	4.19	4.94
Efficiency (%)	92.6	94.7	61.9	36.5	84.3	85.2
Gain (dBi)	3.82	4.25	3.13	2.26	3.53	4.21

- 191

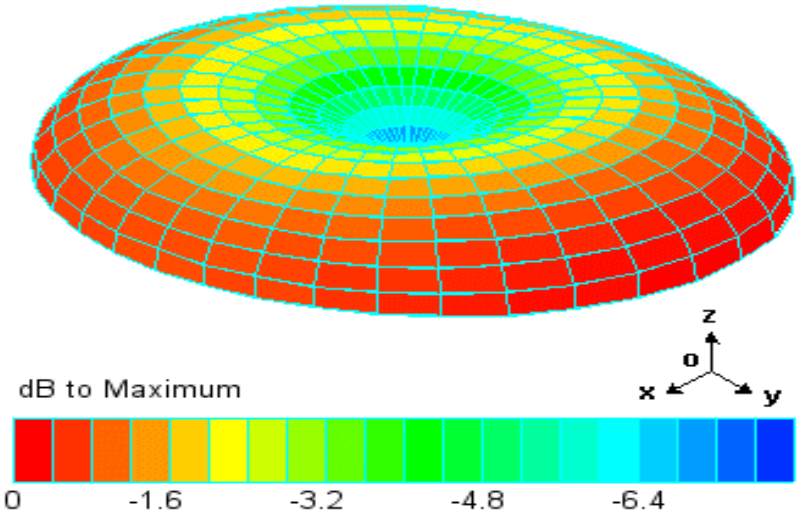

(a)

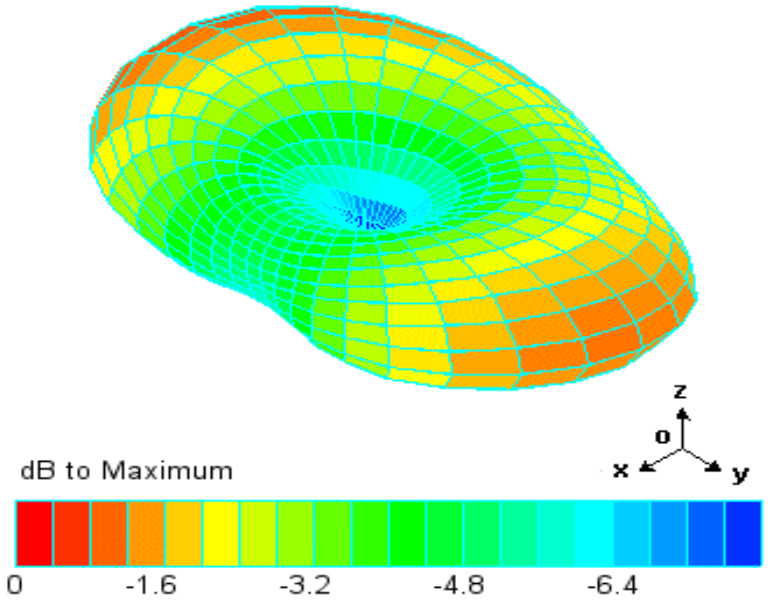

(b)

Figure 7-26 The 3D radiation patterns of the dual-band PIFA covered by a lossy dielectric layer and without an air gap: (a) low band; (b) high band.

- 192

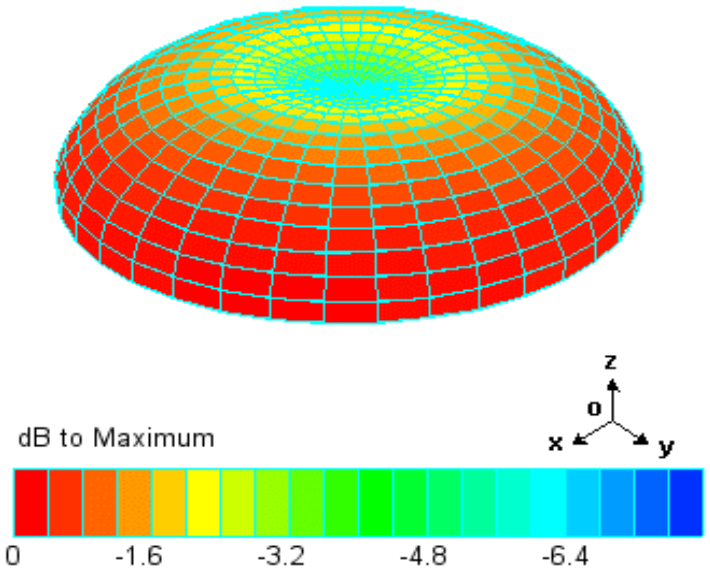

(a)

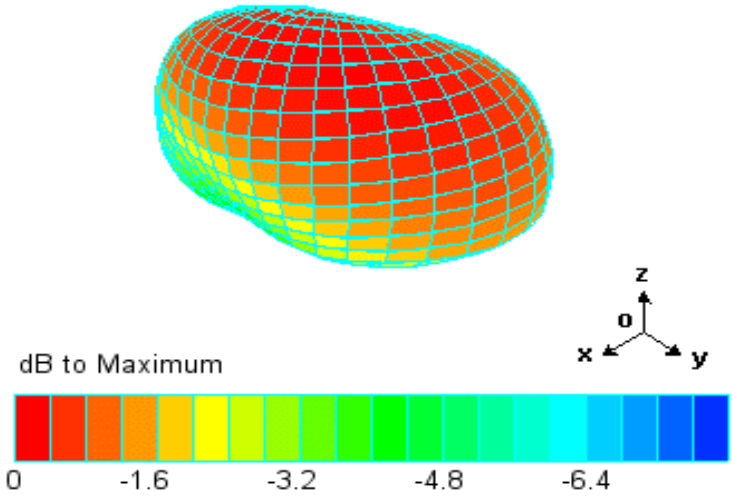

(b)

Figure 7-27 The 3D radiation patterns of dual-band PIFA covered by a lossy dielectric layer and with an air gap: (a) low band; (b) high band.

- 193

7.7 Summary

This chapter presents the analysis and design of a new single feed dual-band PIFA using a capacitive electromagnetic coupling feeding technique. A design example for a dual-band PIFA for 900 MHZ and 2400 MHz ISM applications is given. Computer simulations have been used to investigate the influence of the individual composite parts on the impedance characteristics of the proposed dual-band PIFA. This antenna has been fabricated and the measured results are compared with the simulated results. This new dual-band antenna only has a single feed with a flexible feed configuration that allow the two resonances to be set independently. The effect of the dielectric cover layer on the proposed dual-band PIFA has also been investigated. It is found that the dielectric cover layer could have a significant impact on the input and the radiation characteristics of the PIFA, particularly at the high band.

The analysis and design details for the antenna, including the effect of the dielectric cover layer having loss tangent of 0.0155, (typical for FR-4 fibreglass laminate), is used could be adopted for the initial design of a low-profile dual-band PIFA.

- 194

CHAPTER EIGHT

8. CONCLUSIONS AND RECOMMENDATIONS

8.1 Summary of Results and Conclusions

The growing demand for mobile communications has created a desire for smaller and lighter mobile terminals. This consequently has led to an increasing interest in the development of smaller and lower profile antennas. Various techniques of antenna miniaturisation for mobile radio applications have been proposed in the literature. Some of the commonly employed methods are described in Chapter 2. They include using resistive or reactive loadings, using high-dielectric-constant materials, using short-circuit plates or pins, cutting slots on a resonant patch, and folding the resonant patch or wire. Such techniques have been used in mobile radio communications (Fujimoto *et al*, 1987; James *et al*, 1989; Hirasawa *et al*, 1992; Bokhari, *et al*, 1996; Huang, 2001; Li *et al*, 2002; Wong, 2002; Altshuler *et al*, 2000). However, bandwidth and efficiency limitations, which are fundamental to miniaturising antenna structures, are imposed by the minimum possible Q factor of the antenna. These fundamental relationships between size and performance have been discussed in Chapter 2. It has been concluded that when the volume of an antenna is reduced its bandwidth will become narrower as its minimum possible Q factor increases.

The planar inverted F antenna (PIFA) was introduced to mobile radio applications by Taga *et al* (Taga *et al*, 1987). A survey of the literature covering the origin and performance analysis of the PIFA, sited on an infinite ground plane, is presented in Chapter 3. This survey shows that the PIFA not only has a low profile structure but is also sufficiently flexible in design to allow both easy impedance matching and the simultaneous achievement of a reasonably wide bandwidth, such as 8.5% of the centre frequency. The published research works (Taga *et al*, 1987; Pedersen *et al*, 1994; Jensen *et al*, 1994; Okoniewski *et al*, 1996; Li *et al*, 1997) describing the influence on the performance of PIFA due to the conducting body of a mobile terminal and the

- 195

presence of the head, hand and body of a user, have also been reviewed. This review reports that the bandwidth could double when a PIFA is mounted on a finite conducting body instead of an infinite ground plane. This bandwidth may be further enhanced by selecting the appropriate dimensions for the conducting body. Furthermore, it is found that the gain of the PIFA changes not just with the size and shape of the radio terminal's conducting body and its position on the body, but also varies as a function of the orientation of the radio terminal. The important point derived from this review is that when a conducting body carries a PIFA, it becomes an integral part of the antenna system itself. It is essential, therefore, that the two structures are considered together when designing to achieve an optimal performance available from such an antenna system. Moreover, it is also found that the use of a PIFA could reduce the SAR tenfold due to the smaller backward radiation in the direction of the user, when compared with a conventional whip antenna having an omnidirectional radiation. These advantageous characteristics of the PIFA make it one of the most promising candidates for mobile applications.

A new trend in mobile radio is the use of internal antenna which fits into the case of a mobile radio terminal. This configuration can reduce the possibility of the antenna being physically damaged as well as keeping the outline of the equipment more compact and appealing. However, an internal antenna needs to be mounted on a ground plane, which is often the PCB part of the mobile terminal. To achieve the required compactness of the antenna system, this ground plane is usually quite small compared with the operating wavelength. Diffraction from the edges of such a small finite plane could modify the current distributions of the antenna. These currents will alter the radiation patterns, causing nulls in the forward radiation and even higher cross polarisation levels, as well as changing the input impedance in some cases. Moreover, the material of the terminal case could also have a strong interaction with the operation of the internal antenna, particularly if the case is within the reactive region of the antenna. This interaction may well result in poor performance of the antenna, particularly one having a high Q such as an electrically small antenna. As further reviewed in Chapter 3, no reports have been found on the interaction between the dielectric casing (or radome) and an internal antenna, such as a PIFA. Consequently, the objective of this study has been to investigate the operating performance of a PIFA

- 196

having a dielectric casing or radome. An outcome of this study is to improve the design considerations for such a radome-antenna system.

For accurate analysis of an internal mobile antenna operating in a complex environment, like being located in the dielectric casing or radome, numerical approaches are necessary. As reviewed in Chapter 3, the FDFD and FEM are both volume-based techniques. They are able to model any dielectric of various shapes and electrical properties. Because the cell size is determined by the highest frequency of interest, as well as the smallest detail of concern, the number of cells used in these two methods will have to increase significantly when applied to thin structures. The MOM basically starts with an integral equation for the current density on the surface of the antenna structure. The integral equation technique used in NEC uses the free space Green's function and can be particularly efficient for the analysis of wire antennas or other resonant conducting surfaces (Burke *et al,* 1981). However it cannot model microstrip or other printed antennas in a multilayer environment. As a result, the so-called MPIE has been proposed for the modelling and analysis of multilayered planar antennas of arbitrary shapes (Mosig, 1988). In this technique, a more complex Green's function, which satisfies the stratified dielectric boundary conditions (except the boundary condition on the conducting surface), is used to replace the free space Green's function. The electromagnetic simulator, IE3D from Zeland, adopts this technique (Zheng, 1994). It is noted that the MPIE does not account for the effect of surface-wave reflection and diffraction at the edges of a truncated layer. However, such effects can generally be ignored for an electrically thin layer.

For MOM full wave 3-D modelling of arbitrary conducting and dielectric objects, an SIE approach with a surface formulation has been proposed (Kolundzija, 1997). In this approach, the electromagnetic field inside a homogeneous isotropic and linear region is expressed in terms of an impressed field and the equivalent electric and magnetic currents distributed over its boundary surface. Such an approach is used in the electromagnetic simulator, WIPL-D, which uses entire-domain basis functions to efficiently model arbitrary composite metallic and dielectric objects (Kolundzija *et al*, 2000). MOM, like FEM, however, is a frequency-domain solution. Compared with a time-domain solution like FDTD, the price paid is the need for a number of simulations

- 197

to adequately cover a given frequency range. This can be overcome by using sophisticated interpolation techniques to fill in the missing frequency spectrum (Miller, February 1998 and April 1998 and June 1998; Schlagenhaufer, *et al*., 2001). In this study, the dielectric casing or radome is considered to be a planar structure, thin compared with the operating wavelength. Therefore, MOM is the most suitable method for this research.

An internal antenna is often mounted on a finite ground plane such as a PCB. In this thesis, first the influence on the input characteristics of a PIFA mounted on a finite ground plane due to changes in the positions of the short-circuit plate and feed wire and whereabouts the PIFA is mounted relative to the edges of the ground plane has been studied. This is in order to improve the PIFA design in the later part of Chapter 4. It is found that the short-circuit plate "movement" has a stronger effect on the resonant frequency than "movement" of the feed wire. On the other hand, the effect of the feed point "movement" produces a slighter increase in bandwidth change than the short-circuit plate "movement" does. Also, when an antenna is designed to have a minimum volume, both the feed wire and the short-circuit plate should be located on the same edge of the top patch. However, such a design would suffer from a low minimum achievable bandwidth. Since the feed wire "movement" has a significantly larger influence on the bandwidth than the resonant frequency, it may be a good design compromise to consider fixing the short-circuit plate at the edge of the top plate while moving the feed point away from the edge to obtain the required bandwidth. Moreover, it is observed that the resistance of the antenna at resonance increases when the feed wire is moved away from the short-circuit plate along the x-axis as shown in Figure 4-7. This particular characteristic of the PIFA provides a convenient way to achieve antenna impedance matching. Furthermore, it is observed that the position where the PIFA assembly is located on the finite ground plane could greatly alter the input characteristics of the antenna. For a PIFA to resonate at the lowest frequency, it should be located in the corner of the ground plane. This observation suggests that for a given resonant frequency, the size of a PIFA could be made smaller if it is located at the edge of the ground plane. However, for a PIFA to achieve a maximum bandwidth it is desirable to have it mounted in the middle of the ground plane. It is found that the ratio of the bandwidth to resonant frequency could vary between 3.5 % to 8.5 % just by

- 198

locating the PIFA at different locations on the ground plate. These two seemingly contradictory requirements for small size and wide bandwidth call for some form of compromise in the actual PIFA implementation. The results obtained indicate that the position where the antenna is located on the finite ground plane must be accounted for in the design. Based on this study, a PIFA with a bandwidth of 8.5% (VSWR $\leq$ 2) operated at the 900 MHz band has been designed as a reference antenna for further studies.

When an antenna is integrated as part of an electronic system, some parts, particularly those around the sides of the rectangular dielectric radome, may be further away from the radiation element compared with the top part. In this case the effects of the side parts of the dielectric casing may be ignored and the dielectric casing can be considered to be a dielectric layer of infinite extent. Thus, the MPIE based MOM technique that is used in IE3D can be used to model and analyse this problem. The effect of the top dielectric cover layer on the performance of the reference PIFA, in terms of its resonant frequency, input impedance, bandwidth and efficiency, has been investigated. The dependence of such performance parameters on the electrical properties of the dielectric layer, its thickness and separation between the dielectric layer and antenna has also been examined using IE3D in section 4.4. It is found that the fractional change in the resonant frequency is more than 9%, when the PIFA is covered by a dielectric sheet having a thickness of 0.0092λ (3.048 mm) and a dielectric constant of 4.4. This falls outside the original design bandwidth of 8.5%. Also, the simulated results of the distribution of the surface current on the top patch confirm the type of behaviour exhibited in the study of input impedance. When a dielectric cover layer is located close to the PIFA, the distribution of the surface current on the patch varies noticeably, even though it is still operating in the TM_{100} mode at the new resonant frequency. In such a case, the effective length of the current flow on the top patch becomes longer and the resonant frequency of the antenna is shifted to a lower frequency. These changes in current distribution are mainly determined by the dimensions, positions and dielectric constant of the cover layer. However, the absolute values of the magnitudes of the surface currents are also affected by the loss tangent of the cover layer material. For example, the efficiency of the antenna is lowered to 76.3% from 87.3% when the loss tangent of the dielectric material is changed from 0.0027 (e.g. R4003) to 0.07 (e.g.

- 199

FR4). This result shows that the loss tangent of the cover layer will have a significant impact on the gain of the antenna. These observations help to provide appropriate adjustments to the dimensions of the PIFA to account for the influence of the dielectric layer in the design stage of such a dielectric-covered antenna. Moreover, this study shows that if a sufficiently large air gap, in the order of 0.03λ, is introduced between the dielectric sheet and the top plate of the PIFA, the influence of the dielectric layer is reduced significantly. Finally, measurements were conducted to validate the simulations. A good agreement between them has been achieved.

By contrast an antenna used in an antenna system may sometimes be enclosed tightly within a dielectric radome. In this case, the effect of the side parts of the dielectric radome may not be ignored. In Chapter 5, the performance of a PIFA enclosed within a rectangular dielectric radome has been studied using a MOM electromagnetic simulator, WIPL-D. This simulator has been discussed in Chapter 3 and presented as an efficient way to model and analyse any arbitrary shape radome-antenna structures. To give confidence in the simulation, the parameters of the computer model used are adjusted until both the following two conditions are satisfied. The first ensures that the input and the radiation characteristic results of the model including an air-filled radome and the model without a radome are identical. The second checks the quality of the numerical solution by calculating the power balance. After that, the performance of a PIFA operating at 900 MHz in the presence of a rectangular dielectric radome is analysed. It is found that the resonant frequency of the PIFA is dramatically shifted to a lower frequency when it is enclosed by a dielectric radome. This is mainly because the dielectric constant of the radome directly impacts on the impedance and electrical length of the antenna, with the higher dielectric constant material effectively causing an increase in the antenna electrical length. Also, it is found in section 5.6.5 that in the presence of the dielectric radome the actual value of the dielectric constant can alter the radiation patterns of the antenna. By contrast, the loss tangent of the dielectric material does not seem to alter the radiation patterns but, as expected, it will significantly reduce the gain. These observations can be explained by the distribution of the surface current on the antenna as discussed in section 4.4.3. Due to the presence of the radome, the current density has been changed even though the current flow on the patch still corresponds to the current distribution of the TM_{100} resonant mode at its new resonant

- 200

frequency. The distribution of the surface current on the patch is mainly determined by the dimensions, the positions and dielectric constant of the radome, rather than the loss tangent of the radome material, which determines the surface current magnitude.

Following this, an investigation of the effect due to each individual part of the rectangular radome has been carried out. It is observed that each individual part has a different degree of effect on both the input and the radiation characteristics of the PIFA. The strongest to the weakest effect on the input characteristics, may be listed in the following order: “top”, “side”, “open” and “short”. These results suggest that the short-circuit plate of the PIFA should be located as close as possible to the radome in order to minimise the influence of the radome when its volume is fixed. Considering the effect on the radiation pattern, the “open” is dominant and the “short” has the least effect. These factors are significant and must be taken into account in the early design stages. Next, the effect of the radome on the input impedance of the PIFA due to the separation between the radome and the antenna, radome thickness and its electrical properties has been examined. It is found that the resonant frequency, bandwidth and gain could be easily affected by these radome parameters and in some cases the bandwidth could increase. This indicates that it is possible to improve the bandwidth and simultaneously minimise the size of the PIFA, by choosing appropriately the physical and electrical parameters of the radome and PIFA combination. Finally, the influence of a rectangular radome on the performance of a PIFA operating at a higher frequency of 2400 MHz has been examined and a comparison between the performance at 900 MHz and at 2400 MHz has been made. The results clearly demonstrate that the radome has a greater impact on both the input and the radiation characteristics at 2400 MHz than at the lower frequency of 900 MHz. This is particularly the case with gain. It shows that the effect of the radome at the higher frequency is more significant.

The influences of the dielectric cover layer and the dielectric radome on the input and radiation characteristics of the PIFA have been investigated comprehensively using the numerical approach described in Chapters 4 and 5. However, the long computing time usually encountered in numerical modelling of such problems is disadvantageous for the process of optimising the design parameters. Therefore, an approximation analysis such as the use of the TLM is beneficial in this respect for the initial engineering design. As

- 201

a result, an efficient TLM, applicable for a PIFA covered with a dielectric layer, has been presented in Chapter 6. A comparison between the analytical (TLM) and numerical (full wave MOM) calculations for four PIFAs with different configurations shows a reasonably good agreement. Such a TLM could be integrated into a CAD tool for use in the design a PIFA covered with a large thin dielectric layer to provide initial design parameters for use in accurate numerical modelling, thus saving significant computing resources. However, its application is limited to rectangular patches.

With the increasing popularity of multi-band operation in mobile radio applications, it becomes essential to develop efficient and compact dual-band antennas. Therefore, a new single feed dual-band PIFA which uses a capacitive electromagnetic coupling feeding technique has been proposed in Chapter 7. Computer simulations have been used to investigate the influence of each individual composite part of the antenna on the impedance characteristics of the proposed dual-band PIFA. Also, different feed configurations have been studied. The results show that this new dual-band antenna not only needs just a single feed but most importantly that such a feed configuration is able to control the two band resonances independently. This gives the design great flexibility in choosing the two desired frequencies, as well as providing an easy means to match impedances at each resonant frequency. A design example of a dual-band PIFA for 900 MHZ and 2400 MHz ISM application has been given in section 7.4 and section 7.5. This antenna has been fabricated and tested and the measured results agreed well with the simulation results. Finally, the effect of a dielectric cover layer on this dual-band PIFA has also been studied. It is found that the dielectric cover layer could have a significant impact on the input and radiation characteristics of this dual-band PIFA, particularly for the higher frequency resonance. The analysis and design details for the antenna and the effect of the dielectric cover layer presented here could be adopted as starting points for engineers who are interested in utilising a low-profile dual-band or multi-band PIFA as an internal antenna for new wireless communication devices.

- 202

8.2 Recommendations

The following extensions are recommended as a result from the work carried out in this thesis.

1. The results obtained in this study have shown that a dielectric cover layer or radome has a significant impact on the operating performance of the PIFA when they are located close to one another. This impact can be minimised by rearranging the orientation and location of the antenna within the dielectric enclosure or radome and by choosing the appropriate electrical properties and physical dimensions for the dielectric material used. Also, the results have shown that when the PIFA is enclosed by a dielectric enclosure, the resonant frequency of the antenna decreases but the bandwidth could increase. Such findings indicate that it is possible to optimise the operating performance of a radome-antenna system by finding the best electrical properties of the dielectric material and the best geometry and structure for the radome-antenna system. For this reason, as discussed in section 2.4.6 of Chapter 2, it is recommended that the TLM code developed in Chapter 6 may be combined with an optimisation tool such as a Genetic Algorithm (GA) (Davis, 1987), to search for the appropriate values of these electrical and physical parameters, in order to achieve an optimal performance of the radome-enclosed PIFA. The GA is a global numerical-optimisation method, patterned after the natural process of genetic recombination and evolution and is becoming a promising tool for optimising antenna system design for a particular application (Haupt, 1995, Altshuler *et al*, 2000 and Altshuler, 2002).

2. Also, it will be worth while to investigate the effect of the dielectric radome on the polarisation of the PIFA.

- 203

REFERENCES

Altshuler, E. E., 2002, "Electrically Small Self-Resonant Wire Antennas Optimized Using a Genetic Algorithm", *IEEE Trans. Antennas Propagat.*, Vol. 50, No. 3, pp. 297 - 300.

Altshuler, E. E., and O'Donnell, T., 2000, "Mutual Coupling between Electrically Small Genetic Antennas", *Proceedings of the 2000 Antenna Applications Symposium*, Allerton Park, Monticello, Illinois, pp. 128 - 133.

Bhattacharyya, A. K., 1991, "Effects of Ground Plane Truncation on the Impedance of a Patch Antenna", *Microwaves, Antennas and Propagation, IEE Proceedings H* , Vol. 138, No. 6, pp. 560 - 64.

Bhattacharya, S., Long, S. and Wilton, D**.,** 1987**, "**The Input Impedance of a Monopole Antenna Mounted on a Cubical Conducting Box**",** *IEEE Trans. Antennas Propagat.*, Vol. 35, No. 7, pp. 1987 - 762.

Bokhari, S. A., Zurcher, J. –F., Mosig, J. R. and Gardiol, F. E; 1996, "A Small Microstrip Patch Antenna with a Convenient Turning Option", *IEEE Trans. Antennas Propagat.*, Vol. 44, No. 11, pp. 1521 - 1528.

Burke, G. J., and Poggio, A. J., 1981, *Numerical Electromagnetic Code (NEC) - the Method of Moments*, Technical report, Lawrence Livermore National Laboratory, Livermore, CA, UCID-18834.

Chang, D. C., and Zheng, J. X., 1992, "Electromagnetic Modelling of Passive Circuits in MMIC", *IEEE Trans. Microwave Theory Tech.*, Vol. 40, No. 9, pp. 1741 - 1747.

Chen, Hong-Twu, Wong, Kin-Lu and Chiou, Tzung-Wern, 2003, "PIFA with a Meandered and Folded Patch for the Dual-Band Mobile Phone Application", *IEEE Trans. Antennas Propagat.*, Vol. 51, No. 9, pp. 2468 - 2471.

Chu, L. J., 1948, "Physical Limitations of Omni-Directional Antennas", *Journal of Applied Physics*, Vo. 19, pp.1163 - 1175.

Davis, L., 1987, *Genetic Algorithms and Simulated Annealing*, Morgan Kaufmann Publishers, London.

Derneryd, A.G., 1978, "A Theoretical Investigation of the Rectangular Microstrip Antenna Elements", *IEEE Trans. Antennas Propagat.*, Vol. 26, pp. 532 - 535.

- 204

Evans-Pughe, C., 2003, **"**ZigBee Wireless Standard", IEE Review, Vol. 49, No. 3, pp. 28 – 31.

Fenk, J., 2003, "RF-Trends in Mobile Communication", *Proceedings of the 29th European Solid-State Circuits Conference***,** pp. 21 – 27.

Fujimoto, K., Henderson, A., Hirasawa, K. and James, J. R., 1987, *Small Antennas*, Research Studies Press, Letchworth, Hertfordshire, England.

Fujimoto, K., and James, J. R., 1994, *Mobile Antenna Systems Handbook*, Artech House, Norwood.

Guertler, R., 1977, "Isotropic Transmission-Line Antenna and Its Toroid-Pattern Modification", *IEEE Trans. Antennas Propagat*., Vol. 25, No. 3, pp. 386 - 392.

Hammer, P., Van Bouchaute, D., Verschraeven, D., and Van De Capelle, A., 1979, "A Model for Calculating the Radiation Field of Microstrip Antenna'*, IEEE Trans. Antenna Propagat.*, Vol. 27, No. 3, pp. 267 -270.

Hammerstad, E., and Jensen, O, 1980, "Accurate Models for Microstrip Computer-Aided Design", *Microwave Symposium Digest of the International MTT-S*, Vol. 80, No. 1, pp. 407 - 409.

Harrington, R. F., 1960, "Effect of Antenna Size on Gain, Bandwidth, and Efficiency", *Journal of Research of the National Bureau of Standards-D. Radio Propagat.*, Vol. 64D, No. 1.

Harrington, R. F., 1961, *Time-Harmonic Electromagnetic Fiel*ds, McGraw-Hill, New York, pp. 378.

Harrington, R. F., 1993, *Field Computation by Moment Metho*ds, IEEE Press, New York.

Harrison, C. W., Jr., 1958, *Theory of Inverted-L Antenna with Image*, Technical report, Sandia Corporation, Albuquerque, New Mexico, Vol. 11, No. 14.

Haupt R. L., 1995, "An Introduction to Genetic Algorithms for Electromagnetics", *IEEE Antenna and Propagation Magazine*, Vol. 37, No. 2, pp. 7 - 15.

He, J., 2000, "Strip Inverted-F Antenna for a Laptop Computer", *Proceedings of the 2000 IUEEPS*, Perth.

Hirasawa, K., and Haneshi M., 1992, *Analysis, Design, and Measurement of Small and Low-Profile Antennas*, Artech House, Norwood, MA.

- 205

Hoffmann, R. K., 1987, *Handbook of Microwave Integrated Circuits*, Artech House, Norwood, pp. 305 - 306.

Huang, J., 2001, "Miniaturized UHF Microstrip Antenna for a Mars Mission"*, Antennas and Propagation Society International Symposium, IEEE*, Vol. 4, pp. 486 – 489.

Hubing, T. H., 1991, *Survey of Numerical Electromagnetic Modelling Techniques*, TR91-1-001.3, EMC Laboratory, University of Missouri-Rolla.

James, J. R., and Hall, P. S., 1989, *Handbook of Microstrip Antennas*, P. Peregrinus on behalf of the Institution of Electrical Engineers, London.

Jensen, M. A., and Rahmat-Samii, Y., 1994, "The Electromagnetic Interaction between Biological Tissue and Antennas on a Transceiver Handset", *IEEE Antennas and Propagation Society International Symposium (AP-S Digest)*, Vol. 1, pp. 367 – 370.

Johnson, R. C., and Jasik, H., 1984, *Antenna Engineering and Handbook*, second edition, McGraw-Hill Book Company, pp.44-1 to 44-25.

Jui-Hung Yeh, Jyh-Cheng Chen, and Chi-Chen Lee, 2003, "WLAN Standards*", IEEE, Potentials,* Vol. 22, No. 4, pp. 16 –22.

King, B., Harrison, C. and Denton, D., 1960, "Transmission-Line Missile Antennas", *IRE Trans. Antennas Propagat.*, Vol. 8, No.1, pp. 88 - 90.

Kirschning, M., Jansen, R. H. and Koster, N. H. L., 1981, "Accurate Model for Open End Effect of Microstrip Lines", *Electronics Letters*, Vol. 17, No. 3, pp. 123 - 124.

Kolundzija, B. M., 1999, "Electromagnetic Modelling of Composite Metallic and Dielectric Structures", *IEEE Trans. Antennas Propagat.*, Vol. 47, No. 7, pp.1021 - 1032.

Kolundzija, B., Tasic, M. and Sarkar, T., 1999, "Efficient and Accurate Inclusion of Radomes into Antenna Analysis", *IEEE Antennas and Propagation Society International Symposium*, Vol. 2, pp. 842 - 845.

Kolundzija, B. M., Ognjanovic, J. S. and Sarkar, T. K., 2000, *WIPL-D: Electromagnetic Modelling of Composite Metallic and Dielectric Structures*, Artech House, Norwood.

Kompa, G., and Mehran, R., 1975, "Planar Waveguide Model for Calculating Mictrostrip Components", *Electronics Letters*, Vol. 11, No. 19, pp. 549 - 460.

Lebbar, H., Himdi, M. and Daniel, J. P., 1992, "Transmission Line Analysis of Printed Monopole"*, Electronics Letters*, Vol. 28, No. 14, pp.1326 - 1327.

- 206

Li, Le-Wei, Kooi, Pang-Shyan, Leong, Mook-Seng, Chan, Hse-Ming and Yeo, Tat-Soon, 1997, "FDTD Analysis of Electromagnetic Interactions between Handset Antennas and the Human Head", *Proceedings of Asia-Pacific Microwave Conference (APMC)*, Vol. 3, pp.1189 - 1192.

Li, R. L., DeJean, G., Tsai, E., Tentzeris, E. and Laskar, J., 2002, "Novel Small Folded Shorted-Patch Antennas", *IEEE Antennas and Propagation Society International Symposium*, Vol. 4, pp. 26 - 29.

Liu, Z. D., and Hall, P. S., 1996, "Dual-Band Antenna for Hand Held Portable Telephones", *Electronics Letters*, Vol. 32, No. 7, 28 Mar., pp. 609 – 610.

Lo, T. K.-C., and Hwang, Y., 1998, "Bandwidth Enhancement of PIFA Loaded with Very High Permittivity Material Using FDTD", *IEEE Antennas and Propagation Society International Symposium*, Vol. 2, pp. 798 - 801.

Lo, Y. T., and Lee, S. W., 1988, *Antenna Handbook: Theory, Applications, and Design*, Van Nostrand Reinhold, New York.

Long, S. and Chu, A., 1987, **"**Radiation Patterns of a Monopole Antenna Mounted on a Cubical Conducting Box**",** *Antennas and Propagation Society International Symposium*, Vol. 25, pp. 654 - 657.

Miller, E. K., February 1998, "Model-Based Parameter Estimation in Electromagnetics I: Background and Theoretical Development", *IEEE Antennas and Propagation Magazine*, Vol. 40, No. 1, pp. 42 – 52.

Miller, E. K., April 1998, "Model-Based Parameter Estimation in Electromagnetics II: Applications to EM Observables", *IEEE Antennas and Propagation Magazine*, Vol. 40, No. 2, pp. 51 - 65.

Miller, E. K., June 1998, "Model-based Parameter Estimation in Electromagnetics III: Applications to EM Integral Equations", *IEEE Antennas and Propagation Magazine*, Vol. 40, No. 3, pp. 49 - 66.

Mosig, J. R., 1988, "Arbitrarily Shaped Microstrip Structures and Their Analysis with a Mixed Potential Integral Equation", *IEEE Trans. Microwave Theory Tech*., Vol. 36, No. 2, pp. 314 - 323.

Munson, R. E., 1974, "Conformal Micostrip Antennas and Microstrip Phased Arrays", *IEEE Trans. Antennas Propagat.*, Vol.22, pp.74 - 78.

Nakano, H., Yamauchi, J. and Mimaki, H., 1988, "Backfire Radiation from a Monofilar Helix with a Small Ground Plane", *IEEE Trans. Antennas Propagat.*, Vol. 36, No.10, pp. 1359 - 1364.

- 207

Okoniewski, M., and Stuchly, M. A., 1996, "A Study of the Handset Antenna and Human Body Interaction", *IEEE Trans. Microwave Theory Tech.*, Vol. 44, No. 10, pp. 1855–1864.

Orr, W. I., 1978, *Radio Handbook*, 21st ed., Indianapolis, Ind.: Editors and Engineers.

Owyang, G. H., 1989, *Foundation for Microwave Circuits*, Springer-Verlag, New York, pp. 1 - 39.

Pedersen, G. F., and Andersen, J. B., 1994, "Integrated Antennas for Hand-Held Telephones with Low Absorption", *Proceedings of the 44th IEEE Vehicular Technology Conference*, Vol. 3, pp.153 - 1541.

Pues, H., and Van de Capelle A., 1984, "Accurate Transmission-Line Model for the Rectangular Microstrip Antenna", *IEE Proc. Pt. H.,* Vol. 131, No. 6, pp. 334 - 340.

Rao, S. M., Cha, C.-C., Cravey, R. L. and Wilkes, D. L., 1991, "Electromagnetic Scattering from Arbitrary Shaped Conducting Bodies Coated with Lossy Materials of Arbitrary Thickness", *IEEE Trans. Antennas Propagat.*, Vol. 39, No 5, pp. 627 – 631.

Rowell, C. R., and Murch, R. D., 1997, "A Capacitively Loaded PIFA for Compact Mobile Telephone Handsets", *IEEE Trans. Antennas Propagat.*, Vol. 45, No. 5, pp. 837 – 842.

Rowell, C. R., and Murch, R. D., 1998, "A Compact PIFA Suitable for Dual-Frequency 900/1800-MHz Operation", *IEEE Trans. Antennas Propagat.*, Vol. 46, No. 4, pp. 596 - 598.

Sainati, R. A., 1996, *CAD of Microstrip Antennas for Wireless Applications*, Artech House, Norwood.

Sarkar, T. K., Arvas, E. and Ponnapalli, S., 1989, "Electromagnetic Scattering from Dielectric Bodies", *IEEE Trans. Antennas Propagat.,* Vol. 37, No. 5, pp. 673 – 676.

Schlagenhaufer, F., Fynn, K. and Probol, C., 2001, "Rational Approximation of Transfer Functions for Radiating Structures", *Proceedings of the international IEEE Symp. on EMC*, pp. 864 - 869.

Seale, R., and Chung, K., 1992, "Modified Transmission Line Antenna on a Conducting Box", *Proc. of the International Symposium on Antennas and Propagation*, Sapporo, Japan, pp.665 - 668.

Seale, R. B., 1993, *A Study of Small UHF Antennas*, Masters Thesis, Curtin University of Technology.

- 208

Stutzman, W. L., and Thiele, G. A., 1981, *Antenna Theory and Design*, John Wiley & Sons.

Taga, T., and Tsunekawa, K., 1987, "Performance Analysis of a Built-in Planar Inverted-F Antenna for 800 MHz Band Portable Radio Units", *IEEE Trans. Selected Areas in Communication*, Vol. 5, No. 5, pp. 921 - 929.

The Mathworks, 1984, http://www.mathworks.com/.

Tomar, R. S., and Bhartia, P., 1987, "New Quasi-Static Models for the Computer-Aided Design of Suspended and Inverted Microstrip Line", *IEEE Trans. Microwave, Theory and Tech.*, Vol. 35, No. 4, April 1987, pp. 453 - 457 and corrections No. 11, pp. 1076.

Vandenbosch, G. A. E., 1995, "Capacitive Matching of Microstrip Antenna", *Electronics Letters*, Vol. 31, No. 18, pp.1535 - 1536.

Vandenbosch, G. A. E., 1999, "Network Model for Capacitively Fed Microwave Element", *Electronics Letters*, Vol. 35, No 19, pp.1597 - 1599.

Vandenbosch, G. A. E., and Van de Capelle A. R., 1994, "Study of the Capacitively Fed Microwave Antenna Element", *IEEE Trans. Antennas Propagat.*, Vol. 42, No. 12, pp.1648 - 1652.

Verma, A. K., 1995, "Static Capacitance of Some Multilayered Microstrip Capacitors", *IEEE Trans. Microwave, Theory Tech.*, Vol. MTT-43, No. 5, pp. 1144 - 1152.

Virga, K. L., and Rahmat-Samii, Y., 1997, "Low-Profile Enhanced-Bandwidth PIFA Antennas for Wireless Communications Packaging", *IEEE Trans. Microwave Theory Tech.*, Vol. 45, No. 10, pp. 1879 - 1888.

Weiner, M., 1987, "Monopole Element at the Center of a Circular Ground Plane Whose Radius is Small or Comparable to a Wavelength", *IEEE Trans. Antennas Propagat.*, Vol. 35, No. 5, pp. 488 - 495.

Wheeler, H. A., 1947, "Fundamental Limitations of Small Antennas", *Proceedings of the I.R.E.*, pp. 1479 - 1484.

Williams, J. T., Delgado, H. J. and Long, S. A., Nov. 1990, "An Antenna Pattern Measurement Technique for Eliminating the Fields Scattered from the Edges of a Finite Ground Plane", *IEEE Trans. Antennas Propagat.*, Vol. 38, No. 11, pp. 1815 - 1822.

Wolff, I., and Knoppik, N., 1974, "Rectangular and Circular Microstrip Disk Capacitors and Resonators", *IEEE Trans. Microwave, Theory Tech.*, Vol. MTT-22, No. 10, pp. 857 - 864.

- 209

Wong, Kin-Lu, 2002, *Planar Antennas for Wireless Communications*, Wiley-Interscience.

Wong, Kin-Lu, and Yang, Kai-Ping, 1998, "Modified Planar Inverted F Antenna", *Electronics Letters*, Vol. 34, No. 1, pp. 7 - 8.

Zeland Software, 1996, *IE3D User's Manual*, Version 3.0.

Zheng, J. X., 1994, "Electromagnetic Simulation of Microstrip Patch Antennas", *IEEE Antennas and Propagation Society International Symposium*, AP-S, Digest, Vol. 1, pp. 318 – 321.

- 210

APPENDIX A GALERKIN'S METHOD

The field integral equation belongs to the class of linear operator equations. It can be expressed in the form (Harrington, 1993)

$$L\left[f(\mathbf{r})\right] = g(\mathbf{r}') \tag{A.1}$$

where L is the known linear operator, $g(\mathbf{r}')$ represents the known excitation vector (incident electric field) function, and $f(\mathbf{r})$ represents the unknown current function that should be determined.

Solving this problem directly by taking the inverse of the operator (L^{-1}) is usually difficult, if not impossible. Instead, the solution may be found numerically by using the linearity of the L operator. This is done by first expanding $f(\mathbf{r})$ in n terms of a selected basis function $f_n(\mathbf{r})$ i. e,

$$L\left[\sum_{n=1}^{N} c_n f_n(\mathbf{r})\right] = g(\mathbf{r}') \tag{A.2}$$

where the c_n are constants.

Since L is a linear operator, it can be brought inside the summation as follows:

$$\sum_{n}^{N} c_n L\left[f_n(\mathbf{r})\right] = g(\mathbf{r}') \tag{A.3}$$

Now define a set of test functions w_1, w_2, w_3,… in the range of L, and take the inner product of equation (A.3) with each w_m. The result is

$$\sum_{n=1}^{N} c_n \left\langle w_m(\mathbf{r}), L\left[f_n(\mathbf{r})\right]\right\rangle = \left\langle w_m(\mathbf{r}), g(\mathbf{r}')\right\rangle, m = 1, 2, ...M \tag{A.4}$$

When the test functions are chosen to be the same as the basis functions, this is called the Galerkin method. Thus, equation (A.4) becomes,

$$\sum_{n=1}^{N} c_n \left\langle f_n(\mathbf{r}), L\left[f_n(\mathbf{r})\right]\right\rangle = \left\langle f_n(\mathbf{r}), g(\mathbf{r}')\right\rangle \tag{A.5}$$

Equation (A.5) can be expressed in matrices as in,

$$\begin{bmatrix} \langle f_1(\mathbf{r}), L(f_1(\mathbf{r}))\rangle & \langle f_1(\mathbf{r}), L(f_2(\mathbf{r}))\rangle & \langle f_1(\mathbf{r}), L(f_N(\mathbf{r}))\rangle \\ \langle f_2(\mathbf{r}), L(f_1(\mathbf{r}))\rangle & \langle f_2(\mathbf{r}), L(f_2(\mathbf{r}))\rangle & \langle f_2(\mathbf{r}), L(f_N(\mathbf{r}))\rangle \\ \vdots & \vdots & \vdots \\ \langle f_M(\mathbf{r}), L(f_1(\mathbf{r}))\rangle & \langle f_M(\mathbf{r}), L(f_2(\mathbf{r}))\rangle & \langle f_M(\mathbf{r}), L(f_N(\mathbf{r}))\rangle \end{bmatrix} \begin{bmatrix} c_1 \\ c_2 \\ \vdots \\ c_n \end{bmatrix}$$

$$= \begin{bmatrix} \langle f_1(\mathbf{r}), g(\mathbf{r}')\rangle \\ \langle f_2(\mathbf{r}), g(\mathbf{r}')\rangle \\ \vdots \\ \langle f_M(\mathbf{r}), g(\mathbf{r}')\rangle \end{bmatrix} \tag{A.6}$$

which can be expressed concisely in matrix form as:

$$[L_{mn}][c_n] = [g_m] \tag{A.7}$$

where $[L_{mn}]$, $[c_n]$, and $[g_m]$ are N x N, N x 1, *and* N x 1 matrices (or vectors), respectively. The unknown vector $[c_n]$ can then be found by solving equation (A.7).

APPENDIX B RATIONAL APPROXIMATION OF TRANSFER FUNCTIONS FOR RADIATING STRUCTURES

The input impedance characteristic parameters of a passive antenna system can be approximated by a rational function that interpolates a given function at given frequencies. The approach for the basic rational approximation (Schlagenhaufer *et al*, 2001) is:

$$H(s) = \frac{\sum_{k=0}^{m} a_k \cdot s^k}{\sum_{l=0}^{n} b_l \cdot s^l} \tag{B.1}$$

where $H(s)$ is a complex frequency response, $s = j2\pi f$ is a complex frequency, a_k and b_l are complex coefficients. The transfer function $H(s)$ is known for a certain number of sample points s. The coefficients a_k and b_l characterising the rational function are calculated from equation (B.1). To do this, equation (B.1) can be rewritten as a linear equation system in matrix form

$$\mathbf{A}\vec{x} = \vec{d} \tag{B.2}$$

using

$$H(s) \cdot \sum_{l=0}^{n} s^l \cdot b_l - \sum_{k=0}^{m} s^k \cdot a_k = 0 \tag{B.3}$$

and a constraint has to be introduced to obtain a uniquely defined equation system:

$$\sum_{k=0}^{m} a_k = 1 . \tag{B.4}$$

This constraint has been chosen instead of the commonly used $a_m = 1$ because it is not known of which order the numerator polynomial of the approximating rational function

will be. The coefficient for its highest term may become very small and numerical problems could occur. The constraint described in equation (B.4) overcomes this problem, as any one of the coefficients can become zero (or very small) without introducing numerical difficulties.

The first row of the coefficients A_{lk} of matrix **A** represents this constraint:

$$A_{1k} = \begin{cases} 1 & \text{, for } 1 \le k \le m \\ 0 & \text{, for } m < k \le m+n \end{cases} \text{, for } l = 1 . \tag{B.5}$$

Row 2 to row n+m are defined by the samples:

$$A_{lk} = \begin{cases} H(s_{l-2}) \cdot {s_{l-2}}^{k-1} & \text{, for } 1 \le k \le n \\ -{s_{l-2}}^{k-(n+1)} & \text{, for } n < k \le m+n \end{cases} \text{, for } l \ \ge \ 2 . \tag{B.6}$$

The vectors $\vec{x}$ and $\vec{d}$ are given by

$$\vec{x} = \begin{pmatrix} a_0 & \cdots & a_m & b_0 & \cdots & b_n \end{pmatrix}^{\mathrm{T}}, \tag{B.7}$$

and

$$d = \begin{pmatrix} 1 & 0 & \cdots & 0 \end{pmatrix}^{\mathrm{T}} . \tag{B.8}$$

The linear equation system is uniquely defined if the number of the samples equals n + m - 1.

APPENDIX C RELATION BETWEEN [S] AND [Z] - ONE PORT

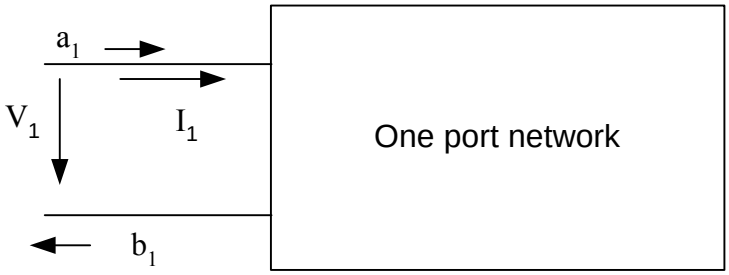

Figure C-1 A one-port network.

Figure C-1 shows an incident wave a_1, reflected wave b_1, current I_1 and the voltage V_1 across the port of a one-port network. The scattering parameter S_{11} is defined to relate the incident and reflected waves at the port as follows (Owyang, 1989):

$$S_{11} = \frac{b_1}{a_1} \tag{C.1}$$

The input impedance at the port is given by

$$Z_{in} = \frac{V_1}{I_1} \tag{C.2}$$

From the transmission line relations, the voltage and current can be expressed in term of the incident wave and reflected waves.

$$\frac{V_1}{\sqrt{Z_0}} = a_1 + b_1 \tag{C.3}$$

$$\sqrt{Z_0} I_1 = a_1 - b_1 \tag{C.4}$$

where Z_0 is the characteristic impedance of the lossless line.

Therefore,

$$Z_{in} = Z_0 \frac{1 + S_{11}}{1 - S_{11}} \tag{C.5}$$

or

$$S_{11} = \frac{Z_{in} - Z_0}{Z_{in} + Z_0} \tag{C.6}$$

This is the relation between [Z] and [S] for a one-port network.

APPENDIX D EXPRESSIONS FOR VALUES OF d_{ij} IN A NEW QUASI-STATIC MODEL FOR THE COMPUTER-AIDED DESIGN OF INVERTED MICROSTRIP LINE

Defining

$$F = \ln \varepsilon_r$$

We have

$$d_{00} = (2359.4010\text{-}97.1644F\text{-}5.7706F^2 + 11.4112F^3)*10^{-3}$$

$$d_{01} = (4855.9472\text{-}3408.5207F + 15296.7300F^2\text{-}2418.1785*F^3)*10^{-5}$$

$$d_{02} = (1763.3400 + 961.0481F\text{-}2089.2800F^2 + 375.8805F^3)*10^{-5}$$

$$d_{03} = (-556.0909\text{-}268.6165F + 623.7094F^2\text{-}119.1402F^3)*10^{-6}$$

$$d_{10} = (219.0660\text{-}253.0864F + 208.7469F^2\text{-}27.3285F^3)*10^{-3}$$

$$d_{11} = (915.5589 + 338.4033F\text{-}253.2933F^2 + 40.4745F^3)*10^{-3}$$

$$d_{12} = (-1957.3790\text{-}1170.9360F + 1480.8570F^2\text{-}347.6403F^3)*10^{-5}$$

$$d_{13} = (486.7425 + 279.83223F\text{-}431.3625F^2 + 108.8240F^3)*10^{-6}$$

$$d_{20} = (5602.7670 + 4403.3560F\text{-}4517.0340F^2 + 743.2717F^3)*10^{-5}$$

$$d_{21} = (-2823.4810\text{-}1562.7820F + 3646.1500F^2\text{-}823.4223F^3)*10^{-5}$$

$$d_{22} = (253.8930 + 158.5529F\text{-}3235.4850F^2\text{-}919.36661F^3)*10^{-6}$$

$$d_{23} = (\text{-}147.0235 + 62.4342F + 887.5211F^2\text{-}270.7555F^3)*10^{-7}$$

$$d_{30} = (\text{-}3170.2100\text{-}1931.8520F + 2715.3270F^2\text{-}519.3420F^3)*10^{-6}$$

$$d_{31} = (596.3251 + 188.1409F\text{-}1741.4770F^2 + 465.6756F^3)*10^{-6}$$

$$d_{32} = (124.9655 + 577.5381F + 1366.4530F^2\text{-}481.1300F^3)*10^{-7}$$

$$d_{33} = (\text{-}530.2099\text{-}2666.3520F\text{-}3220.0960F^2 + 1324.4990F^3)*10^{-9}$$

APPENDIX E PUBLICATIONS

The following conference papers have been published on the topics related to this study.

- He, J. and Chung, K., "Design Considerations of Planar Inverted-F Antenna on Finite Ground Plane", *Proceedings of the Asia Pacific Communications Conference*, Beijing, 2004, pp. 655-659.
- He J. W., "Analysis and Design of a Single Feed Dual-band Low Profile Antenna for Wireless ISM Band Communications", *Proceedings of the PEECS*, Perth, 2003, pp. 186-191.
- He, J. and Chung, K. "Analysis of the Effect of Dielectric Radome of Planar Inverted–F Antenna", *Proceedings of the Asia Pacific Communications Conference*, Bandung, 2002, pp.174-177.
- He. J. W., "Analysis of Interaction between PIFA and Radome at 2.4 GHz WLAN Band", *Proceedings of the IUPEES*, Perth, 2002.
- He, J. and Chung, K., "Planar Inverted-F Antenna Covered with a Dielectric Layer", *Proceedings of the Antenna Applications Symposium*, Illinois, 2000, pp. 323 –337.
- He J. W., "Strip Inverted-F Antenna for Laptop Computers", *Proceedings of the IUPEES*, Perth, 2000, pp.61-62.